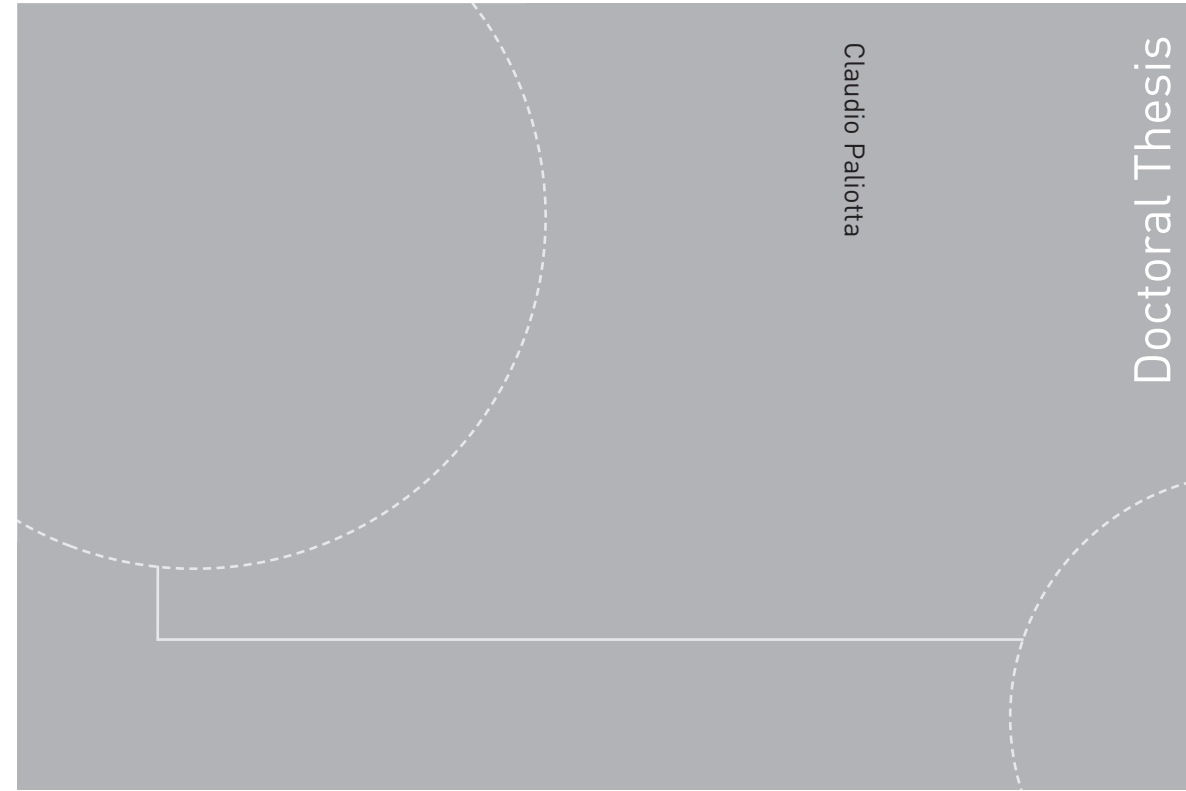


ISBN 978-82-326-2552-9 (printed version)
ISBN 978-82-326-2553-6 (electronic version)
ISSN 1503-8181



Doctoral theses at NTNU, 2017:240

Claudio Paliotta

Control of Under-actuated Marine Vehicles

Doctoral theses at NTNU, 2017:240

NTNU
Norwegian University of
Science and Technology
Faculty of Information Technology,
Mathematics and Electrical Engineering
Department of Engineering Cybernetics

 **NTNU**
Norwegian University of
Science and Technology

 NTNU

 **NTNU**
Norwegian University of
Science and Technology

Claudio Paliotta

Control of Under-actuated Marine Vehicles

Thesis for the degree of Philosophiae Doctor

Trondheim, September 2017

Norwegian University of Science and Technology
Faculty of Information Technology,
Mathematics and Electrical Engineering
Department of Engineering Cybernetics



Norwegian University of
Science and Technology

NTNU

Norwegian University of Science and Technology

Thesis for the degree of Philosophiae Doctor

Faculty of Information Technology,
Mathematics and Electrical Engineering
Department of Engineering Cybernetics

© Claudio Paliotta

ISBN 978-82-326-2552-9 (printed version)

ISBN 978-82-326-2553-6 (electronic version)

ISSN 1503-8181

Doctoral theses at NTNU, 2017:240



Printed by Skipnes Kommunikasjon as

To whom it may concern

Summary

In this dissertation, various topics related to control problems for under-actuated marine vehicles are investigated. The thesis is divided into three parts.

The first part deals with the source-seeking problem for multi-agent systems. It is assumed that a group of vehicles has to identify the location of a source in the ocean space. The source may for instance be an area with a high concentration of a specific chemical substance. The agents have to define the direction of motion towards the source utilizing distributed measurements of the scalar field surrounding the source. It is supposed that the agents are organized in a leader-follower scheme. An approach for kinematic unicycle agents is first presented. In this approach the novelty is a variable-leader scheme. That is, it is assumed that the leader can change during the mission. This allows for a better distribution of the tasks in the group. In particular, there is an agent in the group which has information about the direction where to move in order to explore an area of interest. Then there is also another agent that can take on the role as leader if it gets satisfactory measurements from the environment. This approach is then used in order to develop a strategy for multi-agent systems consisting of under-actuated marine vehicles. In this second case, a synchronization controller is used for the vehicles in order to achieve motion in formation. The leader agent collects information from the followers and is able to compute the direction pointing towards the source, computing the approximated gradient of the field surrounding the source. Simulation case studies are presented in order to validate the approaches.

In the second part of the thesis a novel approach for controlling under-actuated marine vehicles is presented. The approach is inspired by works on control of non-holonomic ground vehicles. The method is based on the definition of a different output for the system. Then an input-output feedback linearization controller is used in order to apply a change of inputs to the system. This method transforms the nonlinear model of an under-actuated marine vehicle into a system with a linear external dynamics and a nonlinear internal dynamics. We use this approach to solve the trajectory tracking control problem, the path following control problem and the leader-follower synchronization control problem for marine vehicles in presence of environmental disturbances. Simulation case studies and experimental results validate the theoretical results.

The third part of the thesis deals with the path following control problem for under-actuated marine vehicles. First the path following control problem is dealt with for unparametrized straight-line paths. A guidance law inspired by a common control approach for aerial vehicles is developed. The guidance is based

on geometric control principles and it is used together with an observer in order to counteract the effect of ocean currents. Almost-global stability of the closed-loop system is proven and a simulation case study validates the theoretical result. Then the path following problem for curved paths is considered. In particular, paths parametrized by a path variable are considered. Two strategies are considered. Both the strategy are based on a parametrization of the curve which is used to propagate a path-tangential frame. The path following errors are defined with respect to the path-tangential frame. The first strategy forces the vehicle to move along the normal of the path-tangential frame. This results in a singularity which makes the strategy valid only locally around the path. The second strategy defines a different path parametrization which is valid globally. Here an ocean current observer is also used in order to counteract the ocean current disturbance. The closed-loop system is proven to be globally asymptotically stable. The theoretical results are verified via numerical simulations. Finally, a novel control strategy for path following of curved paths is presented. The novelty of this last approach is that it does not require any parametrization of the path. In fact, the path is implicitly defined as a manifold in the state space. The control approach is based on geometric control and hierarchical control design. An adaptive controller is used in order to deal with the disturbance caused by ocean currents. The closed-loop system is proven to be asymptotically stable.

Contents

Summary	iii
Contents	v
List of figures	ix
List of tables	xi
Preface	xiii
1 Introduction	1
1.1 Background and motivation	1
1.2 Thesis outline and scientific contributions	8
1.3 Publications	14
2 Model and mathematical preliminaries	17
2.1 The general model for marine vehicles	17
2.2 The relative velocity model	18
I Source seeking strategies for marine vehicles	23
3 Source-seeking with variable leader in the network	25
3.1 System description	26
3.2 The revised agreement protocol	30
3.3 Results	34
3.4 Simulations	36
3.5 Conclusions	37
4 Adaptive source-seeking with marine vehicles	39
4.1 ASV model	40
4.2 Constant bearing guidance law	41
4.3 Leader's heading computation	42
4.4 Source seeking guidance law and synchronization controller	45
4.5 Simulations	45
4.6 Conclusion	46
4.A Function definitions	48

II	Control of marine vehicles using the hand position approach	49
5	Trajectory tracking of marine vehicles	51
5.1	Vehicle model	51
5.2	Hand position: line of reasoning	52
5.3	Control objectives	55
5.4	The controller	57
5.5	Main result	57
5.6	The particular case of straight-line paths	62
5.7	Simulations	64
5.8	Conclusions	65
5.A	Equations	69
6	Path following of marine vehicles	71
6.1	Vehicle model	72
6.2	Hand position: line of reasoning	72
6.3	Problem definition and control objectives	74
6.4	The control system	76
6.5	Main result	77
6.6	The straight-lines case	83
6.7	Unparametrized straight-line paths	85
6.8	Simulation results	87
6.9	Sea trial results	91
6.10	Conclusions	93
7	Multi-agent formation with disturbance rejection	95
7.1	Agents' model and assumptions	96
7.2	Control objective	97
7.3	Control design	98
7.4	Main results	99
7.5	Formation control of marine vehicles	102
7.6	Simulations	107
7.7	Conclusions	110
7.A	Equations	112
III	Path following for marine vehicles	113
8	Geometric guidance for path following of marine vehicles	115
8.1	Vehicle model	116
8.2	Control objectives	117
8.3	The guidance law and the observer	117
8.4	The controllers	121
8.5	Main result	123
8.6	Simulation results	128
8.7	Conclusions	131

8.A	Perturbation terms	131
9	Observer based path following for generic paths: a local approach	133
9.1	Vessel model	134
9.2	Problem definition	134
9.3	Controller, observer, and guidance	137
9.4	Closed-loop analysis	144
9.5	Case study	149
9.6	Conclusion	151
9.A	Proof of Lemma 9.2	153
9.B	Proof of Lemma 9.3	154
9.C	Proof of Lemma 9.4	156
10	Observer based path following for generic paths: a global approach	161
10.1	Vessel model	161
10.2	Problem definition	163
10.3	Controllers, Observer, and Guidance	164
10.4	Closed-Loop Analysis	172
10.5	Case Study	177
10.6	Conclusion	178
10.A	Proof of Lemma 10.1	180
10.B	Proof of Lemma 10.2	182
10.C	Proof of Lemma 10.3	186
11	Path following of unparametrized paths	191
11.1	Preliminaries and notation	192
11.2	The problem	193
11.3	Hierarchical control approach	195
11.4	The case of zero ocean current	196
11.5	The case of non-zero ocean current	203
11.6	Simulation results	208
11.7	Conclusions	210
11.A	Functions used in the model	212
11.B	Curvature computation for Lemma 11.3	213
12	Conclusions and future work	215
12.1	Conclusions	215
12.2	Future work	218
A	Mathematical references	221
A.1	Mathematical References	221
A.2	Graph theory tools	224
B	Numerical simulation models	227
B.1	Numerical model for a supply vessel	227
B.2	Numerical model for the light autonomous under-water vehicle (LAUV)	229
	References	231

List of figures

2.1	Vehicle's states.	19
3.1	Global and body frames	27
3.2	Exchange of the leadership, the agent v_1 is the initial leader, the agent v_2 is the the active follower, the red dots are the sensors	28
3.3	Topology of the agents' graph	38
3.4	Motion of the vehicles.	38
3.5	Investment parameter k	38
4.1	Formation moving towards the source, following a lawn-mower path. . .	47
4.2	Evolution of the variable weight k and synchronization error between the followers and the leader.	47
5.1	The hand position point.	53
5.2	Motion of the ship.	66
5.3	Time evolution of the errors states.	66
5.4	Ocean current estimates.	67
5.5	Time evolution of the surge velocity, sway velocity and yaw rate.	67
6.1	The hand position point.	73
6.2	Path following.	75
6.3	Motion of the vehicle. The black dot represents the motion of the virtual frame VF	88
6.4	Time evolution of the error states.	89
6.5	Time evolution of the surge velocity, sway velocity and yaw rate.	89
6.6	Motion of the vehicle.	91
6.7	Top) Cross-track error, i.e. distance of the vehicle along the perpendicular direction to the path; Bottom) Course error.	92
6.8	Light autonomous underwater vehicle (LAUV).	92
6.9	Motion of the vehicle in the real trial.	93
6.10	Top) Cross-track error in the sea trial; Bottom) Course error in the sea trial.	94
7.1	Illustration of the control approach.	103
7.2	a) The pivot point (P) and the hand position \mathbf{h} . b) Relative velocities in the NED frame.	105

7.3	Desired motion and topology of the communication graph.	108
7.4	Motion of the vehicles.	109
7.5	Trajectory tracking errors of the leader v_0	109
7.6	Formation errors.	110
7.7	Time evolution of the yaw angle and yaw rate of the five agents.	111
8.1	a) Geometric guidance principle for the 2D case; b) Geometric guidance principle for steady state situation	119
8.2	Motion of the vessel. The arrows indicates the direction of the ocean current, but they are not in scale.	129
8.3	Cross-track error.	129
8.4	Ocean current estimate errors.	130
8.5	Top: surge propeller force; bottom: rudder torque	130
9.1	Definition of the ship's kinematic variables.	135
9.2	Definition of the path.	136
9.3	Path of the vessel in the $x - y$ -plane	150
9.4	Path following errors, current estimates, sway velocity, yaw rate, surge velocity , and size of C_r over time.	152
10.1	Definition of the ship's kinematic variables.	162
10.2	Definition of the path.	163
10.3	Path of the vessel in the $x - y$ -plane.	178
10.4	Path following errors, current estimates, sway velocity, yaw rate, surge velocity , and size of C_r over time.	179
11.1	Illustration of the ship's kinematic variables.	193
11.2	Path of the ship and the cassini oval (the ship is not to scale).	209
11.3	Sway velocity of the ship.	209
11.4	Magnitude of $h(p)$ as the vessel converges to the path.	210
11.5	Case of non-zero ocean current. The path of the ship and the Cassini oval (the ship and the ocean current vectors are not to scale).	210
11.6	Case of non-zero ocean current. Sway velocity of the ship.	211
11.7	Case of non-zero ocean current. Magnitude of $h(p)$ as the vessel converges to the path.	211
B.1	A supply vessel. [36]	227
B.2	The LAUV.	230

List of tables

3.1	Initial states and ocean currents affecting the vehicles.	37
5.1	Initial conditions.	65
6.1	Initial conditions.	87
7.1	Way points.	107
7.2	Initial states and ocean currents affecting the vehicles.	108

Preface

This thesis is submitted in partial fulfillment of the requirements for the degree of philosophiae doctor (PhD) at the Norwegian University of Science and Technology (NTNU). The work has been carried out at the Department of Engineering Cybernetics and at the Center for Autonomous Marine Operations and Systems (AMOS). My main supervisor has been Professor Kristin Ytterstad Pettersen and my co-supervisor has been Professor Asgeir Sørensen from the Marine Technology Department.

Acknowledgments

I believe that these few pages of acknowledgement probably are the most important of this dissertation. Even people who will not understand the technical details of the thesis will spend few minutes reading these few lines. I believe that I have to put an extra effort into writing properly these words which are *concluding* this long journey which lasted a little more than three years. As opposed to the rest of the thesis, it is in these pages that I can tell about the contribution of other people to my journey and to my personal growth. And this is by far the most important thing which I obtained from the PhD journey.

If I have to talk about a journey, the first thing to do is to talk about its beginning. I still remember that 19th of December 2013, the day when I got the official contract from NTNU. That contract opened to me two possibilities: stay in the same place as I grew up and continue a life which could have been, to a certain extend, predictable. Or, I could just leave a *familiar* environment and jump into a new adventure, in a foreign country where I had never been before and where I knew nobody. Since you are holding this thesis in yours, you can easily guess that I chose the second option. It took probably few hours to take the decision. After more than three years I can tell that that decision has been the best one of my life so far!

The first person who I must thank for this great opportunity is my supervisor Professor Kristin Ytterstad Pettersen. First of all, I have to thank her because she believed in me the moment she chose me. Furthermore, she has been a great guide and mentor. Without her positive attitude I could never had completed this long path. I will never forget her support and help when I was visibly frustrated by things which were not working. Thanks to her, I achieved things that I thought unachievable at the beginning of this journey.

I would like to thank also my co-supervisor Professor Asgeir J. Sørensen for the time that he dedicated to me, for his inspiring talks at AMOS events and for his encouragement to share and discuss things with our colleagues. The warm and kind environment which he helped to create in AMOS was one of the things which I appreciated the most while working in this center of research.

I would also like to thank my former supervisor Professor Gianluca Antonelli from University of Cassino and Southern Latium. He was the person who helped me to find the open position at NTNU and he encouraged me to apply. Probably, if he had not encouraged me, I would have missed this great opportunity. Talking about my former university I have to thank also Professor Filippo Arrichiello. We started a cooperation about a year ago but time went by too fast to allow us to get to a concrete result. However, future is still ahead and we will see if we are able to get somewhere.

During these years I also had the opportunity and the fortune to work with many people who have been fundamental to obtain the results presented in this thesis. I am grateful for the opportunity to work with Professor Manfredi Maggiore from the University of Toronto. His scientific advice and insights were precious and motivating. The outcomes of our joint works represent some of the highest quality work included in this thesis. I will also remember our interesting and motivating talks outside the work environment.

Another vital cooperation who characterized this thesis is the one with Professor Erjen Lefeber from the University of Eindhoven. During my stay in Eindhoven we worked together for few weeks. It was not a long time but it was very intense. His patience and kindness were tremendously helpful to lift up some of my work. In those few weeks I learnt a lot from him.

I would like also to thank Professor João Sousa at the University of Porto for the opportunity to do experiments with the underwater vehicles of the Laboratório de Sistemas e Tecnologia Subaquática (LSTS). A special thanks goes to José Pinto and Maria Costa for their help to get ready the code and perform the experiments.

Another person who I will remember for our joint work is Mohamed Maghenem from L2S Supélec. It was a great pleasure to have the possibility to work with Mohamed. His incredible ability to dive into theoretical details, his passion and good spirit have been essential to get high quality work in a very short time.

I am grateful to have worked also with Antonio Adaldo from KTH. He came to visit our department and I had the opportunity and the pleasure to work with him. Unfortunately, we were not able to achieve the expected result by the time I started to write this thesis. However, I hope we will find the time to conclude our work.

Last autumn I had also the pleasure to work with Koen Goris from University of Eindhoven. He spent here the semester for an internship and I had the pleasure to be his *guide* during this period.

I would also like to thank all my colleagues at AMOS and the Department of Engineering Cybernetics. Our coffee breaks, parties and ski trips are all good memories and remarkable moments of my life in Trondheim. Listing everyone would take too long. But some people need to be explicitly mentioned here. I will start with Dennis and Albert. Dennis has been my office mate from my first day here in Trondheim up until he finished his PhD. We shared an office, many coffee breaks,

many beers, and we supported each other during the tough period as PhD students. When Asgeir Sørensen said "Your best supervisor may be your office mate" he must have been talking about Dennis. Especially during my first period, we had many discussions which were invaluable for my learning process. Albert is still sitting next door and since the day he arrived he brought that *South European flavor* which was missing during the first months I was here. The many discussions with Dennis and Albert have ranged from trivial jokes to the attempt to solve global problems. I believe that we still have not managed to fix the world. However, I hope that in the future we will find the time to give some more attempts to *World salvation*. I need also to mention Mikkel C. Nielsen, his presence in our coffee breaks has been, and it is still today, very relevant both to reach an high level of silliness and to have a genuine serious talk. Then I need to thank *my partner* in crime Andreas, Anna, Erlend, and Bård for great moments at and outside work.

I also had the fortune to meet many great people outside the work environment which turned out to be also great friends. I can start mentioning my flatmate Luca. It has been a great pleasure to share an apartment and good time with him. Our serious discussions and jokes at home were essential for my survival during the PhD life. I also need to thank Walter, who was one of the first persons who I met here in Trondheim. He was the one who introduced me to a part of the *Italian community* here in this city. I need to mention Luca A. and Maria, Giancarlo and Roberta, Nick and Sepideh, Eleni and Eirini for our great time together. I had great time with each one of you and with all of you together. Ski trips, walks in the woods, *simple* dinners, trips, cabin trips, beers, board games. Each single occasion was great. You all contributed to make my experience in Trondheim memorable.

When I decided to leave Italy, I also knew that some connections would have become weaker. Today I can tell that some of them have become such. But others, even though are characterized by a less frequent communication, do not need many words to be as strong as they were in the past. It is not really possible to list all of them here, but I will have to mention at least Simone and Giuseppe. Often, when I went back for vacation in my home village, we found the time for a beer or two. I hope we will keep this tradition.

Then I must thank my family, my father Bartolomeo, my mother Maria and my brother Riccardo. Their support, during my years while I was there with them and while I was here in Norway, has been constant and unconditioned. Sometimes it has not been easy for them to deal with me.

Least but not the last I need to mention Antonietta. She has been (and is) so close when we have been (and are) so far. Past and future become fuzzy and blurry when I want to describe her influence during these last years. It looks like that it has always been a *far* present with her.

Finally, I would like to thank the many people who consciously or unconsciously have influenced this long and exciting journey.

Claudio Paliotta, April 2017

I have only one regret... that I have not worked harder.

Frederick Henry Royce

Chapter 1

Introduction

This thesis deals with control problems for under-actuated marine vehicles. In particular, it mainly deals with control problems related to autonomous surface vehicles (ASVs) and autonomous underwater vehicles (AUVs). The control problems related to marine vehicles span a broad area in the field of control theory and marine systems. We decide to focus on a few of these problems, in particular:

- source-seeking for multi-vehicle systems;
- path following for a single vehicle;
- trajectory tracking for a single vehicle;
- synchronization control for multi-vehicle systems.

In this chapter we present the motivations and the contributions of this dissertation.

1.1 Background and motivation

In this section we first give a general introduction to the context of marine vehicles. We then present motivations and a general overview of the previous works on the topics dealt with in this thesis.

1.1.1 Modeling of marine vehicles

Autonomous vehicles have drawn the attention of researchers for the last decades. The use of autonomous vehicles is appealing for several real world applications. For instance, autonomous vehicles are particularly suitable for execution of tasks which are dull, hard or impossible to execute for humans. Furthermore, autonomous vehicles are interesting for different fields, and include unmanned vehicles for ground applications (unmanned ground vehicles (UGVs)), unmanned vehicles for aerial applications (unmanned aerial vehicles (UAVs)) and unmanned marine vehicles, that is, autonomous surface vehicles (ASVs) and autonomous underwater vehicles (AUVs). In each one of the aforementioned fields there are many examples of applications. We have autonomous cars which are leading towards profound changes in our concept of transportation [73, 74]. We have extensive use of UAVs for exploration, monitoring and surveillance tasks [35, 79, 127]. Also, autonomous vehicles

have a large potential in applications intended to execute tasks in areas which are inaccessible for humans, for instance space exploration [34, 60, 93], and Arctic [98] or deep water exploration [21, 121, 133].

Another advantage of using autonomous vehicles is that they do not require an operator to maneuver the system. Nevertheless, human operators are still involved in some supervision of the mission. In the context of marine vehicles this may allow savings in the costs of the operation. In fact, fully autonomous vehicles may require less or may not require personnel on a vessel supporting the operation at all. However, the absence of an operator who takes direct control of the vehicle requires the development of more sophisticated control strategies. Indeed, when there is not an operator taking care of the maneuvering of the system, the vehicle has to be able to counteract also the disturbances which may prevent it from fulfilling the assigned task. It is then clear that the development of control strategies requires the necessity of a mathematical model for the system and the disturbance. The type of model and its complexity depend on the particular task and the operation conditions. A possible classification of the models depending on the operational conditions, is between low velocity and high velocity models. The former is suitable for station keeping and dynamic positioning operations where the vehicle is required to remain in a fixed position. The latter is instead used for maneuvering tasks, such as path following [54]. Another important aspect of the model is its complexity. According to Sørensen [131] two main categories may be distinguished between in this sense. The first category is called control plant model. This includes models which are a simplified description of the system containing only the main physical properties of the plant. The control plant model is suitable for control design purposes and theoretical analysis. The second category is the process plant model, and it is a more complex mathematical model which includes a detailed description of the physical system. The process plant model is suitable for high fidelity simulation of the system.

In real applications, ASVs and AUVs may be deployed in order to perform independent tasks or tasks which require cooperation or coordination among the vehicles. In the former case it is important to deal with control strategies which concern a single vehicle and the control feedback depends only on the information available to the vehicle. Instead, in the latter case a high level control which takes care of the coordination among the vehicles, has to be carefully studied and analyzed. In this case, the control strategy requires also an exchange of information among the vehicles in the network.

1.1.2 Source-seeking with multi-vehicle systems

Part I of this thesis concerns the source-seeking problem for marine vehicles.

The source-seeking task deals with the localization of the source of a specific signal. From a mathematical point of view, we call source the position of the maximum (or the minimum) of a function $f(x)$, which describes the scalar field associated with the signal distribution, and where $x \in \mathbb{R}^2$ gives a specific position in space. From a practical point of view, the source can, for instance, be seen as an area in which there is a high concentration of a specific chemical substance or a thermal source.

The source-seeking task may be performed using static or moving agents. In the first case a number of static sensors collect and exchange information in order to identify the location of the source. In the second case a group of mobile agents is equipped with sensors. Each agent can detect scalar measurements of the signal distribution and can exchange information with the rest of the group. The vehicles then use the shared information in order to move towards and reach the source. In this thesis we investigate this second case.

The advantage of using multi-agent systems lies in the fact that having several vehicles allows spacial distributed measurements which can be used in order to determine the position of the source. There are several methods in order to exploit the measurements of the agents. The two most common methods are: gradient based approaches [11, 53, 136, 137, 141, 142] and extremum-seeking [17, 59, 78]. The gradient based approaches are based on the approximation of the gradient of the signal distribution using spacially diffused measurements from the agents [11, 53, 136, 137, 141, 142]. The mobile agents then move to climb the gradient. It is clear that gradient based methods require that the source exists and is unique. The extremum-seeking method also relies on the approximated gradient computation. However, the gradient is approximated by one or several vehicles probing the field, usually with a sinusoidal or a dither motion [17, 59, 78, 139]. In this dissertation we use a gradient based method since we want to exploit the spacial covering of the multi-vehicle system without requiring dither motions of each agent.

When dealing with a multi-agent system, an important aspect of the network is the hierarchy among the agents. We may have leader-follower schemes, where the leader is an agent able to influence the states of the other agents, the followers. There are also leaderless networks where the agents all have the same capabilities and influence each other equally according to a specific communication scheme. Examples of leader-follower networks are [17, 90, 141, 142]. The works [11, 63, 136, 137] deal instead with leaderless networks. In this work we focus on the leader-follower approach.

One of the first studies of this scheme is given in [132]. In [132], the author deals with a group of agents in which the leader is able to control the states of the other agents. The communication among the agents is characterized by a fixed topology graph. Necessary conditions on the structure of the communication graph are given under which the states of the followers are controllable by the leader. Further investigation about the connection between controllability of the leader-follower networks and the topology of the communication scheme is given in [70, 101, 119]. Other authors have focused on the controllability of the leader-follower scheme considering a switching topology graph for communication [69, 95]. In particular, the seminal work [69] gives a thorough analysis of the stability of a network of agents with and without a leader. It is assumed that over a certain interval of time the neighbors of the i -th agent change. Necessary conditions on the connectivity of the agents' graph over time are given to achieve an agreement among the agents. In the case of the leader-follower scheme the followers agree to follow the leader's heading.

Source-seeking tasks can be performed with the leader-follower scheme [17, 53, 105, 141] and with the leaderless scheme [63, 136, 137]. The work [17] deals with a source-seeking mission using the extremum-seeking method. The multi-

agent system is characterized by a leader which is able to get scalar measurements from the field. In order to get distributed measurements, it moves due to a dither motion to compute the approximated gradient. The followers keep an assigned formation around the leader. Their relative position is controlled by a passivity based control law. This controller guarantees that the followers move behind the leader, filtering its dither motion while reaching the source. In [53, 105], a group of fully-actuated agents are used to perform source-seeking using scalar measurements from each agent. In particular, some virtual leaders are used to achieve a prescribed formation using artificial potentials. Each real agent takes scalar measurements that are used to compute the gradient of the environment. A Kalman filter is used to improve the quality of the gradient estimate. Asymptotic convergence to a region that contains local minima is proved. In [141], a source-seeking guidance law for UAVs agents based on a leader-follower scheme is studied. The followers constantly move on a circular trajectory around the leader. Only the followers are able to get scalar measurements from the field. The leader receives the measurements from the followers and uses them to compute the approximated gradient in order to move towards the source. It is necessary that each follower communicates with the leader during the motion. Asymptotic convergence towards the source is proved. The work [105] describes source-seeking performed using a leaderless multi-agent system. The control law of the mission is decoupled to perform formation control and the source-seeking. The motion in formation is achieved using artificial potentials. For the source-seeking, each agent gets scalar measurements and shares it with a central computer. The computer computes the gradient of the field and gives back information to the agents to reach the source. The work [137] presents a source-seeking method for leaderless multi-agent systems not based on the explicit gradient estimation. In particular, the velocity of each agent is decoupled in two parts. The first part is proportional to the scalar measurements from the field. The second part is used for controlling the relative position of the agents. This method is in accordance with the behavior of schools of fish. Convergence to the source while maintaining a certain formation is ensured. The work [136] extends the results to the 3D case.

1.1.3 Trajectory tracking, path following and multi-agent systems

The trajectory tracking problem, the path following problem and the formation control problem are three common problems in the field of marine vehicles. In fact, trajectory tracking and path following tasks are crucial for exploration and surveillance missions, sea-bed scanning and pipeline inspection tasks [121]. Formation control becomes relevant when we want to use multi-vehicle systems in order to explore or monitor larger areas in a shorter time. Indeed, one of the advantages of using multi-agent systems lies in the fact that they offer larger spacial coverage.

Marine vehicles, both ASVs and AUVs, generally operate in challenging operational conditions. In fact, ocean currents and environmental disturbances, generally referred to as sea loads [52], may seriously influence the success of a mission. Furthermore, ASVs and AUVs are generally under-actuated vehicles, i.e., the number of independent control inputs is less than the degrees of freedom in the configura-

tion space. This characteristic is due to common design rules. In fact, commercial marine vehicles are often equipped just with fixed stern propellers and a steering rudder, or with two azimuth propellers. Sometimes they also have tunnel thrusters for lateral motion during docking, but such actuators work only at low speeds [75]. Consequently, the control design for this class of vehicles is challenging due to the absence of a direct actuation in the side direction (sway direction). The challenge is even bigger when environmental disturbances affect the system. At this point it is clear that due to their relevance for real applications and the challenges that characterize marine vehicles, trajectory tracking and path following tasks have drawn the attention of researchers over the years [1, 4, 5, 15, 19, 20, 31, 32, 41–44, 46, 55–57, 62, 71, 80, 87, 100, 103, 116, 117, 130, 135].

Trajectory tracking

The trajectory tracking control problem deals with the design of a controller which steers and stabilizes a vehicle to a geometric path that is parametrized by time, i.e., the vehicle has to follow a geometric path respecting a time constraint. Several works have dealt with this problem, proposing different approaches [1, 4, 5, 41, 62, 71, 87, 116, 117, 130]. Pettersen and Nijmeijer [116] presents one of the first solutions for the full-state stabilization of under-actuated marine vehicles. In particular, [116] gives a trajectory tracking controller for a simplified model of an ASV. The approach is based on the back-stepping and recursive technique given for systems in chained form studied in [72]. The result in [116] was further developed in [118], where some restrictions on the curvature were relaxed. Both [116, 118] do not consider the effect of environmental disturbances, which are dealt with in Pettersen and Nijmeijer [117].

The work [71] presents an approach using Lyapunov’s direct method to solve the trajectory tracking problem of ASVs. Two constructive solutions are proposed by application of Lyapunov’s direct method. Both the proposed controllers are developed exploiting the cascaded structure of the system. However, both the approaches require a persistently exiting (PE) yaw rate. The PE condition is a common feature with the works [116–118] mentioned above.

Do et al. [46] present a result which does not need the PE condition and it is based on a combination of the back-stepping and Lyapunov’s direct methods. However, [46], like [116–118], considers a simplified model of a ship. That is, the mass and damping matrices are assumed to be diagonal. This assumption is removed in Do and Pan [41], where mass and damping matrices with non-zero off diagonal elements are considered. Here a change of coordinates transforms the dynamics into a diagonal form and the same method as in [46] is applied. Nonlinear damping is considered in [45].

Sonnenburg and Woolsey [130] present two solutions for the trajectory tracking control problem for a riverine ASV. The authors first identify the parameters of a Nomoto model in order to describe the motion of the vehicle. Then this model is used for control purposes and two control laws are proposed. The first law is a proportional derivative controller, while the second is derived using the backstepping technique. The results are validated experimentally.

Aguiar et al. [4] presents an interesting approach based on an adaptive switching supervisory control law combined with a nonlinear Lyapunov-based tracking control law. The authors show convergence of the position tracking error to a neighborhood of the origin that can be made arbitrarily small.

Path following

The path following control problem differs from the trajectory tracking control problem because of the time constraints. That is, differently from the trajectory tracking control problem, the path following control problem does not impose any time constraint on the vehicle. The ASV or the AUV is just required to converge to and move along the path without any time constraint. In particular, the vehicle is not required to be at a specific location along the path at a specified time. The path following control problem for marine vehicles has been dealt with in many works [15, 18–20, 30, 32, 44, 45, 48, 50, 55–57, 80, 100, 103, 134, 135].

A well-known guidance control strategy for path following of straight-lines is the line-of-sight (LOS) guidance [19, 54, 56, 57]. The LOS guidance is based on the approach of experienced helmsmen who steer the vessel towards a point lying at a constant distance ahead of the ship along the desired path. Børhaug and Pettersen [18] provides a stability proof for the LOS guidance control using cascaded system theory. The closed-loop system is shown to be κ -exponentially stable and the zero dynamics are carefully studied and proven to be well-behaved. However, [18] does not consider the effect of environmental disturbances. This case is considered in Børhaug et al. [19] where an integral action is added to the LOS guidance. A stability analysis is provided and uniform global asymptotic stability of the closed-loop system is shown. In Caharija et al. [32] the work of Børhaug et al. [19] is revisited. Caharija et al. [32] considers a model based on relative velocities. This approach simplifies the control design and analysis. Wiig et al. [134] proves that the integral-LOS (ILOS) control system is semi-globally exponentially stable. In Fossen et al. [56], the LOS guidance strategy is used together with a switching algorithm in order to make the vehicle move along a piece-wise continuous path, i.e., a path made of segments connecting several way-points. This approach was further developed in Breivik and Fossen [24] for circular paths. However, both [24, 56] do not consider disturbances.

One of the first scientific contributions for path following of marine vehicles for curved-paths is Encarnação et al. [50]. Encarnação et al. [50] applies the approach developed in Micaelli and Samson [102] for unicycles together with an observer in order to compensate for constant disturbances. This approach has some limitations since it is based on a parametrization of the path which is valid only locally. Furthermore, it assumes a constant total velocity, which requires an active and not practical control of the forward speed in order to compensate for variation in the sway velocity induced by the curved motion. This approach has been further developed by Lapierre and Soetanto [80], Lapierre et al. [81]. In fact, [80, 81] present a solution which is based on a globally valid parametrization of the path. This is achieved by proposing a new parametrization of the path where the time update of the parameter s which defines the path, is left as an extra degree of freedom for control purposes. However, [80, 81] do not consider environmental disturbances.

Moe et al. [103] uses the same relative velocity model as in [32]. Then, using the same parametrization as in [80, 81] together with an observer, proposes a control law valid for curved-paths in presence of constant ocean currents.

Multi-agent systems

The works discussed above are all about the trajectory tracking and path following control problem for a single vehicle. However, it is relevant to deal with trajectory tracking and path following control of multi-ASV and multi-AUV systems. In fact, the use of marine vehicles is costly due to the necessity of vessels and personnel supporting off-shore missions. Deploying more vehicles simultaneously implies shorter time for completing the task and consequently cost saving. From a more theoretical point of view, the design of formation control strategies for multi-vehicle systems may be reduced to the the consensus or synchronization problem. That is, all the agents should synchronize their outputs to a common signal. The synchronization control problem for generic multi-agent systems has drawn a lot of attention in the last decades [6, 40, 92, 92, 94, 96, 120, 126, 140]. It may be divided into two different cases, i.e., leaderless synchronization (or the consensus problem) and leader-follower synchronization (or consensus with a leader). In the former case, the agents should synchronize to a common value which depends on the initial states of the system [6, 92, 94, 96, 120, 126]. In general, the final common value reached by the states of each agent cannot be chosen freely, but it is determined by the initial states of the agents. In the leader-follower case we have a group of agents, generally addressed as followers, which have to synchronize their states to the states of a certain agent in the network, the leader agent [40, 92, 140]. Generally, in the leader-follower case, it is assumed that it is possible to assign a desired trajectory to the leader's states. Therefore, this allows the followers' states to be steered to a desired trajectory. For instance, Zhang et al. [140] considers the synchronization problem for a group of identical linear agents. The communication graph is considered directed but it has to contain a spanning tree, that is, there must be at least one agent which can communicate, directly or indirectly, with all the others. A diffusive coupling law which makes the agents synchronize to the reference trajectory of a leader agent is presented. However, [140] does not consider the presence of disturbances affecting the systems. Ding [40] presents a solution for the synchronization problem for a network of linear agents, with or without leader and with the agents affected by disturbances. In particular, the approach in [40] is based on a disturbance observer. The method is suitable for matched disturbances and in general requires some pre-knowledge about the exosystem generating the disturbance. Li et al. [92] gives an H_∞ controller for agent synchronization to a desired reference signal. The controller makes a group of agents interconnected by an undirected graph synchronize to a desired reference signal while rejecting exogenous disturbances.

All the works discussed above considering multi-agent synchronization deal with linear systems. We have already mentioned that the dynamical model of ASVs and AUVs is nonlinear. This implies that all the results mentioned above cannot be directly applied for the synchronization or the coordination control of multi-ASV or multi-AUV systems. In addition, ASVs and AUVs are generally under-actuated.

The problem of multi-vehicle coordination in the context of marine systems has been dealt with in [8, 9, 12, 13, 19, 22, 26, 29, 30, 49, 51, 64–67, 129]. Børhaug et al. [19] tackles the problem of the formation control of under-actuated marine vehicles using a coordinated path following approach. That is, each vehicle has to reach its own path. Once each vehicle reaches its own path, the formation is reached by regulating the along path distance among the vehicles. However, [19] does not consider the effect of disturbances affecting the system. The approach in [19] is then revisited in [12, 13] where the effect of constant irrotational ocean currents is taken into account. Encarnação and Pascoal [49] considers the formation control problem for under-actuated marine vehicles using a leader-follower approach. In particular, a follower vehicle is controlled in order to follow the leader vehicle, keeping a given distance. However, [49] does not consider the effect of ocean currents. Skjetne et al. [129] tackles the problem of formation control for fully-actuated marine vehicles using a virtual structure approach and a backstepping control design. That is, a virtual point moving in the space is defined for each vehicle. Each vehicle is then required to converge to the assigned point and move along with it. When all the vehicles have reached their virtual points, motion in formation is obtained. Skjetne et al. [129] considers the presence of a constant ocean current. Arrichiello et al. [9] uses the Null-Space-Based behavioral control (NSB) approach for solving the formation control problem for a fleet of marine vehicles. The NSB approach is a behavior-based approach. That is, several behaviors are assigned to the agents and the resulting motion is a weighted average of the single behaviors. In [9], the vehicles are required to move in formation and avoid obstacles which may eventually be present in the environment. Under-actuated vehicles are considered, but the presence of environmental disturbances is not taken into account. Ihle et al. [67] combines a path following approach and a coordination law for solving the formation control problem for fully-actuated marine vehicles. The closed-loop system is shown to have passive properties.

1.2 Thesis outline and scientific contributions

This dissertation is divided into three main parts:

1. Source-seeking with multi-vehicle systems: consists of Chapters 3-4;
2. Control of ASVs and AUVs using the hand position point approach: consists of Chapters 5-7;
3. Path following for ASVs and AUVs: consists of Chapters 8-11.

Parts I, II and III are further discussed in the two following subsections.

1.2.1 Source-seeking with multi-vehicle systems

Part I of the thesis deals with the source-seeking problem for marine vehicles. It consists of Chapters 3-4. The content and the scientific contribution of each chapter is discussed separately.

Chapter 3

In this chapter we consider the source-seeking problem using under-actuated vehicles organized in a leader-follower scheme. Here the agents are modeled as kinematic unicycles. We revise the controlled agreement protocol scheme [119, 132] with the addition of a variable leader in order to shift the agreement. Our approach is inspired by the biological model for the migration of birds presented in Couzin et al. [37] and studied in Leonard [88] and Pais and Leonard [106]. According to [37, 88, 106], during the migration, flocks of birds are characterized by leaders and followers. Over generations leaders and followers change according to the so called fitness parameter. Leonard [88], Pais and Leonard [106] study the dynamics of the change of the leadership in the flock of birds over the generations. The role as leader is taken by the most skilled animals, that is, the ones with the best capabilities in detecting the best direction for the migration.

The main scientific contribution of this chapter is inspired by the migration model for flocks of birds. A revised control consensus protocol with a variable leader is applied to the source-seeking problem for multi-agent systems. The main difference in this work compared to previous works is that in our model the leadership is exchanged according to the environment conditions, i.e. the proximity to the source. In particular, the agents move along a definite direction assigned to the initial leader, but if during the motion one of the agents detects a source, they deviate from the initial direction. The sensing agent would then take on the role as leader and would compute a new direction that points towards the source. Being the new leader, it imposes the new direction of motion to the rest of the agents. Which is the current leader, depends on the current value of the investment parameter. This feature makes sure that the group follows the agent that has the best information available about the source they are seeking, and is expected to provide more efficient source-seeking operations.

Chapter 4

In this chapter we consider the source-seeking problem using a multi-agent systems consisting of under-actuated ASVs. The main contribution of this chapter is a method to achieve source-seeking tasks using a multi-agent system without a priori assuming that there is a source in the field. Whereas in the literature the field is often a priori assumed to contain a source. Consequently, it is common practice to compute the heading based only on information from the source regardless of the signal's strength. While in this work an initial path to follow is given to the agents in order to explore a given area. Then, if a source is present in the explored area and the signal from the source is strong enough, i.e. exceeds a given threshold, the group of vehicles will leave the initial path and will move towards the source. The autonomy of the agents is increased because no matter if a source is present or not, the agents can always choose a path to follow and this is in accordance with the best available information from the field. Furthermore, it is shown that the presented source-seeking strategy can easily be integrated with a leader-follower synchronization based formation control strategy for ASVs or AUVs moving in the horizontal plane.

1.2.2 Control of ASVs and AUVs using the hand position point approach

Part II of the thesis deals with the trajectory tracking control problem, the path following control problem and the synchronization control problem for marine vehicles. It consists of Chapter 5-7.

The chapters presented in Part II are based on a different approach to the control problem of trajectory tracking and path following of marine vehicles. In fact, all the works discussed in Section 1.1 have in common that the vehicle has to track a trajectory or follow a path with respect to the center of mass or the pivot point. The latter is a point on the center-line of the vehicle such that its lateral motion (sway motion) is not affected by any of the control inputs. We propose a different approach. We extend the definition of *hand position*, which has been used for ground vehicles in [82, 122], to marine vehicles. The definition of the *hand position* is further discussed in Chapters 5-7, but briefly described it is a point lying along the center-line of the vehicle ahead of the pivot point. Choosing the hand position motion as the output of our system and using an input-output feedback linearizing controller, we perform a change of inputs to our system, which, as typical for feedback-linearized systems, leads to an external dynamics which is linear, and in particular to a double integrator. The advantage of this approach lies in the fact that now we have to deal with a linear system for control purposes.

The content and the contribution of each chapter of Part II is discussed separately in the following.

Chapter 5

In this chapter we consider the model of an ASV or an AUV moving in the horizontal plane, affected by an environmental disturbance, i.e., an unknown constant ocean current. We address the problem of trajectory tracking for straight-line and curved paths. The proposed control strategy is based on the definition of the *hand position* point and an input-output feedback linearizing controller. We present a change of coordinates which is not standard for the input-output feedback linearizing approach. This particular choice for the new set of coordinates allows us to obtain a transformed model where the ocean current affects the system at the level of the linear external dynamics and can be counteracted with a simple integral action. The drawback of this approach is that we obtain a nonlinear internal dynamics which is affected by the input of the external dynamics. Therefore, attention has to be paid to the analysis of the states of the internal dynamics in order to check that they are well-behaved. We show that the integral state is able to give an estimate of the ocean current. We prove that our output, i.e., the *hand position* point, converges to the desired trajectory globally exponentially while the states of the internal dynamics are ultimately bounded. We also show that for the case of straight-line trajectories we have *almost-global asymptotic stability* (AGAS) of the closed-loop system. Finally, the theoretical results are validated by a simulation case study.

Chapter 6

This chapter considers the path following control problem for ASVs and AUVs moving in the horizontal plane. The effect of unknown ocean currents is also taken into account. The path following control problem is tackled using the same approach as in Chapter 5. That is, the hand position point is defined as the output of the system. An input-output feedback linearizing controller is then used in order to obtain a transformed model which is more suitable for control design purposes. We use the same change of coordinates as in Chapter 5. Consequently, we obtain the same advantage as in Chapter 5, i.e., a linear external dynamics which facilitates the control design phase. However, we have the same downside as in Chapter 5, i.e., a nonlinear internal dynamics affected by the input of the external dynamics. We consider parametrized paths, i.e., paths in which each point along the path is uniquely defined by an along path variable s . The path variable is used to propagate a virtual path-tangential frame with respect to which the path following errors are defined. The propagation of the path-tangential frame depends on a time update law for the path variable s . We design the time update law for s dependent on the Euclidean distance of the vehicle from the path-tangential frame. The *hand position* point is proven to converge to the desired path globally exponentially while the states of the internal dynamics are ultimately bounded. The case of parametrized and unparametrized straight-line paths is considered. It is shown that in this case the closed-loop systems is AGAS. A simulation case study validates the theoretical results. Furthermore, the case of unparametrized paths is validated with experimental results.

Chapter 7

In Chapters 5 and 6 we have applied an input-output feedback linearizing controller using the hand position point as output. We have obtained a linear external dynamics and a nonlinear internal dynamics. A major motivation for transforming the system into this form has been to be able to develop synchronization control schemes for multi-vehicle systems consisting of under-actuated marine vehicles. In particular, having a linear external dynamics facilitates the control design phase, and also represents an advantage for designing synchronization control strategies.

Motivated by this and by leader-follower synchronization results in [126] and [140], we propose a diffusive coupling law for leader-follower synchronization of linear systems. In particular, we design a distributed controller for leader-follower synchronization based on the one given in [140]. We add integral action in the control law for each agent inspired by the distributed control in [126] for leaderless synchronization. The integral action is introduced in order to reject the effect of the constant unknown disturbance. The leader agent in the network may be real or virtual. With respect to [140], we relax the condition that the leader is an unforced linear time-invariant (LTI) system. Instead we take into account that the leader may be an agent controlled independently of the followers. As regards the communication scheme, we consider the general case of directed communication among the agents and that the leader only needs to communicate with at least one follower. The diffusive coupling law designed for linear systems is then applied for

synchronization control of multi-ASV systems.

1.2.3 Path following for ASVs and AUVs

Part III consists of Chapters 8-11 and extensively deals with the path following control problem. Solutions for parametrized and unparametrized paths are considered. In Chapter 6, the path following control problem is dealt with considering the aforementioned hand position approach, i.e., applying a change of coordinates to the system in order to obtain a different model for control purposes. In Part III, the path following is instead considered using the standard nonlinear model of marine vehicles.

The content and the contribution of each chapter is discussed separately below.

1.2.4 Chapter 8

In this chapter the path following control problem of unparametrized straight-line paths is considered. The approach in this chapter is different from the one in Chapter 6 due to the choice of the output of the system. In fact, in Chapter 6, the path following control problem is addressed considering the hand position point as output. Instead, in this chapter, the vehicle is controlled with respect to the pivot point. Furthermore, the result in this chapter is limited to unparametrized straight-line paths, while the results in Chapter 6 holds for parametrized curved paths.

The main contribution of this chapter is a guidance law for ASVs and AUVs moving on the horizontal plane in presence of an ocean current with unknown direction and magnitude. We use an observer to estimate the current, such that we can use the estimates in the guidance law in order to counteract its disturbing effect. The method is based on geometric control considerations inspired by common control strategies used for UAVs, in particular quad-copters. Specifically, this work has been inspired by the control approach given in [84, 86]. We define a direction which points towards the path using the cross track error vector and the estimated ocean current vector. Then we make the vehicle align itself with this direction in order to converge to the path. We do not define an explicit desired yaw angle, but instead we use a feedback linearization controller based on an error function developed directly on the $SO(2)$ group [27]. Using cascaded systems theory we prove that the closed-loop system is *almost*-GAS. A simulation case study validates the theoretical results.

1.2.5 Chapter 9

This chapter considers path following of generic paths for under-actuated marine vessels in the presence of constant ocean currents. A line-of-sight guidance law, an ocean current observer, and a local parametrization of the path are used. For the path, we use the same parametrization as used in Samson [124] for mobile ground robots. We add an adaptation to the path parametrization in order to counteract the effect of the unknown ocean currents. This parametrization aims to keep the vessel on the normal of a path-tangential reference frame. However, this is only

possible when the ocean current is known, and therefore the adaptation to the parametrization includes a restoring term that assures that the vessel is brought back to the normal of the path-tangential reference frame once the estimate of the ocean current has converged. The strategy which we apply is similar to the one used in Do and Pan [44]. However, Do and Pan [44] considers a simplified model with diagonal mass and damping matrices. We consider non-diagonal mass and damping matrices and we consider also the presence of ocean currents. Furthermore, compared to Do and Pan [44], in this work the parametrization is adapted to include the effect of the unknown ocean current.

Note that the path following control strategy presented in this chapter differs by the one in Chapter 6 in the choice of the output. In fact, in Chapter 6 the vehicle is controlled with respect to the hand position point, while here with respect to the pivot point. Furthermore, the control approach in Chapter 9 is not limited only to straight-line paths like the one in Chapter 8.

A complete analysis of the sway velocity dynamics is given, taking into account the coupling between the total velocity and the sway velocity. The parametrization which we use is valid only locally around the curve. In particular, it is valid inside a tube around the curve whose dimensions depends on the maximum curvature of the path. It is then proven that the closed-loop system is exponentially stable when the vehicle is inside the tube.

1.2.6 Chapter 10

This chapter deals with the path following control problem for under-actuated marine vessels in the presence of constant ocean currents of generic paths. The approach is an extension of the one presented in Chapter 9. In fact, while the parametrization defined in Chapter 9 holds only locally, here we define a parametrization which holds globally, i.e., the initial error from the path can be arbitrarily large. The guidance law which is presented here is a line-of-sight like guidance where the look-ahead distance is adapted based on the path following errors. Also in this case we use an ocean current observer in order to estimate and compensate for the ocean current. The guidance law is an adaptation from Moe et al. [103], which considers the same problem. The closed-loop system is proven to be globally asymptotically stable under certain conditions for the look-ahead distance and the curvature of the path. The main difference compared with Moe et al. [103] is a different adaptation law and a different choice for the look-ahead distance which is necessary in order to prove stability of the zero dynamics, which were not analyzed in [103].

1.2.7 Chapter 11

In this chapter we present a solution to the path following control problem for unparametrized paths. That is, paths which are described by an implicit equation and not by a path variable, as common in all the works about curved paths discussed in Section 1.1.

The control strategy for path following presented in this chapter differs from all the other path following control approaches discussed in the previous chapters.

In fact, the results of Chapter 11 hold for unparametrized curved paths, while the previous chapters present either solutions for unparametrized straight-line paths or parametrized curved paths.

To the best of our knowledge, in the context of marine vessels, the problem of finding a smooth, static, and time invariant feedback solving the path following problem for unparametrized paths remains open. In this chapter, we present a first solution. The controller is based on geometric considerations and the control design follows from the hierarchical control method presented in [47]. Principles from adaptive control are also used in order to deal with the ocean current effect. Using the hierarchical control method, the closed-loop system is analyzed and proven to be asymptotically stable while the zero dynamics is proven to be well-behaved. We want to remark that this control approach to path following is a *pure* approach compared to the ones discussed in Chapters 6, 8, 9 and 10. In fact, in this approach the path is not parametrized and therefore there is no distinction among the points constituting the curve.

1.3 Publications

This section presents the list of publications related to the work in the rest of this thesis. The list includes publications in conferences and journals, and works which are published and others which are to be submitted.

Journal papers

- D. J. W. Belleter, M. Maghenem, C. Paliotta, and K. Y. Pettersen. Observer based path following for underactuated marine vessels in the presence of ocean currents: a global approach. *Submitted to IEEE Transactions on Control Systems and Technology*, 2017.
- C. Paliotta, E. Lefeber, K. Y. Pettersen, J. Pinto, M. Costa, and J. Sousa. Trajectory tracking and path following for under-actuated marine vehicles. *Submitted to IEEE Transactions on Control Systems and Technology*, 2017

1.3.1 Conference papers

- M. Maghenem, D. J. W. Belleter, C. Paliotta, and K. Y. Pettersen. Observer based path following for underactuated marine vessels in the presence of ocean currents: a local approach. In *IFAC World Congress*, Toulouse, France, 2017.
- C. Paliotta, E. Lefeber, and K. Y. Pettersen. Trajectory tracking of under-actuated marine vehicles. In *Proc. 45th IEEE Conference on Decision and Control*, Las Vegas, Nevada, USA, Dec. 2016.
- C. Paliotta and K. Y. Pettersen. Leader-follower synchronization with disturbance rejection. In *Proc. IEEE Multi-Conference on Systems and Control*, Buenos Aires, Argentina, Sep. 2016.
- D. J. W. Belleter, C. Paliotta, M. Maggiore, and K. Pettersen. Path following for underactuated marine vessels. In *Proc. 10th IFAC Symposium on Nonlinear Control Systems*, Monterey, CA, USA 2016.

- C. Paliotta and K. Y. Pettersen. Geometric path following with ocean current estimation for ASVs and AUVs. In *Proc. 2016 American Control Conference*, Boston, MA, USA, July 2016.
- C. Paliotta, D. J. W. Belleter, and K. Y. Pettersen. Adaptive source seeking with leader-follower formation control. *IFAC-PapersOnLine, Presented at: 10th IFAC Conference on Maneuvering and Control of Marine Crafts*, 2015.
- C. Paliotta and K. Y. Pettersen. Source seeking with a variable leader multi-agent fixed topology network. In *Proc. European Control Conference*, Linz, Austria, 2015.

Publications not part of this thesis

- E. Xidias, C. Paliotta, N. Aspragathos, and K. Y. Pettersen. Path planning for formation control of autonomous vehicles. In *Proc. 25th Conference on Robotics in Alpe-Adria-Danube Region (RAAD16)*, Belgrade, Serbia, 2016.

Chapter 2

Model and mathematical preliminaries

In this dissertation we deal with control problems related to under-actuated marine vehicles, in particular autonomous surface vehicles (ASVs) and autonomous underwater vehicles (AUVs). In this chapter the physical model describing the motion of ASVs and AUVs moving in the horizontal plane is given. The choice of the right model for the description of the motion of the vehicle is not an easy task. In fact, a model can be more or less accurate and therefore more or less complex. A trade-off between accuracy and complexity is needed in order to not overcomplicate the analysis and the control design. Therefore, in this chapter a general model for marine vehicles is first introduced. Then, several considerations are given in order to obtain a simplified model which is suitable for the applications described in this thesis.

2.1 The general model for marine vehicles

In this section we describe the general model for marine vehicles presented in [54].

When we want to describe the motion of a vehicle in a given environment we can start by defining an earth fixed reference frame which we call the global or inertial frame. The motion of the vehicle is analyzed with respect to the inertial frame. For the inertial frame we consider the North-East-Down (NED) convention to hold. That is, we have the x axis of the inertial frame pointing north, the y axis pointing east and the z axis pointing down towards the center of the Earth. We need also to consider a reference frame anchored to the vessel. We call the frame fixed with the vehicle the *body* or *local frame*. For the body frame we consider the x axis directed from stern to bow, the y axis directed to starboard and the z axis pointing from top to bottom. In this dissertation only the case of ASVs and AUVs moving in the horizontal plane is considered. Therefore, the model which is described in the following refers to marine vehicles with 3 degrees of freedom (DOF) and moving in the $x - y$ plane of the NED frame. Note that we consider AUVs moving in the horizontal plane and therefore we do not consider the vertical model of the vehicle. From [54] we have that the equations of motion for ASVs and

AUVs are

$$\dot{\eta} = \mathbf{R}(\psi) \boldsymbol{\nu} \quad (2.1a)$$

$$\mathbf{M}_{RB} \dot{\boldsymbol{\nu}} + \mathbf{C}_{RB}(\boldsymbol{\nu}) \boldsymbol{\nu} + \mathbf{M}_A \dot{\boldsymbol{\nu}} + \mathbf{C}_A(\boldsymbol{\nu}_r) \boldsymbol{\nu}_r + \mathbf{D}(\boldsymbol{\nu}_r) \boldsymbol{\nu}_r = \mathbf{B} \mathbf{f} + \boldsymbol{\tau}_w. \quad (2.1b)$$

The vector $\boldsymbol{\eta} = [x, y, \psi]^T \in \mathbb{R}^3$ where the pair x, y gives the position in the NED frame of the vehicle and ψ , called the yaw angle, gives the orientation. The angle ψ is the angle between the x axis of the NED frame and the x axis of the body frame. The vector $\boldsymbol{\nu} = [u, v, r]^T \in \mathbb{R}^3$ gives the velocity of the vehicle expressed in the body frame, where u is the surge velocity, v the sway velocity and r the yaw rate. Then $\boldsymbol{\nu}_r = \boldsymbol{\nu} - \boldsymbol{\nu}_c$ where $\boldsymbol{\nu}_c = [u_c, v_c, r_c]^T \in \mathbb{R}^3$ is the velocity of the ocean current expressed in the body frame. An illustration of the vehicle's states is given in Figure 2.1. The matrix $\mathbf{B} \in \mathbb{R}^{n \times m}$ is the input configuration matrix, where $n = 3$ is the number of DOF of the system and m is the number of independent inputs to the system. The vector $\mathbf{f} \in \mathbb{R}^m$ is represents the control input in the body frame. Note that when $m < n = 3$ the vehicle is under-actuated, that is, the available number of independent control inputs is smaller than the number of DOF of the system. The vector $\boldsymbol{\tau} = \boldsymbol{\tau}_{wind} + \boldsymbol{\tau}_{wave}$ gives the effect of wind and wave induced forces. Note that $\boldsymbol{\nu}_c, \boldsymbol{\tau}_{wind}, \boldsymbol{\tau}_{wave}$ describe all the environmental disturbances. In this dissertation we consider only the effect of ocean current $\boldsymbol{\nu}_c$ affecting the system and assume that $\boldsymbol{\tau}_{wind} = \boldsymbol{\tau}_{wave} = \mathbf{0}$. The matrix $\mathbf{R}(\psi) \in SO(3)$, where

$$SO(3) = \{\mathbf{R} | \mathbf{R} \in \mathbb{R}^{3 \times 3}, \mathbf{R} \mathbf{R}^T = \mathbf{R}^T \mathbf{R} = \mathbf{I} \wedge \det \mathbf{R} = 1\}.$$

In particular, we have

$$\mathbf{R}(\psi) = \begin{bmatrix} \cos(\psi) & -\sin(\psi) & 0 \\ \sin(\psi) & \cos(\psi) & 0 \\ 0 & 0 & 1 \end{bmatrix}. \quad (2.2)$$

The matrices $\mathbf{M}_{RB} = \mathbf{M}_{RB}^T > 0$ and $\mathbf{C}_{RB}(\boldsymbol{\nu})$ are the rigid body inertia matrix and Coriolis and centripetal matrix, respectively. Then $\mathbf{M}_A = \mathbf{M}_A^T > 0$ and $\mathbf{C}_A(\boldsymbol{\nu})$ are the added mass and added Coriolis and centripetal matrix, respectively. Finally, $\mathbf{D}(\boldsymbol{\nu})$ is the hydrodynamics damping matrix.

2.2 The relative velocity model

In this section we start from the model (2.1) and derive a simpler model which is suitable for the control applications which we deal with in this work.

In this thesis only the presence of constant and irrotational ocean currents is considered. This implies that the ocean current vector expressed in the body frame is $\boldsymbol{\nu}_c = [u_c, v_c, 0]^T$. At this point we can rewrite the model (2.1) in a more convenient form to incorporate the ocean current effect. We can rewrite the ocean current vector in the global frame as

$$\mathbf{V} = \mathbf{R}(\psi) \boldsymbol{\nu}_c \quad (2.3)$$

where $\mathbf{V} = [V_x, V_y, 0]^T \in \mathbb{R}^3$. In [54], it is shown that

$$\mathbf{M}_{RB} \dot{\boldsymbol{\nu}} + \mathbf{C}_{RB}(\boldsymbol{\nu}) \boldsymbol{\nu} = \mathbf{M}_{RB} \dot{\boldsymbol{\nu}}_r + \mathbf{C}_{RB}(\boldsymbol{\nu}_r) \boldsymbol{\nu}_r \quad (2.4)$$

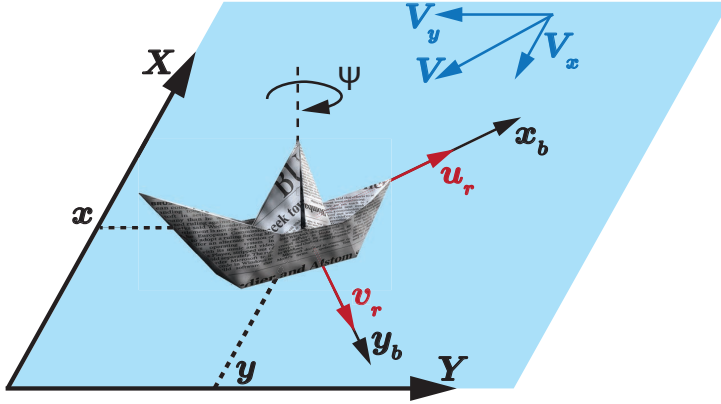


Figure 2.1: Vehicle's states.

Therefore using (2.3) and (2.4) we can rewrite (2.1) as:

$$\dot{\eta} = \mathbf{R}(\psi)\boldsymbol{\nu}_r + \mathbf{V} \quad (2.5a)$$

$$\mathbf{M}\dot{\boldsymbol{\nu}}_r + \mathbf{C}(\boldsymbol{\nu}_r) + \mathbf{D}(\boldsymbol{\nu}_r)\boldsymbol{\nu}_r = \mathbf{B}\mathbf{f}. \quad (2.5b)$$

We have that $\mathbf{M} \triangleq \mathbf{M}_{RB} + \mathbf{M}_A$ and $\mathbf{C}(\boldsymbol{\nu}_r) = \mathbf{C}_{RB}(\boldsymbol{\nu}_r) + \mathbf{C}_A(\boldsymbol{\nu}_r)$. Note that it holds that $\mathbf{M} = \mathbf{M}^T > 0$. The model (2.5) presents the effect of constant and irrotational ocean currents as a kinematic drift. Note also that (2.5) is function only of the relative velocities $\boldsymbol{\nu}_r$. Therefore, during the control design phase we decide to control the state $\boldsymbol{\nu}_r$. This gives a direct control on the direct energy consumption of the vehicle since the hydrodynamics damping depends on $\boldsymbol{\nu}_r$ [31].

Now some assumptions which are supposed to hold for the system, are given. First, we consider the following assumption to hold:

Assumption 2.1. *The vehicle is port-starboard symmetric.*

This assumption holds for the largest part of marine vehicles available on the market. Furthermore, according to Assumption 2.1, the mass matrix \mathbf{M} and the Coriolis matrix $\mathbf{C}(\boldsymbol{\nu}_r)$ have the following structure

$$\mathbf{M} \triangleq \begin{bmatrix} m_{11} & 0 & 0 \\ 0 & m_{22} & m_{23} \\ 0 & m_{32} & m_{33} \end{bmatrix}, \quad \mathbf{C} \triangleq \begin{bmatrix} 0 & 0 & -m_{22}v_r - m_{23}r \\ 0 & 0 & m_{11}u_r \\ m_{22}v_r + m_{23}r & -m_{11}u_r & 0 \end{bmatrix}.$$

It is also assumed that the following assumption holds

Assumption 2.2. *The hydrodynamic damping is linear.*

Remark 2.1. *The nonlinear damping term is not considered to not increase the complexity of the controller. However, due to the passive nature of the damping forces, the stability of the vehicle should still be enforced in case of nonlinear damping.*

According to this Assumption 2.1-2.2 the damping matrix is independent on ν_r , i.e. has constant entries, and has the following structure

$$\mathbf{D} \triangleq \begin{bmatrix} d_{11} & 0 & 0 \\ 0 & d_{22} & d_{23} \\ 0 & d_{32} & d_{33} \end{bmatrix}. \quad (2.6)$$

This dissertation mainly focuses on under-actuated vehicles, that is, vehicles which are characterized by $\mathbf{f} \in \mathbb{R}^m, m < n = 3$. This characteristic implies that the number of independent control inputs which are available for controlling the vehicle is smaller than the number of degrees of freedom. Most marine vehicles available on the market are under-actuated with respect to the sway direction when moving at speeds which are higher than $1 - 2$ [m/s] [22]. Therefore, this is the case which we consider. Then we have $\mathbf{f} = [f_u, f_r]^T \in \mathbb{R}^2$, where f_u is the surge thrust input and f_r is the rudder angle. The matrix \mathbf{B} thus has the following structure

$$\mathbf{B} \triangleq \begin{bmatrix} b_{11} & 0 \\ 0 & b_{22} \\ 0 & b_{32} \end{bmatrix}.$$

Note that generally the term $b_{22} \neq 0$, implying that an input from the rudder, f_r , has an effect also along the sway direction. In order to make the stability properties of the sway easier to analyze, we can perform a change of coordinates which leads to a system in which there is no indirect effect of the control inputs f_u, f_r in the sway direction. We follow the same approach as in Fredriksen and Pettersen [57]. We start by defining the distance ϵ as

$$\epsilon = -\frac{m_{33}b_{22} - m_{23}b_{32}}{m_{22}b_{32} - m_{23}b_{22}}.$$

The distance ϵ is such that the body fixed frame is moved to the so called *pivot point*. An important characteristic of the pivot point is that the sway dynamics is decoupled from the rudder input. Note that ϵ is well defined as long as the vehicle is controllable in yaw. The transformation proposed in [57] is

$$\bar{u}_r = u_r, \quad \bar{v}_r = v_r + \epsilon r, \quad \bar{r} = r \quad (2.7)$$

This transformation corresponds to moving the body fixed frame along the center line of the vehicle for a distance ϵ . Therefore defining

$$\mathbf{H} \triangleq \begin{bmatrix} 1 & 0 & 0 \\ 0 & 1 & -\epsilon \\ 0 & 0 & 1 \end{bmatrix}. \quad (2.8)$$

the equation of motion (2.5) can be transformed as described in [54] and we obtain

$$\dot{\boldsymbol{\eta}} = \mathbf{R}(\psi)\boldsymbol{\nu}_r + \mathbf{V} \quad (2.9a)$$

$$\mathbf{M}^P \dot{\boldsymbol{\nu}}_r + \mathbf{C}^P(\boldsymbol{\nu}_r) + \mathbf{D}^P(\boldsymbol{\nu}_r)\boldsymbol{\nu}_r = \mathbf{B}^P \mathbf{f} \quad (2.9b)$$

where $\mathbf{M}^P \triangleq \mathbf{H}^T \mathbf{M} \mathbf{H}$, $\mathbf{C}^P(\mathbf{v}_r) \triangleq \mathbf{H}^T \mathbf{C}(\mathbf{v}_r) \mathbf{H}$, $\mathbf{D}^P \triangleq \mathbf{H}^T \mathbf{D} \mathbf{H}$, $\mathbf{B}^P \triangleq \mathbf{H}^T \mathbf{B} \mathbf{H}$. Now, it can be verified that

$$(\mathbf{M})^{-1} \mathbf{B}^P \mathbf{f} = \begin{bmatrix} \frac{b_{11}}{m_{11}} f_u \\ 0 \\ \frac{m_{22}b_{32} - m_{23}b_{22}}{m_{22}m_{33} - m_{23}^2} f_r \end{bmatrix} \quad (2.10)$$

and it is clear that the yaw rudder control is not affecting the sway dynamics of the pivot point.

At this point, defining $(\mathbf{M})^{-1} \mathbf{B}^P \mathbf{f} = \boldsymbol{\tau} = [\tau_u, 0, \tau_r]^T$, we can write (2.9) in component form as

$$\dot{x} = u_r \cos(\psi) - v_r \sin(\psi) + V_x \quad (2.11a)$$

$$\dot{y} = u_r \sin(\psi) + v_r \cos(\psi) + V_y \quad (2.11b)$$

$$\dot{\psi} = r \quad (2.11c)$$

$$\dot{u}_r = F_{u_r}(v_r) + \tau_u \quad (2.11d)$$

$$\dot{v}_r = X(u_r)r + Y(u_r)v_r \quad (2.11e)$$

$$\dot{r} = F_r(u_r, v_r, r) + \tau_r. \quad (2.11f)$$

The expressions for $F_{u_r}(v_r)$, $X(u_r)$, $Y(u_r)$, $F_r(u_r, v_r, r)$ are

$$F_{u_r}(v_r, r) \triangleq \frac{1}{m_{11}}(m_{22}v_r + m_{23}r)r - \frac{d_{11}}{m_{11}}u_r, \quad (2.12a)$$

$$X(u_r) \triangleq -X_1u_r + X_2, \quad (2.12b)$$

$$Y(u_r) \triangleq -Y_1u_r - Y_2, \quad (2.12c)$$

$$F_r(u_r, v_r, r) \triangleq \frac{m_{23}d_{22} - m_{22}(d_{32} + (m_{22} - m_{11})u_r)}{m_{22}m_{33} - m_{23}^2}v_r \quad (2.12d)$$

$$+ \frac{m_{23}(d_{23} + m_{11}u_r) - m_{22}(d_{33} + m_{23}u_r)}{m_{22}m_{33} - m_{23}^2}r \quad (2.12e)$$

and

$$X_1(\mathbf{M}) \triangleq \frac{m_{11}m_{33} - m_{23}^2}{m_{22}m_{33} - m_{23}^2} \quad X_2(\mathbf{M}, \mathbf{D}) \triangleq \frac{d_{33}m_{23} - d_{23}m_{33}}{m_{22}m_{33} - m_{23}^2} \quad (2.13)$$

$$Y_1(\mathbf{M}) \triangleq \frac{(m_{11} - m_{22})m_{23}}{m_{22}m_{33} - m_{23}^2} \quad Y_2(\mathbf{M}, \mathbf{D}) \triangleq \frac{d_{22}m_{33} - d_{32}m_{23}}{m_{22}m_{33} - m_{23}^2}. \quad (2.14)$$

The functions $Y(u_r)$, $X(u_r)$ are both linear in u_r and for $Y(u_r)$ the following assumption holds

Assumption 2.3. *The following bounds hold on Y_1, Y_2*

$$Y_1 > 0, \quad Y_2 > 0. \quad (2.15)$$

This clearly implies

$$Y(u_r) \leq -Y^{\min} < 0, \forall u_r \in [\underline{u}, \bar{u}]$$

where $0 < \underline{u} < \bar{u}$.

Remark 2.2. *The conditions $Y_1, Y_2 < 0$ imply $Y(u_r) < 0$, which is a natural assumption. In fact, $Y(u_r) \geq 0$ would result in an unstable sway dynamics, which is unfeasible for commercial marine vehicles by design. This is a common assumption for marine systems control design, e.g. [33].*

Part I

Source seeking strategies for marine vehicles

Chapter 3

Source-seeking with variable leader in the network

In this chapter a new approach to the leader-follower coordination problem of a multi-agent system is considered for source-seeking tasks. The source-seeking problem for marine vehicles is relevant when the objective of a mission is to locate and steer the agents towards a point with a high concentration of a chemical substance or a thermal signal, e.g., from an underwater pipe leak. The main objective of the method presented in this chapter is to improve the capabilities of a group of marine vehicles for exploration and survey operations. In fact, one of the main advantage of using multi-agent systems is the possibility to assign different sensors to different vehicles. In this way, each vehicle has a different task depending on the particular sensor that it has been equipped with. For instance, assuming that the agents can communicate with each other, it may be necessary to equip just one vehicle with a GPS and assign to this specific agent the task of steering the other agents towards a specific area. Then another agent may be equipped with specific sensors for acquiring data from that area. The distribution of the sensors among the vehicles would imply power saving and therefore longer lasting and more efficient missions.

A group of n agents represented by a unicycle model is considered. The objective of the group is to explore a given area moving along a desired direction. Then, if a source is present in the explored area, the agents should leave the initial desired direction of motion and move towards the source. In particular, in the group we define two special agents, the *initial leader* and the *active follower*. The *initial leader* is the agent which is the leader at the beginning of the mission and knows the initial direction in which the agents should move. The *active follower* is an agent which is able to get measurements of a specific signal from the environment. If the measurements from the environment cross a given threshold, then the *active follower* takes on the role as leader and the *initial leader* becomes a follower. In other words, while the active follower is following the leader, it investigates the field. If it gets a relevant signal it will compute the direction that points towards the source of the signal and it will steer the whole group in this new direction. A simple illustration is given in Figure 3.2.

In order to achieve the goal, we revise the controlled agreement protocol scheme

proposed in [119] with the addition of a variable leader in order to shift the agreement. That is, we have two leaders which can influence the other agents in order to achieve an agreement on a given trajectory. Switching between the leaders we switch the agreement among the followers and therefore the direction which the whole group follows. We consider that the leadership may be switched between the *initial leader* and the *active follower*. In order to define a law for the leadership switching we extend to artificial systems the notion of an *investment parameter* which characterizes the migration model of birds [37, 106]. In particular, [106] studies the evolution of leadership among birds based on the model presented in [37]. According to this model, during the migration each animal spends energy in getting information from the environment and from its neighbors. This behavior is expressed by the investment parameter. If a bird spends a lot of energy in sensing the environment, it is characterized by a strong investment parameter. On the other hand, if it gets information only from the neighbors, it is characterized by a low investment parameter. The leaders have a high investment parameter and influence the migration of the followers.

The work presented in this chapter is based on [108].

The chapter is organized as follows: in Section 3.1 the system is described; Section 3.2 describes the proposed revised agreement for source-seeking; Section 3.3 presents the main results; in Section 3.4 some simulations are presented; Section 3.5 gives the conclusions.

3.1 System description

In this section we describe the model which characterizes the agents. The assumptions which hold on the communication network are also presented here.

3.1.1 The agents model

Each agent is characterized by a local coordinate system $\{b\}$. For the frame $\{b\}$ we use the convention typically used for marine vehicles, i.e. the z axis of the frame points downwards. The velocity in the local frame is u_i along x_b , $\dot{\psi}$ around z_b and w_i along y_b . The velocity in the global frame $\{g\}$ is given by $V = [\dot{x}_i, \dot{y}_i, \dot{\psi}_i]^T$. An illustration is given in Figure 3.1. The considered kinematic model is:

$$\dot{x}_i = u_i \cos(\psi_i) \tag{3.1a}$$

$$\dot{y}_i = u_i \sin(\psi_i) \tag{3.1b}$$

$$\dot{\psi}_i = \omega_i. \tag{3.1c}$$

Equation (3.1) gives the model of a unicycle where the control inputs are the forward velocity in the local frame u_i and the angular rate ω_i . In this chapter we design ω_i, u_i independently by each other. That is, we design a distributed law for ω_i in order to reach an agreement on a direction of motion for the group. The direction of motion is decided by the current leader in the group and is therefore subject to change if the leader changes. For the forward velocity u_i a distributed law is also designed but it will be used just to agree on a forward velocity of motion. Note that

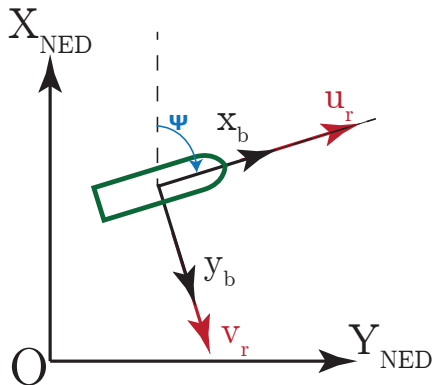


Figure 3.1: Global and body frames

since u_i, ω_i are designed independently, the vehicles do not move respecting relative distances among each other. This aspect does not guarantee collision avoidance during the motion or that the agents stay close to each other during the motion. However, collision avoidance or formation control are not points of discussion in this chapter. The main focus here is the design of a novel agreement protocol based on the switch of the leadership between two agents in the network. Since proximity of the agents is not guaranteed we assume that the agents can communicate also at long distances.

3.1.2 The network

In the following we consider a set of n agents defined by \mathcal{V} , that are indexed as v_i . We model the communication network with a graph $\mathcal{G} = (\mathcal{V}, \mathcal{E})$. Without loss of generality we index the agents such that the agent v_1 is the initial leader of the group. The initial leader's role is to make the group move in the fixed initial direction. This makes the agents move into an area of interest where, based on some a-priori knowledge of the environment, it is supposed that the source is. We consider the case where only one agent is able to sense the environment. This agent is denoted by v_2 , and in the following is called the *active* follower. Finally the agents from v_3 to v_n are the *passive* followers. These cannot sense the environment and may represent agents with different sensors, for instance cameras or antennas. Moreover they might be communication nodes to allow communication among not directly connected agents. This is particularly useful in our case because as we have mentioned above, the model does not guarantee that the agents keep a formation during the motion. But our model requires only a connected communication scheme among the agents, therefore more agents allow to have communication over larger areas.

The following assumption is valid on \mathcal{G} :

Assumption 3.1. *The graph \mathcal{G} , which characterizes the agents, is connected and has a controllable structure with respect to the nodes v_1, v_2 .*

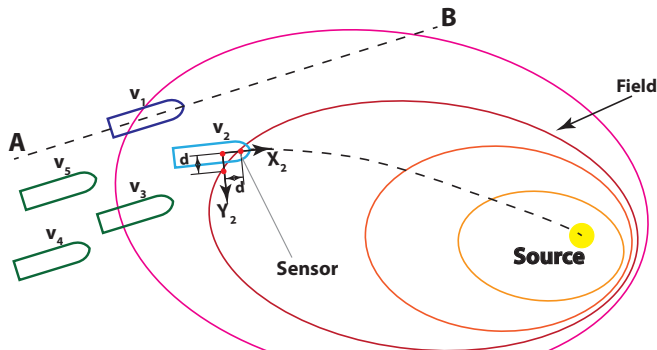


Figure 3.2: Exchange of the leadership, the agent v_1 is the initial leader, the agent v_2 is the the active follower, the red dots are the sensors

Remark 3.1. *The results in [101, 119] demonstrate that connectivity is a necessary condition for a network based on leader-followers scheme to be controllable. Furthermore, this kind of graph scheme does not require an all-to-all communication, which is an advantage for practical implementation. Conditions on the graph structure to be controllable are given in [101, 119, 132]. For instance, a graph has not to be complete or symmetric from the input node in order to be controllable.*

Remark 3.2. *We do not explicitly consider the case of directed graphs, which can have a non-symmetric Laplacian and complex conjugate eigenvalues. However, if the controllability condition with respect to v_1, v_2 is verified also for directed graph, then the following considerations hold also for this case.*

Since we assumed that the communication network may be described by a graph, graph theory tools are used in this chapter. A brief overview of the tools which we use is reported in Section A.2

3.1.3 The field

We assume that the agents have to locate the source of a vector field. The source may be an area with an high concentration of a chemical agent, a possible scenario may be the leak of oil from an underwater pipe. We assume that the location of the source is unknown and that the source generates an unknown scalar field $F(x, y)$ around it. In order to identify where the source is, it is assumed that the *active* follower is equipped with three sensors that can get scalar measurements of the field. One of the sensors is located at the center of the body of the vehicle. The other two are located at a distance d from this one on the axes x_b and y_b , respectively (Figure 3.2). The measurements of v_2 are used to calculate an approximated gradient of the field and determine a direction pointing towards the source. In the following we consider reaching the maximum of a given field $F(x, y)$. But analogous considerations hold to reach a minimum.

Assuming that v_2 is the only agent equipped with sensors able to get measurements from the field does not guarantee good distribution of the measurements,

and therefore does not guarantee a good computation of the gradient of the field. However, as already mentioned above, our main concern in this chapter is not the gradient estimation but rather the design of a novel agreement protocol based on the switching of the leadership.

We assume that at each instant the scalar measurement are available. We assume that the scalar measurement is $\delta(x, y) = hF(x, y)$, where h is a constant parameter which scales the measurements from the field $F(x, y)$ to the sensor. According to [141] it is possible to express the scalar measurement of the field $\delta(x_i, y_i)$ at the generic position (x_i, y_i) according to the following Taylor expansion:

$$\delta(x_i, y_i) \approx \delta(x, y) + \frac{\partial \delta(x, y)}{\partial x}(x_i - x) + \frac{\partial \delta(x, y)}{\partial y}(y_i - y). \quad (3.2)$$

Considering that the active follower is equipped with three sensors it is possible to write:

$$\begin{bmatrix} \delta_{22} - \delta_{21} \\ \delta_{23} - \delta_{21} \end{bmatrix} = \begin{bmatrix} x_2^g - x_1^g & y_2^g - y_1^g \\ x_3^g - x_1^g & y_3^g - y_1^g \end{bmatrix} \begin{bmatrix} \frac{\partial \delta_{21}}{\partial x_1} \\ \frac{\partial \delta_{21}}{\partial y_1} \end{bmatrix} \quad (3.3)$$

where (x_i^g, y_i^g) are the coordinates of the sensors on the agent v_2 expressed in the *global* frame. The index $i \in \{1, 2, 3\}$ refers to the i -th sensor. In particular, $i = 1$ indexes the sensor in the center of the body of v_2 , $i = 2$ and $i = 3$ refer to the sensors on the x_b and y_b local-frame axis of v_2 , respectively. Finally δ_{2i} is the scalar measure that corresponds to the i -th sensor. From (3.3), we can calculate the gradient of the field as follows:

$$\mathbf{G} = \begin{bmatrix} G_x \\ G_y \end{bmatrix} = (P^T P)^{-1} P^T \begin{bmatrix} \delta_2 - \delta_1 \\ \delta_3 - \delta_1 \end{bmatrix} \quad (3.4)$$

where:

$$P = \begin{bmatrix} x_2^g - x_1^g & y_2^g - y_1^g \\ x_3^g - x_1^g & y_3^g - y_1^g \end{bmatrix}. \quad (3.5)$$

The vector \mathbf{G} is directed towards the source, so it is possible to compute the direction ψ_{d2} which points towards the source as follows:

$$\psi_{d2} = \arctan 2(G_y, G_x) = 2 \arctan \left(\frac{G_y}{\sqrt{G_x^2 + G_y^2} + G_x} \right). \quad (3.6)$$

Notice that (3.6) is not defined for $(G_x, G_y) = (0, 0)$ and $0 \geq \psi_{d2} \geq 2\pi$. We design the linear velocity such that the agents stop before arriving to the maximum of the field, where $(G_x, G_y) = (0, 0)$.

In this chapter we consider a time-invariant field $F(x, y) : \mathbb{R}^2 \rightarrow \mathbb{R}^+$ that satisfies the following assumption:

Assumption 3.2. *The field $F(x, y)$ is continuous and convex.*

Remark 3.3. *This assumption ensures that there is only one global maximum on $F(x, y)$, and therefore only one source in the field. A field with several local maxima is equivalent to having several sources in the environment.*

3.2 The revised agreement protocol

In this section we present the distributed control for the agents. In particular, we present our approach based on the controlled agreement protocol characterized by a switch in the leadership. That is, a certain agent takes on the role of a leader or a follower depending on its sensing of the strength of the field. In particular, the closer to the field maximum/minimum the agent is, the more the agent takes on the leader role. In order to make the group move into the area of interest, a fixed initial direction of motion is assigned.

3.2.1 The investment parameter

Before presenting the control law we introduce the concept of investment parameter. In [37, 89, 106], the migration model for birds is studied. This model is characterized by leaders and followers. The leaders are animals with special skills which are able to sense from the environment the right direction for the migration and therefore lead the rest of the group. The followers are animals which are less skilled than the leaders and therefore do not sense the environment but just get information from their neighbors in the group. The difference between leaders and followers is defined by the so called *investment parameter*. Each bird in the group is characterized by an investment parameter $k_i \in [0, 1]$. If $k_i = 0$ the agent v_i is a follower and this means that it invests few energy in getting information from the environment. If $k_i = 1$ then v_i is a leader and this means that the v_i invests a lot of energy in getting information from the environment. The investment parameter k_i for the i -th agent changes over the generation of the animals according to the so called fitness function, which takes into account the evolution of the skills of the birds over the generations. For artificial agents we cannot apply the concept of evolution, but getting inspired by [37, 89, 106] we can define some agents in the network which can change their status of followers or leaders during the mission. In particular, we consider that in the network there are just two agents which can change their status. These two agents are the initial leader v_1 and the active follower v_2 . The agents v_1 and v_2 are characterized by an investment parameter $k_i \in [0, 1]$, for $i \in \{1, 2\}$, which may change according to the environmental conditions. That is, if the agents are far from a source and v_2 does not get good enough measurements, then $k_2 \rightarrow 0$, i.e. v_2 is a follower and the group is led by v_1 . On the other hand, if v_2 senses measurements with a signal which crosses a given threshold, then $k_2 \rightarrow 1$ and v_2 leads the group towards the source.

The investment parameters k_1 and k_2 are defined as follows:

$$k_1 = k, \quad k_2 = 1 - k \quad (3.7)$$

where

$$k = \frac{1}{2} (\cos(\Delta) + 1) \quad (3.8a)$$

$$\Delta = \begin{cases} 0 & \text{if } \delta_{21} \leq \delta_m \\ \pi \frac{\delta_{21} - \delta_m}{\delta_M - \delta_m} & \text{if } \delta_m < \delta_{21} < \delta_M \\ \pi & \text{if } \delta_{21} \geq \delta_M \end{cases} \quad (3.8b)$$

The value $\delta_m > 0$ defines the minimum relevant level for the measurements, $\delta_M > \delta_m$ is the maximum thresholds over which v_2 becomes a full leader, δ_{21} is the strength of the measurement signal that the agent v_2 currently receives to its central sensor. The function k is continuous and such that $k = 1$ for $\delta_{21} \leq \delta_m$ and $k = 0$ for $\delta_{21} \geq \delta_M$. Notice that δ_m, δ_M are not the minimum and the maximum of $F(x, y)$, but only two tuning parameters. The values δ_m, δ_M may be determined by some a-priori knowledge of the the source and the field.

The choice (3.7) ensures that the initial leader and the active follower cannot have their investment parameter equal to 1 or to 0 at the same time. If $k_1 = k_2 = 1$ then they would both be leader. In this case they would not influence each other. Each one would follow its desired direction without caring about the direction of the other one. If $k_1 = k_2 = 0$ they would both be followers. In this case there would not be a leader in the group and all the agents would get an agreement on a common direction that would be the average of their initial direction of motion [101].

The derivative of k is:

$$\dot{k} = \begin{cases} 0 & \text{if } \delta_{21} \leq \delta_m \\ \pi \frac{\dot{\delta}_{21}}{\delta_M - \delta_m} & \text{if } \delta_m < \delta_{21} < \delta_M \\ 0 & \text{if } \delta_{21} \geq \delta_M \end{cases} \quad (3.9a)$$

where $\dot{\delta}_2$ is the velocity with which the signal from the field to the agent v_2 varies. Note that \dot{k} is well defined $\forall \delta_{21}$. We consider that the following Assumption holds for our model:

Assumption 3.3. *The velocity with which the signal from the field to the agent v_2 varies is bounded, i.e. $\|\dot{\delta}_{21}\| \leq c$, where $c > 0$*

Remark 3.4. *This Assumption ensures that the agents move with a finite velocity over the field, and that the field itself has not discontinuities.*

Note that Assumption 3.3 implies that $\dot{k} \leq \frac{\pi c}{\delta_M - \delta_m} = \alpha$.

3.2.2 The coordination law for headings

Inspired by [37, 89, 106], we propose the following law for the heading velocities ω_i of the initial leader v_1 and the active follower v_2 :

$$\omega_1 = k_1(\psi_{d1} - \psi_1) - (1 - k_1) \frac{1}{d(v_1)} \mathbf{L}_1 \boldsymbol{\psi} \quad (3.10a)$$

$$\omega_2 = k_2(\psi_{d2} - \psi_2) - (1 - k_2) \frac{1}{d(v_2)} \mathbf{L}_2 \boldsymbol{\psi} \quad (3.10b)$$

where $d(v_i)$ is the degree number of the i -th agent, \mathbf{L}_i is the i -th row of the Laplacian matrix. The parameters $k_1, k_2 \in [0, 1]$ are given in (3.7). If $k_i = 1$ the agent is a full leader, if $k_i = 0$ it becomes a pure follower. Equation (3.10) is similar to the one in [37, 89, 106], where the leadership is associated with k_i . Except that in this thesis $k_i(t)$ varies according to the scalar signal measured from the source in

the field. When the agent v_2 takes measures that cross a fixed threshold, it becomes the new leader. Finally ψ_{d1} is the initial heading assigned to v_1 , which is the initial leader. Then ψ_{d2} is the desired heading of the active follower given in (3.6), and it depends on current position of the agent v_2 in the field $F(x, y)$.

For the other $n - 2$ passive followers the concept of investment parameter does not apply since they do not participate actively in either leading the rest of the group in a certain direction or sensing relevant information from the environment. Therefore, $k_i = 0 \forall i \in \{3, \dots, n\}$. We assign to their dynamics classic *agreement protocol* [101], that is:

$$\omega_i = -\frac{1}{d(v_i)} \mathbf{L}_i \boldsymbol{\psi} \quad \forall i \in \{3, \dots, n\} \quad (3.11)$$

If the graph is connected the agents will agree on a common direction to follow [101]. In our case this direction is suggested by the current leader.

Equations (3.10) and (3.11) can be rewritten in matrix form:

$$\dot{\boldsymbol{\psi}} = K(\boldsymbol{\psi}_d - \boldsymbol{\psi}) - D^{-1}(I - K)L\boldsymbol{\psi} \quad (3.12)$$

where:

$$K = \begin{bmatrix} \begin{bmatrix} k(t) & 0 \\ 0 & 1 - k(t) \end{bmatrix} & O_{2 \times (n-2)} \\ O_{(n-2) \times 2} & O_{(n-2) \times (n-2)} \end{bmatrix} \quad (3.13)$$

$$\boldsymbol{\psi}_d = \begin{bmatrix} \psi_{d1} \\ \psi_{d2} \\ \mathbf{0}_{(n-2) \times 2} \end{bmatrix} \quad (3.14)$$

where $O_{a \times b}$ is a matrix $[a \times b]$ with all entries equal to zero. The vector $\boldsymbol{\psi}_d$ is the vector of the desired headings. Finally notice that the last $n - 2$ elements of the vector are conventionally assumed to be zeros. In fact the first term $K(\boldsymbol{\psi}_d - \boldsymbol{\psi})$ couples only the dynamics of the agents that can change their investment parameter k_i . The desired headings of the $n - 2$ passive followers can assume whichever value possible, but they are ignored because their k_i is equal to zero. The dynamics of the $n - 2$ passive followers are coupled with the ones of the agents v_1 and v_2 via the term $D^{-1}(I - K)L\boldsymbol{\psi}$. Notice that D^{-1} is the inverse of the degree matrix and this inverse exists since we assume the graph to be connected. Finally I is the $[n \times n]$ identity matrix. The equation can be rearranged and rewritten as:

$$\dot{\boldsymbol{\psi}} = -M\boldsymbol{\psi} + K\boldsymbol{\psi}_d \quad (3.15a)$$

$$M = [K + D^{-1}(I - K)L]. \quad (3.15b)$$

From the matrix K the necessity of our choice in (3.7) is more clear. If both k_1 and k_2 were zero at the same time, the model given by (3.12) would become the classical *agreement protocol* $\dot{\boldsymbol{\psi}} = L\boldsymbol{\psi}$ [101]. If both $k_1 = k_2 = 1$, then both v_1 and v_2 would be leaders, in this case each one follows its desired direction ignoring the other one. The passive followers follow a direction that depends on the characteristics of the connection graph.

3.2.3 The linear velocities

In our approach the control of the linear velocities $\mathbf{u} = [u_1 \ u_2 \ \dots \ u_n]^T$ is done independently from the angular velocities $\dot{\boldsymbol{\psi}}$.

We choose the velocity controllers such that agent v_2 controls the linear velocity of the other agents during the mission. In particular, this means that the active follower v_2 is always the agent in charge of controlling the linear velocity of the remaining $n - 1$ vehicles, initial leader v_1 included, at any time. That is v_2 imposes its own linear velocity to the rest of the agents even though v_1 is leading with respect to headings. The motivation for the choice of v_2 to decide the linear velocity of the group is that it is the only agent which obtains measurements from the field, and it is desirable to adjust the linear velocity with the intensity of the signal from the field. The velocity for v_2 is chosen as:

$$\bar{u}_2 = u_0 - (1 - k_c)u_0 \quad (3.16)$$

where u_0 is the initial constant assigned velocity,

$$k_c = \frac{1}{2} (\cos(\Delta_c) + 1) \quad (3.17a)$$

$$\Delta_c = \begin{cases} 0 & \text{if } \delta_{21} \leq \delta_{mu} \\ \pi \frac{\delta_{21} - \delta_{mu}}{\delta_{Mu} - \delta_{mu}} & \text{if } \delta_{mu} < \delta_{21} < \delta_{Mu} \\ \pi & \text{if } \delta_{21} \geq \delta_{Mu} \end{cases} \quad (3.17b)$$

Note that k_c is a similar function to k and it is used to slow down v_2 and stop it completely when it reaches a point with scalar measurement $\delta_{21} = \delta_{Mu}$.

The linear velocities of the agents are controlled by v_2 . We assign the forward velocities u_i according to the controlled agreement protocol in [132]:

$$\underbrace{\begin{bmatrix} u_1 \\ u_2 \\ u_3 \\ \vdots \\ u_n \end{bmatrix}}_{\mathbf{u}^*} = - \begin{bmatrix} L_{11} & L_{12} & \dots & L_{1n} \\ 0 & 0 & \dots & 0 \\ L_{31} & L_{32} & \dots & L_{3n} \\ \vdots & \vdots & \ddots & \vdots \\ L_{n1} & L_{n2} & \dots & L_{nn} \end{bmatrix} \begin{bmatrix} l_1 \\ l_2 \\ l_3 \\ \vdots \\ l_n \end{bmatrix} + \begin{bmatrix} 0 \\ \bar{u}_2 \\ 0 \\ \vdots \\ 0 \end{bmatrix} \quad (3.18)$$

where L_{ij} is the element (i, j) of the Laplacian matrix L , l_i is the measure of the distance which each agents has traveled. Finally \bar{u}_2 is the control input for the linear velocity of v_2 .

The dynamics of the linear velocities of the agents v_1, v_3, \dots, v_n is:

$$\mathbf{u}^* = -\bar{L}\mathbf{l}^* - \mathbf{r}\bar{u}_2 \quad (3.19)$$

where \bar{L} is a matrix $[(n-1) \times (n-1)]$ obtained by the Laplacian deleting the second column and the second row, i.e. the row and the column that corresponds to v_2 . The vector \mathbf{l}^* is $\mathbf{l}^* = [l_1, l_3, \dots, l_n]^T$. Then the vector \mathbf{r} is the $[(n-1) \times 1]$ vector obtained by the second column of the Laplacian deleting the second element. With this dynamic we want the agents v_1, v_3, \dots, v_n move with the same velocity as v_2 .

At this point is important to specify that the i -th agent moves according to the model (3.1) where u_i is given by (3.18) and ω_i is given in (3.12). As already said, this choice for u_i, ω_i does not guarantee motion in formation or collision avoidance. However, our main concern in this chapter is to design a controlled agreement protocol with a variable leader. This is done with the coordination law (3.12).

3.3 Results

In this section the conditions to have a stable exchange of the leadership within the group are stated and demonstrated. In the following $O_{a \times b}$ is used to indicate an $[a \times b]$ matrix with all the elements equal to zero. The investment parameter $k(t)$ is simply rewritten as k without neglecting its time variant behavior.

The following Lemma is important for the proof of the main Theorem.

Lemma 3.1. *For a connected undirected graph \mathcal{G} the matrix $M = K + D^{-1}(I - K)L$ is positive definite if $K \neq O_{n \times n}$.*

Proof. We want to demonstrate that M is positive definite for each value of k . We observe that M is not symmetric, but according to [76] we know that the positive-definiteness is a property that holds also for non-symmetric matrix. Furthermore, even in the case a non-symmetric matrix is positive definite, this guarantee that its eigenvalues are all positive. So we focus on the following quadratic form:

$$\mathbf{x}^T(K + D^{-1}(I - K)L)\mathbf{x} = \mathbf{x}^T K \mathbf{x} + \mathbf{x}^T D^{-1}(I - K)L \mathbf{x} \geq 0 \quad (3.20)$$

We do not know what are the eigenvalues of $K + D^{-1}(I - K)L$, but if we can prove that there is not a vector different from zero that makes (3.20) zero, then $K + D^{-1}(I - K)L$ is strictly greater than 0, and so positive definite [76].

Let us consider first the case $0 < k < 1$. The matrix K is diagonal and with $n - 2$ null elements on its diagonal, so it is positive semi-definite because k and $1 - k$ are non negative. Its eigenvalues are k , $1 - k$ and 0. The eigenvalue 0 has algebraic and geometric multiplicity $n - 2$, so there are $n - 2$ eigenvectors that correspond to the eigenvalue $\lambda_k = 0$. We call \mathbf{e}_1 and \mathbf{e}_2 the eigenvectors that correspond to the eigenvalues $1 - k$ and k . Then we call \mathbf{e}_i , with $i \in \{3, \dots, n\}$, the $n - 2$ eigenvectors that correspond to $\lambda = 0$. The generic vector \mathbf{e}_i has $n - 1$ null elements and the value 1 in the $i - th$ position:

$$\mathbf{e}_3 = \{0, 0, 1, 0, \dots, 0\}^T \quad (3.21)$$

$$\mathbf{e}_i = \{0, 0, \dots, 1, \dots, 0\}^T \quad (3.22)$$

$$\mathbf{e}_n = \{0, 0, 0, \dots, 1\}^T \quad (3.23)$$

Now it is sufficient to show that none of the eigenvectors \mathbf{e}_i makes the quadratic form (3.20) zero. For this purpose, we consider (3.20) with $\mathbf{x} = \mathbf{e}_i$ where $i \in \{3, \dots, n\}$. We obtain:

$$\mathbf{e}_i^T D^{-1}(I - K)L \mathbf{e}_i = L_{ii} = d(v_i) > 0 \quad (3.24)$$

where L_{ii} is the i -th element on the diagonal of L that is equal to $d(v_i)$, that is the number of neighbors of v_i . Since we have a connected graph, each agent has to have at least one neighbor, so $d(v_i) > 0$.

When $k = 0$ we have $e_1 = \{1, 0, \dots, 0\}^T$ and $e_1^T M e_1 = d(v_1) > 0$.

When $k = 1$ we have $e_2 = \{0, 1, 0, \dots, 0\}^T$ and $e_2^T M e_2 = d(v_2) > 0$.

So we can conclude that there is not a vector that is different by $\mathbf{0}$, which can make zero both the terms of (3.20) at the same time. Consequently we have proved that M is positive definite, and so its eigenvalues are all positive [76]. \square

Now it is possible state the main theorem:

Theorem 3.1. *Consider a group of agents that move according to (3.15) in a time-invariant field $F(x, y)$, and assume that Assumptions 1-3 are satisfied. Then (3.15) is input to state stable (ISS) with respect to the input $K\psi_d$. And if the eigenvalues of \bar{L} are all distinct and the corresponding eigenvectors are not orthogonal to \mathbf{r} , then (3.18) is controllable by u_2 .*

Proof. We want to demonstrate that (3.15) is Input to State Stable (ISS) with input $K\psi_d$. To this purpose we know that M is positive definite according to Lemma 3.1 and we want to focus on the norms of M and \bar{M} . First we focus on M :

$$M = \begin{bmatrix} 1 & -\frac{L_{12}(k-1)}{d_1} & -\frac{L_{13}(k-1)}{d_1} & \dots & -\frac{L_{1n}(k-1)}{d_1} \\ \frac{L_{21}k}{d_2} & 1 & \frac{L_{23}k}{d_2} & \dots & -\frac{L_{2n}k}{d_2} \\ \frac{L_{31}}{d_3} & \frac{L_{32}}{d_3} & 1 & \dots & \frac{L_{3n}}{d_3} \\ \vdots & \vdots & \vdots & \ddots & \vdots \\ \frac{L_{n1}}{d_n} & \frac{L_{n2}}{d_n} & \frac{L_{n3}}{d_n} & \dots & 1 \end{bmatrix} \quad (3.25)$$

where L_{ij} are the (i, j) -th elements of L . According to [101] the sum of the elements on the rows of L is zero. So using this property, the sum of the elements on the rows of M are:

$$r_1 = 1 + \sum_{i=2}^n -\frac{L_{1i}(k-1)}{d_1} = 2 - k \quad (3.26)$$

$$r_2 = \frac{L_{21}k}{d_2} + 1 + \sum_{i=3}^n \frac{L_{2i}}{d_2} = 1 - k \quad (3.27)$$

$$r_j = \sum_{i=1}^{j-1} \frac{L_{ji}}{d_j} + 1 + \sum_{i=j+1}^n \frac{L_{ji}}{d_j} = 0 \quad (3.28)$$

where r_i gives the sum of the elements of the i -th row, and $j \in [3, 4, \dots, n]$. According to this we have:

$$\|M\|_\infty = \max \{2 - k, 1 - k, 0\} \leq 2 \quad (3.29)$$

because $0 \geq k \geq 1$.

Now we focus on \dot{M} :

$$\dot{M} = (I - D^{-1})\dot{K} = \begin{bmatrix} 0 & -\frac{\dot{k}L_{12}}{d_1} & 0 & \dots & 0 \\ \frac{\dot{k}L_{21}}{d_2} & 0 & 0 & \dots & 0 \\ \frac{\dot{k}L_{31}}{d_3} & -\frac{\dot{k}L_{32}}{d_3} & 0 & \dots & 0 \\ \vdots & \vdots & \vdots & \ddots & \vdots \\ \frac{\dot{k}L_{n1}}{d_n} & -\frac{\dot{k}L_{n2}}{d_n} & 0 & \dots & 0 \end{bmatrix} \quad (3.30)$$

According to the definition of the Laplacian we have $L_{ij} \in \{0, -1\}$ for $i \neq j$. So considering also Assumption 3.3 we have:

$$\|\dot{M}\|_\infty = \max \left\{ -\frac{\dot{k}L_{12}}{d_1}, \frac{\dot{k}L_{21}}{d_2}, \frac{\dot{k}L_{31} - \dot{k}L_{32}}{d_3}, \dots, \frac{\dot{k}L_{n1} - \dot{k}L_{n2}}{d_n} \right\} \quad (3.31)$$

$$< \max \left\{ \frac{\dot{k}}{d_1}, -\frac{\dot{k}}{d_2}, \pm \frac{\dot{k}}{d_3}, \dots, \pm \frac{\dot{k}}{d_n}, 0 \right\} \quad (3.32)$$

$$\leq \frac{\dot{k}}{\min\{d_i\}} \quad \text{for } i \in [1, 2, \dots, n] \quad (3.33)$$

$$\leq \alpha_1 \quad (3.34)$$

where α_1 is a constant. According to the properties of M and \dot{M} we can conclude that:

$$\dot{\psi} = -M\psi \quad (3.35)$$

is globally exponentially stable (GES), according to [123, Theorem 8.7]. Moreover $0 \geq \psi_{d2} \geq 2\pi$ because of its definition. And we have:

$$\|K\|_\infty = \max\{1 - k, k, 0\} \leq 1 \quad \forall k \in [0, 1] \quad (3.36)$$

because of the definition of K . So (3.15) is ISS according to [77, Lemma 4.6].

As regards the linear velocities, the system (3.18) is controllable by u_2 if [132, Theorem IV.1] applies. According to [101, 132] if Assumption 3.1 holds then the eigenvalues of \bar{L} are all distinct and the corresponding eigenvectors are not orthogonal to \mathbf{r} . Therefore the conditions of [132, Theorem IV.1] are satisfied and v_2 can control the velocities of the other agents. \square

The solution of (3.15) is $\psi = [K + D^{-1}(I - K)L]^{-1}K\psi_d$. Considering the chosen function for k we know that it evolves over the field between the values 1 and 0. So when $k = 1$ and v_2 is the leader the matrix $[K + D^{-1}(I - K)L]^{-1}K$ gives $\psi = [\psi_{d2}, \dots, \psi_{d2}]^T$. When we have $k = 0$ the agent v_1 is the leader and the solution is $\psi = [\psi_{d1}, \dots, \psi_{d1}]^T$. The direction ψ_{d2} points towards the source [141].

3.4 Simulations

In this section simulation results are presented to illustrate the behavior of the presented model.

Table 3.1: Initial states and ocean currents affecting the vehicles.

	$x _{t_0}$ [m]	$y _{t_0}$ [m]	$\psi _{t_0}$ [deg]
v_1	90	0	90
v_2	87	3	120
v_3	96	-6	60
v_4	84	-9	30
v_5	81	-12	10

We consider a group of five agents described by a graph $(\mathcal{G}, \mathcal{V})$. The graph is connected but without a directed connection between v_1 and v_2 . In other words we assume a graph topology in which v_1 and v_2 do not directly exchange the information about their relative position. The graph topology for the communication scheme of the relative position is illustrated in Figure 3.3. The following Laplacian matrix corresponds to the illustrated topology:

$$L = \begin{bmatrix} 2 & 0 & -1 & -1 & 0 \\ 0 & 2 & -1 & 0 & -1 \\ -1 & -1 & 2 & 0 & 0 \\ -1 & 0 & 0 & 1 & 0 \\ 0 & -1 & 0 & 0 & 1 \end{bmatrix} \quad (3.37)$$

We assign $u_0 = 1$ m/s. The considered field is:

$$F(x, y) = e^{(-0.1A(0.055(x+130)-10)^2 - 0.2B0.04(y+170)-11)^2} \quad (3.38)$$

where $A = e^{0.005(x+130)}$, $B = e^{0.005(y+170)}$. Notice that $F(x, y)$ respects Assumption 3.2. The thresholds for k are $\delta_m = 0.08$ and $\delta_M = 0.5$. The thresholds for the variation of the velocity u are $\delta_{mu} = 0.8$ and $\delta_{Mu} = 0.95$. The initial conditions for the agents are summarized in Table 3.1. Figure 3.4 shows motion of the agent. It is clear that they start with different directions and they all agree on the direction that the leader v_1 imposes to them. When they arrive close to the source the active follower v_2 takes on the role as leader and steers the agents to the source. Figure 3.5 shows when v_2 becomes leader, that is, when the investment parameter $k_2 = 1 - k$ becomes 1.

3.5 Conclusions

The objective of this chapter was the design of a controlled agreement protocol with switching of the leadership, which is applied to the headings of a multi-agent systems where each agent has been modeled by a unicycle kinematic model. In particular, in a network of n agents two special agents have been defined, the initial leader v_1 and the active follower v_2 . These are the two agents which can take on the role as leader. The actual leader is defined by the investment parameter, a parameter which defines the role of birds during migration. Extending the concept of investment parameter to artificial agents, we have presented a coordination law

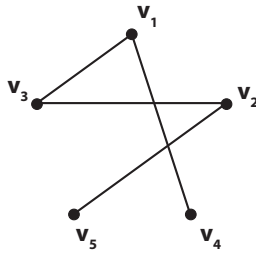


Figure 3.3: Topology of the agents' graph

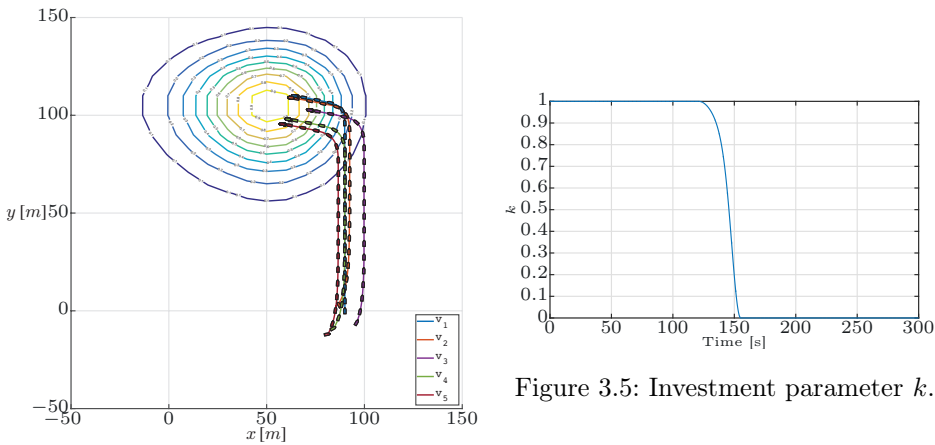


Figure 3.5: Investment parameter k .

Figure 3.4: Motion of the vehicles.

which exchanges the leadership between v_1 and v_2 according to the environmental conditions, i.e. considering the proximity of the group to the source of a scalar field. It is assumed that only the agent v_2 can take distributed scalar measurements of the field and is able to compute the direction pointing towards the source. The agent v_1 , i.e. the initial leader, has the role to take on the leadership when the signal of the source is weak and steer the agents in a desired direction.

For the linear velocities a parallel controlled agreement for which v_2 is the only leader, without switching, was used. With this choice the linear velocities can be made proportional to the strength of the signal from the source, since v_2 is the only agent able to get measurements from the environment. The linear velocity which v_2 imposes on the others is such that it is zero when the agents are sufficiently close to the source.

Chapter 4

Adaptive source-seeking with marine vehicles

In this chapter we consider the source seeking problem using a multi-agent system consisting of autonomous underwater vehicles (ASVs). It is assumed that a group of n agents has to explore a given area where, based on a-priori knowledge, there is supposed to be the source of a scalar field. The source may be an area where there is a high concentration of a chemical substance, for instance, the leak from an underwater pipe line may be considered a source in this context. In general, when source-seeking algorithms are developed, it is always assumed that a source is present in the explored area. Here a method which does not require this assumption is presented. The method aims to increase the autonomy of the system. In this sense, it is assumed that the group of agents moves along a given path in order to explore a given area. Then, if the signal that the agents get from the environment is sufficiently strong, the agents should leave the initial path meant to explore the area, calculate a path which points towards the source and move towards it. According to this approach, if a source is present in the area, then the agents leave the initial path. On the other hand, if the measurement from the field are not strong enough to suppose that a source is nearby, the agents do not leave the safe initial desired path.

In order to achieve the exploration task described above, a system of n agents characterized by a leader-follower scheme is considered. The leader is an agent which influences the states of the followers, and the followers have no influence on the leader's states. In particular, the leader is the only agent which knows the desired path to follow and the followers have to follow the leader, keeping a prescribed formation. It is assumed that each agent in the network is equipped with a sensor which can get scalar measurements of the field around the source. These measurements are used to compute the approximated gradient of the field. Using the gradient of the field and the intensity of the scalar measurements from the field, a guidance law which adapts the desired heading of the leader is present. In particular, an initial heading, which is meant to steer the agents towards an area where the source is supposed to be, is assigned to the leader. The initial heading is computed using a-priori knowledge of the environment. Then using the scalar

measurements of the field, the direction towards the source is computed by means of the approximated gradient. According to the intensity of the scalar measurements from the environment, the heading law assigned to the leader weighs the initial headings and the one computed from the approximated gradient. In particular, if the intensity of the signal exceeds a given threshold, the heading pointing towards the source is considered more relevant than the initial heading, and the group moves following the former. On the other hand, if the intensity of the signal is poor, that is below a fixed threshold, the group moves on keeping the initial heading. The leader-follower synchronization controller presented in [13] is used in order to achieve motion in formation. The motion in formation is important in order to distribute the agents in the environment in such a way that the measurements that they get are good for gradient computation. That is, it is undesirable to have sensors aligned along a level curve or overlapping in a single point, since then it would not be possible to compute the gradient.

The work in this chapter is based on [111].

The chapter is organized as follows. Section 4.1 gives a brief description of the used model for the agents. Section 4.2 introduces the constant bearing guidance law and the synchronization controller for the followers. Then in Section 4.3 the source seeking guidance law for the leader is presented. In Section 4.4 we describe the properties of the proposed heading guidance and the synchronization controller. Section 4.5 presents a case study and simulation results for this. Finally Section 4.6 gives the conclusions.

4.1 ASV model

In this chapter the model of an ASV or an AUV moving in the horizontal plane introduced in Section 2.2 is used. Recall that this model can be written in component form as

$$\dot{x} = u \cos(\psi) - v \sin(\psi) \quad (4.1a)$$

$$\dot{y} = u \sin(\psi) + v \cos(\psi) \quad (4.1b)$$

$$\dot{\psi} = r \quad (4.1c)$$

$$\dot{u} = F_u(v, r) + \tau_u \quad (4.1d)$$

$$\dot{v} = X(u)r + Y(u)v \quad (4.1e)$$

$$\dot{r} = F_r(u, v, r) + \tau_r \quad (4.1f)$$

where $F_u(v, r)$, $X(u)$, $Y(u)$, $F_r(u, v, r)$ are given in Appendix 4.A. From the model (4.1), it is clear that the vehicles are under-actuated in sway. Note that in this chapter the effect of environmental disturbances is not considered, i.e., $\nu_c = \mathbf{0}$. Therefore, in (4.1) we have used $\nu = \nu_r$. This implies that a guidance method to achieve motion in formation of the followers with respect to the leader has to be suitably chosen. We decide to use the *constant bearing* guidance law [54].

4.2 Constant bearing guidance law

The constant bearing (CB) guidance law is briefly discussed here as presented in [23, 54]. This guidance law is used for the followers to track the leader and assume a desired relative positions with respect to it.

The constant bearing guidance law is:

$$\mathbf{v}_d^n = \mathbf{v}_l^n + \mathbf{v}_a^n \quad (4.2a)$$

$$\mathbf{v}_a^n = -k \frac{\tilde{\mathbf{p}}^n}{\|\tilde{\mathbf{p}}^n\|} \quad (4.2b)$$

$$\tilde{\mathbf{p}}^n = \mathbf{p}^n - \mathbf{p}_l^n \quad (4.2c)$$

where $\mathbf{v}_l^n \triangleq [\dot{x}_l, \dot{y}_l]^T$ is the velocity of the leader in the NED frame, which has to be matched to achieve synchronization. The term \mathbf{v}_a^n is proportional to the relative distance between the leader and the follower $\tilde{\mathbf{p}}^n$ expressed in the NED frame and defined as

$$\tilde{\mathbf{p}}^n \triangleq [(x_f - x_l), (y_f - y_l)]^T. \quad (4.3)$$

Then the term \mathbf{p}_l^n is defined as

$$\mathbf{p}_l^n \triangleq \mathbf{p}_{l,true}^n + \mathbf{R}(\psi_l)\mathbf{p}_r. \quad (4.4)$$

The term $\mathbf{p}_{l,true}^n$ is the actual position of the leader and $\mathbf{R}(\psi_l)\mathbf{p}_r$ is an off-set distance expressed in the NED frame which imposes the relative distance $\mathbf{p}_r = [x_r, y_r]^T \in \mathbb{R}^2$ between the follower and the leader. Finally

$$k = U_{a,max} \frac{\|\tilde{\mathbf{p}}\|}{\sqrt{(\tilde{\mathbf{p}}^n)^T \tilde{\mathbf{p}}^n + \Delta_{\bar{p}}^2}} \quad (4.5)$$

where $U_{a,max}$ is the maximum approach velocity and $\Delta_{\bar{p}}$ is a tuning parameter.

From (4.2b) and (4.5), it is clear that the approach speed approaches to zero when the relative distance approaches to zero, i.e. $\mathbf{v}_a^n \rightarrow 0$ for $\tilde{\mathbf{p}}^n \rightarrow 0$. On the other hand, if $\tilde{\mathbf{p}}^n \rightarrow \infty$ we have $\mathbf{v}_a^n \rightarrow U_{a,max}$ and the CB guidance law commands the maximum allowed velocity in order to make the follower catch up with the leader.

Remark 4.1. For curved paths the velocity \mathbf{v}_l^n should be calculated in the off-set point to track the curvature with minimal error.

Remark 4.2. Note that for the implementation of the CB guidance scheme information is needed about the leader's position and its inertial frame velocity. This information can be obtained through communication of GPS data or data from an underwater acoustic network for AUVs.

4.2.1 The controller

In this section the controllers, used together with the CB guidance law described in Section 4.2, are described. The closed-loop stability properties of these controllers are described and analyzed in [13].

The control objectives for each follower are:

$$\lim_{t \rightarrow \infty} \tilde{\mathbf{p}} = \mathbf{0} \quad (4.6)$$

$$\lim_{t \rightarrow \infty} \tilde{\mathbf{v}} \triangleq \mathbf{v}^n - \mathbf{v}_d^n = \mathbf{0} \quad (4.7)$$

$$\lim_{t \rightarrow \infty} \tilde{\psi} \triangleq \psi - \psi_d = 0. \quad (4.8)$$

These conditions correspond to synchronization among leader and followers. That is, each follower follows the leader with a prescribed desired velocity and with a desired relative position and heading.

These objectives are achieved using a feedback linearizing controller. For the surge the following controller is used:

$$\tau_u = -F_u(v, r) + \dot{u} - k_u(u - u_d) \quad (4.9)$$

where k_u is a positive constant gain. This controller is a feedback linearizing P controller. For the yaw rate actuation the following controller is used

$$\tau_r = -F_r(u, v, r) + \ddot{\psi} - k_\psi(\psi - \psi_d) - k_r(\dot{\psi} - \dot{\psi}_d) \quad (4.10)$$

where k_ψ and k_r are positive gains.

The desired surge velocity u_d can be calculated from $\tilde{\mathbf{v}}^n$ using the transformations:

$$\begin{bmatrix} \tilde{\psi} \\ \tilde{u} \\ \tilde{v} \end{bmatrix} = \begin{bmatrix} 1 & 0 & 0 \\ 0 & \cos(\tilde{\psi} + \psi_d) & \sin(\tilde{\psi} + \psi_d) \\ 0 & -\sin(\tilde{\psi} + \psi_d) & \cos(\tilde{\psi} + \psi_d) \end{bmatrix} \begin{bmatrix} \tilde{\psi} \\ \tilde{\mathbf{v}}^n \end{bmatrix} \quad (4.11)$$

where $\tilde{u} = u - u_d$ and $\tilde{v} = v$. The desired heading angle ψ_d is calculated from the inner and outer product of \mathbf{v}^n and \mathbf{v}_d^n , see [25]. This implies that \mathbf{v}^n is aligned with \mathbf{v}_d^n . These controllers are the same as presented in [13, 14].

4.3 Leader's heading computation

In this section we describe how we compute the leader's heading. The heading for the leader is computed taking into account the current gradient information from the field. In particular, with our approach the leader, and therefore the group, follows an initial given path and leaves this one in favor of the one pointing towards the source only if the signal's strength from the field exceeds a predefined threshold.

The main objective for the group is to explore an area of the environment where the source of a scalar signal is supposed to be and eventually converge to the origin of the source if it is present. The signal of the source can be assumed to be the concentration of a chemical agent or an electromagnetic or thermal signal. We assume that the distribution of a possibly present source is given by a map $F(x, y) : \mathbb{R}^2 \rightarrow \mathbb{R}$ whose shape is not known to the agents. Furthermore, we consider that the following assumption holds for $F(x, y)$:

Assumption 4.1. *The map $F(x, y)$ is time-invariant, continuous and characterized by only one global maximum which corresponds to the origin of the source, e.g. the maximum concentration of a chemical agent or the maximum value of a thermal signal.*

Remark 4.3. *This assumption ensures that only one source may be present in the explored environment. Considering a time-invariant map $F(x, y)$ we exclude the possibility that turbulences are present in the field. In the case that turbulences are present and their magnitude is small compared to the mean value of the measurements, then considering the non-stationary nature of the turbulence and the fact that the vehicle's dynamics act as a filter to fast changes, the source may still be found. To actively deal with the occurrence of turbulence, high-frequency filters can be applied to the measurements to remove the effect of high-frequency turbulence.*

We consider a group of $n = 3$ agents with only one leader. The leader is addressed with the index l , while the followers are indexed with the index f_i with $i \in [1, 2] \subset \mathbb{N}$.

We define the leader's reference yaw rate to be:

$$\dot{\psi}_{l,r} = k(\psi_{l,d_1} - \psi_{l,r}) + (1 - k)(\psi_{l,d_2} - \psi_{l,r}) \quad (4.12)$$

where ψ_{l,d_1} is the initial heading assigned to the leader in order to explore an area where the source is supposed to be. This is assumed to be bounded. The heading ψ_{l,d_2} points towards the source and it is computed using the gradient of the field. The law to compute ψ_{l,d_2} is given later. Finally $k(t) \in [0, 1]$ is a variable weight proportional to the strength of the signal from the source given by:

$$k = \frac{1}{2} (\cos(\Delta) + 1) \quad (4.13a)$$

$$\Delta = \begin{cases} 0 & \text{if } \delta_{21} \leq \delta_m \\ \pi \frac{\delta_{21} - \delta_m}{\delta_M - \delta_m} & \text{if } \delta_m < \delta_{21} < \delta_M \\ \pi & \text{if } \delta_{21} \geq \delta_M \end{cases} \quad (4.13b)$$

where $\delta_m > 0$ is the minimum level for the measurements to be considered, $\delta_M > \delta_m$ is the maximum threshold for the adaptation after which the heading $\psi_{l,d_2}(t)$ is followed, $\delta_l(t)$ is the strength of the measured signal that the leader receives. The function k is continuous and such that $k = 1$ for $\delta_{21} \leq \delta_m$ and $k = 0$ for $\delta_{21} \geq \delta_M$. Notice that δ_m, δ_M are not the minimum and the maximum of $F(x, y)$, but only two tuning parameters. The values δ_m, δ_M may be determined by some rough a-priori knowledge of the the source and the field.

What is new in our method with respect to past works is that the updating law (4.12) is adapting the current reference heading with respect to two desired headings $\psi_{l,d_1}(t)$ and $\psi_{l,d_2}(t)$. In [63], [141], the authors consider the agents to be in an environment where a source is surely present. Therefore the agents follow the heading computed via the approximated gradient. Our method is more general and assumes that a source may not be present in the environment. So in our heading updating law (4.12) we add the term $k(t)(\psi_{l,d_1}(t) - \psi_{l,r})$ which takes into account the possibility to stay on a given desired trajectory if a source is not present. The current reference heading for the group is defined in (4.12) by means of the weight $k(t)$, which according to (4.13) depends on the current strength of the signal. A strong signal gives a $k(t) \rightarrow 1$ which makes the agent leave the initial assigned trajectory and to steer on a trajectory which goes towards the source.

The heading ψ_{l,d_2} is computed using an estimation of the gradient obtained via the single measurements of each vehicle and we assume that these are available at each time instant. According to [141] it is possible to express the scalar measure of the field $\delta(x_i, y_i)$ at the generic position (x_i, y_i) using the following Taylor expansion:

$$\delta(x_i, y_i) \approx \delta(x, y) + \frac{\partial \delta(x, y)}{\partial x} (x_i - x) + \frac{\partial \delta(x, y)}{\partial y} (y_i - y) \quad (4.14)$$

Considering that each vehicle has a sensor we write:

$$\vec{\delta} = \begin{bmatrix} \delta_{f_1} - \delta_l \\ \delta_{f_2} - \delta_l \end{bmatrix} = \begin{bmatrix} x_{f_1} - x_l & y_{f_1} - y_l \\ x_{f_2} - x_l & y_{f_2} - y_l \end{bmatrix} \begin{bmatrix} \frac{\partial \delta_l}{\partial x_l} \\ \frac{\partial \delta_l}{\partial y_l} \end{bmatrix} \quad (4.15)$$

where (x_l, y_l) is the position of the leader expressed in the NED frame and (x_{f_i}, y_{f_i}) with $i = 1, 2$ are the positions of the followers. Finally δ_l and δ_{f_i} are the scalar measurements that corresponds to the leader and the i -th follower, respectively. From (4.15) it is possible to write:

$$\vec{G} = \begin{bmatrix} G_x \\ G_y \end{bmatrix} = (P^T P)^{-1} P^T \begin{bmatrix} \delta_{f_1} - \delta_l \\ \delta_{f_2} - \delta_l \end{bmatrix} \quad (4.16)$$

where:

$$P = \begin{bmatrix} x_{f_1} - x_l & y_{f_1} - y_l \\ x_{f_2} - x_l & y_{f_2} - y_l \end{bmatrix} \quad (4.17)$$

Notice that in the case of $n > 3$ agents with only one leader the computation of the gradient requires only an extended matrix P of dimensions $[(n - 1) \times 2]$ and the vector $\vec{\delta}$ of dimension $[(n - 1) \times 1]$ with i -th element $(\delta_{f_i} - \delta_l)$.

The vector \vec{G} is directed towards the source, so we compute $\psi_{l,d_2} \in [-\pi, \pi)$ as follows:

$$\psi_{l,d_2} = \arctan 2(G_y, G_x) - \pi + 2 \arctan \left(\frac{\delta_d}{\delta_l} \right) \quad (4.18)$$

As shown in [141] the first term of (4.18) points towards the source while the second and third terms allow the formation to track a level curve with signal strength δ_d . Notice that $\arctan 2(G_y, G_x)$ is not verified for $(G_x, G_y) = (0, 0)$ which corresponds to the formation being at the maximum of the vector field. Therefore we use (4.18) to steer the agents towards the source but instead of approaching the maximum we make them track the level curve which corresponds to δ_d which is close to the maximum of the vector field.

To guarantee convergence of the source seeking strategy we require the following assumption on the communication scheme to hold:

Assumption 4.2. *Each follower can communicate its measurement from the field to the leader, such that the leader can compute the gradient of the field.*

Remark 4.4. *This assumption is easily satisfied for ASVs and can be satisfied for AUVs using acoustic communication. Especially for AUVs continuous communication might be resource heavy, however, to reduce communication costs communication can be made event driven, meaning that communication will take place with a*

specified minimum frequency outside the field. This frequency will be made higher if the measurements of the field becomes stronger. In this way the communication is reduced to a minimum outside the field and significantly reduced within the field. The communication frequency can be changed by defining thresholds above and below the last communicated measurement, and if the threshold is crossed then the communication frequency is increased or decreased, respectively.

4.4 Source seeking guidance law and synchronization controller

In this section we show that combining the synchronization controller presented in Section 4.2 and 4.2.1 with the source seeking guidance law given in Section 4.3 does not affect the stability properties of the formation control.

The synchronization controller in [13] gives the control laws (4.9) and (4.10) for the followers. These controllers allow the followers to track the current position of the leader. As shown in [13], it does not matter which heading or direction the leader follows as long as the leader's input remains bounded.

To prove that the guidance law (4.12) gives bounded reference heading angles to the leader for bounded values of $\psi_{l,d1}$ and $\psi_{l,d2}$, we rewrite the update law for the heading angle (4.12) as:

$$\dot{\psi}_l = -\psi_l + (1 - k)\psi_{l,d2} + k\psi_{l,d1} \quad (4.19)$$

Consequently, it can easily be verified that (4.19) is input-to-state stable (ISS) with input $u = (1 - k(t))\psi_{l,d2} + k\psi_{l,d1}$. The reference input to the leader is thus bounded as long as k , $\psi_{l,d1}$ and $\psi_{l,d2}$ are bounded, which they are by design (4.13),(4.18). Furthermore, the solution of (4.19) is $\psi_l = (1 - k)\psi_{l,d2} + k\psi_{l,d1}$. Considering that $k \in [0, 1]$ we have $\psi_l = \psi_{l,d1}$ for $k = 1$ and $\psi_l = \psi_{l,d2}$ for $k = 0$.

Therefore if we use the guidance law (4.12) for the leader the closed-loop stability properties of the formation control strategy hold.

4.5 Simulations

In this section a case study is presented to validate the proposed method. A scenario where the agents move in a triangular formation along a path made of circular arcs and straight lines to explore a certain area is considered. This is a version of the well-known lawn-mower pattern, which is much used in mapping, monitoring and search and survey operation.

We consider three ASVs v_1, v_2, v_3 whose initial positions and orientations expressed in the inertial frame are $\eta_{v_1} = [-1500 \text{ m}, -5500 \text{ m}, 0 \text{ rad}]^T$, $\eta_{v_2} = [-2000 \text{ m}, -5000 \text{ m}, \pi \text{ rad}]^T$, and $\eta_{v_3} = [-2000 \text{ m}, -6000 \text{ m}, \pi \text{ rad}]^T$ respectively. The surge velocity of the leader v_1 is $u_{v_1} = 3 \text{ [m/s]}$. The followers v_2 and v_3 regulate their motion according to the CB guidance law (4.2a). For v_2 , the off-set distance with respect to the leader expressed in the leader body frame is $[-200, 200]^T \text{ [m]}$. For v_3 , it is $[-200, -200]^T \text{ [m]}$. Each agent takes scalar measurements from the field. The leader computes the approximated gradient according to (4.16), then computes the

desired direction ψ_{l,d_2} according to (4.18), and uses (4.12) to decide the direction to follow. For the thresholds in (4.13) we choose $\delta_m = 1$ and $\delta_M = 5$. The level curve to track in order to move around the source is defined by $\delta_d = 0.9$. The agents have no a priori knowledge of the existence and shape of the source. In this simulation there is a source at the point $[5000, 5000]^T$ [m] and the field is described by $F = 10 \exp(-(.0005x - 2.5)^2 - (.0005y - 2.5)^2)$. The lawn-mower pattern like initial trajectory assigned to the leader is made of straight lines and circle's arcs and it is given by:

$$\psi_{l,d_1} = \begin{cases} 0 & \text{for } \Delta t_x = 3500 \text{ [s]} \\ \frac{u_{v_1}}{R}(t - t_c) & \text{for } \Delta t_y = 2191 \text{ [s]} \end{cases} \quad (4.20)$$

where u_{v_1} is the surge velocity of the leader, $R = 2100$ [m] is the radius of circle arc path along which the group will move after the straight line, t is the current time instant and t_c is the time at which the circular path starts. Notice that this value is to be updated each time the agents start to turn. Furthermore note that u_{v_1}/R is the angular velocity the group should have to move along a circular path of radius R . The choice of $\Delta t_y = 2191$ [s] corresponds to moving on the circular path until a half circle is traversed at the speed $u_{v_1} = 3$ [m/s]. The results for this case study are given in the Figures 4.1 and 4.2. From Figure 4.1 we see that agents travel along the assigned path as long as they do not meet the field. When the group meets the field around the source and starts to sense relevant measurements from the environment it starts to turn towards the source. When the measurements exceeds the threshold δ_M the initial path is not followed anymore and the agents move towards the source. When they arrive on the desired level curve $\delta_d = 0.9$ they track it and move around the source. The synchronization error converges to zero during the linear motion but it is not zero during turning and becomes constant when the agents start to move in a circle. However, it still stays under 0.5 [m] which is small compared to the off-set distance. The error is caused by the circular motion which perturbs the under-actuated sway dynamics. Since each agent moves along a curve with different radius the dynamics are perturbed differently and a steady-state error remains due to the under-actuation.

4.6 Conclusion

In this chapter we have presented a method to perform source seeking with a multi-agent system consisting of under-actuated ASVs or AUVs moving in a plane and organized in a leader-follower scheme. Our method is based on a heading guidance law which chooses the heading to follow between an initial heading assigned to the leader and one computed from measurements from the field. The guidance law chooses the best heading to follow according to the information from the environment. A synchronization controller based on a CB guidance law has been used to achieve the motion of the agents in formation. We have also shown that our source seeking guidance law does not influence the stability properties of the closed-loop system of the synchronization controller.

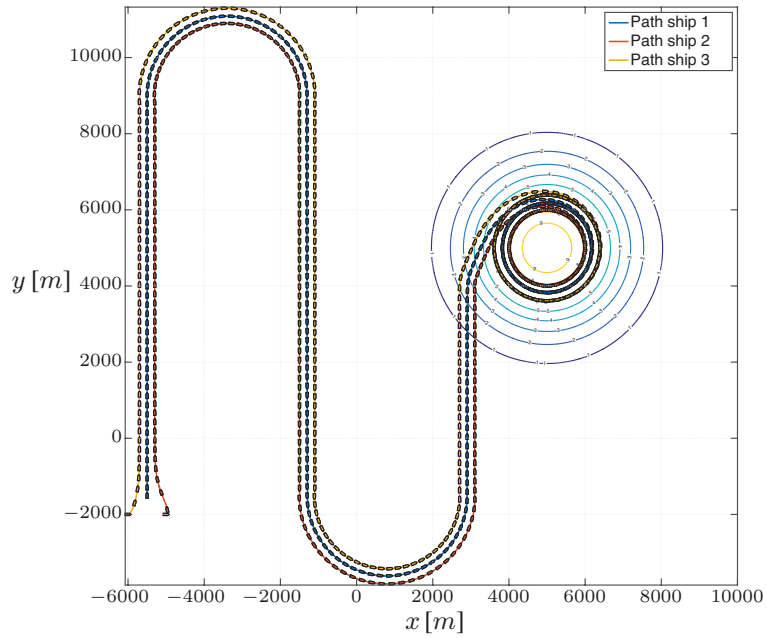


Figure 4.1: Formation moving towards the source, following a lawn-mower path.

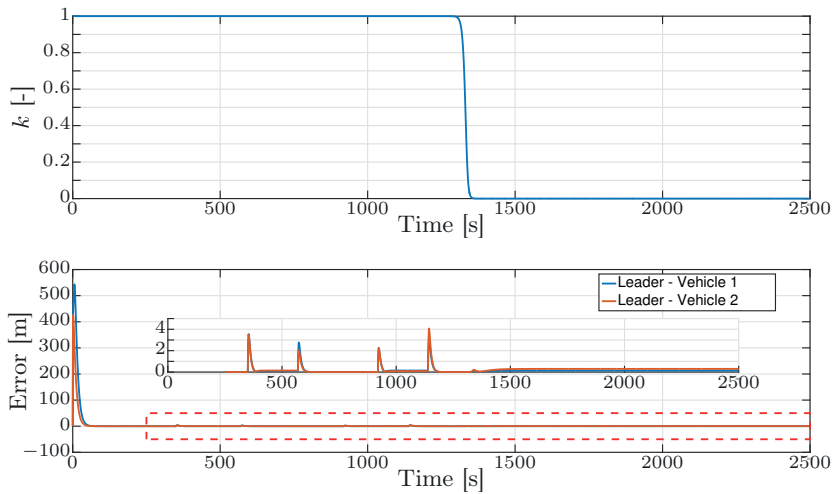


Figure 4.2: Evolution of the variable weight k and synchronization error between the followers and the leader.

4.A Function definitions

The functions F_{u_r} , $X(u_r)$, $Y(u_r)$, and F_r are given by:

$$F_{u_r} \triangleq \frac{1}{m_{11}}(m_{22}v_r + m_{23}r)r, \quad (4.21)$$

$$X(u_r) \triangleq \frac{m_{23}^2 - m_{11}m_{33}}{m_{22}m_{33} - m_{23}^2}u_r + \frac{d_{33}m_{23} - d_{23}m_{33}}{m_{22}m_{33} - m_{23}^2}, \quad (4.22)$$

$$Y(u_r) \triangleq \frac{(m_{22} - m_{11})m_{23}}{m_{22}m_{33} - m_{23}^2}u_r - \frac{d_{22}m_{33} - d_{32}m_{23}}{m_{22}m_{33} - m_{23}^2}, \quad (4.23)$$

$$F_r(u_r, v_r, r) \triangleq \frac{m_{23}d_{22} - m_{22}(d_{32} + (m_{22} - m_{11})u_r)}{m_{22}m_{33} - m_{23}^2}v_r + \frac{m_{23}(d_{23} + m_{11}u_r) - m_{22}(d_{33} + m_{23}u_r)}{m_{22}m_{33} - m_{23}^2}r. \quad (4.24)$$

Part II

Control of marine vehicles using the hand position approach

Chapter 5

Trajectory tracking of marine vehicles

In this chapter we consider the model of an ASV and an AUV moving in the horizontal plane affected by an environmental disturbance, i.e. an unknown constant ocean current. We address the problem of trajectory tracking control for curved paths. The proposed control strategy is based on the definition of the *hand position* point and an input-output feedback linearizing controller. We present a change of coordinates which is not standard for the input-output feedback linearizing approach, but that allows us to obtain a transformed model where the ocean current affects the system at the level of the linear external dynamics and can be counteracted with a simple integral action. We show that the integral state is able to give an estimate of the ocean current. We prove that our output, i.e. the *hand position* point, converges to the desired trajectory globally exponentially while the states of the internal dynamics are ultimately bounded. We show also that for the case of straight-line trajectories we have *almost-global asymptotic stability* (AGAS) of the closed-loop system.

The work discussed in this chapter is based on [110, 112].

The chapter is organized as follows: Section 5.1 presents the model of the class of vehicles which we consider; in Section 5.2 we describe our control approach; in Section 5.3 we formalize the trajectory tracking control problem and give the control objectives; Section 5.4 presents the proposed controller; in Section 5.5 we present the main result for trajectory tracking in the form of a theorem and present a rigorous mathematical proof; then in Section 5.6 the theoretical results is specialized to the case of straight-line trajectories; in Section 5.7 we present simulation results in order to validate the theoretical outcomes; finally in Section 5.8 the conclusions are given.

5.1 Vehicle model

This section briefly recalls the 3 DOF model for under-actuated marine vehicles introduced in Chapter 2.

We consider the model for ASVs and AUVs moving in the horizontal plane introduced in Chapter 2, i.e. we consider Assumption 2.1-2.3 to hold and the model (2.11) in component form:

$$\dot{x} = u_r \cos(\psi) - v_r \sin(\psi) + V_x \quad (5.1a)$$

$$\dot{y} = u_r \sin(\psi) + v_r \cos(\psi) + V_y \quad (5.1b)$$

$$\dot{\psi} = r \quad (5.1c)$$

$$\dot{u}_r = F_{u_r}(v_r) + \tau_u \quad (5.1d)$$

$$\dot{v}_r = X(u_r)r + Y(u_r)v_r \quad (5.1e)$$

$$\dot{r} = F_r(u_r, v_r, r) + \tau_r. \quad (5.1f)$$

The states x, y give the position of the vehicle in the NED frame, the state ψ is the yaw angle and gives the orientation of the vehicle in the NED frame. The states u_r, v_r are the surge and sway relative velocity, respectively. The state r is the yaw rate, V_x, V_y are the component of the ocean current vector \mathbf{V} . The expressions for $F_{u_r}(u_r), F_r(u_r, v_r, r)$ are given in Appendix 5.A. Furthermore, $X(u_r) = -X_1 u_r + X_2, Y(u_r) = -Y_1 u_r - Y_2$ and X_1, X_2, Y_1, Y_2 are reported in Appendix 5.A. We consider the following assumption to hold:

Assumption 5.1. *The ocean current in the inertial frame $\mathbf{V} = [V_x, V_y]^T$ is constant, irrotational and bounded, i.e., $\exists V_{\max} \geq 0$ such that $\sqrt{V_x^2 + V_y^2} \leq V_{\max}$.*

5.2 Hand position: line of reasoning

Before describing the trajectory tracking problem, in this section we present our different approach to the general control problem of a marine vehicle. We present the considerations which justify a different choice of the output for the system described by (5.1) compared to previous literature. In previous works on trajectory tracking of ASV and AUV the output of the system has been chosen as either the center of mass or the pivot point $\mathbf{p} = [x, y]^T$, which was then defined as the origin of the body-fixed frame (cf. Figure 5.1). Inspired by the work of Lawton and Beard [82], we choose the motion of a certain point on the center line of the vehicle, which we call *hand position*, as the output of the system.

The work [82] deals with the control problem of first-order non-holonomic vehicles, in particular unicycles whose model is

$$\dot{x} = u_1 \cos(\psi) \quad (5.2a)$$

$$\dot{y} = u_1 \sin(\psi) \quad (5.2b)$$

$$\dot{\psi} = u_2. \quad (5.2c)$$

where u_1, u_2 are the control inputs, $\mathbf{p}_{gv} = [x, y]^T$ is the position in the global frame and ψ is the yaw angle. In particular, u_1 is the forward velocity and u_2 is the yaw rate. The model (5.2) is similar to (5.1a-5.1c). They differ just because of the under-actuated state v_r , which is characterized by the uncontrolled dynamics (5.1e), and because of the ocean current that affects the system. Note also that

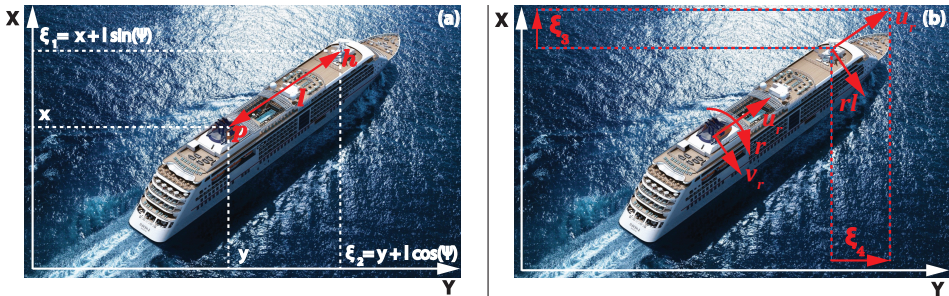


Figure 5.1: The hand position point.

(5.1) has control inputs in the surge and yaw directions like in (5.2), but on the dynamic level instead of on a purely kinematic level.

The aforementioned similarities between the kinematic model of unicycles and ASVs and AUVs motivate us to choose a different output from the commonly used pivot point for AUVs and ASVs. Based on this, we extend the definition of the *hand position* point to marine vehicles and similarly to [82] by defining $\mathbf{h} = [\xi_1, \xi_2]^T$ with

$$\xi_1 = x + l \cos(\psi) \quad (5.3a)$$

$$\xi_2 = y + l \sin(\psi), \quad (5.3b)$$

where x, y give the position of the pivot point in the NED frame, ψ is the yaw angle and $l > 0$ is a constant. An illustration of the hand position point is given in Figure 5.1. For practical applications the constant l may be chosen such that the point \mathbf{h} coincides with the position of a certain sensor of the vehicle. For instance, in case of an exploration mission, \mathbf{h} may be chosen similar to the position of a camera, such that \mathbf{h} tracks a prescribed path in order to take specific images of the area which is explored. From Figure 5.1 it is also clear that the point \mathbf{h} is indirectly actuated by the control inputs acting on \mathbf{p} . In particular, note that an actuation on \mathbf{p} along the surge direction generates an actuation in the surge direction of \mathbf{h} . Then, an actuation around the yaw axis in \mathbf{p} generates an actuation in the sway direction of \mathbf{h} , which is directly proportional to the constant l . Note that we therefore have two indirect control inputs available which actuate the point \mathbf{h} with a linear motion in two perpendicular directions, while in \mathbf{p} we have available two control inputs which generate motion in the linear direction of surge and in the rotational direction of yaw, respectively.

The next step is to apply the output feedback linearization method [68] with \mathbf{h} chosen as output. Note, however, that the output feedback linearization method [43] cannot be straightforwardly applied, but needs to be adjusted because of the ocean currents that affect the system. This will be described later in this section. First, we need to check if (5.1) is input-output feedback linearizable with output \mathbf{h} , i.e., we need to check if the vector relative degree $\rho = [\rho_{\xi_1}, \rho_{\xi_2}]^T$ is well defined

[68] . Deriving ξ_1, ξ_2 twice we obtain

$$\begin{aligned} \begin{bmatrix} \ddot{\xi}_1 \\ \ddot{\xi}_2 \end{bmatrix} &= \begin{bmatrix} \cos(\psi) & -\sin(\psi) \\ \sin(\psi) & \cos(\psi) \end{bmatrix} \begin{bmatrix} F_{u_r}(v_r, r) - v_r r - l r^2 \\ u_r r + X(u_r)r + Y(u_r)v + F_r(u_r, v_r, r)l \end{bmatrix} \\ &+ \underbrace{\begin{bmatrix} \cos(\psi) & -l \sin(\psi) \\ \sin(\psi) & l \cos(\psi) \end{bmatrix}}_{\mathbf{B}(\psi)} \begin{bmatrix} \tau_u \\ \tau_r \end{bmatrix}. \end{aligned} \quad (5.4)$$

From (5.4), we see that the system has a well-defined vector relative degree since $\rho_{\xi_1} = \rho_{\xi_2} = 2$ for $l \neq 0$, since $\mathbf{B}(\psi)$ is non-singular for $l \neq 0$. Note that $l = 0$ makes $\mathbf{B}(\psi)$ singular and therefore the system does not have a well-defined relative degree when the pivot point is chosen as output.

Now we define the following change of coordinates

$$z_1 = \psi \quad (5.5a)$$

$$z_2 = r \quad (5.5b)$$

$$\xi_1 = x + l \cos(\psi) \quad (5.5c)$$

$$\xi_2 = y + l \sin(\psi) \quad (5.5d)$$

$$\xi_3 = u_r \cos(\psi) - v_r \sin(\psi) - r l \sin(\psi) \quad (5.5e)$$

$$\xi_4 = u_r \sin(\psi) + v_r \cos(\psi) + r l \cos(\psi). \quad (5.5f)$$

Note that we cannot choose $\xi_3 = \dot{\xi}_1, \xi_4 = \dot{\xi}_2$ since this choice would imply that ξ_3, ξ_4 are functions of the ocean current, which is unknown. Our change of coordinates results in $\xi_3 = \dot{\xi}_1 - V_x, \xi_4 = \dot{\xi}_2 - V_y$. Therefore, ξ_3, ξ_4 are the relative velocities of the vehicle in the global frame.

Applying (5.5), (5.1) becomes

$$\dot{z}_1 = z_2 \quad (5.6a)$$

$$\dot{z}_2 = F_{z_2}(z_1, \xi_3, \xi_4) + \tau_r \quad (5.6b)$$

$$\begin{bmatrix} \dot{\xi}_1 \\ \dot{\xi}_2 \end{bmatrix} = \begin{bmatrix} \xi_3 \\ \xi_4 \end{bmatrix} + \begin{bmatrix} V_x \\ V_y \end{bmatrix} \quad (5.6c)$$

$$\begin{bmatrix} \dot{\xi}_3 \\ \dot{\xi}_4 \end{bmatrix} = \begin{bmatrix} F_{\xi_3}(z_1, \xi_3, \xi_4) \\ F_{\xi_4}(z_1, \xi_3, \xi_4) \end{bmatrix} + \begin{bmatrix} \cos(z_1) & -l \sin(z_1) \\ \sin(z_1) & l \cos(z_1) \end{bmatrix} \begin{bmatrix} \tau_u \\ \tau_r \end{bmatrix} \quad (5.6d)$$

where

$$\begin{bmatrix} F_{\xi_3}(\cdot) \\ F_{\xi_4}(\cdot) \end{bmatrix} = \begin{bmatrix} \cos(\psi) & -\sin(\psi) \\ \sin(\psi) & \cos(\psi) \end{bmatrix} \begin{bmatrix} F_{u_r}(\cdot) - v_r r - d r^2 \\ u_r r + X(\cdot)r + Y(\cdot)v_r + F_r(\cdot)l \end{bmatrix} \quad (5.7)$$

and $F_{z_2}(z_1, \xi_3, \xi_4)$ is obtained from $F_r(u_r, v_r, r)$ substituting $u_r = \xi_3 \cos(z_1) + \xi_4 \sin(z_1)$, $v_r = -\xi_3 \sin(z_1) + \xi_4 \cos(z_1) - z_2 l$, and $r = z_2$. Note that choosing $\xi_3 \neq \dot{\xi}_1, \xi_4 \neq \dot{\xi}_2$ in (5.5) is not a standard approach for feedback llinearization. However, this choice is necessary to make ξ_3, ξ_4 independent on the unknown ocean current. Note also that with this choice for ξ_3, ξ_4 the environmental disturbance is

affecting the system at the level of the linear external dynamics where, as it will become clear from the next sections, it is possible to counteract it using an integral action.

Now we apply the following change of input in order to linearize the external dynamics

$$\begin{bmatrix} \tau_u \\ \tau_r \end{bmatrix} = \begin{bmatrix} \cos(\psi) & -l \sin(\psi) \\ \sin(\psi) & l \cos(\psi) \end{bmatrix}^{-1} \begin{bmatrix} -F_{\xi_3}(z_1, \xi_3, \xi_4) + \mu_1 \\ -F_{\xi_4}(z_1, \xi_3, \xi_4) + \mu_2 \end{bmatrix}. \quad (5.8)$$

The terms μ_1, μ_2 in (5.8) are new inputs which are to be defined in Section 5.4 in order to solve the trajectory tracking problem. Substituting (5.8) in (5.6) we obtain

$$\dot{z}_1 = z_2 \quad (5.9a)$$

$$\begin{aligned} \dot{z}_2 = & - \left(\left(Y_1 - \frac{X_1 - 1}{l} \right) U \cos(z_1 - \phi) + Y_2 + \frac{X_2}{l} \right) z_2 \\ & - \left(\frac{Y_1}{l} (\xi_3 \cos(z_1) + \xi_4 \sin(z_1)) + \frac{Y_2}{l} \right) U \sin(z_1 - \phi) \\ & - \frac{\mu_1 \sin(z_1)}{l} + \frac{\mu_2 \cos(z_1)}{l} \end{aligned} \quad (5.9b)$$

$$\dot{\xi}_1 = \xi_3 + V_x \quad (5.9c)$$

$$\dot{\xi}_2 = \xi_4 + V_y \quad (5.9d)$$

$$\dot{\xi}_3 = \mu_1 \quad (5.9e)$$

$$\dot{\xi}_4 = \mu_2 \quad (5.9f)$$

where

$$U = \sqrt{\xi_3^2 + \xi_4^2} \quad (5.10)$$

$$\phi = \arctan \left(\frac{\xi_4}{\xi_3} \right). \quad (5.11)$$

Note that z_1 appears only as an argument of trigonometric functions with period 2π . Therefore, we can consider (5.9a-5.9b) to take values on the manifold $\mathbb{M} = \mathbb{S} \times \mathbb{R}$ where \mathbb{S} is the one-dimensional sphere.

The main advantage of choosing \mathbf{h} as output is clear from (5.9). In fact, the transformed model (5.9) is characterized by a linear external dynamics (5.9c-5.9f) and a nonlinear internal dynamics (5.9a-5.9b) as common for feedback linearized systems. Therefore, as opposed to considering the model (5.1), we can consider the external dynamics which is linear, for control purposes. The price to pay is clearly the fact that the inputs μ_1, μ_2 , which are to be designed in order to fulfill the control objectives, are affecting also the internal dynamics (5.9a-5.9b), and we have carefully to check the internal stability properties of the states z_1, z_2 .

5.3 Control objectives

In this section the trajectory tracking control problem is formalized. Based on the arguments in Section 5.2, our control objective is to make the point \mathbf{h} follow an

assigned generic trajectory. Without loss of generality we consider a trajectory which starts at origin of the NED frame. We consider the desired trajectory $\Gamma(t) = \{(\xi_{1_d}(t), \xi_{2_d}(t), \xi_{3_d}(t), \xi_{4_d}(t)) | t \in \mathbb{R}^+\}$ to be parametrized by the time t . We consider the following assumption to hold:

Assumption 5.2. *There exist constants $\underline{\xi}_3, \bar{\xi}_3, \underline{\xi}_4, \bar{\xi}_4, \underline{\xi}_{3_d}^*, \bar{\xi}_{3_d}^*, \underline{\xi}_{4_d}^*, \bar{\xi}_{4_d}^*$ such that*

$$\xi_3 \leq \xi_{3_d}(t) \leq \bar{\xi}_3 \quad (5.12a)$$

$$\underline{\xi}_4 \leq \xi_{4_d}(t) \leq \bar{\xi}_4 \quad (5.12b)$$

$$\underline{\xi}_{3_d}^* \leq \dot{\xi}_{3_d}(t) \leq \bar{\xi}_{3_d}^* \quad (5.12c)$$

$$\underline{\xi}_{4_d}^* \leq \dot{\xi}_{4_d}(t) \leq \bar{\xi}_{4_d}^* \quad (5.12d)$$

Remark 5.1. *Assumption 5.2 implies that the desired linear velocity and acceleration of the vehicle are upper and lower bounded. The lower bound on the velocity is necessary for the under-actuated vehicle to be controllable. The upper bound on the velocity is required for the desired linear velocity to be bounded, and thus create a feasible trajectory. The bounds on the acceleration are necessary in order to have a smooth motion of the vehicle.*

The control objectives can be formalized as

$$\lim_{t \rightarrow \infty} (\xi_1 - \xi_{1_d}(t)) = 0 \quad (5.13a)$$

$$\lim_{t \rightarrow \infty} (\xi_2 - \xi_{2_d}(t)) = 0 \quad (5.13b)$$

$$\lim_{t \rightarrow \infty} (\xi_3 - (\xi_{3_d}(t) - V_x)) = 0 \quad (5.13c)$$

$$\lim_{t \rightarrow \infty} (\xi_4 - (\xi_{4_d}(t) - V_y)) = 0. \quad (5.13d)$$

Note that (5.13c-5.13d) require the relative velocities ξ_3, ξ_4 in the global frame to converge to the values $\xi_{3_d} - V_x, \xi_{4_d} - V_y$. This is necessary because we want the absolute velocities in the NED frame to converge to ξ_{3_d}, ξ_{4_d} , which allow the vehicle to track the desired trajectory $\Gamma(t)$. Note that (5.13c-5.13d) depend on V_x, V_y which are unknown, however, as discussed previously, we will cope with this by introducing an integral action in our controller.

We consider the following assumption to hold

Assumption 5.3. *The total relative velocity is such that*

$$U_d = \sqrt{(\xi_{3_d}^2 - V_x)^2 + (\xi_{4_d} - V_y)^2} > 0.$$

Furthermore, the vehicle's thrusters provide enough power in order to overcome the ocean current disturbance.

Remark 5.2. *This is a necessary assumption in order to have forward motion of the vehicle, which again is necessary for the controllability of under-actuated marine vehicles.*

Remark 5.3. *Note that Assumption 5.2 implies that $\underline{U}_d \leq U_d \leq \bar{U}_d$, where $\underline{U}_d, \bar{U}_d$ are constants.*

5.4 The controller

In this section we present our choice for the control inputs $\mu = [\mu_1, \mu_2]^T$ in (5.9) which solve the control problem described in Section 5.3. In order to make the point \mathbf{h} track the desired trajectory $\Gamma(t)$ we choose

$$\mu_1 = -k_{v_x}(\xi_3 - \xi_{3_d}) - k_{p_x}(\xi_1 - \xi_{1_d}) - k_{I_x}(\xi_{1_I} - \xi_{1_{d_I}}) + \dot{\xi}_{3_d} \quad (5.14a)$$

$$\mu_2 = -k_{v_y}(\xi_4 - \xi_{4_d}) - k_{p_y}(\xi_2 - \xi_{2_d}) - k_{I_y}(\xi_{2_I} - \xi_{2_{d_I}}) + \dot{\xi}_{4_d} \quad (5.14b)$$

where $k_{p_x}, k_{p_y}, k_{v_x}, k_{v_y}, k_{I_x}, k_{I_y}$ are positive real gains, $\xi_{i_I} = \int_0^t \xi_i(\tau) d\tau$ where $i \in \{1, 2, 1_d, 2_d\}$. The integral action in (5.14) is necessary to reject the constant disturbance, i.e. the ocean current \mathbf{V} , affecting the system [10].

5.5 Main result

The main result is presented in this section. The following theorem gives the conditions under which the control objectives (5.13a) are fulfilled using the controller (5.8).

Theorem 5.1. *Consider an under-actuated marine vehicle described by the model (5.1). Consider the hand position point $\mathbf{h} = [\xi_1, \xi_2]^T = [x + l \cos(\psi), y + l \sin(\psi)]^T$, where $[x, y]^T$ is the position of the pivot point of the ship, l is a positive constant and ψ is the yaw angle of the vehicle. Then define*

$$U_d = \sqrt{(\xi_{3_d} - V_x)^2 + (\xi_{4_d} - V_y)^2} > 0 \quad (5.15)$$

as the desired relative velocity magnitude and

$$\phi_1 = \arctan\left(\frac{\xi_{4_d} - V_y}{\xi_{3_d} - V_x}\right) \quad (5.16)$$

as the crab angle. If Assumption 5.3 is satisfied and if

$$0 < \underline{U}_d < \frac{Y_2}{Y_1} \quad (5.17)$$

$$k_{v_i} > 0, k_{p_i} > 0, k_{I_i} > 0, i \in \{x, y\} \quad (5.18)$$

$$k_{v_i} k_{p_i} > k_{I_i} \quad i \in \{x, y\} \quad (5.19)$$

$$l > \max\left\{\frac{m_{22}}{m_{23}}, -\frac{X_2}{Y_2}\right\} \quad (5.20)$$

$$\bar{U}_d^* \leq \frac{2 \min\{a(\underline{d} - \underline{c}), b\}}{\left((\bar{a} + \sqrt{\bar{a}^2 + 1})(Y_1 - \frac{X_1 - 1}{l}) + \frac{2Y_1 \bar{U}_d}{l}\right)} \quad (5.21)$$

then the controller (5.8), where the new inputs μ_1, μ_2 are given by (5.14), guarantees the achievement of the control objectives (5.13). In particular,

$$(\xi_1, \xi_2, \xi_3, \xi_4) \rightarrow (\xi_{1_d}, \xi_{2_d}, \xi_{3_d}, \xi_{4_d})$$

globally exponentially and (z_1, z_2) are globally ultimately bounded. Furthermore, the steady state values of the integral variables give an estimate of the ocean current:

$$\hat{V}_x = \lim_{t \rightarrow \infty} \frac{k_{v_x}(\xi_{1_I} - \xi_{1_{I_d}})}{k_{I_x}}, \quad \hat{V}_y = \lim_{t \rightarrow \infty} \frac{k_{v_y}(\xi_{2_I} - \xi_{2_{I_d}})}{k_{I_y}}. \quad (5.22)$$

Remark 5.4. Notice that we assume an unknown ocean current and therefore also the crab angle ϕ , which is necessary in order to counteract the currents and follow the trajectory, is unknown. However, the integral action in (5.8) takes care of compensating for the unknown value of the constant disturbance.

Proof. First of all we define the following change of coordinates

$$\tilde{z}_1 = z_1 - \phi_1, \quad \tilde{\xi}_{1_I} = \xi_{1_I} - \int_0^t \xi_{1_d} d\tau - \frac{k_{I_x} V_x}{k_{v_x}}, \quad (5.23a)$$

$$\tilde{z}_2 = z_2 - \dot{\phi}_1, \quad \tilde{\xi}_{2_I} = \xi_{2_I} - \int_0^t \xi_{2_d} d\tau - \frac{k_{I_y} V_y}{k_{v_y}}, \quad (5.23b)$$

$$\tilde{\xi}_1 = \xi_1 - \xi_{1_d}, \quad \tilde{\xi}_4 = \xi_4 - (\xi_{4_d} - V_y), \quad (5.23c)$$

$$\tilde{\xi}_2 = \xi_2 - \xi_{2_d}, \quad \tilde{\xi}_3 = \xi_3 - (\xi_{3_d} - V_x). \quad (5.23d)$$

Defining the vectors $\tilde{z}_s = [\sin(\tilde{z}_1), \tilde{z}_2]^T$, $\tilde{\xi} = [\tilde{\xi}_{1_I}, \tilde{\xi}_{2_I}, \tilde{\xi}_1, \tilde{\xi}_2, \tilde{\xi}_3, \tilde{\xi}_4]^T$, the closed-loop system becomes

$$\dot{\tilde{z}} = H_{\tilde{z}}(\tilde{z}_1) \tilde{z}_s + G(\tilde{z}, \tilde{\xi}_3, \tilde{\xi}_4) \tilde{\xi} + \Delta(\dot{\phi}_1, \ddot{\phi}_1, \tilde{z}_1) \quad (5.24a)$$

$$\dot{\tilde{\xi}} = H_{\tilde{\xi}} \tilde{\xi} \quad (5.24b)$$

where $G(\cdot)$ is reported in Appendix 5.A and

$$H_{\tilde{z}}(\tilde{z}) = \begin{bmatrix} 0 & 1 \\ -(c \cos(z_1) + d) & -(a \cos(z_1) + b) \end{bmatrix} \quad (5.25)$$

$$\Delta(\dot{\phi}_1, \ddot{\phi}_1, \tilde{z}_1) = \begin{bmatrix} 0 \\ \delta(\dot{\phi}_1, \ddot{\phi}_1, \sin(\tilde{z}_1)) \end{bmatrix} \quad (5.26)$$

$$\begin{aligned} \delta(\cdot) = & -(a \cos(\tilde{z}_1) + b) \dot{\phi}_1 + \ddot{\phi}_1 \\ & + (\dot{\xi}_{4_d} \cos(\tilde{z}_1) - \dot{\xi}_{3_d} \sin(\tilde{z}_1)) \cos(\phi_1) \\ & + (-\dot{\xi}_{4_d} \sin(\tilde{z}_1) + \dot{\xi}_{3_d} \cos(\tilde{z}_1)) \sin(\phi_1) \end{aligned} \quad (5.27)$$

$$a = \left(Y_1 - \frac{X_1 - 1}{l} \right) U_d \quad b = Y_2 + \frac{X_2}{l} \quad (5.28)$$

$$c = \frac{Y_1 U_d^2}{l} \quad d = \frac{Y_2 U_d}{l} \quad (5.29)$$

$$H_{\tilde{\xi}} = \begin{bmatrix} 0 & 0 & 1 & 0 & 0 & 0 \\ 0 & 0 & 0 & 1 & 0 & 0 \\ 0 & 0 & 0 & 0 & 1 & 0 \\ 0 & 0 & 0 & 0 & 0 & 1 \\ -k_{V_x} & 0 & -k_{p_x} & 0 & -k_{v_x} & 0 \\ 0 & -k_{V_y} & 0 & -k_{p_y} & 0 & -k_{v_y} \end{bmatrix}. \quad (5.30)$$

According to Assumption 2.3 ($Y_1, Y_2 > 0$), we have $c, d > 0$ and (5.17) implies $d > c \forall t$. We also have $a, b > 0 \forall t$ because of (5.20). Note also that from $\underline{U}_d \leq U_d \leq \bar{U}_d$ we have $\bar{a} > a > \underline{a}, \bar{c} > c > \underline{c}, \bar{d} > d > \underline{d}$ with $\bar{a}, \underline{a}, \bar{c}, \underline{c}, \bar{d}, \underline{d}$ positive constants. Finally, we have also that $\delta \leq \bar{\delta}$ since function of bounded signals. We now study the stability properties of the external dynamics (5.24b) and the tracking dynamics (Equation (5.24a) with $G(\tilde{z}, \tilde{\xi}_3, \tilde{\xi}_4)\tilde{\xi} = 0$) and then the stability properties of the total system (5.24).

5.5.1 The external dynamics

The equilibrium point of (5.24b) is $\tilde{\xi} = \mathbf{0}$. The matrix $H_{\tilde{\xi}}$ is Hurwitz for $k_{v_i}, k_{p_i}, k_{I_i}$ respecting (5.18-5.19).

5.5.2 The internal dynamics

Consider the

$$\dot{\tilde{z}}_1 = \tilde{z}_2 \quad (5.31a)$$

$$\begin{aligned} \dot{\tilde{z}}_2 = & -(a \cos(\tilde{z}_1) + b)\tilde{z}_2 - (c \cos(\tilde{z}_1) + d) \sin(\tilde{z}_1) \\ & + \delta(\dot{\phi}_1, \ddot{\phi}_1, \tilde{z}_1). \end{aligned} \quad (5.31b)$$

The subsystem (5.31) does not have an equilibrium point at the origin due to the presence of the disturbance $\delta(\cdot)$. Thus, we study the ultimately boundedness of the states \tilde{z}_1, \tilde{z}_2 .

Define the following Lyapunov function candidate (LFC)

$$W = \frac{1}{2} \tilde{z}_s^T \underbrace{\begin{bmatrix} a^2 + c & a \\ a & 1 \end{bmatrix}}_{P_{z_s}} \tilde{z}_s + (ab + d)(1 - \cos(\tilde{z}_1)). \quad (5.32)$$

We have that $W > 0 \forall (\cos(\tilde{z}_1), \sin(\tilde{z}_1), \tilde{z}_2) \in \mathbb{M} - \{[1, 0, 0]\}$ and $W = 0$ only for $(\cos(\tilde{z}_1), \sin(\tilde{z}_1), \tilde{z}_2) = (1, 0, 0)$. The time derivative is

$$\begin{aligned} \dot{W} = & -\tilde{z}_s^T \begin{bmatrix} a(d + c \cos(\tilde{z}_1)) & 0 \\ 0 & b \end{bmatrix} \tilde{z}_s + \frac{\partial W}{\partial \tilde{z}_s} \Delta \tilde{z} \\ & + \tilde{z}_s^T \begin{bmatrix} 2\dot{a}a + \dot{c} & \dot{a} \\ \dot{a} & 0 \end{bmatrix} \tilde{z}_s + (\dot{a}b + \dot{d})(1 - \cos(\tilde{z}_1)). \end{aligned} \quad (5.33)$$

Note that \dot{a} , \dot{c} , \dot{d} all depend on \dot{U}_d . Since $\dot{U}_d \leq \bar{U}_d^*$ due to Assumption 5.3, we have $\dot{a} \leq \bar{a}^*$, $\dot{c} \leq \bar{c}^*$, $\dot{d} \leq \bar{d}^*$. Then we have

$$\begin{aligned} \dot{W} \leq & -\tilde{z}_s^T \underbrace{\begin{bmatrix} a(d-c) & 0 \\ 0 & b \end{bmatrix}}_{Q_{\tilde{z}}} \tilde{z}_s + \frac{\partial W}{\partial \tilde{z}_s} \Delta_{\tilde{z}} + (\bar{a}^* b + \bar{d}^*)(1 - \cos(\tilde{z}_1)) \\ & + \frac{1}{2} \tilde{z}_s^T \underbrace{\begin{bmatrix} 2\bar{a}^* \bar{a} & \bar{a}^* \\ \bar{a}^* & 0 \end{bmatrix}}_{\Lambda_1} \tilde{z}_s + \frac{1}{2} \tilde{z}_s^T \underbrace{\begin{bmatrix} \bar{c}^* & 0 \\ 0 & 0 \end{bmatrix}}_{\Lambda_2} \tilde{z}_s. \end{aligned} \quad (5.34)$$

From the definition of $\Delta_{\tilde{z}}$ we have that

$$\left\| \frac{\partial W}{\partial \tilde{z}_s} \right\| \|\Delta_{\tilde{z}}\| \leq \alpha_1 \bar{\delta} \|\tilde{z}_s\| \quad (5.35)$$

where $\alpha_1 = \max\{1, a\}$ and $\bar{\delta}$ is the upperbound of $\delta(t)$, i.e. $\delta(t) \leq \bar{\delta}$ since $\delta(t)$ is function of bounded signals. Then we obtain

$$\dot{W} \leq - \underbrace{(\lambda_{Q_{\tilde{z}}}^{\min} - \lambda_{\Lambda_1}^{\max} - \lambda_{\Lambda_2}^{\max})}_{\sigma} \|\tilde{z}_s\|^2 + \alpha_1 \bar{\delta} \|\tilde{z}_s\| + 2(\bar{a}^* b + \bar{d}^*) \quad (5.36)$$

where $\lambda_{Q_{\tilde{z}}}^{\min} = \min\{a(d-c), b\}$ is the minimum eigenvalue of $Q_{\tilde{z}}$, $\lambda_{\Lambda_1}^{\max} = \frac{1}{2}(\bar{a} + \sqrt{\bar{a}^2 + 1})\bar{a}^*$ and $\lambda_{\Lambda_2}^{\max} = \frac{1}{2}\bar{c}^*$ are the maximum eigenvalues of Λ_1, Λ_2 , respectively. We have $\sigma > 0$ when (5.21) holds. Thus we obtain

$$\dot{W} \leq -(1-\theta)\sigma \|\tilde{z}_s\|^2 < 0 \quad \forall \|\tilde{z}_s\| \geq \frac{\alpha_1 \bar{\delta} + \sqrt{8\sigma(\bar{a}^* b + \bar{d}^*)} - \alpha_1^2}{2\theta\sigma} \quad (5.37)$$

where $0 < \theta < 1$.

The important conclusion which can draw from the considerations above is that the state \tilde{z}_2 , which is the only one that may grow unbounded on the manifold \mathbb{M} , stays bounded when the external dynamics is at steady state.

5.5.3 Stability of the complete system

Since (5.24b) is GES, there exist two positive definite matrices P_ξ , Q_ξ such that they satisfy the Lyapunov equation $H_\xi^T P_\xi + P_\xi H_\xi = -Q_\xi$. Thus, we choose the following LFC

$$V = W + \kappa \tilde{\xi}^T P_\xi \tilde{\xi} \quad (5.38)$$

where W is the same as in (5.32), and $\kappa > 0$ still to be determined. Deriving (5.38) along the directions of (5.24) we obtain

$$\dot{V} \leq -\sigma \|\tilde{z}_s\|^2 - \kappa \tilde{\xi}^T Q_\xi \tilde{\xi} + \frac{\partial W}{\partial \tilde{z}} G(\cdot) \tilde{\xi} + \frac{\partial W}{\partial \tilde{z}_2} \delta(\cdot) \quad (5.39)$$

The following bounds hold for $G(\cdot)$ and W :

$$G(\tilde{z}, \tilde{\xi}_3, \tilde{\xi}_4) \leq G_1(\|\tilde{\xi}\|) \|\tilde{z}_s\| + G_2(\|\tilde{\xi}\|) \leq \bar{G}_1 \|\tilde{z}_s\| + \bar{G}_2 \quad (5.40)$$

$$\left\| \frac{\partial W}{\partial \tilde{z}} \right\| \leq \|\tilde{z}_s\| \left\| \begin{bmatrix} a^2 + c + \frac{ab+d}{2} & a \\ a & 1 \end{bmatrix} \right\| \leq \alpha_2 \|\tilde{z}_s\|, \quad (5.41)$$

where $\bar{G}_1 = G_1(\bar{\xi})$, $\bar{G}_2 = G_2(\bar{\xi})$, and $\bar{\xi}$ is the upperbound of $\|\xi\|$. Let $\lambda_{P_{z_s}}^{\min}$, $\lambda_{P_\xi}^{\min}$, $\lambda_{Q_\xi}^{\min}$ denote the minimal eigenvalue of P_{z_s} , P_ξ , Q_ξ respectively. The closed-loop external dynamics (5.24b) is GES, therefore there exists a time t^* such that for all $t \geq t^*$: $\|\tilde{\xi}(t)\| \leq \sigma/(2\alpha_2\bar{G}_1)$. For $t \leq t^*$ and

$$\kappa > \frac{\alpha_2^2 \bar{G}_2^2}{\sigma \lambda_{Q_\xi}^{\min}} + \frac{2\alpha_2 \bar{G}_1 \bar{\xi} \lambda_{P_\xi}^{\min}}{\lambda_{Q_\xi}^{\min} \lambda_{P_{z_s}}^{\min}} \quad (5.42)$$

we have

$$\begin{aligned} \dot{V} &\leq -\sigma \|\tilde{z}_s\|^2 - \kappa \tilde{\xi}^T Q_\xi \tilde{\xi} \\ &\quad + \alpha_2 \|\tilde{z}_s\| (\bar{G}_1 \|\tilde{z}_s\| + \bar{G}_2) \tilde{\xi} + \alpha_1 \bar{\delta} \|\tilde{z}_s\| \\ &\leq -\sigma \|\tilde{z}_s\|^2 + \alpha_2 \bar{G}_1 \bar{\xi} \|\tilde{z}_s\|^2 + \alpha_2 \bar{G}_2 \|\tilde{z}_s\| \|\tilde{\xi}\| \\ &\quad - \kappa \lambda_{Q_\xi}^{\min} \|\tilde{\xi}\|^2 + \alpha_1 \bar{\delta} \|\tilde{z}_s\| \\ &\leq -\frac{1}{2} \sigma \|\tilde{z}_s\|^2 - \left(\frac{\alpha_2^2 \bar{G}_2^2}{\sigma \lambda_{Q_\xi}^{\min}} + \frac{2\alpha_2 \bar{G}_1 \bar{\xi} \lambda_{P_\xi}^{\min}}{\lambda_{Q_\xi}^{\min} \lambda_{P_{z_s}}^{\min}} \right) \lambda_{Q_\xi}^{\min} \|\tilde{\xi}\|^2 \\ &\quad + \alpha_2 \bar{G}_1 \bar{\xi} \|\tilde{z}_s\|^2 + \alpha_2 \bar{G}_2 \|\tilde{z}_s\| \|\tilde{\xi}\| \\ &\quad - \frac{1}{2} \sigma \|\tilde{z}_s\|^2 + \alpha_1 \bar{\delta} \|\tilde{z}_s\| \end{aligned} \quad (5.43)$$

for $\|\tilde{z}_s\| \geq \frac{2\alpha_1 \bar{\delta}}{\sigma}$ we have

$$\begin{aligned} \dot{V} &\leq -\frac{1}{2} \sigma \|\tilde{z}_s\|^2 + \alpha_2 \bar{G}_2 \|\tilde{z}_s\| \|\tilde{\xi}\| - \frac{\alpha_2^2 \bar{G}_2^2}{\sigma} \|\tilde{\xi}\|^2 \\ &\quad - \frac{2\alpha_2 \bar{G}_1 \bar{\xi} \lambda_{P_\xi}^{\min}}{\lambda_{P_{z_s}}^{\min}} \|\tilde{\xi}\|^2 + \alpha_2 \bar{G}_1 \bar{\xi} \|\tilde{z}_s\|^2 \\ &\leq \frac{2\alpha_2 \bar{G}_1 \bar{\xi} \lambda_{P_\xi}^{\min}}{\lambda_{P_{z_s}}^{\min}} \|\tilde{\xi}\|^2 + \alpha_2 \bar{G}_1 \bar{\xi} \|\tilde{z}_s\|^2 \\ &\leq \frac{2\alpha_2 \bar{G}_1 \bar{\xi} \lambda_{P_\xi}^{\min}}{\lambda_{P_{z_s}}^{\min}} \|\tilde{\xi}\|^2 + \alpha_2 \bar{G}_1 \bar{\xi} \|\tilde{z}_s\|^2 \\ &\quad \pm \frac{2\alpha_2 \bar{G}_1 \bar{\xi}}{\lambda_{P_{z_s}}^{\min}} (ad + c)(1 - \cos(\tilde{z}_1)) \\ &\leq \frac{2\alpha_2 \bar{G}_1 \bar{\xi}}{\lambda_{P_{z_s}}^{\min}} V + 4 \frac{\alpha_2 \bar{G}_1 \bar{\xi}}{\lambda_{P_{z_s}}^{\min}} (ad + c), \end{aligned} \quad (5.44)$$

so for $t < t^* \wedge \|\tilde{z}_s\| \geq \frac{2\alpha_1\bar{\delta}}{\sigma}$ the trajectories are bounded. For $t < t^* \wedge \|\tilde{z}_s\| < \frac{2\alpha_1\bar{\delta}}{\sigma}$ we have

$$\begin{aligned}
 \dot{V} &\leq -\frac{1}{2}\sigma\|\tilde{z}_s\|^2 + \alpha_2\bar{G}_2\|\tilde{z}_s\|\|\tilde{\xi}\| - \frac{\alpha_2^2\bar{G}_2^2}{\sigma}\|\tilde{\xi}\|^2 \\
 &\quad - \frac{\alpha_2\bar{G}_1\bar{\xi}\lambda_{P_{z_s}}^{\min}}{\lambda_{P_{z_s}}^{\min}}\|\tilde{\xi}\|^2 + \alpha_2\bar{G}_1\bar{\xi}\|\tilde{z}_s\|^2 + \alpha_1\bar{\delta}\|\tilde{z}_s\| \\
 &\leq \frac{\alpha_2\bar{G}_1\bar{\xi}\lambda_{P_{z_s}}^{\min}}{\lambda_{P_{z_s}}^{\min}}\|\tilde{\xi}\|^2 + \alpha_2\bar{G}_1\bar{\xi}\|\tilde{z}_s\|^2 + \bar{\delta}\frac{2\alpha_1^2}{\sigma} \\
 &\leq \alpha_2\bar{G}_1\bar{\xi}\|\tilde{z}_s\|^2 + \frac{2\alpha_2\bar{G}_1\bar{\xi}\lambda_{P_{z_s}}^{\min}}{\lambda_{P_{z_s}}^{\min}}\|\tilde{\xi}\|^2 + \bar{\delta}\frac{2\alpha_1^2}{\sigma} \\
 &\quad \pm \frac{2\alpha_2\bar{G}_1\bar{\xi}}{\lambda_{P_{z_s}}^{\min}}(ad+c)(1-\cos(\tilde{z}_1)) \\
 &\leq \frac{2\alpha_2\bar{G}_1\bar{\xi}}{\lambda_{P_{z_s}}^{\min}}V + \bar{\delta}\frac{2\alpha_1^2}{\sigma} + 4\frac{\alpha_2\bar{G}_1\bar{\xi}}{\lambda_{P_{z_s}}^{\min}}(ad+c), \tag{5.45}
 \end{aligned}$$

so $V(t)$ remains bounded also for the case $t \leq t^* \wedge \|\tilde{z}_s\| < \frac{2\alpha_1}{\sigma}$, meaning that the trajectories are bounded for any $t < t^*$.

For $t \geq t^*$ we have

$$\begin{aligned}
 \dot{V} &\leq -\sigma\|\tilde{z}_s\|^2 - \kappa\lambda_{Q_\xi}^{\min}\|\tilde{\xi}\|^2 + \alpha_2\|\tilde{z}_s\|(\bar{G}_1\|\tilde{z}_s\| + \bar{G}_2)\tilde{\xi} + \alpha_1\bar{\delta}\|\tilde{z}_s\| \\
 &\leq -\frac{1}{2}\sigma\|\tilde{z}_s\|^2 + \alpha_2\bar{G}_2\|\tilde{z}_s\|\|\tilde{\xi}\| - \kappa\lambda_{Q_\xi}^{\min}\|\tilde{\xi}\|^2 + \alpha_1\bar{\delta}\|\tilde{z}_s\| \\
 &\leq -\frac{1}{2}\theta\sigma\|\tilde{z}_s\|^2 + \alpha_2\bar{G}_2\|\tilde{z}_s\|\|\tilde{\xi}\| - \kappa\lambda_{Q_\xi}^{\min}\|\tilde{\xi}\|^2 \\
 \forall\|\tilde{z}_s\| &> \frac{2\alpha_1\bar{\delta}}{(1-\theta)\sigma} \wedge 0 < \theta < 1, \tag{5.46}
 \end{aligned}$$

which is negative definite for $\kappa > \alpha_2^2\bar{G}_2^2/(\sigma\lambda_{Q_\xi}^{\min})$. We can conclude that $\tilde{\xi} \rightarrow 0$ globally exponentially while the states z_1, z_2 are ultimately bounded. \square

5.6 The particular case of straight-line paths

Now we draw our attention to straight-line paths and constant desired forward velocity. Without loss of generality, consider a path which is aligned along the x axis of the NED frame. This implies $\dot{\xi}_{3_d} = \dot{\xi}_{4_d} = \xi_{4_d} = 0$. Furthermore, since we assume that the desired forward velocity is constant we have $\xi_{3_d} = 0$. As a result, we have $\delta(\phi_1, \ddot{\phi}_1, \sin(\tilde{z}_1)) = 0$ and ϕ_1 is a constant angle. Under this conditions, we can derive the following corollary from Theorem 5.1.

Corollary 5.1. *Consider an under-actuated marine vehicle described by the model (5.1). Consider the hand position point $\mathbf{h} = [x_1, y_1]^T = [x + l \cos(\psi), y + l \sin(\psi)]^T$, where $[x, y]^T$ is the position of the pivot point of the ship, l is a positive constant and ψ is the yaw angle of the vehicle. Then define $U_d = \sqrt{(u_d - V_x)^2 + V_y^2} > 0$ as*

the desired relative velocity magnitude and $\phi = \arctan\left(\frac{-V_y}{u_d - V_x}\right)$ as the crab angle. If Assumption 5.3 is satisfied and if

$$0 < U_d < \frac{Y_2}{Y_1} \quad (5.47)$$

$$k_{v_i} > 0, k_{p_i} > 0, k_{I_i} > 0, i \in \{x, y\} \quad (5.48)$$

$$k_{v_i} k_{p_i} > k_{I_i} \quad i \in \{x, y\} \quad (5.49)$$

$$l > \max\left\{\frac{m_{22}}{m_{23}}, -\frac{X_2}{Y_2}\right\} \quad (5.50)$$

then the controller (5.8), where the new inputs μ_1, μ_2 are given by (5.14), guarantees the achievement of the control objectives (5.13). In particular,

$$(z_1, z_2, \xi_1, \xi_2, \xi_3, \xi_4) \rightarrow (\phi, 0, u_d t, 0, u_d - V_x, -V_y)$$

almost-globally asymptotically. Furthermore, the steady state values of the integral variables give an estimate of the ocean current:

$$\hat{V}_x = \lim_{t \rightarrow \infty} \frac{k_{I_x}(\xi_{1_I} - \xi_{1_{I_d}})}{k_{v_x}} + u_d, \quad \hat{V}_y = \lim_{t \rightarrow \infty} \frac{k_{I_y}(\xi_{2_I} - \xi_{2_{I_d}})}{k_{v_y}}. \quad (5.51)$$

Proof. The proof follows along the lines of the proof of Theorem 5.1.

5.6.1 The external dynamics

The same considerations given in 5.5.1 hold here.

5.6.2 The internal dynamics

The tracking dynamics now becomes

$$\dot{\tilde{z}}_1 = \tilde{z}_2 \quad (5.52a)$$

$$\dot{\tilde{z}}_2 = -(a \cos(\tilde{z}_1) + b)\tilde{z}_2 - (c \cos(\tilde{z}_1) + d) \sin(\tilde{z}_1). \quad (5.52b)$$

The system (5.52) can be studied on the manifold $\mathbb{M} = \mathbb{S} \times \mathbf{R} = \{(\cos(\theta), \sin(\theta), r) \mid \theta \in \mathbf{R}, r \in \mathbf{R}\}$. The system (5.52) has two equilibria, and they are

$$E_s = (1, 0, 0) \in \mathbb{M}, \quad E_u = (-1, 0, 0) \in \mathbb{M}. \quad (5.53)$$

The point E_s is a stable node, while E_u is a saddle point since we assumed $d > c$. Note that E_u is a hyperbolic equilibrium. Choosing (5.32) as Lyapunov function we obtain

$$\dot{W} = -\tilde{z}_s^T Q_{\tilde{z}} \tilde{z}_s \leq 0 \quad \forall (\sin(\tilde{z}_1), \tilde{z}_2) \neq (0, 0). \quad (5.54)$$

Equation 5.54 implies that the state $(\sin(\tilde{z}_1), \tilde{z}_2) = (0, 0)$ is GAS. However, $\sin(\tilde{z}_1) = 0$ corresponds either to $\cos(\tilde{z}_1) = 1$ or $\cos(\tilde{z}_1) = -1$ on the one-dimensional unit sphere. That is, if the vehicle is required to move along a straight-line path it may move forward ($\cos(\psi) = 1$) or backwards ($\cos(\psi) = -1$). But, linearizing

(5.52) about the origin, we have that the equilibrium $E_u = \{\cos(\tilde{z}_1), \sin(\tilde{z}_1), \tilde{z}_2) = (-1, 0, 0)\} \in \mathbb{M}$ is unstable and hyperbolic. Then, recalling Theorem A.2 we deduce that E_u is characterized by a stable and an unstable manifold $\mathcal{W}_u^s, \mathcal{W}_u^u$, respectively. The unstable manifold \mathcal{W}_u^u is tangent to the eigenspace spanned by the positive real part eigenvalue of the Jacobian matrix of the system (5.52) evaluated at E_u . This manifold is therefore one-dimensional and converges to the only other equilibrium point of the system, that is $E_s = \{\cos(\tilde{z}_1), \sin(\tilde{z}_1), \tilde{z}_2) = (1, 0, 0)\} \in \mathbb{M}$. The stable manifold \mathcal{W}_u^s is also one-dimensional since it is spanned by the negative real part eigenvalue of the Jacobian matrix of (5.52). Since the system (5.52) evolves on the manifold $\mathbb{M} = \mathbb{S} \times \mathbb{R}$, which is 2-dimensional (it is a "pipe-shaped" manifold, that is, it is a cylindrical surface in the space), we have that \mathcal{W}_u^s has one dimension less than \mathbb{M} and has therefore zero Lebesgue measure. At this point we can conclude that all the trajectories which do not start on \mathcal{W}_u^s converge to the point E_s . Furthermore, since \mathcal{W}_u^s has zero Lebesgue measure, we can say that E_s is *almost*-GAS.

5.6.3 Stability of the total system

The stability of the total system follows from the same considerations as in Subsection 5.5.3. \square

5.7 Simulations

In this section we present the results of a simulation case study. We consider the model of the Light Autonomous Underwater Vehicle (LAUV) of the Laboratório de System y Tecnologia Subaquatica (LSTS) at the University of Porto. The model of the vehicle is give [38] and reported in Appendix B.

We consider that the vehicle has to track a circle centered at the origin of the NED frame. We consider a circle with radius $R = 80$ m. The circle is parametrized by the time t and the the vehicle has to travel with constant tangential velocity to the circle such that it completes a round in $T = 80$ s. The desired signals are

$$\xi_{1_d} = R \cos(\omega t) \tag{5.55a}$$

$$\xi_{2_d} = R \sin(\omega t) \tag{5.55b}$$

$$\xi_{3_d} = -R\omega \sin(\omega t) \tag{5.55c}$$

$$\xi_{4_d} = R\omega \cos(\omega t) \tag{5.55d}$$

$$\dot{\xi}_{3_d} = -R\omega^2 \cos(\omega t) \tag{5.55e}$$

$$\dot{\xi}_{4_d} = -R\omega^2 \sin(\omega t) \tag{5.55f}$$

where $\omega = -|1/T| = -0.0125$ 1/s . Note that the negative sign just implies that the ship has to travel counterclockwise along the circle.

We choose the constant $l = 1$ m in (5.3a) The initial conditions of the vehicle are summarized in Table 5.1. From Table 5.1 we have that

Table 5.1: Initial conditions.

t_0	$x _{t_0}$ m	$y _{t_0}$ m	$\psi _{t_0}$ rad	u_r m/s	v_r m/s	r rad/s
t_0	0	140	$-\pi$	0	0	0

$$\xi_{1_0} = 0 \text{ m} \quad (5.56a)$$

$$\xi_{2_0} = 139 \text{ m} \quad (5.56b)$$

$$\xi_{3_0} = 0 \text{ m/s} \quad (5.56c)$$

$$\xi_{4_0} = 0 \text{ m/s} \quad (5.56d)$$

$$z_{1_0} = 0 \text{ rad} \quad (5.56e)$$

$$z_{2_0} = 0 \text{ rad/s.} \quad (5.56f)$$

The gains in (5.14) are

$$k_{p_x} = k_{p_y} = 0.5 \quad (5.57a)$$

$$k_{v_x} = k_{v_y} = 10 \quad (5.57b)$$

$$k_{I_x} = k_{I_y} = 0.007. \quad (5.57c)$$

The ocean current is $\mathbf{V} = [-0.05, 0.16]^T$ m/s. According to the choice of the gains and the properties of the path described above, the conditions under which Theorem 5.1 holds are satisfied.

The results of the simulation are shown in Figures 5.2-5.5. In Figure 5.2 we can see the motion of the vehicle. We see that the vehicle converges to the trajectory counteracting the ocean current. In Figure 5.3, the time evolution of the error states $\tilde{\xi}_1, \tilde{\xi}_2, \tilde{\xi}_3, \tilde{\xi}_4$ confirms that the trajectory tracking task is fulfilled. In fact, all the error states converge to zero. Figure 5.4 shows the the ocean current estimates calculated from the integral states. It is clear that when the vehicle reaches the steady state the ocean current estimate error converges to zero. Finally, in Figure 5.5 the relative surge velocity u_r , the relative sway velocity v_r and the yaw rate r are shown. Note that u_r and v_r are not constants. In fact, since the ocean current is not constant in the local frame even though it is constant in the NED frame, we have that u_r, v_r have to be time varying in order to make the vehicle travel with absolute velocity constant and tangential to the circle as required. This is clear also from the inversion of the change of coordinates (5.5). In fact it results in

$$u_r = (\xi_3 - V_x) \cos(\psi) + (\xi_4 - V_y) \sin(\psi) \quad (5.58a)$$

$$v_r = -(\xi_3 - V_x) \sin(\psi) + (\xi_4 - V_y) \cos(\psi) - lr. \quad (5.58b)$$

Finally note that from Figure 5.5 we see that $r = z_2$ is bounded as expected.

5.8 Conclusions

In this chapter we considered the relative velocity model of a marine vehicle. In particular, the model of an ASV or an AUV moving on the horizontal plane. We considered that a constant and irrotational ocean current affects the vehicle. We

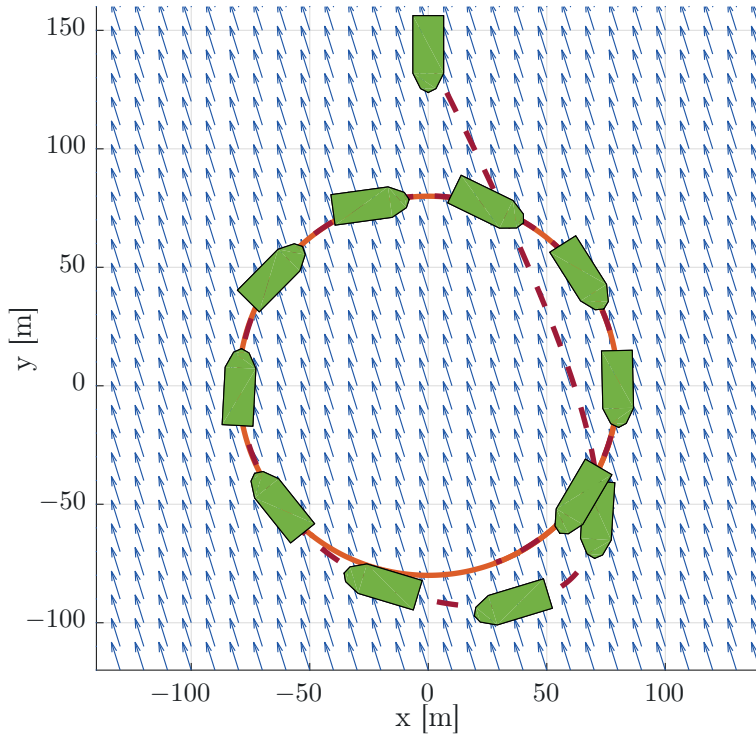


Figure 5.2: Motion of the ship.

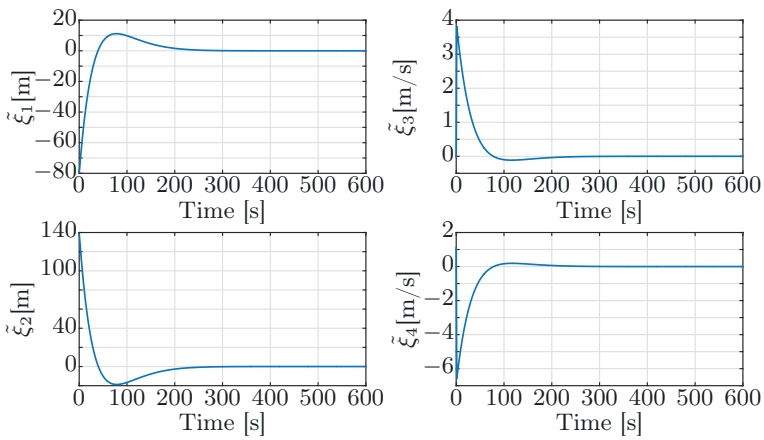


Figure 5.3: Time evolution of the errors states.

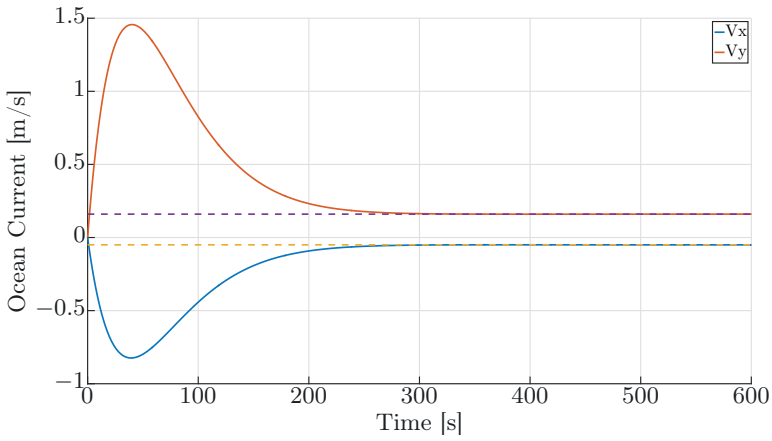


Figure 5.4: Ocean current estimates.

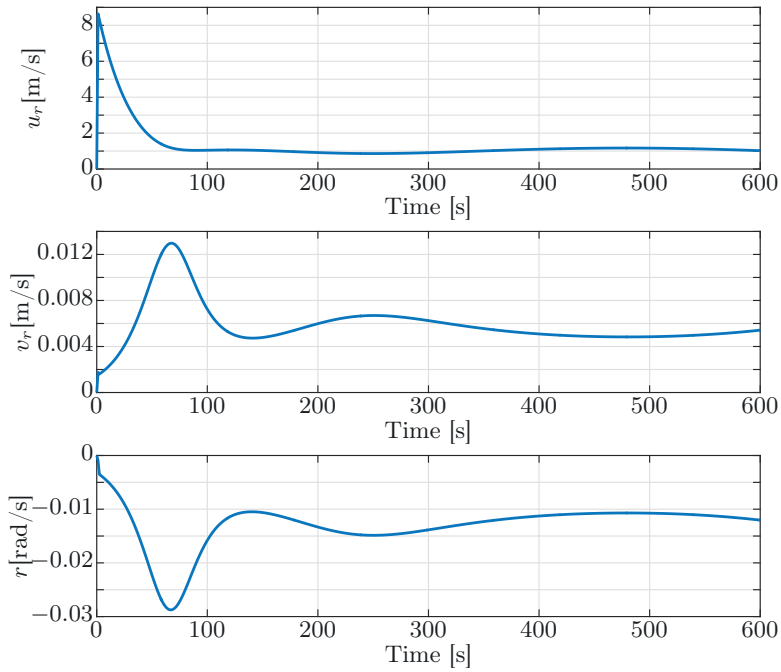


Figure 5.5: Time evolution of the surge velocity, sway velocity and yaw rate.

dealt with the trajectory tracking problem, that is we wanted the vehicle to follow a given trajectory parametrized by the time t . The solution which we proposed is based on a novel approach for marine vehicles. The approach was inspired by the work of Lawton and Beard [82]. In particular, we extended the definition of hand position, given in [82] for ground vehicles, to ASVs and AUVs. Then we used the input-output feedback linearization method using the hand position point motion as output. In this way we transformed the nonlinear model of the AUV in a model with a linear external dynamics and a nonlinear internal dynamics. The advantage of the transformed model is that we had to deal with a double integrator dynamics, that is, the linear external dynamics, for control purposes. The price to pay is that the stability properties of the nonlinear internal dynamics had to be carefully studied since the internal dynamics are affected by the control input designed for the linear external dynamics. The proposed controller makes the vehicle achieve the control objectives. We showed that the closed-loop system has a GES external dynamics and internal dynamics with ultimately bounded states. Finally, we have also shown that in case of straight-line paths the closed-loop system is *almost*-GAS. That is, the control objectives are achieved for almost all the initial conditions and the states of the internal dynamics converge to constant signals. In particular, the yaw rate converges to zero and the yaw angle converges to a constant angle, the crab angle, dependent on the ocean current components and the desired linear velocities.

5.A Equations

The nonlinear terms appearing in (5.1) and (5.24b) are reported here:

$$F_{u_r}(v_r, r) \triangleq \frac{1}{m_{11}}(m_{22}v_r + m_{23}r)r - \frac{d_{11}}{m_{11}}u_r, \quad (5.59)$$

$$X_1(\mathbf{M}) \triangleq \frac{m_{11}m_{33} - m_{23}^2}{m_{22}m_{33} - m_{23}^2} \quad X_2(\mathbf{M}, \mathbf{D}) \triangleq \frac{d_{33}m_{23} - d_{23}m_{33}}{m_{22}m_{33} - m_{23}^2} \quad (5.60)$$

$$Y_1(\mathbf{M}) \triangleq \frac{(m_{11} - m_{22})m_{23}}{m_{22}m_{33} - m_{23}^2} \quad Y_2(\mathbf{M}, \mathbf{D}) \triangleq \frac{d_{22}m_{33} - d_{32}m_{23}}{m_{22}m_{33} - m_{23}^2} \quad (5.61)$$

$$X(u_r) \triangleq -X_1u_r + X_2 \quad Y(u_r) \triangleq -Y_1u_r - Y_2, \quad (5.62)$$

$$F_r(u_r, v_r, r) \triangleq \frac{m_{23}d_{22} - m_{22}(d_{32} + (m_{22} - m_{11})u_r)}{m_{22}m_{33} - m_{23}^2}v_r \quad (5.63)$$

$$+ \frac{m_{23}(d_{23} + m_{11}u_r) - m_{22}(d_{33} + m_{23}u_r)}{m_{22}m_{33} - m_{23}^2}r, \quad (5.64)$$

$$G(\tilde{z}, \tilde{\xi}_3, \tilde{\xi}_4) \triangleq \begin{bmatrix} 0 & 0 & 0 & 0 & 0 & 0 \\ -\frac{\sin(\tilde{z}_1)}{l} & \frac{\cos(\tilde{z}_1)}{l} & 0 & 0 & \alpha(\tilde{z}, \tilde{\xi}_3) & \beta(\tilde{z}, \tilde{\xi}_3, \tilde{\xi}_4) \end{bmatrix} \quad (5.65)$$

$$\begin{aligned} \alpha(\tilde{z}, \tilde{\xi}_3) \triangleq & -((Y_1U_d \cos(\tilde{z}_1)^2 + Y_1U_d \cos(\tilde{z}_1) \sin(\tilde{z}_1) \\ & + Y_2 \sin(\tilde{z}_1) + Y_2\tilde{\xi}_3 \sin(\tilde{z}_1) \cos(\tilde{z}_1) \\ & + \left(-Y_1 + \frac{X_1 - 1}{d}\right) \tilde{z}_2 \cos(\tilde{z}_1)) \end{aligned} \quad (5.66)$$

$$\begin{aligned} \beta(\tilde{z}, \tilde{\xi}_3, \tilde{\xi}_4) \triangleq & Y_1U_d \sin(\tilde{z}_1) \cos(\tilde{z}_1) + Y_1U_d \cos(\tilde{z}_1)^2 \\ & + Y_2 \cos(\tilde{z}_1) + Y_1\tilde{\xi}_3 \sin(\tilde{z}_1) + Y_1 \cos(\tilde{z}_1)^2 \tilde{\xi}_3 \\ & - Y_1 \cos(\tilde{z}_1) \sin(\tilde{z}_1) \tilde{\xi}_4 + \left(-Y_1 + \frac{X_1 - 1}{d}\right) \tilde{z}_2 \sin(\tilde{z}_1) \end{aligned} \quad (5.67)$$

Chapter 6

Path following of marine vehicles

In this chapter we address the path following control problem of curved and straight-line paths for ASVs and AUVs. We consider paths that are parameterized by the arc length s . The control strategy proposed in this chapter builds on the approach presented in Chapter 5. In particular, we use the same input-output feedback linearizing controller presented in Section 5.2. The main contribution of this chapter is a guidance control strategy for parametrized curved paths which depends on the Euclidean distance of the vehicle from the path, and propose an update law for the path variable s which depends on the Euclidean distance from the path. It is also considered that a constant and unknown ocean current affects the system. We show that the hand position point converges exponentially to the desired path while the states of the internal dynamics are ultimately bounded. Furthermore, it is shown that for the case of straight-line paths the closed-loop system is *almost-global asymptotic stability* (AGAS). Finally, we consider also the case of unparametrized straight-line paths. This case is of particular interest for practical applications, and we show that we can deal with it using the approach presented in this chapter. Simulation case studies and experimental results are presented in order to validate the theoretical results. The structure and results of this chapter are similar to Chapter 5 since the control approach is the same as in Chapter 5. However, the hand position point approach is used here for solving the path following control problem.

The work discussed in this chapter is based on [110, 112].

The chapter is organized as follows: Section 6.1 presents the model of the class of vehicles which is considered; Section 6.2 recalls the definition of the hand position point from Chapter 5 and illustrates our general approach; in Section 6.3 the control problem is described and formalized; Section 6.4 introduces the controller proposed in order to solve the path following problem; in Section 6.5 the main result of this chapter is given; Section 6.6 deals with the special case of straight-line paths; Section 6.7 shows how the results of this chapter can be applied also to the case of unparametrized straight-line paths; in Section 6.8 two simulation case studies are presented. One using simulations performed with Matlab for the case of curved paths and one using the simulator *DUNE* for the case of straight-line paths; Section 6.9 presents experimental results for straight-line paths; finally, Section 6.10 gives

the conclusions.

6.1 Vehicle model

In this section we recall the model for ASVs and AUVs moving in the horizontal plane introduced in Chapter 2.

We consider Assumptions 2.1-2.3 to hold and the model (2.11) in component form:

$$\dot{x} = u_r \cos(\psi) - v_r \sin(\psi) + V_x \quad (6.1a)$$

$$\dot{y} = u_r \sin(\psi) + v_r \cos(\psi) + V_y \quad (6.1b)$$

$$\dot{\psi} = r \quad (6.1c)$$

$$\dot{u}_r = F_{u_r}(v_r) + \tau_u \quad (6.1d)$$

$$\dot{v}_r = X(u_r)r + Y(u_r)v_r \quad (6.1e)$$

$$\dot{r} = F_r(u_r, v_r, r) + \tau_r. \quad (6.1f)$$

The states x, y give the position of the vehicle in the NED frame, the state ψ is the yaw angle and gives the orientation of the vehicle in the NED frame. The states u_r, v_r are the surge and sway relative velocity, respectively. The state r is the yaw rate. The ocean current disturbance in the NED frame is given by $\mathbf{V} = [V_x, V_y]^T$. The expressions for $F_{u_r}(u_r), F_r(u_r, v_r, r)$ are given in Appendix 5.A. Furthermore, $X(u_r) = -X_1 u_r + X_2, Y(u_r) = -Y_1 u_r - Y_2$ and X_1, X_2, Y_1, Y_2 are reported in Appendix 5.A. We consider the following assumption to hold:

Assumption 6.1. *The ocean current in the inertial frame $\mathbf{V} = [V_x, V_y]^T$ is constant, irrotational and bounded, i.e., $\exists V_{\max} \geq 0$ such that $\sqrt{V_x^2 + V_y^2} \leq V_{\max}$.*

6.2 Hand position: line of reasoning

Before describing the path following problem, in this section we recall the approach based on the definition of the hand position point already introduced in Chapter 5. The reader is referred to Section 5.2 for a more detailed discussion.

Inspired by the work of Lawton and Beard [82], we define the hand position point as $\mathbf{h} = [\xi_1, \xi_2]^T$ with

$$\xi_1 = x + l \cos(\psi) \quad (6.2)$$

$$\xi_2 = y + l \sin(\psi), \quad (6.3)$$

where x, y give the position of the pivot point in the NED frame, ψ is the yaw angle and $l > 0$ is a constant. An illustration of the hand position point is given in Figure 6.1.

In Section 5.2 we have already shown that (6.1) is input-output feedback linearizable with output \mathbf{h} since the vector relative degree $\rho = [\rho_{\xi_1}, \rho_{\xi_2}]^T$ is well

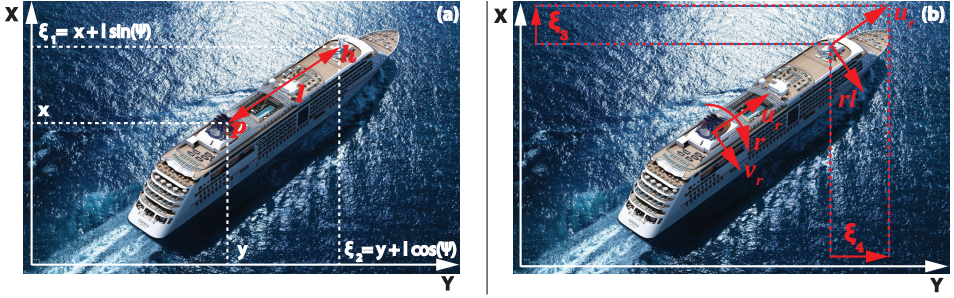


Figure 6.1: The hand position point.

defined if $l > 0$. Therefore we can apply the following change of coordinates

$$z_1 = \psi \quad (6.4a)$$

$$z_2 = r \quad (6.4b)$$

$$\xi_1 = x + l \cos(\psi) \quad (6.4c)$$

$$\xi_2 = y + l \sin(\psi) \quad (6.4d)$$

$$\xi_3 = u_r \cos(\psi) - v_r \sin(\psi) - rl \sin(\psi) \quad (6.4e)$$

$$\xi_4 = u_r \sin(\psi) + v_r \cos(\psi) + rl \cos(\psi). \quad (6.4f)$$

together with the feedback linearizing controller

$$\begin{bmatrix} \tau_u \\ \tau_r \end{bmatrix} = \begin{bmatrix} \cos(\psi) & -l \sin(\psi) \\ \sin(\psi) & l \cos(\psi) \end{bmatrix}^{-1} \begin{bmatrix} -F_{\xi_3}(z_1, \xi_3, \xi_4) + \mu_1 \\ -F_{\xi_4}(z_1, \xi_3, \xi_4) + \mu_2 \end{bmatrix}. \quad (6.5)$$

We obtain

$$\dot{z}_1 = z_2 \quad (6.6a)$$

$$\begin{aligned} \dot{z}_2 = & - \left(\left(Y_1 - \frac{X_1 - 1}{l} \right) U \cos(z_1 - \phi) + Y_2 + \frac{X_2}{l} \right) z_2 \\ & - \left(\frac{Y_1}{l} U \cos(z_1 - \phi) + \frac{Y_2}{l} \right) U \sin(z_1 - \phi) \\ & - \frac{\mu_1 \sin(z_1)}{l} + \frac{\mu_2 \cos(z_1)}{l} \end{aligned} \quad (6.6b)$$

$$\dot{\xi}_1 = \xi_3 + V_x \quad (6.6c)$$

$$\dot{\xi}_2 = \xi_4 + V_y \quad (6.6d)$$

$$\dot{\xi}_3 = \mu_1 \quad (6.6e)$$

$$\dot{\xi}_4 = \mu_2 \quad (6.6f)$$

where

$$U = \sqrt{\xi_3^2 + \xi_4^2} \quad (6.7)$$

$$\phi = \arctan \left(\frac{\xi_4}{\xi_3} \right). \quad (6.8)$$

The terms μ_1, μ_2 in (6.5) are new inputs which are to be defined in Section 6.4 in order to solve the path following problem. Note that z_1 appears only as an argument of trigonometric functions with period 2π . Therefore, we can consider (6.6a-6.6b) to take values on the manifold $\mathbb{M} = \mathbb{S} \times \mathbb{R}$ where \mathbb{S} is the one-dimensional sphere.

The main advantage of choosing \mathbf{h} as output is clear from (6.6). In fact, the transformed model (6.6) is characterized by a linear external dynamics (6.6c-6.6f) and a nonlinear internal dynamics (6.6a-6.6b) as common for feedback linearized systems. Therefore, as opposed to considering the model (6.1), we can consider the external dynamics which are linear, for control purposes. The drawback is that the inputs μ_1, μ_2 , which are to be designed in order to fulfill the control objectives, are affecting also the internal dynamics (6.6a-6.6b), and we have carefully to check the internal stability properties of the states z_1, z_2 .

6.3 Problem definition and control objectives

In this section we formalize the path following control problem.

The path following task requires the vehicle to follow a given curve $\gamma(s) = \{(x(s), y(s)) | s \in \mathbb{R}\}$, where s is a scalar parameter, and travel along the curve with a constant velocity $\bar{U} > 0$ in the global frame. This task can be fulfilled by an under-actuated vehicle if its total velocity U_t is tangential to the path, where

$$U_t = \sqrt{(\xi_3 + V_x)^2 + (\xi_4 + V_y)^2}.$$

The main difference between the path following task and the trajectory tracking discussed in Section 6.3 is that for the path following the path is parametrized by a generic variable s and not necessarily by the time t . This implies that the vehicle is not required to be in a given position along the curve at a specific time instant t , instead the vehicle is required just to converge to the path and move along it with a prescribed velocity. We consider that $\gamma(s) \in \mathcal{C}^2$, this can be formalized by the following assumption

Assumption 6.2. *The path $\gamma(s)$ is a \mathcal{C}^2 function.*

Remark 6.1. *This assumption implies that*

$$\frac{\partial x(s)}{\partial s}, \frac{\partial y(s)}{\partial s}, \frac{\partial^2 x(s)}{\partial s^2}, \frac{\partial^2 y(s)}{\partial s^2}$$

are all continuous. Therefore the curvature κ of $\gamma(s)$ is continuous and the curve is smooth.

We assume also that the path $\gamma(s)$ is parametrized by the arc length s . This way the tangent vector T is given by

$$T = \left[\frac{\partial x(s)}{\partial s} \quad \frac{\partial y(s)}{\partial s} \right]^T$$

and it is a unit vector, that is

$$\|T\| = \sqrt{\left(\frac{\partial x(s)}{\partial s}\right)^2 + \left(\frac{\partial y(s)}{\partial s}\right)^2} = 1.$$

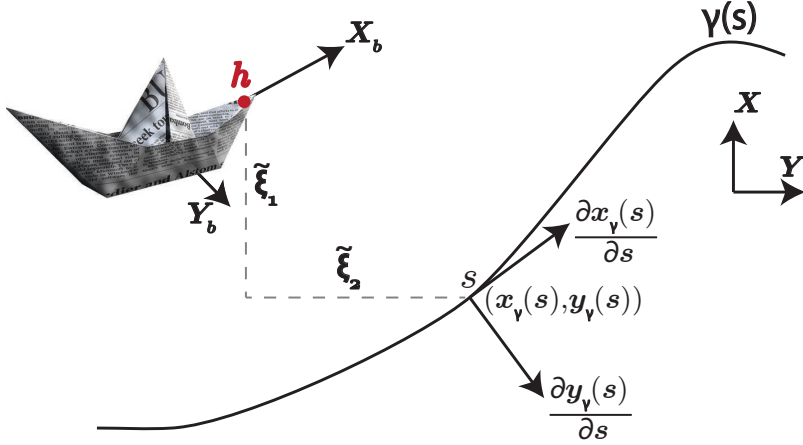


Figure 6.2: Path following.

According to this choice of the parametrization, we can consider that a virtual frame VF moves along $\gamma(s)$. The position along the curve of the origin of VF , which we call x_γ, y_γ , is defined by the parameter s . The x axis of VF is given by the unit tangent vector to the curve T . The y axis is given by the normal vector N and it is chosen by rotating clock-wise T of $\pi/2$ radian (recall that the z axis of the NED frame points downwards). The velocity in the NED frame with which VF moves along $\gamma(s)$ is given by

$$\dot{x}_\gamma(s) = \frac{\partial x_\gamma(s)}{\partial s} \dot{s} \quad \dot{y}_\gamma(s) = \frac{\partial y_\gamma(s)}{\partial s} \dot{s}.$$

Note that its norm is

$$U_\gamma = \dot{s} \sqrt{\left(\frac{\partial x_\gamma(s)}{\partial s}\right)^2 + \left(\frac{\partial y_\gamma(s)}{\partial s}\right)^2} = \dot{s}$$

because of our choice of the parametrization for $\gamma(s)$. An illustration is given in Figure 6.2.

Our objective is to make the vehicle converge to the path $\gamma(s)$ and move along it with an assigned constant velocity \bar{U} . In other words, we want that the point \mathbf{h} converges to (x_γ, y_γ) . Then we want \mathbf{h} to move with total velocity vector $\mathbf{U}_t = [\xi_3 + V_x, \xi_4 + V_y]^T$ aligned with the vector T and with magnitude $U_t = \bar{U}$. The control objectives can be formalized as follows

$$\lim_{t \rightarrow \infty} (\xi_1 - x_\gamma(s)) = 0 \quad (6.9a)$$

$$\lim_{t \rightarrow \infty} (\xi_2 - y_\gamma(s)) = 0 \quad (6.9b)$$

$$\lim_{t \rightarrow \infty} (U_t - \bar{U}) = 0. \quad (6.9c)$$

Remark 6.2. Note that the control objectives require the vehicle to track the point (x_γ, y_γ) . We want to remark that this approach still identifies a path following

control problem. In fact, the trajectory tracking control problem requires the vehicle to be at a certain position in the space at a specific time. With the control objectives (6.9) we are requiring the vehicle to track the point (x_γ, y_γ) and its propagation on γ is defined by \dot{s} . It will be clear in the next section that \dot{s} does not depend on time, but rather on the motion of the vehicle.

6.4 The control system

In this section we discuss our choice for the dynamics \dot{s} which is a design parameter and can be chosen in order to ease the convergence of the vehicle to the path. Then we introduce the control law which we use to achieve the control objectives (6.9).

6.4.1 The parameter s

Our control objective is to make the vehicle move along $\gamma(s)$. Therefore, we can define the error variables

$$\tilde{\xi}_1 = \xi_1 - x_\gamma(s) \quad \tilde{\xi}_2 = \xi_2 - y_\gamma(s). \quad (6.10)$$

$$(6.11)$$

We want to define a law for \dot{s} such that if the Euclidean distance between VF and the vehicle is large, i.e., $\sqrt{\tilde{\xi}_1^2 + \tilde{\xi}_2^2}$ is large, then VF should slow down and wait for the vehicle to catch up. To this purpose we define the following law for \dot{s}

$$\dot{s} = \bar{U} \left(1 - \epsilon \tanh \left(\sqrt{\tilde{\xi}_1^2 + \tilde{\xi}_2^2} \right) \right). \quad (6.12)$$

The value $\epsilon > 0$ is a constant. According to (6.12), $\dot{s} \rightarrow 0$ if $\sqrt{\tilde{\xi}_1^2 + \tilde{\xi}_2^2} \rightarrow \infty$, that is the frame tends to stop if the vehicle is far away from the path. On the other hand, if $\sqrt{\tilde{\xi}_1^2 + \tilde{\xi}_2^2} \rightarrow 0$ we have $\dot{s} \rightarrow \bar{U}$.

We consider the following assumption to hold

Assumption 6.3. *The velocity \bar{U} is such that $\bar{U} > \|\mathbf{V}\|$.*

6.4.2 The controller

In order to make the vehicle converge to the path we define the the following control inputs μ_1, μ_2

$$\mu_1 = -k_{v_x}(\xi_3 - \dot{x}_\gamma(s)) - k_{p_x}(\xi_1 - x_\gamma(s)) - k_{I_x} \left(\xi_{1I} - \int_0^t x_\gamma(s) d\tau \right) + \ddot{x}_\gamma^*(s) \quad (6.13a)$$

$$\mu_2 = -k_{v_y}(\xi_4 - \dot{y}_\gamma(s)) - k_{p_y}(\xi_2 - y_\gamma(s)) - k_{I_y} \left(\xi_{2I} - \int_0^t y_\gamma(s) d\tau \right) + \ddot{y}_\gamma^*(s) \quad (6.13b)$$

where

$$\dot{x}_\gamma(s) = \dot{s} \frac{\partial x_\gamma(s)}{\partial s} \quad \ddot{x}_\gamma^*(s) = \dot{s}^2 \bar{U} \frac{\partial^2 x_\gamma(s)}{\partial s^2} \quad (6.14)$$

$$\dot{y}_\gamma(s) = \dot{s} \frac{\partial y_\gamma(s)}{\partial s} \quad \ddot{y}_\gamma^*(s) = \dot{s}^2 \bar{U} \frac{\partial^2 y_\gamma(s)}{\partial s^2}. \quad (6.15)$$

The terms $\ddot{x}_\gamma^*(s)$, $\ddot{y}_\gamma^*(s)$ are two feed-forward terms. Note $\ddot{x}_\gamma^*(s) \neq \ddot{x}_\gamma(s)$, $\ddot{y}_\gamma^*(s) \neq \ddot{y}_\gamma(s)$. We cannot choose $\ddot{x}_\gamma(s)$, $\ddot{y}_\gamma(s)$ as feed-forward terms since the expression of \dot{s} depends on V_x, V_y , which are unknown. Finally, $k_{v_x}, k_{v_y}, k_{p_x}, k_{p_y}, k_{I_x}, k_{I_y}$ are all positive constants.

6.5 Main result

In this section the main result of this chapter is presented in the following theorem.

Theorem 6.1. *Consider an under-actuated marine vehicle described by the model (6.1). Consider the hand position point $\mathbf{h} = [x_1, y_1]^T = [x + l \cos(\psi), y + l \sin(\psi)]^T$, where $[x, y]^T$ is the position of the pivot point of the ship, l is a positive constant and ψ is the yaw angle of the vehicle. Then define*

$$U_d = \sqrt{\left(\bar{U} \frac{\partial x_\gamma(s)}{\partial s} - V_x\right)^2 + \left(\bar{U} \frac{\partial y_\gamma(s)}{\partial s} - V_y\right)^2} > 0 \quad (6.16)$$

as the desired relative velocity magnitude and

$$\bar{\phi}_1 = \arctan \left(\frac{\bar{U} \frac{\partial x_\gamma(s)}{\partial s} - V_y}{\bar{U} \frac{\partial y_\gamma(s)}{\partial s} - V_x} \right) \quad (6.17)$$

as the crab angle. Consider Assumptions 6.3-6.2 and the following conditions to hold

$$0 < U_d < \frac{Y_2}{Y_1} \quad (6.18)$$

$$k_{v_i} > 0, k_{p_i} > 0, k_{I_i} > 0, i \in \{x, y\} \quad (6.19)$$

$$k_{v_i} k_{p_i} > k_{I_i} \quad i \in \{x, y\} \quad (6.20)$$

$$l > \max \left\{ \frac{m_{22}}{m_{23}}, -\frac{X_2}{Y_2} \right\} \quad (6.21)$$

$$\epsilon < \frac{\lambda_Q^{\min}}{2\lambda_P^{\max}} \quad (6.22)$$

$$\kappa \leq \frac{2 \min\{a(d - c), b\}}{\left(\bar{a} + \sqrt{\bar{a}^2 + 1} \left(Y_1 - \frac{X_1 - 1}{l} + \frac{2Y_1 \bar{U}_d}{l}\right)\right) \bar{U}} \quad (6.23)$$

where κ is the curvature of $\gamma(s)$. Then, the controller (6.5), where the new inputs μ_1, μ_2 are given by (6.13), guarantees the achievement of the control objectives (6.9).

Remark 6.3. Before going we want to remark the differences among the velocities U_γ , U_t , U_d and \bar{U} .

- U_γ is the magnitude velocity of the VF frame in the NED frame;
- U_t is the absolute velocity of the vehicle. We want this quantity to converge to a constant which is $\bar{U} > 0$;
- U_d is the desired relative velocity, note $U_d \neq U_t$;
- \bar{U} is the desired value for U_t .

Note that when $U_t \rightarrow \bar{U}$, the relative velocity vector is such that $[\xi_3, \xi_4]^T \rightarrow \bar{U}T - \mathbf{V}$.

Proof. First of all we define the following change of coordinates

$$\tilde{z}_1 = z_1 - \bar{\phi}_1 \quad \tilde{z}_2 = z_2 - \dot{\bar{\phi}}_1 \quad (6.24a)$$

$$\tilde{\xi}_{1_I} = \xi_{1_I} - \int_0^t x_\gamma(s) d\tau - \frac{k_{v_x} V_x}{k_{I_x}} \quad \tilde{\xi}_{2_I} = \xi_{2_I} - \int_0^t y_\gamma(s) d\tau - \frac{k_{v_y} V_y}{k_{I_y}} \quad (6.24b)$$

$$\tilde{\xi}_1 = \xi_1 - x_\gamma(s) \quad \tilde{\xi}_2 = \xi_2 - y_\gamma(s) \quad (6.24c)$$

$$\tilde{\xi}_3 = \xi_3 - \left(\bar{U} \frac{\partial x_\gamma(s)}{\partial s} - V_x \right) \quad \tilde{\xi}_4 = \xi_4 - \left(\bar{U} \frac{\partial y_\gamma(s)}{\partial s} - V_y \right). \quad (6.24d)$$

Defining the vectors $\tilde{z}_s = [\sin(\tilde{z}_1), \tilde{z}_2]^T$, $\tilde{\xi} = [\tilde{\xi}_{1_I}, \tilde{\xi}_{2_I}, \tilde{\xi}_1, \tilde{\xi}_2, \tilde{\xi}_3, \tilde{\xi}_4]^T$ the closed-loop system becomes

$$\dot{\tilde{z}} = H_{\tilde{z}}(\tilde{z}_1) \tilde{z}_s + G(\tilde{z}, \tilde{\xi}_3, \tilde{\xi}_4) \tilde{\xi} + \Delta_{\tilde{z}}(\dot{\bar{\phi}}_1, \ddot{\bar{\phi}}_1, \tilde{z}_1) \quad (6.25a)$$

$$\dot{\tilde{\xi}} = H_{\tilde{\xi}} \tilde{\xi} + \Delta_{\tilde{\xi}}(\tilde{\xi}_1, \tilde{\xi}_2) \quad (6.25b)$$

where $G(\cdot)$ is reported in Appendix 5.A and

$$H_{\tilde{z}}(\tilde{z}) = \begin{bmatrix} 0 & 1 \\ -(c \cos(\tilde{z}_1) + d) & -(a \cos(\tilde{z}_1) + b) \end{bmatrix} \quad (6.26)$$

$$\Delta_{\tilde{z}}(\dot{\bar{\phi}}_1, \ddot{\bar{\phi}}_1, \tilde{z}_1) = \begin{bmatrix} 0 \\ \delta(\dot{\bar{\phi}}_1, \ddot{\bar{\phi}}_1, \sin(\tilde{z}_1)) \end{bmatrix} \quad (6.27)$$

$$\begin{aligned} \delta(\cdot) = & -(a \cos(\tilde{z}_1) + b) \dot{\bar{\phi}}_1 + \ddot{\bar{\phi}}_1 \\ & + (\dot{\xi}_{4_d} \cos(\tilde{z}_1) - \dot{\xi}_{3_d} \sin(\tilde{z}_1)) \cos(\bar{\phi}) \\ & + (-\dot{\xi}_{4_d} \sin(\tilde{z}_1) + \dot{\xi}_{3_d} \cos(\tilde{z}_1)) \sin(\bar{\phi}) \end{aligned} \quad (6.28)$$

$$a = \left(Y_1 - \frac{X_1 - 1}{l} \right) U_d \quad b = Y_2 + \frac{X_2}{l} \quad (6.29)$$

$$c = \frac{Y_1 U_d^2}{l} \quad d = \frac{Y_2 U_d}{l} \quad (6.30)$$

$$H_{\tilde{\xi}} = \begin{bmatrix} 0 & 0 & 1 & 0 & 0 & 0 \\ 0 & 0 & 0 & 1 & 0 & 0 \\ 0 & 0 & 0 & 0 & 1 & 0 \\ 0 & 0 & 0 & 0 & 0 & 1 \\ -k_{I_x} & 0 & -k_{p_x} & 0 & -k_{v_x} & 0 \\ 0 & -k_{I_y} & 0 & -k_{p_y} & 0 & -k_{v_y} \end{bmatrix} \quad (6.31)$$

$$\Delta_{\tilde{\xi}}(\tilde{\xi}_1, \tilde{\xi}_2) = \epsilon \begin{bmatrix} 0 \\ 0 \\ \bar{U} \frac{\partial x_\gamma(s)}{\partial s} \tanh\left(\sqrt{\tilde{\xi}_1^2 + \tilde{\xi}_2^2}\right) \\ \bar{U} \frac{\partial y_\gamma(s)}{\partial s} \tanh\left(\sqrt{\tilde{\xi}_1^2 + \tilde{\xi}_2^2}\right) \\ 0 \\ 0 \end{bmatrix}. \quad (6.32)$$

Assumption 2.3 implies $c, d > 0$ and (6.18) implies $d > c \forall t$. We also have $a, b > 0$ because of (6.21). Note also that we have U_d which is not constant since $\frac{\partial x_\gamma(s)}{\partial s}, \frac{\partial y_\gamma(s)}{\partial s}$ varies along $\gamma(s)$, however we have $\underline{U}_d \leq U_d \leq \bar{U}_d$ since $\gamma(s) \in \mathcal{C}^2$ by Assumption 6.2. Therefore, we have $\bar{a} > a > \underline{a}, \bar{c} > c > \underline{c}, \bar{d} > d > \underline{d}$ with $\bar{a}, \underline{a}, \bar{c}, \underline{c}, \bar{d}, \underline{d}$ positive constants. We now study the stability properties of the external dynamics (6.25b) and the internal dynamics (Equation (6.25a) with $G(\tilde{z}, \tilde{\xi}_3, \tilde{\xi}_4)\tilde{\xi} = 0$) and then the stability properties of the total system (6.25).

6.5.1 The external dynamics

Since $H_{\tilde{\xi}}$ is Hurwitz because of (6.19-6.20), there exists a positive definite matrix P which satisfies

$$H_{\tilde{\xi}}^T P_{\tilde{\xi}} + P_{\tilde{\xi}}^T H_{\tilde{\xi}} = -Q_{\tilde{\xi}}.$$

where Q is a positive definite matrix. Choosing the following LFC

$$V_{\tilde{\xi}} = \tilde{\xi}^T P_{\tilde{\xi}} \tilde{\xi} \quad (6.33)$$

we have

$$\dot{V}_{\tilde{\xi}} = -\tilde{\xi}^T Q_{\tilde{\xi}} \tilde{\xi} + \frac{\partial V_{\tilde{\xi}}}{\partial \tilde{\xi}} \Delta_{\tilde{\xi}}(\cdot) \quad (6.34)$$

$$\leq -\lambda_{Q_{\tilde{\xi}}}^{\min} \|\tilde{\xi}\|^2 + 2\|P_{\tilde{\xi}}\| \|\tilde{\xi}\| \epsilon \|\tilde{\xi}\| \quad (6.35)$$

$$\leq -\lambda_{Q_{\tilde{\xi}}}^{\min} \|\tilde{\xi}\|^2 + 2\epsilon \lambda_{P_{\tilde{\xi}}}^{\max} \|\tilde{\xi}\|^2 \quad (6.36)$$

$$\leq -\lambda \|\tilde{\xi}\|^2. \quad (6.37)$$

We have $\lambda > 0$ for $\epsilon < \frac{\lambda_{Q_{\tilde{\xi}}}^{\min}}{2\lambda_{P_{\tilde{\xi}}}^{\max}}$. Choosing ϵ this way implies also that $\|\tilde{\xi}\| = 0$ is GES.

6.5.2 The internal dynamics

Let us now focus on the internal dynamics:

$$\dot{\tilde{z}}_1 = \tilde{z}_2 \quad (6.38a)$$

$$\dot{\tilde{z}}_2 = -(a \cos(\tilde{z}_1) + b)\tilde{z}_2 - (c \cos(\tilde{z}_1) + d) \sin(\tilde{z}_1) + \delta(\dot{\phi}_1, \ddot{\phi}_1, \tilde{z}_1). \quad (6.38b)$$

Since (6.38) does clearly not have an equilibrium point at the origin due to the presence of the disturbance $\delta(\cdot)$, we study the ultimately boundedness of the states \tilde{z}_1, \tilde{z}_2 . Now note that $\delta \leq \bar{\delta}$ since function of bounded signals. In fact, δ is function of $\dot{\phi}, \ddot{\phi}$ which in turn are functions of $\dot{x}(s), \dot{y}(s), \ddot{x}(s), \ddot{y}(s)$ which are bounded.

Now we define the following Lyapunov function candidate (LFC)

$$W = \frac{1}{2} \tilde{z}_s^T \underbrace{\begin{bmatrix} a^2 + c & a \\ a & 1 \end{bmatrix}}_{P_{z_s}} \tilde{z}_s + (ab + d)(1 - \cos(\tilde{z}_1)). \quad (6.39)$$

We have that $W > 0 \forall (\cos(\tilde{z}_1), \sin(\tilde{z}_1), \tilde{z}_2) \in \mathbb{M} - \{[1, 0, 0]\}$ and $W = 0$ only for $(\cos(\tilde{z}_1), \sin(\tilde{z}_1), \tilde{z}_2) = (1, 0, 0)$. The time derivative is

$$\begin{aligned} \dot{W} = & -\tilde{z}_s^T \begin{bmatrix} a(d + c \cos(\tilde{z}_1)) & 0 \\ 0 & b \end{bmatrix} \tilde{z}_s + \frac{\partial W}{\partial \tilde{z}_s} \Delta_{\tilde{z}} \\ & + \frac{1}{2} \tilde{z}_s^T \begin{bmatrix} 2\dot{a}a + \dot{c} & \dot{a} \\ \dot{a} & 0 \end{bmatrix} \tilde{z}_s + (\dot{a}b + \dot{d})(1 - \cos(\tilde{z}_1)). \end{aligned} \quad (6.40)$$

Note that $\dot{a}, \dot{c}, \dot{d}$ all depend on \dot{U}_d . According to (6.16), the velocity vector \mathbf{U}_d is

$$\mathbf{U}_d = \bar{U}T - \mathbf{V},$$

where $T = [\frac{\partial x_\gamma(s)}{\partial s}, \frac{\partial y_\gamma(s)}{\partial s}]^T$ is unit tangent vector to the path at s . Thus

$$\dot{\mathbf{U}}_d = \kappa \dot{s} N.$$

where κ is the curvature of $\gamma(s)$ and N is the unit normal vector of $\gamma(s)$ at s . It is clear that $\|\dot{\mathbf{U}}_d\| = \dot{U}_d \leq \bar{U}_d^* = \kappa \bar{U}$. This implies that also $\dot{a}, \dot{c}, \dot{d}$ are upper bounded, that is, $\dot{a} \leq \bar{a}^*, \dot{c} \leq \bar{c}^*, \dot{d} \leq \bar{d}^*$. Then we have

$$\begin{aligned} \dot{W} \leq & -\tilde{z}_s^T \underbrace{\begin{bmatrix} a(d - c) & 0 \\ 0 & b \end{bmatrix}}_{Q_{\tilde{z}}} \tilde{z}_s + \frac{\partial W}{\partial \tilde{z}_s} \Delta_{\tilde{z}} + (\bar{a}^* b + \bar{d}^*)(1 - \cos(\tilde{z}_1)) \\ & + \frac{1}{2} \tilde{z}_s^T \underbrace{\begin{bmatrix} 2\bar{a}^* \bar{a} & \bar{a}^* \\ \bar{a}^* & 0 \end{bmatrix}}_{\Lambda_1} \tilde{z}_s + \frac{1}{2} \tilde{z}_s^T \underbrace{\begin{bmatrix} \bar{c}^* & 0 \\ 0 & 0 \end{bmatrix}}_{\Lambda_2} \tilde{z}_s. \end{aligned} \quad (6.41)$$

From the definition of $\Delta_{\tilde{z}}$ we have that

$$\left\| \frac{\partial W}{\partial \tilde{z}_s} \right\| \|\Delta_{\tilde{z}}\| \leq \alpha_1 \bar{\delta} \|\tilde{z}_s\| \quad (6.42)$$

where $\alpha_1 = \max\{1, a\}$ and $\bar{\delta}$ is the upperbound of $\delta(t)$, i.e. $\delta(t) \leq \bar{\delta}$ since $\delta(t)$ is function of bounded signals. Then we obtain

$$\dot{W} \leq - \underbrace{(\lambda_{Q_{\tilde{z}}}^{\min} - \lambda_{\Lambda_1}^{\max} - \lambda_{\Lambda_2}^{\max})}_{\sigma} \|\tilde{z}_s\|^2 + \alpha_1 \bar{\delta} \|\tilde{z}_s\| + 2(\bar{a}^* b + \bar{d}^*) \quad (6.43)$$

where $\lambda_{Q_{\tilde{z}}}^{\min} = \min\{a(d-c), b\}$ is the minimum eigenvalue of $Q_{\tilde{z}}$, $\lambda_{\Lambda_1}^{\max} = \frac{1}{2}(\bar{a} + \sqrt{\bar{a}^2 + 1})\bar{a}^*$ and $\lambda_{\Lambda_2}^{\max} = \frac{1}{2}\bar{c}^*$ are the maximum eigenvalues of Λ_1, Λ_2 , respectively. We have $\sigma > 0$ when (6.23) holds. Thus we obtain

$$\dot{W} \leq -(1-\theta)\sigma \|\tilde{z}_s\|^2 < 0 \quad \forall \|\tilde{z}_s\| \geq \frac{\alpha_1 \bar{\delta} + \sqrt{8\sigma(\bar{a}^* b + \bar{d}^*)} - \alpha_1^2}{2\theta\sigma} \quad (6.44)$$

where $0 < \theta < 1$. The important conclusion which we can draw from the considerations above is that the state \tilde{z}_2 , which is the only one that may grow unbounded on the manifold \mathbb{M} , stays bounded when the external dynamics is at steady state.

6.5.3 Stability of the complete system

We choose the following LFC

$$V = W + \kappa_1 V_{\tilde{\xi}} \quad (6.45)$$

where W is the same as in (6.39), and $\kappa_1 > 0$ is a constant still to be determined. Deriving (6.45) along the directions of (6.25) we obtain

$$\begin{aligned} \dot{V} &\leq -\sigma \|\tilde{z}_s\|^2 - \kappa_1 \tilde{\xi}^T Q_{\xi} \tilde{\xi} + \frac{\partial W}{\partial \tilde{z}} G(\cdot) \tilde{\xi} + \frac{\partial W}{\partial \tilde{z}_2} \delta(\cdot) + \kappa_1 \frac{\partial V_{\tilde{\xi}}}{\partial \tilde{\xi}} \Delta_{\tilde{\xi}}(\cdot) \\ &\leq -\sigma \|\tilde{z}_s\|^2 - \kappa_1 \lambda \|\tilde{\xi}\|^2 + \frac{\partial W}{\partial \tilde{z}} G(\cdot) \tilde{\xi} + \frac{\partial W}{\partial \tilde{z}_2} \delta(\cdot) \end{aligned} \quad (6.46)$$

The following bounds hold for $G(\cdot)$ and W :

$$G(\tilde{z}, \tilde{\xi}_3, \tilde{\xi}_4) \leq G_1(\|\tilde{\xi}\|) \|\tilde{z}_s\| + G_2(\|\tilde{\xi}\|) \leq \bar{G}_1 \|\tilde{z}_s\| + \bar{G}_2 \quad (6.47)$$

$$\left\| \frac{\partial W}{\partial \tilde{z}} \right\| \leq \|\tilde{z}_s\| \left\| \begin{bmatrix} a^2 + c + \frac{ab+d}{2} & a \\ a & 1 \end{bmatrix} \right\| \leq \alpha_2 \|\tilde{z}_s\|, \quad (6.48)$$

where $\bar{G}_1 = G_1(\bar{\xi})$, $\bar{G}_2 = G_2(\bar{\xi})$, and $\bar{\xi}$ is the upperbound of $\|\xi\|$. Let $\lambda_{P_{z_s}}^{\min}$, $\lambda_{P_{\xi}}^{\min}$, $\lambda_{Q_{\tilde{z}}}^{\min}$, $\lambda_{Q_{\xi}}^{\min}$ denote the minimal eigenvalue of P_{z_s} , P_{ξ} , $Q_{\tilde{z}}$, Q_{ξ} respectively. The closed-loop external dynamics (6.25b) is GES, therefore there exists a time t^* such that for all $t \geq t^*$: $\|\tilde{\xi}(t)\| \leq \sigma/(2\alpha_2 \bar{G}_1)$. For $t \leq t^*$ and

$$\kappa_1 > \frac{\alpha_2^2 \bar{G}_2^2}{\sigma \lambda} + \frac{\alpha_2 \bar{G}_1 \bar{\xi} \lambda_{P_{\xi}}^{\min}}{\lambda \lambda_{P_{z_s}}^{\min}} \quad (6.49)$$

we have

$$\begin{aligned}
 \dot{V} &\leq -\sigma \|\tilde{z}_s\|^2 - \kappa_1 \lambda \|\tilde{\xi}\|^2 \\
 &\quad + \alpha_2 \|\tilde{z}_s\| (\bar{G}_1 \|\tilde{z}_s\| + \bar{G}_2) \tilde{\xi} + \alpha_1 \bar{\delta} \|\tilde{z}_s\| \\
 &\leq -\frac{1}{2} \sigma \|\tilde{z}_s\|^2 - \left(\frac{\alpha_2^2 \bar{G}_2^2}{\sigma \lambda} + \frac{\alpha_2 \bar{G}_1 \bar{\xi} \lambda_{P_\xi}^{\min}}{\lambda \lambda_{P_{z_s}}^{\min}} \right) \lambda \|\tilde{\xi}\|^2 \\
 &\quad + \alpha_2 \bar{G}_1 \bar{\xi} \|\tilde{z}_s\|^2 + \alpha_2 \bar{G}_2 \|\tilde{z}_s\| \|\tilde{\xi}\| \\
 &\quad - \frac{1}{2} \sigma \|\tilde{z}_s\|^2 + \alpha_1 \bar{\delta} \|\tilde{z}_s\|
 \end{aligned} \tag{6.50}$$

for $\|\tilde{z}_s\| \geq \frac{2\alpha_1}{\sigma}$ we have

$$\begin{aligned}
 &\leq -\frac{1}{2} \sigma \|\tilde{z}_s\|^2 + \alpha_2 \bar{G}_2 \|\tilde{z}_s\| \|\tilde{\xi}\| - \frac{\alpha_2^2 \bar{G}_2^2}{\sigma} \|\tilde{\xi}\|^2 \\
 &\quad - \frac{2\alpha_2 \bar{G}_1 \bar{\xi} \lambda_{P_\xi}^{\min}}{\lambda_{P_{z_s}}^{\min}} \|\tilde{\xi}\|^2 + \alpha_2 \bar{G}_1 \bar{\xi} \|\tilde{z}_s\|^2 \\
 &\leq 2\alpha_2 \bar{G}_1 \bar{\xi} \|\tilde{z}_s\|^2 + \frac{2\alpha_2 \bar{G}_1 \bar{\xi} \lambda_{P_\xi}^{\min}}{\lambda_{P_{z_s}}^{\min}} \|\tilde{\xi}\|^2 \\
 &\quad + \frac{2\alpha_2 \bar{G}_1 \bar{\xi}}{\lambda_{P_{z_s}}^{\min}} (ad + c)(1 - \cos(\tilde{z}_1)) - \frac{2\alpha_2 \bar{G}_1 \bar{\xi}}{\lambda_{P_{z_s}}^{\min}} (ad + c)(1 - \cos(\tilde{z}_1)) \\
 &\leq \frac{2\alpha_2 \bar{G}_1 \bar{\xi}}{\lambda_{P_{z_s}}^{\min}} V + \frac{4\alpha_2 \bar{G}_1 \bar{\xi}}{\lambda_{P_{z_s}}^{\min}} (ad + c),
 \end{aligned} \tag{6.51}$$

so for $t < t^* \wedge \|\tilde{z}_s\| \geq \frac{2\alpha_1}{\sigma}$ the trajectories are bounded. For $t < t^* \wedge \|\tilde{z}_s\| < \frac{2\alpha_1}{\sigma}$ we have

$$\begin{aligned}
 \dot{V} &\leq -\frac{1}{2} \sigma \|\tilde{z}_s\|^2 + \alpha_2 \bar{G}_2 \|\tilde{z}_s\| \|\tilde{\xi}\| - \frac{\alpha_2^2 \bar{G}_2^2}{\lambda_{Q_z}^{\min}} \|\tilde{\xi}\|^2 \\
 &\quad - \frac{\alpha_2 \bar{G}_1 \bar{\xi} \lambda_{P_\xi}^{\min}}{\lambda_{P_{z_s}}^{\min}} \|\tilde{\xi}\|^2 + \alpha_2 \bar{G}_1 \bar{\xi} \|\tilde{z}_s\|^2 + \alpha_1 \bar{\delta} \|\tilde{z}_s\| \\
 &\leq \alpha_2 \bar{G}_1 \bar{\xi} \|\tilde{z}_s\|^2 + \frac{2\alpha_2 \bar{G}_1 \bar{\xi} \lambda_{P_\xi}^{\min}}{\lambda_{P_{z_s}}^{\min}} \|\tilde{\xi}\|^2 + \bar{\delta} \frac{2\alpha_1^2}{\sigma} \\
 &\quad + \frac{2\alpha_2 \bar{G}_1 \bar{\xi}}{\lambda_{P_{z_s}}^{\min}} (ad + c)(1 - \cos(\tilde{z}_1)) - \frac{2\alpha_2 \bar{G}_1 \bar{\xi}}{\lambda_{P_{z_s}}^{\min}} (ad + c)(1 - \cos(\tilde{z}_1)) \\
 &\leq \frac{2\alpha_2 \bar{G}_1 \bar{\xi}}{\lambda_{P_{z_s}}^{\min}} V + \bar{\delta} \frac{2\alpha_1^2}{\sigma} + \frac{4\alpha_2 \bar{G}_1 \bar{\xi}}{\lambda_{P_{z_s}}^{\min}} (ad + c),
 \end{aligned} \tag{6.52}$$

so $V(t)$ remains bounded also for the case $t \leq t^* \wedge \|\tilde{z}_s\| < \frac{2\alpha_1}{\sigma}$, meaning that the trajectories are bounded for any $t < t^*$.

For $t \geq t^*$ we have

$$\begin{aligned}
 \dot{V} &\leq -\sigma \|\tilde{z}_s\|^2 - \kappa_1 \lambda \|\tilde{\xi}\|^2 + \alpha_2 \|\tilde{z}_s\| (\bar{G}_1 \|\tilde{z}_s\| + \bar{G}_2) \tilde{\xi} + \alpha_1 \bar{\delta} \|\tilde{z}_s\| \\
 &\leq -\frac{1}{2} \sigma \|\tilde{z}_s\|^2 + \alpha_2 \bar{G}_2 \|\tilde{z}_s\| \|\tilde{\xi}\| - \kappa_1 \lambda \|\tilde{\xi}\|^2 + \alpha_1 \bar{\delta} \|\tilde{z}_s\| \\
 &\leq -\frac{1}{2} \theta \sigma \|\tilde{z}_s\|^2 + \alpha_2 \bar{G}_2 \|\tilde{z}_s\| \|\tilde{\xi}\| - \kappa_1 \lambda \|\tilde{\xi}\|^2 \\
 \forall \|\tilde{z}_s\| &> \frac{2\alpha_1 \bar{\delta}}{(1-\theta)\sigma} \wedge 0 < \theta < 1,
 \end{aligned} \tag{6.53}$$

which is negative definite for $\kappa_1 > \alpha_2^2 \bar{G}_2^2 / (\sigma \lambda)$. We can conclude that $\tilde{\xi} \rightarrow 0$ globally exponentially while the states z_1, z_2 are ultimately bounded. Finally, this implies that the control objectives (6.9) are fulfilled. \square

Remark 6.4. *Note the condition (6.23). This condition is needed in order to guarantee boundedness of the internal dynamics. In Chapter 5 we have seen that for the case of trajectory tracking the boundedness of the states of the internal dynamics is guaranteed with a similar condition on the magnitude of the total desired acceleration. Given a desired tangential velocity $U_d T$, where T is the unit tangent vector to the curve, we know that*

$$\dot{U}_d = U_d \kappa N + \dot{U}_d T$$

where N is the unit normal vector. As shown above, for the path following case, where the tangential velocity of the frame VF is considered constant, we have $\dot{U}_d = 0$. Thus, the condition needed for the boundedness of the states z_1, z_2 can be reduced to a condition just on the curvature κ . On the other hand, the case of trajectory tracking considered in Chapter 5 is more general. We do not restrict to the case of trajectory tracking with constant tangential velocity, that is, $\dot{U}_d \neq 0$. Thus, the condition for the boundedness of z_1, z_2 has to be more general and involve boundedness of the magnitude of the desired tangential acceleration.

6.6 The straight-lines case

In this section we discuss about the specific case of straight-line paths. This case is of particular interest for practical applications since lawn-mower paths, paths made of a series of straight-line segments, are standard for marine vehicles when required to execute surveillance and scanning tasks in the ocean.

Without loss of generality, consider a path which is aligned along the x axis of the NED frame. This implies $\gamma(s) = \{(x(s), y(s)) | y(s) = 0 \wedge s \in \mathbb{R}\}$. Then we have

$$T = \begin{bmatrix} \frac{\partial x_\gamma(s)}{\partial s} & \frac{\partial y_\gamma(s)}{\partial s} \end{bmatrix}^T = [1 \quad 0]^T.$$

Note that velocity in the NED frame with which VF moves along $\gamma(s)$ is given by

$$\dot{x}_\gamma(s) = \frac{\partial x_\gamma(s)}{\partial s} \dot{s} = \dot{s}, \quad \dot{y}_\gamma(s) = 0.$$

For the special case considered in this section, we can derive the following corollary from Theorem 6.1.

Corollary 6.1. Consider an under-actuated marine vehicle described by the model (6.1). Consider the hand position point $\mathbf{h} = [x_1, y_1]^T = [x + l \cos(\psi), y + l \sin(\psi)]^T$, where $[x, y]^T$ is the position of the pivot point of the ship, l is a positive constant and ψ is the yaw angle of the vehicle. Then define

$$U_d = \sqrt{(\bar{U} - V_x)^2 + V_y^2} > 0 \quad (6.54)$$

as the desired relative velocity magnitude and

$$\bar{\phi}_2 = \arctan\left(\frac{-V_y}{u_d - V_x}\right) \quad (6.55)$$

as the crab angle. If Assumptions 6.2-6.3 are satisfied and if

$$0 < U_d < \frac{Y_2}{Y_1} \quad (6.56)$$

$$k_{v_i} > 0, k_{p_i} > 0, k_{I_i} > 0, i \in \{x, y\} \quad (6.57)$$

$$k_{v_i} k_{p_i} > k_{I_i} \quad i \in \{x, y\} \quad (6.58)$$

$$l > \max\left\{\frac{m_{22}}{m_{23}}, -\frac{X_2}{Y_2}\right\} \quad (6.59)$$

then the controller (6.5), where the new inputs μ_1, μ_2 are given by (6.13), guarantees the achievement of the control objectives (6.9). In particular,

$$(z_1, z_2, \xi_1, \xi_2, \xi_3, \xi_4) \rightarrow (\bar{\phi}_2, 0, u_d, 0, u_d - V_x, -V_y)$$

almost-globally asymptotically. Furthermore, the steady state values of the integral variables give an estimate of the ocean current:

$$\hat{V}_x = \frac{k_{I_x}(\xi_{1_I} - \xi_{1_{I_d}})}{k_{v_x}}, \quad \hat{V}_y = \frac{k_{I_y}(\xi_{2_I} - \xi_{2_{I_d}})}{k_{v_y}}. \quad (6.60)$$

Proof. The proof of this Corollary follows from the proof of Theorem 6.1. Applying the change of coordinates (6.24) we obtain the closed loop system (6.25). However, note that now $\dot{U}_d = 0$ and $\dot{\bar{\phi}}_2 = 0$. This implies that a, b, c and d are constants. Furthermore, $\delta(\cdot) = 0$.

6.6.1 The external dynamics

The proof that $\tilde{\xi} = \mathbf{0}$ is GES follows from Theorem 6.1.

6.6.2 The internal dynamics

The internal dynamics is

$$\dot{\tilde{z}}_1 = \tilde{z}_2 \quad (6.61a)$$

$$\dot{\tilde{z}}_2 = -(a \cos(\tilde{z}_1) + b)\tilde{z}_2 - (c \cos(\tilde{z}_1) + d) \sin(\tilde{z}_1). \quad (6.61b)$$

The system (6.61) has two equilibria , and they are

$$E_s = (1, 0, 0) \in \mathbb{M}, \quad E_u = (-1, 0, 0) \in \mathbb{M}. \quad (6.62)$$

The point E_s is a stable node, while E_u is a saddle point since we assumed $d > c$. Note that E_u is a hyperbolic equilibrium. Use W in (6.39) as Lyapunov function candidate. Since a, b, c, d are constants and $\delta(\cdot) = 0$, the time derivative is

$$\dot{W} = -\tilde{z}_s^T Q_{\tilde{z}} \tilde{z}_s \leq 0 \quad \forall (\sin(\tilde{z}_1), \tilde{z}_2) \neq (0, 0). \quad (6.63)$$

Equation 6.63 implies that the state $(\sin(\tilde{z}_1), \tilde{z}_2) = (0, 0)$ is GAS. However, $\sin(\tilde{z}_1) = 0$ corresponds either to $\cos(\tilde{z}_1) = 1$ or $\cos(\tilde{z}_1) = -1$ on the one-dimensional unit sphere. That is, if the vehicle is required to move along a straight-line path it may move forward ($\cos(\psi) = 1$) or backwards ($\cos(\psi) = -1$). Linearizing (6.61) around the origin, it is easy to verify that

$$E_u = \{(\cos(\tilde{z}_1), \sin(\tilde{z}_1), \tilde{z}_2) = (-1, 0, 0)\} \in \mathbb{M}$$

is unstable and hyperbolic. Then, invoking Theorem A.2 we infer that E_u is characterized by a stable and an unstable manifold $\mathcal{W}_u^s, \mathcal{W}_u^u$, respectively. Both $\mathcal{W}_u^s, \mathcal{W}_u^u$ are one-dimensional since spanned by the positive and the negative eigenvalue of the Jacobian matrix of (6.61), respectively. Recall that the system (6.25a) evolves on the manifold $\mathbb{M} = \mathbb{S} \times \mathbb{R}$, which is 2-dimensional (it is a "pipe-shaped" manifold, that is, it is a cylindrical surface in the space). Then \mathcal{W}_u^s has therefore zero Lebesgue measure since it has one dimension less than \mathbb{M} . So we can conclude that E_s is *almost*-GAS since all the trajectories which do not start on \mathcal{W}_u^s converge to E_s .

6.6.3 Stability of the complete system

Following the same approach as in Theorem 6.1 it is straightforward to conclude that the closed loop system is AGAS and that the control objectives (6.9) are satisfied. \square

6.7 Unparametrized straight-line paths

In this section we discuss about the specific case of unparametrized straight-line paths. This case is of particular interest for practical applications. In fact, when an ASVs or an AUVs is used for surveillance or exploration tasks, it is required to follow a path made of a series of unparametrized straight-line segments, generally a lawn-mower path.

Without loss of generality, we consider a path which is aligned along the x axis of the NED frame. The fact that the path is left unparametrized means that there is not a parameter s which is associated to the points of the path. Then the path can be simply defined as $\mathcal{P} = \{(x, y) | y = 0\}$ [32, 33]. Then, it is also clear that there is not the freedom to design the time update for the parameter s . However, in order to have the vehicle to move along \mathcal{P} , it is enough to regulate the state ξ_2 to zero and the forward velocity ξ_3 to a constant value \bar{U} . It is important to notice

that the state ξ_1 can be left uncontrolled since now we cannot define a virtual frame VF propagating along \mathcal{P} .

The path following control objectives for the unparametrized straight-line paths can be formalized as

$$\lim_{t \rightarrow \infty} \xi_2 = 0 \quad (6.64a)$$

$$\lim_{t \rightarrow \infty} \xi_3 - \bar{U} = 0. \quad (6.64b)$$

Since the state ξ_1 cannot be specified, we have to leave it uncontrolled. We define the following controller μ

$$\mu_1 = -k_{v_x}(\xi_3 - \bar{U}) \quad (6.65a)$$

$$\mu_2 = -k_{v_y}\xi_4 - k_{p_y}\xi_2 - k_{I_y}\left(\xi_{2I} - \int_0^t x_\gamma(s)d\tau\right). \quad (6.65b)$$

The intent of (6.65) is to regulate ξ_2 and ξ_4 while counteracting the ocean current by means of an integral action. Note that since ξ_1 cannot be specified, we cannot counteract the along path component of the ocean current \mathbf{V} . Therefore, if we regulate ξ_3 to \bar{U} the absolute velocity of the vehicle in the along path direction is $\xi_3 - V_x$.

We can derive the following corollary from Theorem 6.1 and 6.1

Corollary 6.2. *Consider an under-actuated marine vehicle described by the model (6.1). Consider the hand position point $\mathbf{h} = [x_1, y_1]^T = [x + l \cos(\psi), y + l \sin(\psi)]^T$, where $[x, y]^T$ is the position of the pivot point of the ship, l is a positive constant and ψ is the yaw angle of the vehicle. Then define*

$$U_d = \sqrt{\bar{U} + V_y^2} > 0 \quad (6.66)$$

as the desired relative velocity magnitude and

$$\bar{\phi}_3 = \arctan\left(\frac{-V_y}{\bar{U}}\right) \quad (6.67)$$

as the crab angle. If Assumptions 6.2-6.3 are satisfied and if

$$0 < U_d < \frac{Y_2}{Y_1} \quad (6.68)$$

$$k_{v_i} > 0, k_{p_i} > 0, k_{I_i} > 0, i \in \{x, y\} \quad (6.69)$$

$$k_{v_i}k_{p_i} > k_{I_i} \quad i \in \{x, y\} \quad (6.70)$$

$$l > \max\left\{\frac{m_{22}}{m_{23}}, -\frac{X_2}{Y_2}\right\} \quad (6.71)$$

then the controller (6.5), where the new inputs μ_1, μ_2 are given by (6.65), guarantees the achievement of the control objectives (6.64). In particular,

$$(z_1, z_2, \xi_1, \xi_2, \xi_3, \xi_4) \rightarrow (\bar{\phi}_3, 0, u_d t, 0, u_d - V_x, -V_y)$$

almost-globally asymptotically.

The proof of this corollary follows from the proofs of Theorem 6.1 and Corollary 6.1.

Table 6.1: Initial conditions.

	$x _{t_0}$ m	$y _{t_0}$ m	$\psi _{t_0}$ rad	u_r m/s	v_r m/s	r rad/s
t_0	0	150	$-\pi$	0	0	0

6.8 Simulation results

In this section we present two simulation case studies in order to validate the theoretical results presented above. The first case study considers the case of parametrized curved paths while the second case deals with unparametrized straight-line paths.

6.8.1 Curved paths

We consider the model of the Light Autonomous Underwater Vehicle (LAUV) of the Laboratório de System y Tecnologia Subaquática (LSTS) at the University of Porto. The model of the vehicle is given [38] and reported in Appendix B.

We consider that the vehicle has to track a circle centered at the origin of the NED frame. We consider a circle with radius $R = 80$ m. The desired signals are

$$x_\gamma = R \cos\left(\frac{s}{R}\right) \quad (6.72a)$$

$$y_\gamma = R \sin\left(\frac{s}{R}\right) \quad (6.72b)$$

$$\dot{x}_\gamma = -\dot{s} \sin\left(\frac{s}{R}\right) \quad (6.72c)$$

$$\dot{y}_\gamma = \dot{s} \cos\left(\frac{s}{R}\right) \quad (6.72d)$$

$$\ddot{x}_\gamma^* = -\frac{\dot{s}^2}{R} \cos\left(\frac{s}{R}\right) \quad (6.72e)$$

$$\ddot{y}_\gamma^* = -\frac{\dot{s}^2}{R} \sin\left(\frac{s}{R}\right). \quad (6.72f)$$

We choose the constant $l = 1$ m in (6.2). The initial conditions of the vehicle are summarized in Table 6.1. From Table 6.1 we have that

$$\xi_{1_0} = 0 \text{ m} \quad (6.73a)$$

$$\xi_{2_0} = 149 \text{ m} \quad (6.73b)$$

$$\xi_{3_0} = 0 \text{ m/s} \quad (6.73c)$$

$$\xi_{4_0} = 0 \text{ m/s} \quad (6.73d)$$

$$z_{1_0} = 0 \text{ rad} \quad (6.73e)$$

$$z_{2_0} = 0 \text{ rad/s}. \quad (6.73f)$$

The gains in (6.13) are

$$k_{p_x} = k_{p_y} = 0.5 \quad (6.74a)$$

$$k_{v_x} = k_{v_y} = 10 \quad (6.74b)$$

$$k_{I_x} = k_{I_y} = 0.007. \quad (6.74c)$$

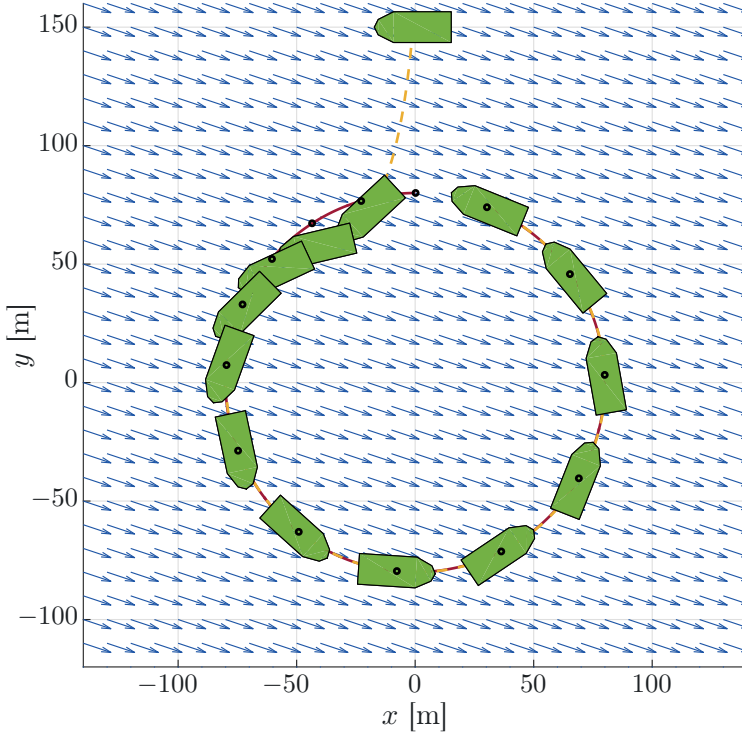


Figure 6.3: Motion of the vehicle. The black dot represents the motion of the virtual frame VF .

The ocean current is $\mathbf{V} = [-0.15, 0.05]^T$ m/s. According to the choice of the gains and the properties of the path described above, the conditions under which Theorem 6.1 holds are satisfied.

For the path parametrization, we choose the initial position of the virtual frame VF such that the distance between the vehicle and the path is minimum. This implies that the initial value of the path parameter is chosen as $s_0 = R\pi/2$. For the update law (6.12), we choose $\epsilon = 0.5$.

Remark 6.5. *Under the conditions chosen for this simulation, we would need $\epsilon < \frac{\lambda_Q^{\min}}{2\lambda_P^{\max}} \approx 10^{-5}$. This condition is conservative due to the conservativeness of the Lyapunov analysis. We choose instead $\epsilon = 0.5 > 10^{-5}$ which would be more suitable for practical applications.*

The results of the simulation are shown in Figures 6.3-6.5. Figure 6.3 shows the motion of the vehicle. The black dot on the circle represents the origin of the

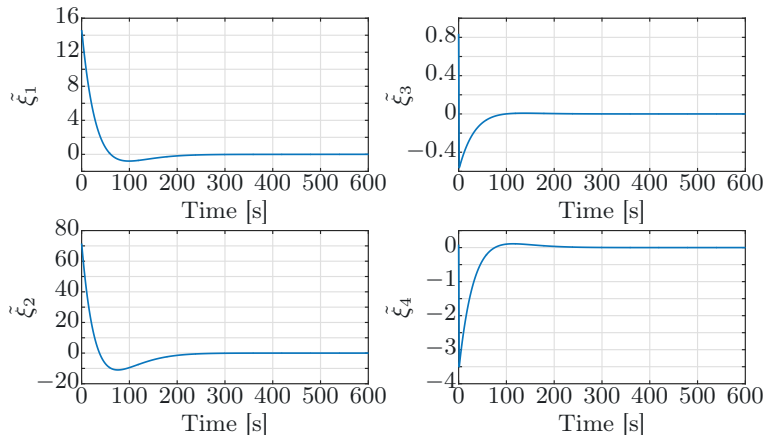


Figure 6.4: Time evolution of the error states.

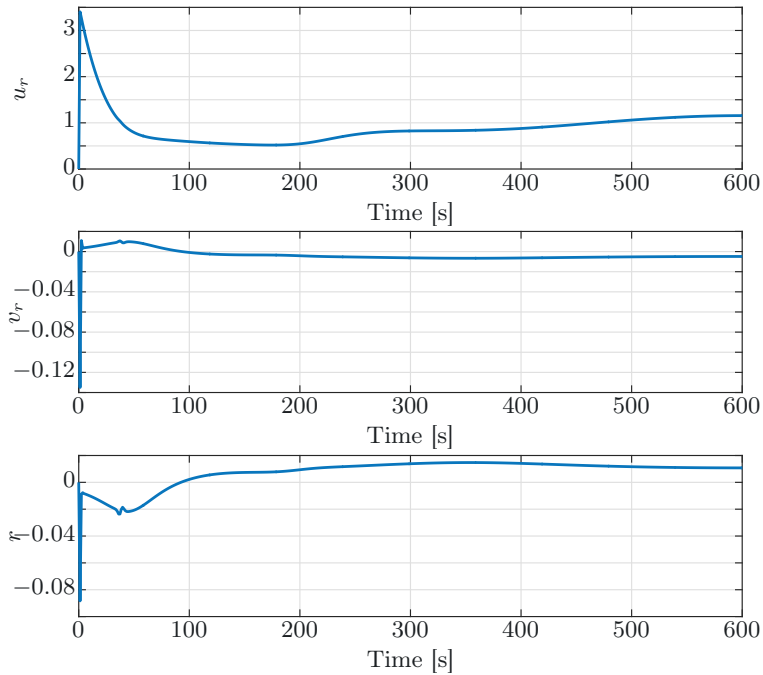


Figure 6.5: Time evolution of the surge velocity, sway velocity and yaw rate.

virtual frame VF . It is clear that the vehicle converges to the circle and moved with VF . We see also that while the vehicle is not on the path, the frame VF slows down. In Figure 6.4, the time evolution of the error states $\tilde{\xi}_1, \tilde{\xi}_2, \tilde{\xi}_3, \tilde{\xi}_4$ confirms that the trajectory tracking task is fulfilled. In fact, all the error states converge to zero. Finally, in Figure 6.5 the relative surge velocity u_r , the relative sway velocity v_r and the yaw rate r are shown. Note that that $r = z_2$ is bounded as expected.

6.8.2 Straight-line paths

We use the model of the LAUV (light autonomous underwater vehicle) given in Appendix B and define a lawn-mower path in order to simulate the path following case described in Section 6.7. The simulation will also be a benchmark for the sea trial results which are presented in Section 6.9, and we therefore consider the special case of straight-line paths which is what we could implement in the experiments. The choice of such a kind of path is driven by the fact that lawn-mower paths are standard for marine vehicles when required to execute surveillance and scanning tasks in the ocean. We perform the simulation using the simulator of DUNE [39], software developed by the Laboratório de Sistemas e Tecnologia Subaquática (LSTS) at University of Porto, and running on the LAUVs. In fact, DUNE has a very detailed model of the LAUV and there are nodes in the software which realistically simulate the behavior of the sensors on-board the real vehicle, i.e. they also simulate noises.

As regards the desired motion, the vehicle is required to move with a constant forward velocity of $U_d = 1.2$ m/s while traveling along a lawn-mower path made of four long straight-lines $l_1 = 130$ m connected by three perpendicular straight-lines $l_2 = 27$ m. The depth of the path is set to 2 [m] under the surface. We do not implement any depth controller but rather use the depth controller already available on the LAUV. In the simulation we assign an ocean current $\mathbf{V} = [V_x, V_y]^T = [0.1, 0.2]^T$ m/s which is unknown to the vehicle. For the point \mathbf{h} we choose $l = 1$ m. Since we have chosen a lawn-mower path we decide to deal with the case of unparametrized paths as discussed in Section 6.7, i.e. we define $k_{p_x} = k_{I_x} = \epsilon = 0$. The other gains are

$$k_{v_x} = k_{v_y} = 1, k_{p_y} = 0.2, k_{I_y} = 0.01.$$

We have required the vehicle to move from its initial random position in the environment to the point $(-136.5, 106.5)$ m in order to bring it closer to the defined lawn-mower path. This action is done just to facilitate the motion of the vehicle towards the path and limit the saturation of the thrusters due to a large initial error. Figure 6.6 shows the motion of the vehicle, and it is readily seen from this figure that the path following task is fulfilled. Note that along the short side of the path the transient is not long enough in order to have $\tilde{\xi}_2 \rightarrow 0$. This is not a problem for real applications, e.g. sonar scanning, since the data collection is performed along the long sides of the path. In Figure 6.7, the cross-track error, i.e. the state $\tilde{\xi}_2$, is shown and we see that along the long side of the path it converges to zero. Figure 6.7 shows also the state $\tilde{z}_1 = \psi - \phi$ converging to a constant $\phi = \left(\frac{V_y}{U}\right)$, i.e. the crab angle, where V_y is the component of \mathbf{V} acting in the perpendicular direction

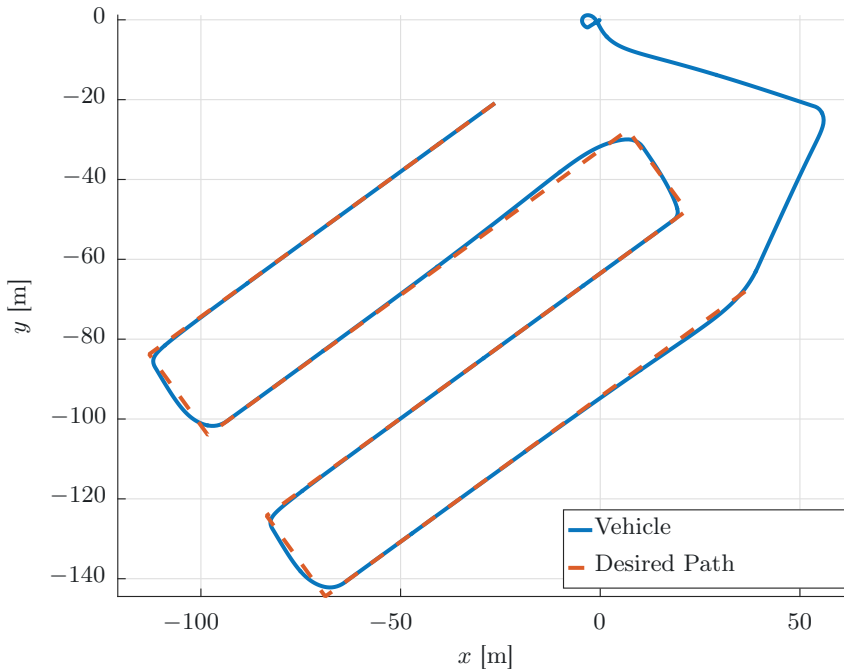


Figure 6.6: Motion of the vehicle.

with respect to the straight-line the vehicle is traveling. This is in accordance with Corollary 6.2. We have zoomed the behavior in the range $(200, 300)[s]$ which characterizes the motion of the vehicle in the North-East direction. Note that $\tilde{z}_1 \rightarrow 0.5^\circ$ and we expect $\phi = 0.6^\circ$. The value do not coincide due to the presence of simulated noises in the sensors' nodes.

6.9 Sea trial results

In this section we present the results from the sea trial. The experiments have been performed in Porto, Portugal using the LAUV (see Figure 6.8) of the LSTS. The LAUV is a lightweight, one-man-portable under-water vehicle. It is easy to operate since it require minimal operational setup. The LAUV is equipped with a computational system and navigation sensors. However, its capabilities can be enhanced adding optional payloads. The task assignment for the vehicle is the same as in the simulation case study described in Section 6.8. Note that in the real trial we do not know the value of the ocean current so we cannot compute the expected angle ϕ .

Figure 6.9 shows the motion of the vehicle compared to the desired trajectory. We see that the vehicle fulfills the path following task. This is also confirmed by

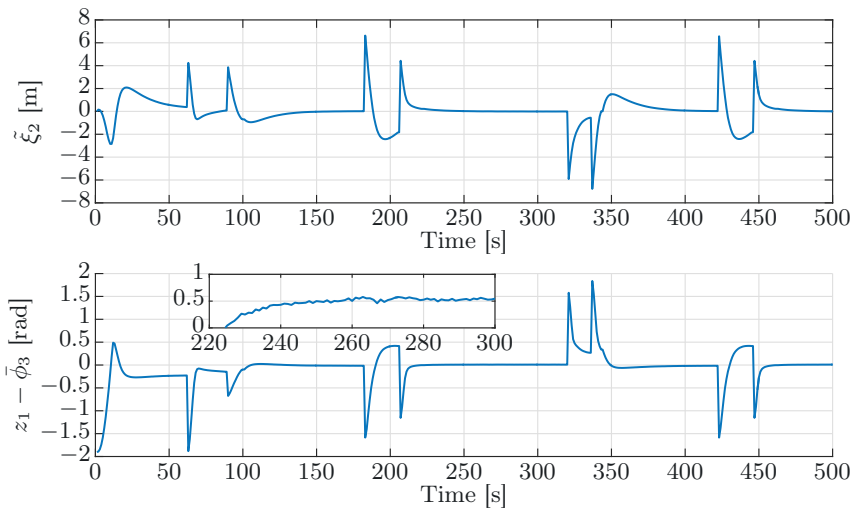


Figure 6.7: Top) Cross-track error, i.e. distance of the vehicle along the perpendicular direction to the path; Bottom) Course error.



Figure 6.8: Light autonomous underwater vehicle (LAUV).

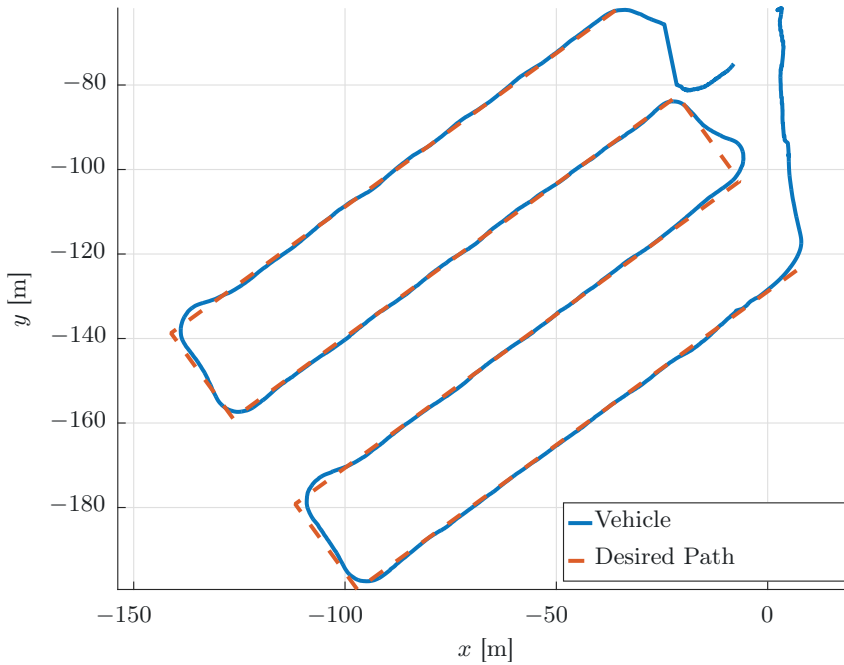


Figure 6.9: Motion of the vehicle in the real trial.

Figure 6.10 where the cross-track error is reported, and it is possible to see how it converges to zero during the motion along the long sides of the path.

From Figures 6.9-6.10, it is also clear that the behavior of the vehicle from the experimental results is in line with what to expect from the simulations.

6.10 Conclusions

In this chapter we have dealt with the path following control problem for ASVs and AUVs moving in the horizontal plane. A disturbance affecting the system, that is, an unknown ocean current, has been considered. The same control strategy as in Chapter 5 has been used for solving the path following control problem. In particular, we have used the definition of the hand position point for ASVs and AUVs in order to apply an input-output linearization. Like in Chapter 5, we obtain a linear external dynamics to deal with for control purposes. This simplifies the control design phase. Furthermore, we obtain a nonlinear internal dynamics which is affected by the control inputs designed for the external dynamics. Paths parametrized using the arc length have been considered. The time update for the path parameter is free to be designed. We have designed the time update for the path parameter dependent on the Euclidean distance of the vehicle from the path. That is, the tangential velocity of the path parameter has been chosen dependent

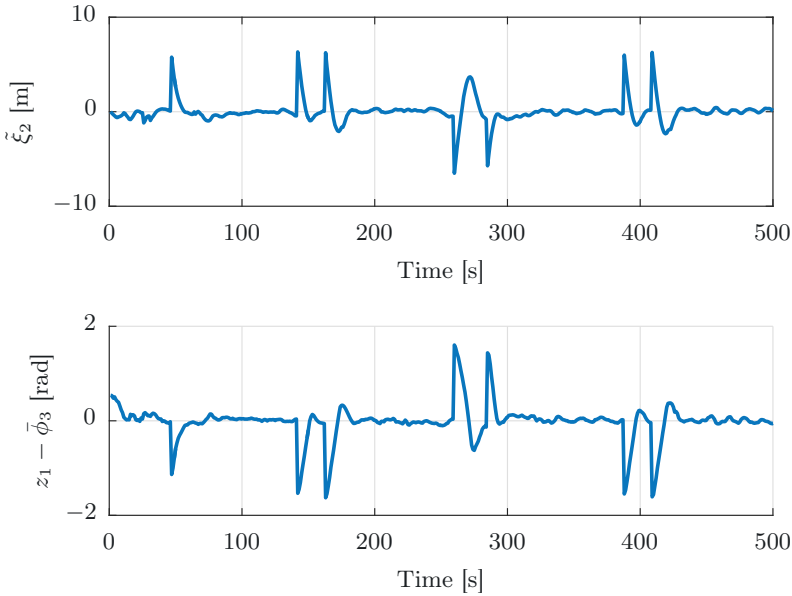


Figure 6.10: Top) Cross-track error in the sea trial; Bottom) Course error in the sea trial.

on the distance between the path and the vehicle. The tangential velocity of the parameter decreases if the vehicle is far in order to help the vehicle to catch up with the path. We have shown that our approach solves the path following control problem. In particular, we have that the external dynamics converges globally exponentially to the desired states, while the states of the internal dynamics are ultimately bounded. We have also shown that in the case of straight-line paths the closed-loop system is almost-global asymptotically stable. Furthermore, we have also considered the case of unparametrized straight-line paths and shown that the results of this chapter apply also in this case. Simulations and experimental results have been presented in order to validate the theoretical results.

Chapter 7

Multi-agent formation with disturbance rejection

In this chapter the leader-follower synchronization problem is considered. We consider a group of $N + 1$ linear agents affected by an unknown constant disturbance, which does not necessarily have to be equal for each agent. The network of agents is characterized by one leader and n followers. The leader is an agent which can influence the other N agents and it is not influenced by them. On the other hand, the remaining N agents, called followers, can influence each other and can be influenced by the leader. We assume that the communication scheme of the agents is described by a graph which has fixed topology. We assume also that the leader can communicate with at least one follower which is a root node in the graph.

The synchronization problem is solved using a diffusive coupling law. In particular, each agent tries to synchronize with its neighbors and the leader if it can directly communicate with these. An integral action is introduced in the control law in order to reject the effect of the constant unknown disturbance. The proposed solution to the leader-follower synchronization problem in this chapter is inspired by the approaches in [126] and [140]. In particular, we design a distributed controller for leader-follower synchronization based on the one given in [140] and we add integral action in the control law for each agent inspired by the distributed control in [126] for leaderless synchronization. The integral action is introduced in order to reject the effect of the constant unknown disturbance. The leader agent in the network may be real or virtual. With respect to [140], we relax the condition that the leader is an unforced linear time-invariant (LTI) system. Instead we take into account that the leader may be an agent controlled independently of the followers. As regards the communication scheme, we consider the general case of directed communication among the agents and that the leader only needs to communicate with at least one follower.

The approach described above for linear systems is then applied for formation control of marine vehicles. In particular, the nonlinear model described in Chapter 2 is used for ASVs and AUVs moving in the horizontal plane. Since the model in Chapter 2 is nonlinear, the considerations developed for linear systems cannot be directly applied. Therefore, the control approach based on the definition of the

hand position as output of the system and presented in Chapters 5, 6 is used to linearize the model of the marine vehicles. In fact, with the hand position as output, we obtain a linearized external dynamics to which it is possible to apply the synchronizing controller which has been developed for LTI systems, together with an internal dynamics which is asymptotically stable for bounded states of the external dynamics. The main idea is similar to the one presented in [125]. That is, the input-output feedback linearizing controller is used at a local level in order to linearize the dynamics of each agent. Then, a diffusive coupling law is used at the network level in order to achieve synchronization of the agents. We show that the desired motion in formation is achieved for the nonlinear under-actuated marine vehicles, even though ocean currents of different unknown constant magnitudes and directions are affecting each vehicle.

This chapter is based on [107].

The chapter is organized as follows: Section 7.1 gives the model and the assumptions for the agents in the network; in Section 7.2 the control objective for each agent is defined; Section 7.3 gives the control design and some considerations on the controller; in Section 7.4 the main result of this chapter is presented; in Section 7.5 we show how the feedback linearizing controller of [110] makes it possible to apply the leader-follower synchronization controller presented in Section 7.3 to under-actuated marine vehicles; in Section 7.6 a simulation case study which illustrates the effectiveness of our controller is presented; finally, in Section 7.7, the conclusions are given.

7.1 Agents' model and assumptions

In this section we will describe the class of linear systems for which we address the leader-follower synchronization problem. Furthermore, we introduce the assumptions which characterize the system.

The i -th agent is characterized by the LTI dynamics

$$\dot{\Phi}_i = A\Phi_i + B\mu_i + Pd_i \quad (7.1a)$$

$$Y_i = C\Phi_i \quad (7.1b)$$

where $\Phi_i \in \mathbb{R}^n$, $\mu_i \in \mathbb{R}^m$, $Y_i \in \mathbb{R}^k$, $m \leq n$, $k \leq n$ and $m, n, k \in \mathbb{N}$. We assume that the dimension of the disturbance is the same as of the control input μ_i , i.e. $d_i \in \mathbb{R}^m$. Then $A \in \mathbb{R}^{n \times n}$, $B \in \mathbb{R}^{n \times m}$, $P \in \mathbb{R}^{n \times m}$, $C \in \mathbb{R}^{k \times n}$. The vector μ_i is the control input and we will in the following design the control law for μ_i of every vehicle in order to achieve the output synchronization. The vector d_i is a constant disturbance, which in general may or may not be different for every agent. Finally, Y_i is the output of the system. Note that we consider $i = 0, \dots, N$, i.e. the leader is identical to the followers. This is different from [140].

We consider the following assumption to hold for the leader:

Assumption 7.1. *The control action $\mu_0 = \mathbf{f}(Y_0 - Y_{0a})$ is able to counteract a disturbance which may affect the leader. Furthermore, $\mathbf{f}(Y_0 - Y_{0a})$ is a globally Lipschitz function such that $|Y_0 - Y_{0a}|$ globally asymptotically converges to zero, i.e. $\mathbf{f}(Y_0 - Y_{0a}) \rightarrow 0$.*

Remark 7.1. *Assumption 7.1 implies that the control action $\mu_0 = \mathbf{f}(Y_0 - Y_{0_d})$ regulates the leader to a constant reference. The special case in which $\mu_0 = 0 \Leftrightarrow Y_0 = Y_{0_d} \forall t \geq 0$ corresponds to the case considered in [91, 140].*

Remark 7.2. *The followers will synchronize to the leader's output regardless of the fact that the leader converges or not to its desired output. That is, if μ_0 is not able to counteract a constant disturbance such that the leader's output converges instead to $|Y_0 - Y_{0_d}| = \epsilon$, then the followers will synchronize their outputs to the resulting output state of the leader.*

In the following we will focus only on the design of the control inputs for the followers $\mu_i, i = \{1, \dots, N\}$.

Remark 7.3. *Note that the leader v_0 described by the model (7.1) may be real or virtual. That is, the leader may be a real vehicle which is moving with the group of followers, or it may be a reference signal, generated by the linear model (7.1), which is available to only some followers.*

We will now assume the following assumption to hold on the network communication:

Assumption 7.2. *The followers communicate among each other according to a digraph $\mathcal{G} = (\mathcal{V}, \mathcal{E})$ which has at least one spanning tree. The leader agent v_0 communicates its state to at least one root node of the digraph \mathcal{G} .*

Since we assumed that the communication network may be described by a graph, graph theory tools are used in this chapter. A brief overview of the tools which we use is reported in Section A.2.

7.2 Control objective

In this section we will describe the control objective which we want to achieve.

The main goal is to design a distributed control law for each follower such that they will synchronize their output states to the output states of the leader. This can be expressed as

$$\lim_{t \rightarrow \infty} ((Y_i + \Gamma_i) - Y_0) = 0 \quad \forall i \in \{1, \dots, N\} \quad (7.2)$$

where $\Gamma_i \in \mathbb{R}^k$ is a vector which prescribes an offset with respect to the leader output. Non zero Γ_i assign relative distances between the i -th follower and the leader position, and may be used in order to assign a desired formation for the agents, while with $\Gamma_i = 0$ Equation (7.2) presents the consensus objective. Note that in the following we will consider Γ_i constant, which corresponds to assigning a rigid formation. Note that each agent v_i is affected by an unknown constant disturbance which must be rejected in order to achieve the control objective (7.2).

7.3 Control design

In this section we design a control law which will achieve the control objective described in Section 7.2.

The model for the i -th follower (7.1) is affected by the presence of a constant disturbance d_i . Since we want to design a control law able to reject this disturbance, we will include an integral action. In order to do this, we consider an augmented model of (7.1)

$$\dot{\Phi}_{i_A} = A_A \Phi_{i_A} + B_A \mu_i + P_A d_i \quad (7.3a)$$

$$Y_i = C_A \Phi_{i_A} \quad (7.3b)$$

where

$$\Phi_{i_A} = \begin{bmatrix} \xi_i \\ \Phi_i \end{bmatrix} A_A = \begin{bmatrix} 0 & C \\ 0 & A \end{bmatrix} B_A = \begin{bmatrix} 0 \\ B \end{bmatrix} P_A = \begin{bmatrix} 0 \\ P \end{bmatrix} C_A = \begin{bmatrix} 0 \\ C \end{bmatrix} \quad (7.4)$$

and $\xi_i \in \mathbb{R}^k$ is such that $\dot{\xi}_i = Y_i = C \Phi_i$. The matrices 0 in A_A, B_A, P_A are matrices with zero entries of appropriate dimensions. Note that also for the leader we consider an augmented model

$$\dot{\Phi}_{0_A} = A_A \Phi_{0_A} + B_A \mu_0 + P_A d_0 \quad (7.5a)$$

$$Y_0 = C_A \Phi_{0_A} \quad (7.5b)$$

We need to assume that the integral state of the leader is available to the followers which are receiving information from it. The reason why this information is needed will be clarified in the following.

We design the following control law for the i -th agent

$$\begin{aligned} \mu_i = & K_P \left(\sum_{j \in \mathcal{N}_i} ((\Phi_i + \Gamma_i) - (\Phi_j + \Gamma_j)) + g_i (\Phi_0 - (\Phi_i + \Gamma_i)) \right) \\ & + K_I \left(\sum_{j \in \mathcal{N}_i} \left(\left(\xi_i + C \int_0^t \Gamma_i d\tau \right) - \left(\xi_j + C \int_0^t \Gamma_j d\tau \right) \right) \right. \\ & \left. + g_i \left(\xi_0 - \left(\xi_i - C \int_0^t \Gamma_i d\tau \right) \right) \right) \end{aligned} \quad (7.6)$$

where $K_P \in \mathbb{R}^{m \times n}$ and $K_I \in \mathbb{R}^{m \times k}$ are matrices with positive constants as entries. For convenience in the notation and without loss of generality, in the following we will consider $\Gamma_i = 0$. Then, we rewrite (7.6) using the augmented model of the i -th agent (7.3), and we obtain

$$\mu_i = \underbrace{\begin{bmatrix} K_I & K_P \end{bmatrix}}_{K_A} \left(\sum_{j \in \mathcal{N}_i} (\Phi_{i_A} - \Phi_{j_A}) + g_i (\Phi_{0_A} - \Phi_{i_A}) \right) \quad (7.7)$$

where clearly $K_A \in \mathbb{R}^{m \times (n+k)}$. We can rewrite the controller as a function of the communication topology matrix, L, G , and the other agents' states as

$$\mu_i = K_A \left((-L_{r,i} \otimes I_{m+k}) \bar{\Phi}_A + (G_{r,i} \otimes I_{m+k}) (\bar{\Phi}_A - \bar{\Phi}_{0A}) \right) \quad (7.8)$$

where \otimes represents the Kronecker product, I_{n+k} is the $(n+k) \times (n+k)$ identity matrix, $L_{r,i}, G_{r,i}$ are the i -th row of the Laplacian and pinning matrix, respectively. Finally, $\bar{\Phi}_A \in \mathbb{R}^{N(n+k)}$ is a vector in which all the states of the all N followers are stacked and has the form $\bar{\Phi}_A = [\Phi_{1A}^T \dots \Phi_{NA}^T]^T$ while $\bar{\Phi}_{0A} = [\Phi_{0A}^T \dots \Phi_{0A}^T]^T \in \mathbb{R}^{N(n+k)}$ is a vector in which the leader's augmented state Φ_{0A} is stacked N times.

At this point we can give some observations about the control law for the followers. First, note that (7.7) can be rearranged as

$$\begin{aligned} \mu_i = & -(\Delta_i + g_i) K_A \left(\Phi_i - \underbrace{\frac{\sum_{j \in \mathcal{N}_i} \Phi_j + g_i \Phi_0}{\Delta_i + g_i}}_{r'_i} \right) \\ & - (\Delta_i + g_i) K_I \left(\xi_i - \underbrace{\frac{\sum_{j \in \mathcal{N}_i} \xi_j + g_i \xi_0}{\Delta_i + g_i}}_{r_{iI}} \right) \end{aligned} \quad (7.9)$$

From (7.9), it is clear that r_i is the reference signal for the i -th agent v_i . The signal r_i is an average of the states of the neighbors of v_i , and the agent leader if $g_i \neq 0$. In order to reject a constant disturbance, we include the integral signal $r_{iI} = \int r_i d\tau$. This implies that we need information about the leader's integral state and the neighbors' integral state since r_{iI} is a function of the leader's and agents' state. Furthermore, the controller (7.9) differs from the controller in [140] because of the integral action, i.e. the main difference is the term r_{iI} . While the main difference of (7.9) with respect to the controller presented in [126] is given by the influence of a leader on the reference signals, i.e. in [126] $g_i = 0 \forall i \in \{1, \dots, N\}$.

7.4 Main results

In this section we present the result for the agents described by the LTI dynamics (7.1) controlled by the distributed control law (7.7).

The closed-loop analysis has to consider the behavior of the entire group of agents. Therefore, based on (7.3), we write the dynamics of the whole group of agents as

$$\dot{\bar{\Phi}}_A = (I_N \otimes A_A) \bar{\Phi}_A + (I_N \otimes B_A) \bar{\mu} + (I_N \otimes P_A) \bar{d} \quad (7.10)$$

where $\bar{d} = [d_1^T, d_2^T, \dots, d_N^T]^T \in \mathbb{R}^{Nn}$.

The controller (7.7) in stacked form for (7.10) is

$$\bar{\mu} = \left((-L + G) \otimes K_A \right) \bar{\Phi}_A + \left((L + G) \otimes K_A \right) \bar{\Phi}_{0A} \quad (7.11)$$

where we have used the Kronecker product's properties and the fact that $(G \otimes I_{n+k})\bar{\Phi}_{0_A} = ((L + G) \otimes I_{n+k})\bar{\Phi}_{0_A}$. Substituting (7.11) for $\bar{\mu}$ in (7.10) we obtain

$$\begin{aligned} \dot{\bar{\Phi}}_A &= \underbrace{((I_N \otimes A_A) - ((L + G) \otimes B_A K_A))}_{A_c} \bar{\Phi}_A \\ &\quad + ((L + G) \otimes B_A K_A) \bar{\Phi}_{0_A} + (I_{m+k} \otimes P_A) \bar{d} \end{aligned} \quad (7.12)$$

At this point we present a lemma which will be used for the proof of the main theorem

Lemma 7.1. *Under Assumptions 7.1-7.2 and if there exists a matrix $K_A = [K_I \ K_P]$ which makes the following matrix Hurwitz*

$$\begin{bmatrix} 0 & -\lambda_i C \\ -\lambda_i B K_I & A - \lambda_i B K_P \end{bmatrix} \quad (7.13)$$

where $\lambda_i \forall i \in \{1, \dots, N\}$ are the eigenvalues of $L + G$, then the matrix A_c is Hurwitz, and therefore invertible.

Proof. First, we recall Lemma 3.3 in [91] in order to prove that the matrix $L + G$ has eigenvalues $\lambda_i > 0 \forall i \in \{1, \dots, N\}$. The conditions for Lemma 3.3 in [91] are straightforwardly satisfied by Assumption 7.2.

Then we can apply a Jordan decomposition to the matrix $L + G$

$$J = P^{-1}(L + G)P = \begin{bmatrix} J_1(\lambda_1) & & \\ & \ddots & \\ & & J_p(\lambda_p) \end{bmatrix} \quad (7.14)$$

where P is a nonsingular matrix which exists for every square matrix $L + G$. Then, $J_j(\lambda_j)$ is a Jordan block of the form

$$J_j = \begin{bmatrix} \lambda_j & 1 & & \\ & \lambda_j & 1 & \\ & & \ddots & \\ & & & \lambda_j \end{bmatrix} \quad (7.15)$$

where in each Jordan block the j -th eigenvalue is repeated with its algebraic multiplicity.

We apply the similarity transformation $(P^{-1} \otimes I_N)A_c(P \otimes I_N)$ to A_c and we get

$$\bar{A}_c = I_N \otimes A_A - J \otimes B_A K_A \quad (7.16)$$

Since similar matrices share the eigenvalues, if we can show that the eigenvalues of \bar{A}_c are all negative then we also have that A_c is Hurwitz.

The matrix \bar{A}_c is block upper triangular of the form

$$\bar{A}_c = \begin{bmatrix} A_A - \lambda_1 B_A K_A & \star & & \\ & \ddots & & \\ & & \ddots & \star \\ & & & A_A - \lambda_N B_A K_A \end{bmatrix} \quad (7.17)$$

where the \star replaces a block of the form $-B_A K_A$ if the j -th eigenvalue has multiplicity larger than one, or a zero entries block otherwise. However, it is not important which block is in the place of the \star since the matrix is block upper triangular and its eigenvalues are therefore determined only by the eigenvalues of the diagonal blocks. That is, the eigenvalues of \bar{A}_c are given by the union of the eigenvalues of blocks $A_A - \lambda_j B_A K_A \forall j \in \{1, \dots, N\}$. At this point, we need to show that the j -th diagonal block is Hurwitz

$$T_j = \begin{bmatrix} 0 & -\lambda_j C \\ -\lambda_j B K_I & A - \lambda_j B K_P \end{bmatrix} \quad (7.18)$$

Applying another similarity transformation using $S = \text{diag}(\lambda_j I_k, I_n)$ we obtain

$$\begin{aligned} \bar{T}_j &= S^{-1} T_j S \\ &= \begin{bmatrix} -\frac{1}{\lambda_j} I_k & \\ & I_m \end{bmatrix} \begin{bmatrix} 0 & -\lambda_j C \\ -\lambda_j B K_I & A - \lambda_j B K_P \end{bmatrix} \begin{bmatrix} -\lambda_j I_k & \\ & I_m \end{bmatrix} \\ &= \begin{bmatrix} 0 & -\lambda_j C \\ -\lambda_j B K_I & A - \lambda_j B K_P \end{bmatrix} = A_A - \lambda_j B_A K_A \end{aligned} \quad (7.19)$$

which is Hurwitz for every $j \in \{1, \dots, N\}$ and for a suitable choice of K_A .

To sum up, we have \bar{T}_j Hurwitz for every $j \in \{1, \dots, N\}$, which implies T_j to be Hurwitz for every $j \in \{1, \dots, N\}$, which implies \bar{A}_c to be Hurwitz, which in turn implies A_c to be Hurwitz, and therefore invertible. \square

At this point we are ready to introduce the theorem presenting the main result of this chapter:

Theorem 7.1. *Consider a group of $N + 1$ agents consisting of N follower agents and one leader agent, v_0 . Consider that the dynamics of the $N + 1$ agents are described by the LTI system (7.1) and that Assumptions 7.1-7.2 hold. If the matrix pair (A, B) is stabilizable and if the matrix A_c is Hurwitz, then the controller (7.11) makes each agent achieve the control objective (7.2). In particular, $Y_i - Y_0 \rightarrow 0$ globally asymptotically.*

Proof. First, we will apply the change of variables $\delta = \bar{\Phi}_A - \bar{\Phi}_{0_A}$ which reflects the disagreement error of the followers with respect to the leader. Then, applying Lemma 7.1 and Lemma 4.6 in [77], we will show that the disagreement dynamics is input-to-state stable (ISS) with respect to the leader control input since Assumption 7.1 holds. Finally, we will show that, since $\mu_0 \rightarrow 0$ globally asymptotically, then also the disagreement dynamics converges globally asymptotically to zero.

In order to perform the change of variables $\delta = \bar{\Phi}_A - \bar{\Phi}_{0_A}$, we take into account that

$$\dot{\bar{\Phi}}_{0_A} = (I_N \otimes A_A) \bar{\Phi}_{0_A} + (I_N \otimes B_A) \bar{\mu}_0 \quad (7.20)$$

where $\bar{\mu}_0 = [\mu_0^T, \dots, \mu_0^T]^T \in \mathbb{R}^{mN}$. Furthermore, note that, without loss of generality and for convenience in the notation, we have considered $d_0 = 0$, since, according to Assumption 7.1, we assume that μ_0 is able to compensate for a possible disturbance affecting the leader. Then, we get

$$\dot{\delta} = A_c \delta + (I_N \otimes P_A) \bar{d} + (I_N \otimes B_A) \bar{\mu}_0 \quad (7.21)$$

Since the conditions required by Lemma 7.1 hold, we have that A_c^{-1} exists. Then, we define $\delta^* = A_c^{-1} (I_N \otimes P_A) \bar{d}$. The value δ^* is constant since we have assumed that d_i is constant for every agent v_i . Now we can apply another change of variables $\bar{\delta} = \delta - \delta^*$ which gives

$$\dot{\bar{\delta}} = A_c \bar{\delta} + (I_N \otimes B_A) \bar{\mu}_0 \quad (7.22)$$

Because of Assumption 7.1 we have that $(I_N \otimes B_A) \bar{\mu}_0 \rightarrow 0$ globally asymptotically, independently of the behavior of $\bar{\delta}$, and $\bar{\mu}_0(Y_0 - Y_{0_a}(t))$ is a globally Lipschitz function. Furthermore, the unforced system $\dot{\bar{\delta}} = A_c \bar{\delta}$ is GES since A_c is Hurwitz due to Lemma 7.1. Therefore, the conditions of Lemma 4.6 in [77] are respected. This implies that (7.22) is ISS. Moreover, since $(I_N \otimes B_A) \bar{\mu}_0 \rightarrow 0$, we have that $\bar{\delta} \rightarrow 0$ globally asymptotically. According to the considerations above, we have that $\delta \rightarrow \delta^*$ globally asymptotically.

Now we have to also show that $Y_i - Y_0 = \xi_i - \xi_0 \rightarrow 0$ for the synchronization objective (7.2) to be satisfied. In order to do this, we note that

$$\delta = \begin{bmatrix} \Phi_{1_A} - \Phi_{0_A} \\ \vdots \\ \Phi_{i_A} - \Phi_{0_A} \\ \vdots \\ \Phi_{N_A} - \Phi_{0_A} \end{bmatrix} = \begin{bmatrix} \begin{bmatrix} \xi_1 - \xi_0 \\ \Phi_1 - \Phi_0 \end{bmatrix} \\ \vdots \\ \begin{bmatrix} \xi_i - \xi_0 \\ \Phi_i - \Phi_0 \end{bmatrix} \\ \vdots \\ \begin{bmatrix} \xi_N - \xi_0 \\ \Phi_N - \Phi_0 \end{bmatrix} \end{bmatrix} \rightarrow \begin{bmatrix} \begin{bmatrix} \xi_1^* \\ \Phi_1^* \end{bmatrix} \\ \vdots \\ \begin{bmatrix} \xi_i^* \\ \Phi_i^* \end{bmatrix} \\ \vdots \\ \begin{bmatrix} \xi_N^* \\ \Phi_N^* \end{bmatrix} \end{bmatrix} = \delta^* \quad (7.23)$$

Then, since δ^* is constant, we have that

$$\begin{bmatrix} \dot{\xi}_i - \dot{\xi}_0 \\ \dot{\Phi}_i - \dot{\Phi}_0 \end{bmatrix} \rightarrow 0 \quad (7.24)$$

The fact that $\dot{\xi}_i - \dot{\xi}_0 = Y_i - Y_0 \rightarrow 0$ proves that the control objective is achieved. \square

Remark 7.4. A suitable matrix K_A may be chosen according to the method given in [91, 92, 126], which requires to solve a Riccati equation. As shown in [91], this is equivalent to solve the optimization problem

$$J_i = \int_0^\infty (x_i^T Q x_i + u_i^T R u_i) dt \quad (7.25)$$

where $Q = Q^T > 0, R = R^T > 0$ and x_i, u_i are the states and control vector of each agent, respectively.

7.5 Formation control of marine vehicles

In this section we show that the distributed controller defined in Section 7.3 can be applied to solve the formation control problem of under-actuated marine vehicles. The presented approach is similar to the one given in [125]. In particular, [125]

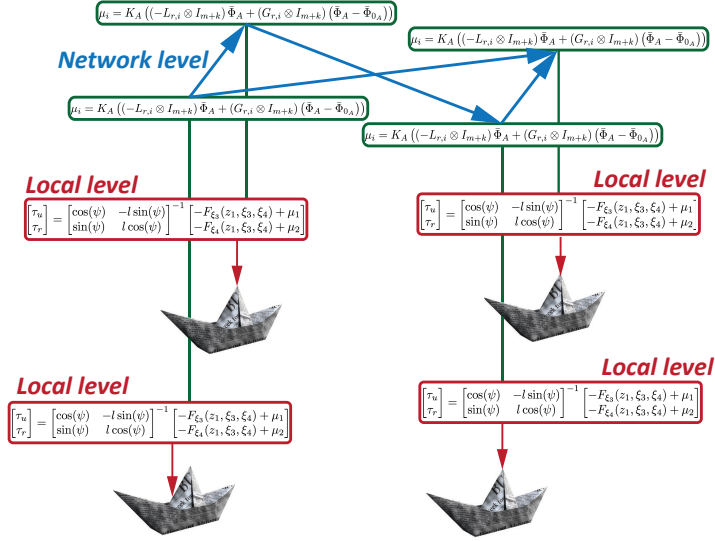


Figure 7.1: Illustration of the control approach.

presents a hierarchical strategy for the coordination of nonlinear agents. That is, the control strategy is divided into two phases. The first phase requires a controller acting at a local level, that is, the controller is independent for each agent. The second phase is characterized by a controller developed at the network level, that is, the controller couples the behavior of all the agents. Note that in [125] it is considered a leaderless scheme for the agents. In our case, we apply this hierarchical approach to the followers. The input-output feedback linearizing controller given in Chapter 5 is used at a local level in order to linearize the dynamics of each agent. This phase takes place for each agent independently from the others. Then the diffusive coupling controller presented in Section 7.3 is applied to the linearized dynamics and it is used in order to coordinate the agents. As regards the leader, a different approach holds. In fact, the leader is meant to influence the followers and to not be influenced by them. Therefore, the leader can be imagined at the top of this hierarchy. That is, the leader influences the coordination of the network being the reference signal in the diffusive coupling control law presented in Section 7.3. Note that the leader may be real or virtual. However, without loss of generality, in the following we assume the leader to be a vehicle which has the same dynamics as the followers. This means that we apply an input-output feedback linearizing controller also to the leader. Figure 7.1 gives a visual understanding of this approach.

7.5.1 Model

In this section we consider a system consisting of $N + 1$ agents characterized by the nonlinear model for ASVs and AUVs presented in Chapter 2. We briefly recall the model here.

We assume that the motion of the i -th vehicle is described in 3 DOF, i.e. surge, sway and yaw, and that the vehicle is port-starboard symmetric. We study the motion of the vehicles in an inertial frame for which we use the *North-East-Down* frame (NED) convention [54]. We consider that the ocean current affecting the i -th vehicle is given in the inertial frame by the vector $V_i = [V_{x_i}, V_{y_i}]^T$. Then, we assume that V_i is constant, irrotational and bounded, i.e. $\exists V_{\max} \geq 0$ such that $\sqrt{V_{x_i}^2 + V_{y_i}^2} \leq V_{\max}$. We assume that in general $V_i \neq V_j$.

The pose of the vehicle, i.e. the position and the orientation of the i -th vehicle, in the NED frame is given by the vector $\eta_i = [x_i, y_i, \psi_i]^T$. The motion of an ASV or an AUV moving in a horizontal plane, is given by the following 3 DOF maneuvering model given in [54] which we report here in component form

$$\dot{x}_i = u_{r_i} \cos(\psi_i) - v_{r_i} \sin(\psi_i) + V_{x_i} \quad (7.26a)$$

$$\dot{y}_i = u_{r_i} \sin(\psi_i) + v_{r_i} \cos(\psi_i) + V_{y_i} \quad (7.26b)$$

$$\dot{\psi}_i = r_i \quad (7.26c)$$

$$\dot{u}_{r_i} = F_{u_{r_i}}(v_{r_i}) - \frac{d_{11}}{m_{11}} u_{r_i} + \tau_{u_i} \quad (7.26d)$$

$$\dot{v}_{r_i} = X(u_{r_i})r_i + Y(u_{r_i})v_{r_i} \quad (7.26e)$$

$$\dot{r}_i = F_{r_i}(u_i, v_{r_i}, r_i) + \tau_{r_i} \quad (7.26f)$$

The expressions for $F_{u_{r_i}}(\cdot)$, $X(\cdot)$, $Y(\cdot)$ and $F_{r_i}(\cdot)$ are given in Appendix 7.A.

As it is clear from (7.26), the i -th vehicle is actuated only along the surge direction, i.e. by the surge force τ_{u_i} , and around the local z axis, i.e. by the yaw moment τ_{r_i} . Therefore, the model describes an under-actuated vehicle, in particular, a second order non-holonomic vehicle [54]. Equation (7.26) describes the motion of the pivot point of a ship.

7.5.2 The local controller

The model (7.26) is nonlinear and it is not possible to directly apply the distributed controller derived in Section 7.3 to a group of vehicles described by (7.26). Therefore, we now apply the results of Chapter 5, which achieves a LTI external dynamics and an internal dynamics which is asymptotically stable for bounded states of the external dynamics.

In particular, in Chapter 5 the concept of hand position $h_i = [\xi_{1_i}, \xi_{2_i}]^T = [x_i + l_i \cos(\psi_i), y_i + l_i \sin(\psi_i)]^T$, where $l_i > 0$ is constant, $[x_i, y_i]^T$ is the pivot point and ψ_i the yaw angle (cf. Figure 7.2), has been applied to under-actuated marine vehicles. Using h_i as output, it has been shown that the model is output-feedback linearizable. Thus, for each vehicle, it is possible to define the following change of coordinates

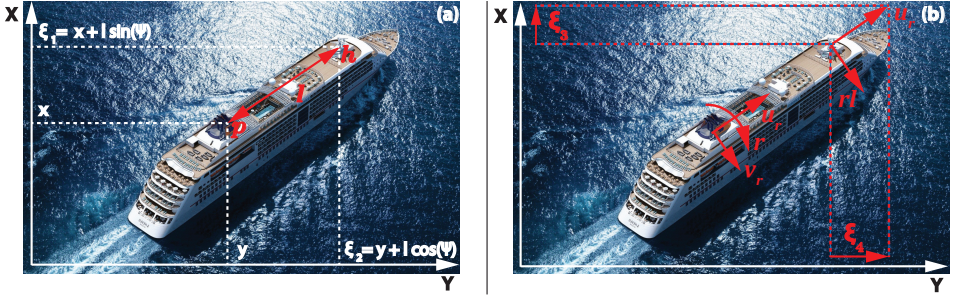


Figure 7.2: a) The pivot point (P) and the hand position h . b) Relative velocities in the NED frame.

$$z_{1_i} = \psi_i \quad (7.27a)$$

$$z_{2_i} = r_i \quad (7.27b)$$

$$\xi_{1_i} = x_i + l_i \cos(\psi_i) \quad (7.27c)$$

$$\xi_{2_i} = y_i + l_i \sin(\psi_i) \quad (7.27d)$$

$$\xi_{3_i} = u_{r_i} \cos(\psi_i) - v_{r_i} \sin(\psi_i) - r_i l_i \sin(\psi_i) \quad (7.27e)$$

$$\xi_{4_i} = u_{r_i} \sin(\psi_i) + v_{r_i} \cos(\psi_i) + r_i l_i \cos(\psi_i) \quad (7.27f)$$

and the controller

$$\begin{bmatrix} \tau_{u_i} \\ \tau_{r_i} \end{bmatrix} = \begin{bmatrix} \cos(\psi_i) & -l_i \sin(\psi_i) \\ \sin(\psi_i) & l_i \cos(\psi_i) \end{bmatrix}^{-1} \begin{bmatrix} -F_{\xi_{3_i}}(z_{1_i}, \xi_{3_i}, \xi_{4_i}) + \mu_{1_i} \\ -F_{\xi_{4_i}}(z_{1_i}, \xi_{3_i}, \xi_{4_i}) + \mu_{2_i} \end{bmatrix}. \quad (7.28)$$

The terms $F_{\xi_{3_i}}(z_{1_i}, \xi_{3_i}, \xi_{4_i})$, $F_{\xi_{4_i}}(z_{1_i}, \xi_{3_i}, \xi_{4_i})$ gather some nonlinearities and are given in Appendix 7.A. Applying (7.27) and (7.28) to each vehicle, we obtain

$$\dot{z}_{1_i} = z_{2_i} \quad (7.29a)$$

$$\dot{z}_{2_i} = f(z_{1_i}, z_{2_i}, \xi_{1_i}, \xi_{2_i}, \xi_{3_i}, \xi_{4_i}, \mu_{1_i}, \mu_{2_i}) \quad (7.29b)$$

$$\dot{\xi}_{1_i} = \xi_{3_i} + V_{x_i} \quad (7.29c)$$

$$\dot{\xi}_{2_i} = \xi_{4_i} + V_{y_i} \quad (7.29d)$$

$$\dot{\xi}_{3_i} = \mu_{1_i} \quad (7.29e)$$

$$\dot{\xi}_{4_i} = \mu_{2_i}. \quad (7.29f)$$

The function $f(\cdot)$ is a nonlinear function given in Appendix 7.A. In particular, (7.29a-7.29b) represent the internal dynamics which, in Chapter 5, has been proven to be asymptotically stable for bounded states of the external dynamics. This implies that for bounded values of ξ_{3_i} , ξ_{4_i} we have bounded z_{1_i} , z_{2_i} . Finally, note that the external dynamics (7.29c-7.29f) can be rewritten in canonical form, i.e. in

the form

$$\begin{bmatrix} \dot{\xi}_{1_i} \\ \dot{\xi}_{2_i} \\ \dot{\xi}_{3_i} \\ \dot{\xi}_{4_i} \end{bmatrix} = \underbrace{\begin{bmatrix} 0 & 0 & 1 & 0 \\ 0 & 0 & 0 & 1 \\ 0 & 0 & 0 & 0 \\ 0 & 0 & 0 & 0 \end{bmatrix}}_A \begin{bmatrix} \xi_{1_i} \\ \xi_{2_i} \\ \xi_{3_i} \\ \xi_{4_i} \end{bmatrix} + \underbrace{\begin{bmatrix} 0 & 0 \\ 0 & 0 \\ 1 & 0 \\ 0 & 1 \end{bmatrix}}_B \begin{bmatrix} \mu_{1_i} \\ \mu_{2_i} \end{bmatrix} + \underbrace{\begin{bmatrix} 1 & 0 \\ 0 & 1 \\ 0 & 0 \\ 0 & 0 \end{bmatrix}}_P \begin{bmatrix} V_{x_i} \\ V_{y_i} \end{bmatrix} \quad (7.30a)$$

$$Y_i = h_i = \begin{bmatrix} \xi_{1_i} \\ \xi_{2_i} \end{bmatrix} = \underbrace{\begin{bmatrix} 1 & 0 & 0 & 0 \\ 0 & 1 & 0 & 0 \end{bmatrix}}_C \begin{bmatrix} \xi_{1_i} \\ \xi_{2_i} \\ \xi_{3_i} \\ \xi_{4_i} \end{bmatrix} \quad (7.30b)$$

which respects the conditions required by Theorem 1 in Section 7.4.

7.5.3 The leader and the followers

Without loss of generality we label the leader agent as v_0 and the N followers as $v_i \ i \in \{1, \dots, N\}$.

Since we consider that the leader is a real vehicle, we want to define a controller for (7.29) such that the leader converges to a desired path. We consider here the case of linear paths. This case is the most common for practical applications. For instance, lawn-mower paths are standard for exploring or mapping tasks. The control objective for the leader is formalized as

$$\lim_{t \rightarrow \infty} (h_0 - h_{0_d}(t)) = 0, \quad (7.31)$$

where $h_{0_d}(t)$ is a time parametrized linear trajectory. In particular, we assign $h_{0_d}(t)$ as a piece-wise linear trajectory defined by way-points [54]. We want the leader vehicle to move along the segments defined by the way points with a constant forward velocity U_d . We choose the following PID controller

$$\mu_{1_0} = -k_{v_{x_0}}(\xi_{3_0} - \xi_{3_{d_0}}) - k_{p_{x_0}}(\xi_{1_0} - \xi_{1_{d_0}}) - k_{I_{x_0}}(\xi_{1_{I_0}} - \xi_{1_{d_{I_0}}}) + \dot{\xi}_{3_{d_0}} \quad (7.32a)$$

$$\mu_{2_0} = -k_{v_{y_0}}(\xi_{4_0} - \xi_{4_{d_0}}) - k_{p_{y_0}}(\xi_{2_0} - \xi_{2_{d_0}}) - k_{I_{y_0}}(\xi_{2_{I_0}} - \xi_{2_{d_{I_0}}}) + \dot{\xi}_{4_{d_0}} \quad (7.32b)$$

where $k_{p_{x_0}}, k_{p_{y_0}}, k_{v_{x_0}}, k_{v_{y_0}}, k_{I_{x_0}}, k_{I_{y_0}}$ are positive real gains, $\xi_{i_I} = \int_0^t \xi_i(\tau) d\tau$ where $i \in \{1, 2, 1_d, 2_d\}$.

For the followers we decide to solve the synchronization problem, i.e.

$$\lim_{t \rightarrow \infty} (h_i - h_0) = 0,$$

assigning $\mu_{\xi_{3_i}}, \mu_{2_i}$ according to (7.8).

7.5.4 The result for marine vehicles

According to the choice that we have done above, we can formulate the following corollary which states the conditions under which the linear diffusive coupling law (7.8), developed in Section 7.3, can be applied for solving the formation control problem for marine vehicles.

Table 7.1: Way points.

	x [m]	y [m]
WP_1	0	0
WP_2	3500	0
WP_3	3500	3500
WP_4	0	3500

Corollary 7.1. *Consider a network of $N+1$ agents described by (7.26). Define the hand position $h_i = [x_i + d \cos(\psi_i), y_i + d \sin(\psi_i)]^T$ as output for each vehicle. Define the input-output feedback linearizing controller (7.28) for each vehicle and apply it with $[\mu_{1_i}, \mu_{6_i}]^T$ chosen as (7.8) for all the followers, and choose $[\mu_{1_0}, \mu_{2_0}]^T$ as in (7.32) for the leader. If the conditions of Theorem 1 are satisfied by the external dynamics (7.29c-7.29f) then the control objective (7.2) is achieved. Furthermore, the internal dynamics of each follower (7.29a-7.29b) stays bounded by the bounded states of the respective external dynamics.*

Proof. The proof of this corollary is a direct consequence of Theorem 5.1 in Chapter 5 and Theorem 7.1. \square

7.6 Simulations

In this section a simulation case study is presented in order to validate the theoretical results.

For our simulations we consider for each vehicle the ASV model given in [57] and reported in Appendix B. We consider four followers and one leader which communicate via the graph given in Figure 7.3. We use the controller (7.28) together with (7.8) for the followers and (7.28) together with (7.32) for the leader. The desired formation is for the followers to move behind the leader, forming a pentagon with side length 200[m]. The leader has to travel along a piece-wise continuous line trajectory $\gamma(t)$ made of three line segments, that is, $\gamma(t) = \gamma_1(t) \cup \gamma_2(t) \cup \gamma_3(t)$. We consider

$$\begin{aligned}
 \gamma_1 &= \{(x_{0_d}(t), y_{0_d}(t)) \mid x_{0_d}(t) = 3t \text{ [m]}, y_{0_d} = 0 \text{ [m]}\} \\
 \gamma_2 &= \{(x_{0_d}(t), y_{0_d}(t)) \mid x_{0_d}(t) = 3500 \text{ [m]}, y_{0_d} = 3(t - t_1) \text{ [m]}\} \\
 \gamma_3 &= \{(x_{0_d}(t), y_{0_d}(t)) \mid x_{0_d}(t) = -3(t - t_2) + 3500 \text{ [m]}, y_{0_d} = 3500 \text{ [m]}\}.
 \end{aligned} \tag{7.33}$$

Note that t_1 is the time instant at which the vehicle arrives nearby WP_2 and t_2 the time instant at which it arrives nearby WP_3 . An illustration of the path and of the desired configuration for the agents is given in Figure 7.3.

It is clear that $\gamma(t)$ is delimited by the four way points listed in Table 7.1. The switch from $\gamma_i(t)$ to $\gamma_{i+1}(t)$ is made with the circle of acceptance method [54]. That is, the desired path switches from $\gamma_1(t)$ to $\gamma_2(t)$ when the vehicle is inside a circle of radius $R = 200$ [m] centered at WP_2 . The switch from $\gamma_2(t)$ to $\gamma_3(t)$ happens in the same way when the distance between the vehicle and WP_3 is smaller than 200[m]. Table 7.2 gives the agents' initial positions and the ocean current affecting each one of them. Note that the currents are strongly different

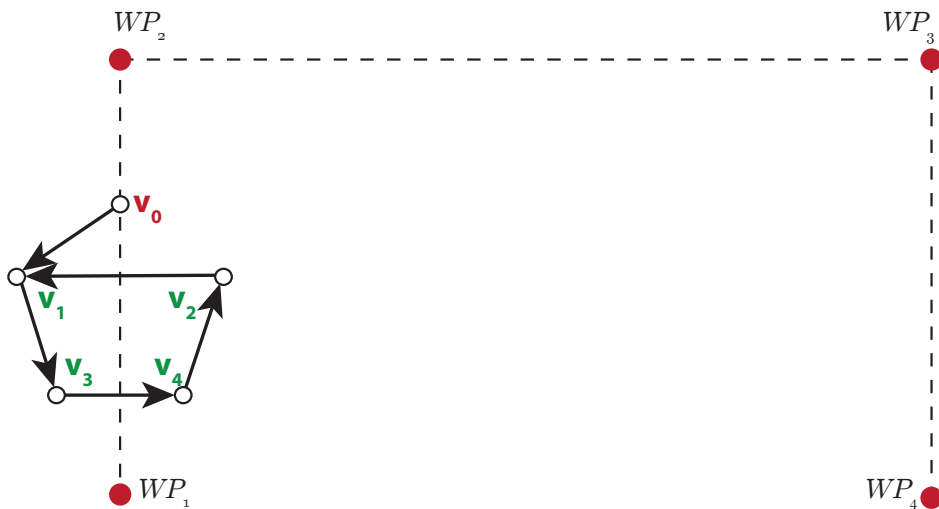


Figure 7.3: Desired motion and topology of the communication graph.

Table 7.2: Initial states and ocean currents affecting the vehicles.

	$x _{t_0}$ [m]	$y _{t_0}$ [m]	$\psi _{t_0}$ [deg]	V_x [m/s]	V_y [m/s]
v_0	-10	50	10	-0.7	-0.9
v_1	-100	50	50	0.5	-1
v_2	-300	300	30	0.2	-0.5
v_3	-300	-150	20	-1	-0.8
v_4	0	100	15	1	-0.3

for each vehicle. This is a somewhat unrealistic situation, but we use it in order to show the generality of our theoretical result. During our simulation we consider saturation for both the rudder and the propeller using the same saturation limit as in [57]. The maximum rudder angle of the ASV is 35° and the maximum rudder turning rate $10[^\circ/\text{s}]$. The maximum available propeller force is $1600[\text{kN}]$. Finally, we consider $l_i = l_j = 50[\text{m}] \forall i, j \in \{1, \dots, N\}$. Figures 7.4-7.7 show the results of the simulation.

From Figure 7.4 we see that the leader vehicle v_0 converges to the desired path while the four followers converge to the desired formation. Figure 7.5 shows the trajectory tracking error of the leader. It is clear that the control objective of the leader, that is tracking $\gamma(t)$ is achieved. Note that when v_0 is close to the way points we have a jump in the error. This corresponds to a switch from a segment to the other of the path. However, the error is driven to zero again. Figure 7.6 shows the error between the output of each agent, that is the hand position point h_i of the i -th agent, and the output of the leader, that is h_0 . It is clear that also the formation task is achieved. Also in this case note how the formation error jumps from zero to a high value when a way point is reached. However, also in this

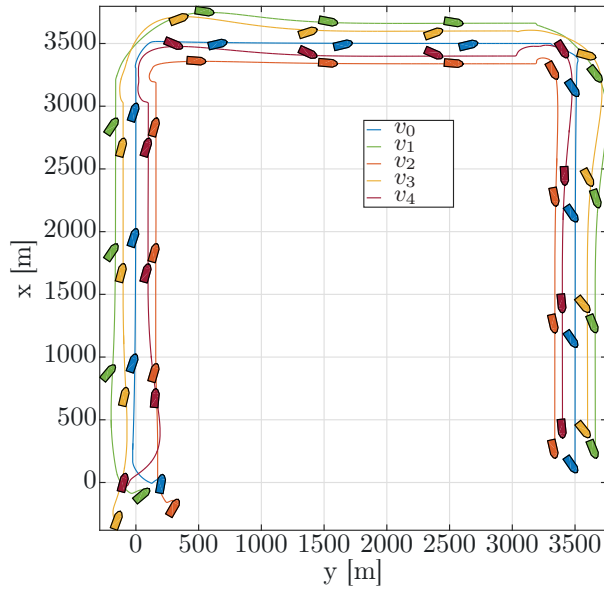
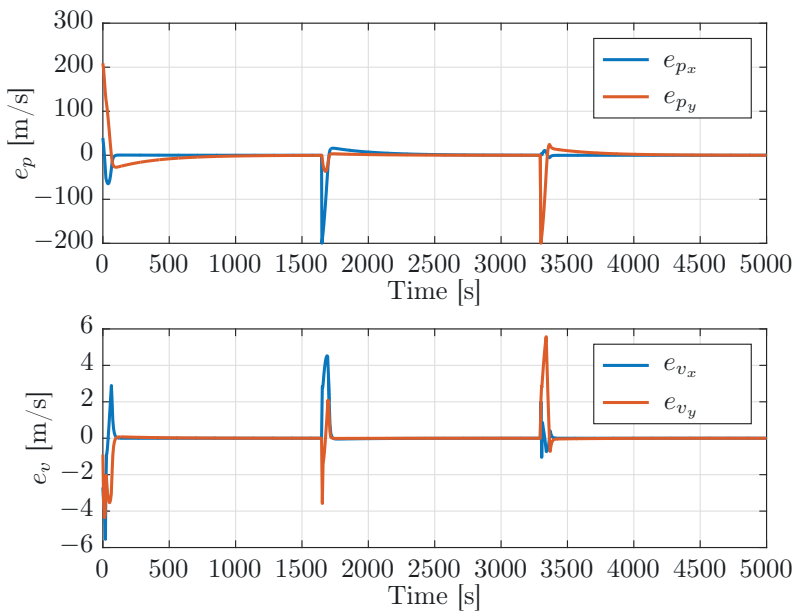


Figure 7.4: Motion of the vehicles.

Figure 7.5: Trajectory tracking errors of the leader v_0 .

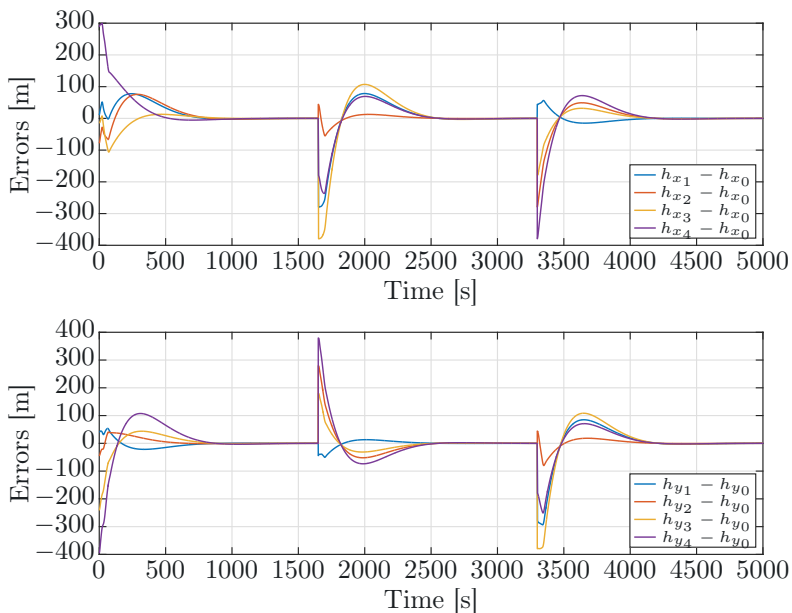


Figure 7.6: Formation errors.

case the formation error is then driven to zero again. Finally, Figure 7.7 shows the states z_{1_i}, z_{2_i} for the five agents. They are all bounded as expected from Theorem 7.1.

7.7 Conclusions

In this chapter we have presented a leader-follower strategy for agents with LTI dynamics. We have considered that each agent is affected by an unknown constant disturbance. We have proved that our approach gives global asymptotic synchronization of the followers' output with the leader's output. We have also considered that the leader may be a controlled linear system, or a virtual leader generated by the LTI dynamics (7.1). Furthermore, we have applied the proposed synchronizing controller to the formation control problem for nonlinear under-actuated marine vehicles. In particular, we have applied recent results on how to develop a feedback linearized system with stable internal dynamics by choosing the concept of hand position as system output, and applied the proposed leader-follower synchronization approach to the resulting LTI system. The theoretical results have been validated with a simulation case study.

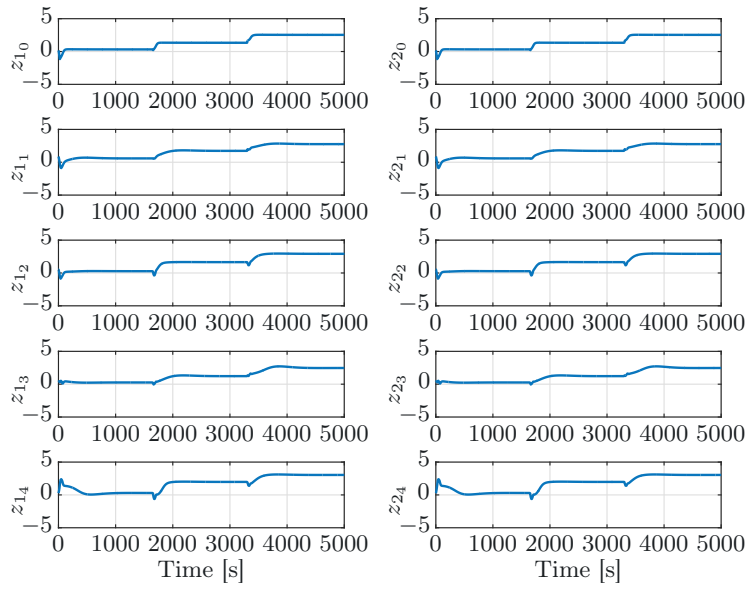


Figure 7.7: Time evolution of the yaw angle and yaw rate of the five agents.

7.A Equations

$$F_{u_r}(v_r, r) \triangleq \frac{1}{m_{11}}(m_{22}v_r + m_{23}r)r - \frac{d_{11}}{m_{11}}u_r, \quad (7.34)$$

$$X_1(\mathbf{M}) \triangleq \frac{m_{11}m_{33} - m_{23}^2}{m_{22}m_{33} - m_{23}^2} \quad X_2(\mathbf{M}, \mathbf{D}) \triangleq \frac{d_{33}m_{23} - d_{23}m_{33}}{m_{22}m_{33} - m_{23}^2} \quad (7.35)$$

$$Y_1(\mathbf{M}) \triangleq \frac{(m_{11} - m_{22})m_{23}}{m_{22}m_{33} - m_{23}^2} \quad Y_2(\mathbf{M}, \mathbf{D}) \triangleq \frac{d_{22}m_{33} - d_{32}m_{23}}{m_{22}m_{33} - m_{23}^2} \quad (7.36)$$

$$X(u_r) \triangleq -X_1u_r + X_2 \quad Y(u_r) \triangleq -Y_1u_r - Y_2, \quad (7.37)$$

$$F_r(u_r, v_r, r) \triangleq \frac{m_{23}d_{22} - m_{22}(d_{32} + (m_{22} - m_{11})u_r)}{m_{22}m_{33} - m_{23}^2}v_r \\ + \frac{m_{23}(d_{23} + m_{11}u_r) - m_{22}(d_{33} + m_{23}u_r)}{m_{22}m_{33} - m_{23}^2}r, \quad (7.38)$$

$$f(z_1, z_2, \xi_1, \xi_2, \xi_3, \xi_4, \mu_1, \mu_2) \triangleq - \left(\left(Y_1 - \frac{X_1 - 1}{l} \right) U \cos(z_1 - \phi) + Y_2 + \frac{X_2}{l} \right) z_2 \\ - \left(\frac{Y_1}{l} U \cos(z_1 - \phi) + \frac{Y_2}{l} \right) U \sin(z_1 - \phi) \\ - \frac{\mu_1 \sin(z_1)}{l} + \frac{\mu_2 \cos(z_1)}{l} \\ U \triangleq \sqrt{\xi_3^2 + \xi_4^2} \quad \wedge \quad \phi \triangleq \arctan \left(\frac{\xi_4}{\xi_3} \right) \quad (7.39)$$

$$\begin{bmatrix} F_{\xi_{3_i}}(\cdot) \\ F_{\xi_{4_i}}(\cdot) \end{bmatrix} \triangleq \begin{bmatrix} \cos(\psi_i) & -\sin(\psi_i) \\ \sin(\psi_i) & \cos(\psi_i) \end{bmatrix} \begin{bmatrix} F_{u_{r_i}}(\cdot) - v_{r_i}r_i - lr_i^2 \\ u_{r_i}r_i + X(\cdot)r_i + Y(\cdot)v_{r_i} + F_{r_i}(\cdot)l \end{bmatrix} \quad (7.40)$$

Part III

Path following for marine vehicles

Chapter 8

Geometric guidance for path following of marine vehicles

In this chapter the path following control problem of unparametrized straight-line paths is considered. ASVs and AUVs moving in the horizontal plane and affected by an constant and unknown ocean current are considered. We use an observer to estimate the current, such that we can use the estimates in the guidance law in order to counteract its disturbing effect. The method is inspired by common control strategies for UAVs, in particular quad-copters, that are based on differential geometry considerations. Specifically, this work has been inspired by the control approach given in [83, 84, 86].

The method presented here is based on the following approach. We define a direction which points towards the path using the cross track error vector and the estimated ocean current vector. Then we make the vehicle align itself with this direction in order to converge to the path. We do not define an explicit desired yaw angle, but instead we use a feedback linearizing controller based on an error function developed directly on the $SO(2)$ group [27, 84, 86]. Furthermore, notice that in [86] environmental disturbances are not considered, while our controller takes into account the rejection of disturbances due to ocean currents. Moreover, in our guidance approach the desired linear velocity is defined using the ocean current estimate and a desired value for the along path velocity.

The way the desired velocity and the desired orientation are defined allows the vehicle to move along the path with an assigned along path velocity, i.e. speed over ground. In other guidance methods, e.g. the ILOS [33], it is only possible to control the relative surge velocity, which is not aligned with the path if the system is affected by an ocean current. This misalignment, i.e. the side-slip angle, is different for different ocean current vectors and the same relative surge velocity. Consequently, with the ILOS the speed over ground and forward along path velocity will depend on the magnitude of the ocean current velocity.

The main difference between the control approach presented in Chapter 6 and the one presented in this chapter stays in the choice of the output of the system. In fact, while in Chapter 6 an input-output feedback linearizing controller was applied choosing the motion of the hand position point as output, in this chapter

the vehicle is controlled with respect to the pivot point. Furthermore, the control strategy presented in Chapter 6 was valid for parametrized curved paths, while the approach presented here is valid only for unparametrized straight-line paths.

Furthermore, the guidance approach in this chapter presents two main differences with respect to control approach presented in Chapter 6. First, the approach developed here is valid only for unparametrized straight-line paths. Second, we control the marine vehicle without applying any change of inputs to the model presented in Chapter 2, as instead done in Chapter 6.

Using cascaded systems theory we prove that the closed-loop system is *almost*-globally asymptotically stable (AGAS). The work presented in this chapter is based on [109].

The chapter is organized as follows: in Section 8.1 the model for under-actuated marine vehicles is given and briefly described; Section 8.2 introduces the path following control problem; in Section 8.3 the proposed guidance strategy is given and discussed; Section 8.4 gives the controller; Section 8.5 presents the main result of this chapter; in Section 8.6 a simulation case study is given in order to validate the theoretical result; finally, Section 8.7 gives the conclusions.

8.1 Vehicle model

In this chapter the relative velocity model for ASVs and AUVs moving in the horizontal plane discussed in Chapter 2 is used. Assumptions 2.1-2.3 are considered to hold. The model (2.11) in component form is recalled here:

$$\begin{bmatrix} \dot{x} \\ \dot{y} \end{bmatrix} = \mathbf{R} \begin{bmatrix} u_r \\ v_r \end{bmatrix} + \begin{bmatrix} V_x \\ V_y \end{bmatrix} \quad (8.1a)$$

$$\dot{\psi} = r \quad (8.1b)$$

$$\dot{u}_r = F_{u_r}(v_r) - \frac{d_{11}}{m_{11}}u_r + \tau_u \quad (8.1c)$$

$$\dot{v}_r = X(u_r)r + Y(u_r)v_r \quad (8.1d)$$

$$\dot{r} = F_r(u_r, v_r, r) + \tau_r \quad (8.1e)$$

where u_r is the relative surge velocity, v_r the relative sway velocity and V_x, V_y are the x and y components of the ocean current $\mathbf{V} = [V_x, V_y]^T$, respectively. The expressions for $F_{u_r}(u_r), X(u_r), Y(u_r), F_r(u_r, v_r, r)$ are given in Appendix 8.A. The matrix $\mathbf{R} \in SO(2)$, that is, \mathbf{R} is a roation matrix and is such that

$$\mathbf{R} = [\mathbf{b}_1 \quad \mathbf{b}_2] \quad (8.2a)$$

$$\mathbf{b}_1^T \mathbf{b}_2 = 0 \quad (8.2b)$$

$$\mathbf{b}_1^T \mathbf{b}_1 = 1 \quad (8.2c)$$

$$\mathbf{b}_2^T \mathbf{b}_2 = 1. \quad (8.2d)$$

The model (8.1) describes a planar motion, therefore \mathbf{R} describes the orientation of the vehicle on the 1-dimensional unit sphere \mathbb{S}^1 , where $\mathbb{S}^1 = \{\zeta \in \mathbb{R}^2 \mid \|\zeta\| = 1\}$.

This implies that the orientation on the Euclidean plane can be described by a single parameter, that is the yaw angle ψ . Then we have

$$\mathbf{R} = \begin{bmatrix} \cos(\psi) & -\sin(\psi) \\ \sin(\psi) & \cos(\psi) \end{bmatrix}. \quad (8.3)$$

In this chapter we present a control strategy based on an attitude tracking error evolving directly in $SO(2)$. This is because the derivation of our approach results more intuitive if used to design a desired rotation matrix \mathbf{R}_d to describe the desired orientation. However, even though for the development of the theory we use \mathbf{R} , for practical reasons in real applications the matrix \mathbf{R} would be computed as in (8.3) since the on-board sensors would provide the yaw angle ψ and not the vectors $\mathbf{b}_1, \mathbf{b}_2$.

We consider the following assumption to hold:

Assumption 8.1. *The ocean current in the inertial frame $\mathbf{V}_c = [V_x, V_y]^T$ is constant, irrotational and bounded, that is, $V_{max} \geq \sqrt{V_x^2 + V_y^2}$ with V_{max} constant.*

8.2 Control objectives

In this section the path following control problems for straight-lines in the presence of unknown ocean current is described and formalized.

Without loss of generality we choose the desired path to be $\mathcal{P} = \{(x, y) \in \mathbb{R}^2 | y = 0\}$. This implies \mathcal{P} is aligned along the x -axis of the NED frame, which in turn implies that the y coordinate is equal to the cross-track error $y = e$, i.e., the minimum distance from the path. The path \mathcal{P} represents a set in the space which we want to stabilize. The control objectives can be stated as follows:

$$\lim_{t \rightarrow \infty} y = 0 \quad (8.4a)$$

$$\lim_{t \rightarrow \infty} (u_r - u_{r_d}) = 0 \quad (8.4b)$$

$$\lim_{t \rightarrow \infty} \tilde{\mathbf{R}} = \lim_{t \rightarrow \infty} \mathbf{R}_d^T \mathbf{R} = \mathbf{I} \quad (8.4c)$$

The values \mathbf{R}_d and u_{r_d} are the desired rotation matrix and the surge relative velocity, respectively. They will be defined in the next section.

8.3 The guidance law and the observer

In this section we present our guidance approach. First, the desired surge velocity u_{r_d} and the desired rotation \mathbf{R}_d are presented and discussed in this section. Then we describe the liner observer presented in [3]. The use of the observer is necessary due to the presence of the constant ocean current \mathbf{V} affecting the system (8.1). We use the observer in order to estimate and compensate for the effect of the unknown ocean current.

8.3.1 Surge velocity

For the desired value of the surge velocity we choose

$$u_{r_d}(u_x, \hat{V}) = \sqrt{(u_x - \hat{V}_x)^2 + (-\hat{V}_y)^2} \quad (8.5)$$

where u_x is a constant. The steady state surge velocity $u_{r_d,ss}$ which is reached when the observer has converged is given by $u_{r_d,ss} = \sqrt{(u_x - V_x)^2 + (-V_y)^2}$. This implies that the vehicle moves with a constant absolute along path velocity u_x , see Figure 8.1.

This differs from previous works considering straight-line path following, for instance, [20, 32], in which only the relative surge velocity is controlled to a constant independent of the ocean current. In particular, they only require $u_{r_d} > \|\mathbf{V}\|$, which implies that when the vehicle is on the path it moves with an unknown along-path velocity depending on $u_{r_d} > \|\mathbf{V}\|$.

Finally we consider the following assumption to hold

Assumption 8.2. *The desired along path velocity respects the following condition*

$$|u_x| \geq V_x. \quad (8.6)$$

Remark 8.1. *This assumption ensures that there will be forward motion along the path \mathcal{P} . Note that when the vehicle is not on the path, $u_{r_d} > \|\mathbf{V}\|$ by definition. This guarantees that the vehicle is able to counteract the disturbing effect of the vehicle as long as the thrusts are able to provide enough power.*

In order to guide the vehicle towards the path, we define a desired rotation matrix \mathbf{R}_d

$$\mathbf{b}_{1d} = \mathbf{u}_x - \mathbf{e} - \hat{\mathbf{V}} \quad (8.7)$$

$$\mathbf{R}_d = \begin{bmatrix} \frac{\mathbf{b}_{1d}}{\|\mathbf{b}_{1d}\|} & \frac{\mathbf{b}_{2d}}{\|\mathbf{b}_{2d}\|} \end{bmatrix} = \begin{bmatrix} \frac{u_x - \hat{V}_x}{\hat{N}} & \frac{ke + \hat{V}_y}{\hat{N}} \\ -k\hat{e} - \hat{V}_y & \frac{u_x - \hat{V}_x}{\hat{N}} \end{bmatrix} \quad (8.8)$$

where $\mathbf{u}_x = [u_x, 0]^T$ is the desired constant along path velocity expressed in the NED frame, $\mathbf{e} = [0, k\hat{e}]^T$ gives the cross-track error scaled by the constant gain k , $\hat{\mathbf{V}} = [\hat{V}_x, \hat{V}_y]^T$ is the estimation of the current, and

$$\hat{N} = \|\hat{\mathbf{V}} + \mathbf{u}_x + \mathbf{e}\| = \sqrt{(u_x - \hat{V}_x)^2 + (-ke - \hat{V}_y)^2}. \quad (8.9)$$

Note that in order to have a well defined guidance law we need $\hat{N} \neq 0 \forall t$. This can be assured by a careful design of the observer for the ocean current \mathbf{V} and it will be discussed in the next section. The unit vector $\frac{\mathbf{b}_{2d}}{\|\mathbf{b}_{2d}\|}$ is chosen such that

$$\left(\frac{\mathbf{b}_{1d}}{\|\mathbf{b}_{1d}\|} \right)^T \frac{\mathbf{b}_{2d}}{\|\mathbf{b}_{2d}\|} = 0. \quad (8.10)$$

This implies that $\mathbf{R}_d \in SO(2)$, i.e. \mathbf{R}_d is an orthogonal matrix [128].

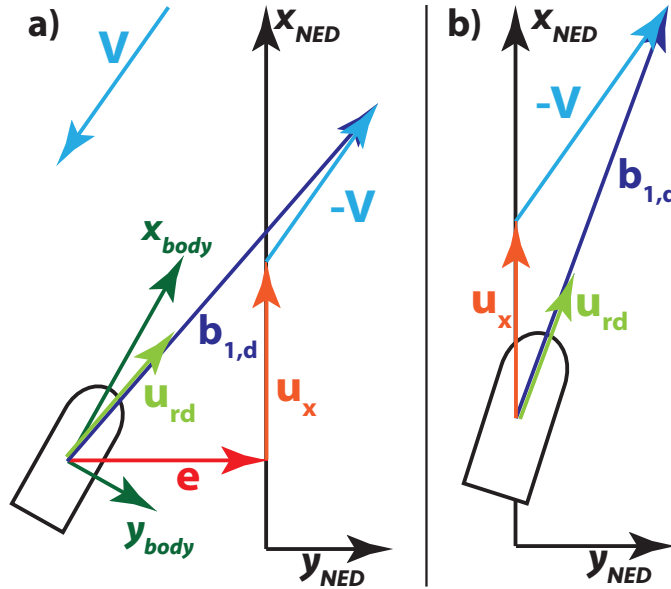


Figure 8.1: a) Geometric guidance principle for the 2D case; b) Geometric guidance principle for steady state situation

The meaning of the vector $\mathbf{b}_{1,d}$ is clear from Figure 8.1. In particular, the vector $\mathbf{b}_{1,d}$ is the sum of \mathbf{e} , \mathbf{u}_x , $-\hat{\mathbf{V}}$. Therefore, no matter what the sign or direction of the current is, if the vehicle is not on the path it will have a non zero component pointing towards the path due to the vector \mathbf{e} . This implies that the rotation imposed by \mathbf{R}_d is also pointing towards \mathcal{P} . Note also that in the vector sum for $\mathbf{b}_{1,d}$ there is $\hat{\mathbf{V}}$, which compensates for the effects of the ocean current when it converges to the real value of the ocean current. This is illustrated in Figure 8.1. Finally, when \mathbf{e} is zero the final desired direction is such that the orientation of the vehicle counteracts the current and moves along the path with velocity u_x . This situation is shown in Figure 8.1b.

To sum up: what we aim to do with our guidance approach is to define the direction $\mathbf{b}_{1,d}$ due to geometric considerations. This direction points towards the path and is used to define a desired rotation matrix \mathbf{R}_d which aligns the surge axis of the vehicle along $\mathbf{b}_{1,d}$. In fact, since we consider under-actuated vehicles the only way for the vehicle to move with the assigned absolute velocity is to align its x axis along the direction of the desired absolute velocity.

8.3.2 The observer

In order to estimate the ocean current, we use the Luenberger observer for AUVs proposed in [3]

$$\dot{\hat{\eta}} = \mathbf{R}\nu_r + \hat{\mathbf{V}} + \mathbf{K}_1\tilde{\eta} \quad (8.11a)$$

$$\dot{\hat{\mathbf{V}}} = \mathbf{K}_2\tilde{\eta} \quad (8.11b)$$

where $\hat{\eta} = [\hat{x}, \hat{y}]^T$ contains the estimates of the positions, $\hat{\mathbf{V}} = [\hat{V}_x, \hat{V}_y]^T$ contains the estimates of the current velocities, and $\mathbf{K}_1 = \text{diag}\{k_{x_1}, k_{y_1}\}$ and $\mathbf{K}_2 = \text{diag}\{k_{x_2}, k_{y_2}\}$ are diagonal matrices of positive constant values. From (8.1a-8.1b) and (8.11) we obtain the following error dynamics

$$\underbrace{\begin{bmatrix} \dot{\tilde{x}} \\ \dot{\tilde{y}} \\ \dot{\tilde{V}}_x \\ \dot{\tilde{V}}_y \end{bmatrix}}_{\dot{\xi}_1} = \begin{bmatrix} -k_{x_1} & 0 & 1 & 0 \\ 0 & -k_{y_1} & 0 & 1 \\ -k_{x_2} & 0 & 0 & 0 \\ 0 & -k_{y_2} & 0 & 0 \end{bmatrix} \underbrace{\begin{bmatrix} \tilde{x} \\ \tilde{y} \\ \tilde{V}_x \\ \tilde{V}_y \end{bmatrix}}_{\xi_1} \quad (8.12)$$

where the tilde quantities represent the estimation error, and are chosen such that $\tilde{a} = a - \hat{a}$ with $a \in \{x, y, V_x, V_y\}$. It is important to note that the injection term of the observer depends on the states x, y which are the real x and y position in the NED frame of the vehicle. The values of x and y in the NED frame can be obtained by a GPS sensor for surface vessels or via acoustic network for AUVs.

At this point, note that in order to have a well defined $\mathbf{R}_d \forall t$ we need that $\hat{N} \neq 0 \forall t$. This is guaranteed if the two terms $u_x - \hat{V}_x, -ke - \hat{V}_y$ are not zero at the same time. It then suffices to have $u_x > \hat{V}_{max} \forall t$. This can be guaranteed with an opportune initialization of the of states of the observer, for instance

$$[\hat{x}(t_0), \hat{y}(t_0), \hat{V}_x(t_0), \hat{V}_y(t_0)]^T = [x(t_0), y(t_0), 0, 0]^T.$$

This implies an initial error for the observer that is

$$[\tilde{x}(t_0), \tilde{y}(t_0), \tilde{V}_x(t_0), \tilde{V}_y(t_0)]^T = [0, 0, V_x, V_y]^T \leq \mathbf{V}_{max} \quad (8.13)$$

Now define the following Lyapunov function

$$W(t) = \tilde{x}^2 + \tilde{y}^2 + \frac{1}{k_{x_2}}\tilde{V}_x^2 + \frac{1}{k_{y_2}}\tilde{V}_y^2. \quad (8.14)$$

We obtain the following derivative

$$\dot{W}(t) = -2k_{x_1}\tilde{x}^2 - 2k_{y_1}\tilde{y}^2 \leq 0. \quad (8.15)$$

This implies that $W(t) \leq \|W(t_0)\|$. According to our choice of initial conditions we have

$$\|W(t_0)\| = \frac{V_x^2}{k_{x_2}} + \frac{V_y^2}{k_{y_2}} \leq \frac{1}{\min(k_{x_2}, k_{y_2})} V_{\max}^2. \quad (8.16)$$

From (8.14) we also have

$$\frac{1}{\max(k_{x_2}, k_{y_2})} \|\tilde{\mathbf{V}}(t)\|^2 \leq W(t). \quad (8.17)$$

Without loss of generality we can choose $k_{x_2} = k_{y_2}$, and combining (8.16), (8.17) we obtain

$$\|\tilde{\mathbf{V}}(t)\|^2 \leq V_{\max}^2. \quad (8.18)$$

Finally according to Assumption 8.2, we have $u_x > \hat{V}_{max} \geq V_x$.

8.4 The controllers

In this section we present the controller design to achieve our control objectives (8.4). We first define an attitude error function. In fact, in Section 8.3 we have presented a guidance law which defines a desired rotation matrix \mathbf{R}_d in order to steer the vehicle towards the desired path \mathcal{P} . This requires the definition of an attitude error function which is defined in the $SO(2)$ space. Finally, we present two feedback linearizing controllers for tracking the desired surge velocity u_{r_d} and the desired rotation matrix \mathbf{R}_d .

8.4.1 Attitude error function

With the purpose of driving the system towards the desired orientation given by \mathbf{R}_d , we define a controller which works directly in the $SO(2)$ space defining an attitude error function $\Psi(\mathbf{R}, \mathbf{R}_d) : SO(2) \times SO(2) \rightarrow \mathbb{R}$ such that $\Psi(\mathbf{R}_d, \mathbf{R}_d) = 0$ [27, 84] and then we choose its derivative as yaw tracking error. This approach is similar to the one in [84, 86].

We define $\Psi(\mathbf{R}, \mathbf{R}_d)$ as follows:

$$\Psi(\mathbf{R}, \mathbf{R}_d) = \frac{1}{2} \text{tr} \left[I - \mathbf{R}_d^T \mathbf{R} \right]. \quad (8.19)$$

and its derivative with respect to \mathbf{R} is [28, 84, 86]

$$\mathbf{D}_R \Psi(\mathbf{R}, \mathbf{R}_d) = e_R = \frac{1}{2} (\mathbf{R}_d^T \mathbf{R} - \mathbf{R}^T \mathbf{R}_d)^\vee \quad (8.20)$$

where $(\mathbf{R}_d^T \mathbf{R} - \mathbf{R}^T \mathbf{R}_d)$ is a 2×2 skew-symmetric matrix and $^\vee$ is an operator such that

$$a = \mathbf{S}(a)^\vee = \left(\begin{bmatrix} 0 & -a \\ a & 0 \end{bmatrix} \right)^\vee. \quad (8.21)$$

Note that $\Psi(\mathbf{R}, \mathbf{R}_d) \in [0, 2]$. In particular, $\Psi(\mathbf{R}_d, \mathbf{R}_d) = 0$ corresponds to the situation for which the x axis of the local frame of the vehicle is aligned along the desired direction \mathbf{b}_{1d} , that is, the vehicle is moving with the desired orientation. While $\Psi(-\mathbf{R}_d, \mathbf{R}_d) = 2$ corresponds to the situation for which the x axis of the local frame of the vehicle is aligned along $-\mathbf{b}_{1d}$, that is, the vehicle is pointing in the opposite direction with respect to the desired one.

According to [83], the following properties hold for $\Psi(\mathbf{R}, \mathbf{R}_d)$

Properties 8.1. $\Psi(\mathbf{R}, \mathbf{R}_d)$ respects the following properties:

- (i.) $\Psi(\mathbf{R}, \mathbf{R}_d)$ is positive definite about $\mathbf{R} = \mathbf{R}_d$
- (ii.) the critical points of $\Psi(\mathbf{R}, \mathbf{R}_d)$, i.e. the points in at which the derivative of $\Psi(\mathbf{R}, \mathbf{R}_d)$ is zero, are $\{\mathbf{R}_d\} \cup \{\pm\pi\hat{s}\}$ for $s \in \mathbb{S}^1$, and there exists only one critical point $\{\mathbf{R}_d\}$ in the sublevel set $L_2 = \{\mathbf{R} \in SO(2) | \Psi(\mathbf{R}, \mathbf{R}_d) < 2\}$
- (iii.) $\Psi(\mathbf{R}, \mathbf{R}_d)$ is locally quadratic on L_2

$$\frac{1}{2}\|e_R\|^2 \leq \Psi(\mathbf{R}, \mathbf{R}_d) \leq \frac{1}{2-\psi}\|e_R^2\|. \quad (8.22)$$

where $\psi < 2$.

Property ii tells that the derivative of $\Psi(\mathbf{R}, \mathbf{R}_d)$ is zero, i.e. $e_R = 0$, when the x axis of the body frame of the vehicle is aligned with \mathbf{b}_{1d} and when it points the opposite direction of \mathbf{b}_{1d} . That is, $e_R = 0$ when $\mathbf{R} = \mathbf{R}_d$ and $e_R = 0$ when $\mathbf{R} = -\mathbf{R}_d$, that is, when the orientation given by \mathbf{R} differs by 180° of the one given by \mathbf{R}_d . Note also that the sublevel set L_2 almost covers the space $SO(2)$ since it includes all the rotation matrices \mathbf{R} which give orientations that differ by 180° from the orientation given by \mathbf{R}_d .

The yaw rate error is defined as

$$\tilde{r} = r - r_d \quad (8.23)$$

and the desired signal r_d can be calculated from

$$r_d = \mathbf{S}(r_d)^\vee = \left(\mathbf{R}_d^T \dot{\mathbf{R}}_d \right)^\vee \quad (8.24)$$

$$\mathbf{S}(r_d) = \begin{bmatrix} 0 & -r_d \\ r_d & 0 \end{bmatrix}. \quad (8.25)$$

For $\Psi(\mathbf{R}, \mathbf{R}_d)$ we have that

$$\frac{d\Psi(\mathbf{R}, \mathbf{R}_d)}{dt} = e_R \tilde{r} \quad (8.26)$$

Then we have that

$$\begin{aligned} \dot{e}_R &= \frac{1}{2} \left(\text{tr} \left(\mathbf{R}_d^T \dot{\mathbf{R}} \right) \mathbf{I}_{2 \times 2} \mathbf{S}(\tilde{r}) \right)^\vee \\ &= \frac{1}{2} \underbrace{\text{tr} \left(\mathbf{R}^T \dot{\mathbf{R}}_d \right)}_C \tilde{r} \end{aligned} \quad (8.27)$$

where

$$\mathbf{S}(r) = \begin{bmatrix} 0 & -r \\ r & 0 \end{bmatrix}. \quad (8.28)$$

Note that $|C| \leq 1$ and this implies $|\dot{e}_R| \leq |\tilde{r}| \forall t$.

Remark 8.2. Note that in order to implement our guidance law, the rotation matrix \mathbf{R} , which gives the actual orientation of the vehicle is needed. The matrix \mathbf{R} can be calculated using the yaw angle ψ measured by the on-board magnetometer.

8.4.2 The controller

Motivated by [20] and [33], we choose the following *feedback linearizing* controller

$$\tau_u = -F_{u_r}(v_r) - k_u \underbrace{(u_r - u_{r_d})}_{\tilde{u}_r} + \frac{d_{11}}{m_{11}} u_{r_d} + \dot{u}_{r_d} \quad (8.29a)$$

$$\tau_r = -F_r(u_r, v_r, r) - k_r \tilde{r} - k_R e_R + \dot{r}_d \quad (8.29b)$$

where $F_{u_r}(v_r), F_r(u_r, v_r, r)$ cancel out the non-linearities of the surge and yaw dynamics in (8.1c),(8.1e). We decide not to cancel out the damping term d_{11}/m_{11} in order to obtain some robustness with respect to modeling errors in d_{11} and m_{11} . The values k_u, k_r, k_R are all positive constants. The main difference between this controller and the one in [20, 33] is that in our case the orientation error is defined using an attitude error function defined on the $SO(2)$ group. Note that in the following we will use $\tilde{u}_r = u_r - u_{r_d}(\cdot)$.

8.5 Main result

In this section we present the main result of the chapter stating a theorem which includes the conditions under which the observer (8.11) and the controller (8.29) make the system achieve the control objectives (8.4). In the following the notation $\mathbf{0}_{a \times b}$, with $a, b \in \mathbb{R}$, is used for a $a \times b$ matrix with zero entries. The notation $\mathbf{0}_a$ is used for vectors with dimension $a \in \mathbb{R}$.

Theorem 8.1. *Consider an under-actuated vessel described by the dynamic model (8.1). If Assumptions 8.1-8.2 hold and*

$$k_{x_1}, k_{y_1}, k_{x_2}, k_{y_2} > 0 \quad (8.30)$$

$$0 < k < \frac{Y_m(u_x - V_x)}{2X_M} \quad (8.31)$$

then the observer (8.11) has a GES equilibrium point $(\hat{x}, \hat{y}, \hat{V}_x, \hat{V}_y) = (x, y, V_x, V_y)$. Furthermore, the controller (8.29), where u_{r_d} and \mathbf{R}_d are given by (8.5) and (8.8), respectively, guarantees the achievement of the control objectives (8.4) for almost all the initial conditions.

Proof. In order to prove Theorem 8.1, we first substitute (8.29) in (8.1), we define $N = \sqrt{(u_x - V_x)^2 + (ke + V_y)^2}$, $\xi_1 = [\tilde{x}, \tilde{y}, \tilde{V}_x, \tilde{V}_y]^T$, $\xi_2 = [\tilde{u}, e_R, \tilde{r}]^T$, $z = [e, v_r]^T$

and after rearranging we obtain the following closed-loop system

$$\begin{aligned} \begin{bmatrix} \dot{e} \\ \dot{v}_r \end{bmatrix} &= \begin{bmatrix} -\frac{ku_{r_d}}{N} & \frac{u_x - V_x}{N} \\ k^2 X(u_{r_d})(u_x - V_x) & -\frac{kX(u_{r_d})(u_x - V_x)^2}{N^3} + Y(u_{r_d}) \end{bmatrix} \begin{bmatrix} e \\ v_r \end{bmatrix} \\ &+ \begin{bmatrix} \left(1 - \frac{u_{r_d}}{N}\right) \\ \left(1 - \frac{u_{r_d}}{N}\right) \frac{k^2 X(u_{r_d})(u_x - V_x)^2}{N} \end{bmatrix} V_y + \underbrace{\begin{bmatrix} g_e(\xi_1, \xi_2, z) \\ g_{v_r}(\xi_1, \xi_2, z) \end{bmatrix}}_{G(\xi_1, \xi_2, z)} \end{aligned} \quad (8.32a)$$

$$\begin{bmatrix} \dot{e}_R \\ \dot{\tilde{r}} \end{bmatrix} = \begin{bmatrix} 0 & C \\ -k_R & -k_r \end{bmatrix} \begin{bmatrix} e_R \\ \tilde{r} \end{bmatrix} \quad (8.32b)$$

$$\dot{\tilde{u}}_r = -\left(k_u + \frac{d_{11}}{m_{11}}\right) \tilde{u}_r \quad (8.32c)$$

$$\underbrace{\begin{bmatrix} \dot{\tilde{x}} \\ \dot{\tilde{y}} \\ \dot{\tilde{V}}_x \\ \dot{\tilde{V}}_y \end{bmatrix}}_{\mathbf{H}} = \underbrace{\begin{bmatrix} -k_{x_1} & 0 & 1 & 0 \\ 0 & -k_{y_1} & 0 & 1 \\ -k_{x_2} & 0 & 0 & 0 \\ 0 & -k_{y_2} & 0 & 0 \end{bmatrix}}_{\mathbf{H}} \begin{bmatrix} \tilde{x} \\ \tilde{y} \\ \tilde{V}_x \\ \tilde{V}_y \end{bmatrix}. \quad (8.32d)$$

The closed-loop system (8.33) can be seen as a cascaded system of the form

$$\dot{z} = \mathbf{f}_z(z, \xi) + G(\xi, z) \quad (8.33a)$$

$$\dot{\xi} = \mathbf{f}_\xi(\xi) \quad (8.33b)$$

with $z = [e, v_r]^T \in \mathbb{R}^2$, $\xi = [\xi_1, \xi_2]^T \in \mathbb{R}^7$.

The proof can be divided in four steps:

- (i.) prove that the estimates of the observer (8.11) globally exponentially converges to the real values of the ocean current, i.e. $\xi_1 = \mathbf{0}_4$ is GES;
- (ii.) prove that $(e_R, \tilde{r}) \rightarrow (0, 0)$ globally asymptotically, but in particular $R \rightarrow R_d$ almost-globally asymptotically;
- (iii.) prove that $(e, v_r) = (0, 0)$ is GAS when (8.32a) is unperturbed, i.e. $(e, v_r) = (0, 0)$ is GAS for $g_e(\cdot) = g_{v_r}(\cdot) = 0$;
- (iv.) prove that the origin of the closed loop-system system is GAS and implies that the control objectives are fulfilled for *almost all* initial conditions.

In the following we will use $X(u_{r_d}) = X$ and $Y(u_{r_d}) = Y$ for ease of notation.

8.5.1 Observer stability

From (8.32d), we note that \mathbf{H} is a Hurwitz matrix. Therefore there exists a symmetric positive definite matrix $P_{\xi_1} > 0$ such that

$$P_{\xi_1}^T \mathbf{H}_{\xi_1} + \mathbf{H}_{\xi_1}^T P_{\xi_1} = -Q_{\xi_1}$$

for a given positive definite matrix $Q_{\xi_1} > 0$. Then we have

$$V_1 = \xi_1^T P_{\xi_1} \xi_1 \quad (8.34)$$

$$\dot{V}_1 = -\xi_1^T Q_{\xi_1} \xi_1. \quad (8.35)$$

Thus the equilibrium point $(\tilde{x}, \tilde{y}, \tilde{V}_x, \tilde{V}_y) = (0, 0, 0, 0)$ is GES. This implies that

$$(\hat{x}, \hat{y}, \hat{V}_x, \hat{V}_y) \rightarrow (x, y, V_x, V_y)$$

exponentially.

8.5.2 Stability of the surge error dynamics

The error dynamics of \tilde{u}_r (8.32c) is clearly exponentially stable since $k_u, d_{11}/m_{11} > 0$. Therefore $\tilde{u}_r = 0$ is a GES equilibrium point. This implies that $u_r \rightarrow u_{r_d} = \sqrt{(u_x - \hat{V}_x)^2 + (-\hat{V}_y)^2}$ globally exponentially.

8.5.3 Stability of the attitude error dynamics

The equilibrium point of (8.32b) is $(e_R, \tilde{r}) = (0, 0)$. Note that

$$e_R|_{\mathbf{R}=\mathbf{R}_d} = e_R|_{\mathbf{R}=-\mathbf{R}_d} = 0.$$

That is, $e_R = 0$ for $\mathbf{R} = \mathbf{R}_d$ and $\mathbf{R} = -\mathbf{R}_d$.

Let us define the following Lyapunov function candidate

$$V_2 = \frac{1}{2}\tilde{r}^2 + k_R\Psi. \quad (8.36)$$

Since $\Psi > 0 \forall e_R \neq 0$, $V_2 > 0$ for $\tilde{r} \neq 0$ and $e_R \neq 0$. The derivative of V_2 is

$$\dot{V}_2 \leq -k_r\tilde{r}^2 \leq 0. \quad (8.37)$$

This implies that $\tilde{r} \rightarrow 0$. Then, invoking the La Salle invariance principle we know that $e_R \rightarrow 0$ as well. According to the definition of e_R we have $e_R = 0$ for $\mathbf{R} = \mathbf{R}_d \wedge \mathbf{R} = -\mathbf{R}_d$. Differentiating the dynamics (8.32b) with respect to the states e_R, \tilde{r} we obtain the following Jacobian matrix

$$J = \begin{bmatrix} 0 & \text{tr}(\mathbf{R}_d^T \mathbf{R}) \\ -k_R & -k_r \end{bmatrix}. \quad (8.38)$$

In particular, we have that $J|_{\mathbf{R}=\mathbf{R}_d}$ has two eigenvalues with negative real part and $J|_{(\mathbf{R}=-\mathbf{R}_d)}$ has one eigenvalue with negative real part and one eigenvalue with positive real part. This implies that $(e_R, \tilde{r})|_{\Psi(\mathbf{R}, \mathbf{R}_d)=0} = (0, 0) \Leftrightarrow \mathbf{R} = \mathbf{R}_d$ is a stable equilibrium point, while $(e_R, \tilde{r})|_{\Psi(\mathbf{R}, \mathbf{R}_d)=2} = (0, 0) \Leftrightarrow \mathbf{R} = -\mathbf{R}_d$ is unstable and in particular hyperbolic. This implies that $\Psi(\mathbf{R}, \mathbf{R}_d) = 0$ is a stable condition, that is, the motion of the vehicle with the desired orientation given by \mathbf{R}_d is stable. On the other hand, $\Psi(\mathbf{R}, \mathbf{R}_d) = 2$ is unstable, that is, if the vehicle moves with an orientation which differs by 180° to the desired one, the motion is unstable.

Then, according to Theorem A.2 and [85] we have that the equilibrium

$$(e_R, \tilde{r})|_{\mathbf{R}=-\mathbf{R}_d} = (0, 0)$$

has a stable and an unstable manifold \mathcal{W}_u^s and \mathcal{W}_u^u , respectively. Both \mathcal{W}_u^s and \mathcal{W}_u^u are one-dimensional. In fact, the manifold \mathcal{W}_u^u is spanned by the eigenvalue

with positive real part of the $J|_{\mathbf{R}=-\mathbf{R}_d}$. While \mathcal{W}_u^s , is spanned by the eigenvalue with negative real part of $J|_{\mathbf{R}=-\mathbf{R}_d}$ [85]. Since the system (8.32b) evolves on the 2-dimensional manifold \mathbb{R}^2 , we have that \mathcal{W}_u^s has zero Lebesgue measure. The discussion above implies that $(e_R, \tilde{r}) \rightarrow (0, 0)$ is GAS. In particular, if $(\mathbf{R}, r) \rightarrow (\mathbf{R}_d, r_d)$ if $(e_R, \tilde{r})_{t_0} \in \mathbb{R}^2 \setminus \mathcal{W}_u^s$, then the control objective (8.4c) is satisfied for *almost-all* the initial conditions, that is, almost globally. Note also that $(\mathbf{R}, r) = (\mathbf{R}_d, r_d)$ is locally exponentially stable (LES). Finally, note also that $\Psi(\mathbf{R}, \mathbf{R}_d) \rightarrow 0$ *almost-globally* asymptotically and locally exponentially.

8.5.4 Stability of the sway error dynamics

We now pay attention to the unperturbed sway dynamics (8.32a), that is, we pay attention to the dynamics of e, v_r when $\xi_1 = \mathbf{0}_4, \tilde{u} = e_R = \tilde{r} = 0$.

Let us define the Lyapunov candidate function

$$V_3 = \frac{1}{2} (e^2 + \kappa_2 v_r^2) \quad (8.39)$$

with $\kappa_2 > 0$ to be determined. We obtain

$$\begin{aligned} \dot{V}_3 &= e\dot{e} + \kappa_2 v_r \dot{v}_r \\ &= e \left(-\frac{k u_{r_d}}{N} + \frac{u_x - V_x}{N} v_r + \left(1 - \frac{u_{r_d}}{N}\right) V_y \right) + \\ &\quad + \kappa_2 v_r \left(\frac{k^2 X (u_x - V_x)}{N^3} e - \frac{k X (u_x - V_x)^2}{N^3} v_r + Y v_r + \right. \\ &\quad \left. - \frac{k X (u_x - V_x)}{N^2} \left(1 - \frac{u_{r_d}}{N}\right) V_y \right). \end{aligned} \quad (8.40)$$

Recall that $N = \sqrt{(u_x - V_x)^2 + (k e - V_y)^2}$. Then, when $e = 0$, we have $u_d = N$. Thus, the following inequalities hold

$$-\frac{k u_{r_d}}{N} e + \left(1 - \frac{u_{r_d}}{N}\right) V_y \leq -\frac{k (u_{r_d} - |V_y|) e}{N} \quad (8.41a)$$

$$-\left(1 - \frac{u_{r_d}}{N}\right) V_y \leq \frac{k |V_y| e}{N}. \quad (8.41b)$$

We obtain

$$\begin{aligned} \dot{V}_3 &\leq -\frac{k (u_{r_d} - |V_y|)}{N} e^2 + (u_x - V_x) \left[1 + \kappa_2 \frac{k^2 X (u_{r_d} + |V_y|)}{N^2} \right] \frac{|v_r| |e|}{N} + \\ &\quad + \kappa_2 \left(-Y_m + \frac{k X_M}{(u_x - V_x)} \right) v_r^2. \end{aligned} \quad (8.42)$$

Define now the variable

$$|z| = \frac{|e|}{N} = \frac{|e|}{\sqrt{(u_x - V_x)^2 + (k e - V_y)^2}}. \quad (8.43)$$

We have that

$$-\frac{k(u_{r_d} - |V_y|)}{N}e^2 = -Nk(u_{r_d} - |V_y|)z^2 \leq -(u_x - V_x)k(u_{r_d} - |V_y|)z^2 \quad (8.44)$$

and

$$\begin{aligned} \dot{V}_3 &\leq -(u_x - V_x)k(u_{r_d} - |V_y|)z^2 + (u_x - V_x) \left[1 + \kappa_2 \frac{k^2 X(u_{r_d} + |V_y|)}{N^2} \right] |v_r||z| \\ &\quad + \kappa_2 \left(-Y_m + \frac{kX_M}{(u_x - V_x)} \right) v_r^2 \end{aligned} \quad (8.45)$$

$$\begin{aligned} &\leq -(u_x - V_x)k(u_{r_d} - |V_y|)z^2 + (u_x - V_x) \left[1 + \kappa_2 \frac{k^2 X(u_{r_d} + |V_y|)}{(u_x - V_x)^2} \right] |v_r||z| \\ &\quad + \kappa_2 \left(-Y_m + \frac{kX_M}{(u_x - V_x)} \right) v_r^2 \end{aligned} \quad (8.46)$$

$$(8.47)$$

Choosing

$$\kappa_2 = \frac{(2\alpha - 1)(u_x - V_x)^2}{k^2(u_{r_d} + |V_y|)} \quad (8.48a)$$

$$\alpha = \frac{(u_{r_d} - |V_y|)}{(u_{r_d} + |V_y|)} \left[\frac{Y_m(u_x - V_x)}{kX_M} - 1 \right] \quad (8.48b)$$

we obtain

$$\dot{V}_3 \leq -(u_x - V_x) \left[k(u_{r_d} - |V_y|)z^2 - 2\alpha|v_r||z| + \frac{\alpha(2\alpha - 1)}{k(u_{r_d} - |V_x|)}v_r^2 \right] \quad (8.49)$$

$$\begin{aligned} &\leq -(u_x - V_x) \left[k(u_{r_d} - |V_y|)z^2 - 2\alpha|v_r||z| + \frac{\alpha^2}{k(u_{r_d} - |V_x|)}v_r^2 \right] \\ &\quad - (u_x - V_x) \frac{\alpha(\alpha - 1)}{k(u_{r_d} - |V_x|)}v_r^2 \end{aligned} \quad (8.50)$$

$$\begin{aligned} &\leq -(u_x - V_x) \left[\frac{\sqrt{k}\sqrt{(u_{r_d} - |V_y|)}e}{\sqrt{(u_x - V_x)^2 + (ke + V_y)^2}} - \frac{\alpha v_r}{\sqrt{k}\sqrt{(u_{r_d} - |V_y|)}} \right]^2 \\ &\quad - (u_x - V_x) \frac{\alpha(\alpha - 1)}{k(u_{r_d} - |V_x|)}v_r^2 \end{aligned} \quad (8.51)$$

$$\leq -\phi(e, v_r). \quad (8.52)$$

The function $\phi(e, v_r)$ is negative definite if $\alpha > 1$. Recalling the condition (8.31) and noticing that $\alpha > 1$ requires

$$k < \frac{Y_m(u_x - V_x)(u_{r_d} - |V_y|)}{2X_M u_{r_d}} \leq \frac{Y_m(u_x - V_x)}{2X_M u_{r_d}} \quad (8.53)$$

we can conclude that $-\phi(e, v_r)$ is negative definite. This implies that $(e, v_r) = (0, 0)$ is GAS. Furthermore, we have that near the origin $\phi(e, v_r) \leq -\lambda_e e^2 - \lambda_{v_r} v_r^2$, implying that $(e, v_r) = (0, 0)$ is also locally exponentially stable (LES).

8.5.5 Stability of the complete system

As mentioned above, our system respects the structure (8.33). Therefore, in order to prove that the origin of the closed-loop system (8.32) is GAS, we use the results of Theorem A.1. We need to check that the three conditions of Theorem A.1 are satisfied. That is:

- (i.) The unperturbed e, v_r dynamics, that is, (8.32a), have GAS origin when $G(\xi)\xi = 0$. This has been proven in Section 8.5.4;
- (ii.) The perturbing dynamics $\xi_1, \tilde{u}, e_R, \tilde{r}$ respect the integrability condition. This holds since $\xi_1, \tilde{u}, e_R, \tilde{r}$ are all GAS and LES;
- (iii.) The perturbing term $G(z, \xi)\xi$ has to have at most linear growth with respect to the state z . Also this property holds since

$$G(\xi) \leq G_1(\|\xi\|)\|z\| + G_2(\|z\|) \leq \bar{G}_1\|z\| + \bar{G}_2. \quad (8.54)$$

Since all conditions required by Theorem A.1 are satisfied we can tell that the origin of (8.32) is GAS. Thus $e = y \rightarrow 0, u \rightarrow u_{r_d}$ and the control objectives (8.4a-8.4b) are fulfilled. Finally, we have $e_R \rightarrow 0$ which implies that either $\mathbf{R} \rightarrow \mathbf{R}_d$ or $\mathbf{R} \rightarrow -\mathbf{R}_d$ according to the initial conditions. According to what is proven in Section 8.5.3, we have that $\mathbf{R} \rightarrow \mathbf{R}_d$ for *almost all* the initial conditions. \square

8.6 Simulation results

In this section the simulation of a case study is reported in order to validate the theoretical results.

For our simulations we consider the model of an ASV given in [57]. We consider that at the time instant $t_0 = 0$ the ASV is stationary ($u|_{t=0} = 0$) at the initial position $\mathbf{p}|_{t=0} = [50, -1100]^T$ [m]. We assume that the system is affected by an ocean current $\mathbf{V} = [V_x, V_y]^T = [-0.6, 0.7]^T$ [m/s]. The vehicle will have an estimate of the current given by the observer (8.11). The initial value of the estimation of the ocean current is $\hat{\mathbf{V}}|_{t=0} = [0, 0]^T$ m/s. As regard the position estimation the observer is initialized with the value $\mathbf{p}_0 = [50, -1100]^T$ m. This respects our considerations in Section 8.3 in order to not have overshoot in the estimation of \mathbf{V} . At $t = 0$ the vehicle is pointing in the direction $\mathbf{b}_1/\|\mathbf{b}_1\| = [0.854, -0.5197]^T$ which corresponds to an initial angle $\psi|_{t=0} = -34, 4^\circ$. The gains for the controller are $k = 0.01, k_r = 0.04, k_R = 0.004$ and $k_u = 1$. Without loss of generality we have chosen a desired straight path fixed along the x axis of the NED frame. Therefore, considering also the disturbance due to the ocean current, the desired direction for the vehicle in order to move along the path is given by $\mathbf{b}_{1,d}/\|\mathbf{b}_{1,d}\| = [0.99 - 0.12]^T$. During our simulation we consider saturation for both the rudder and the propeller using the same saturation limit as in [57]. The maximum rudder angle of the ASV is 35° and the maximum rudder turning rate $10[^\circ/\text{s}]$. The maximum available propeller force is $1600[\text{kN}]$.

In Figure 8.2, we can see how the vehicle converges to the path. It is clear that when the vehicle is on the path, its orientation is non-zero due to the necessary side-slip angle to counteract the ocean current. Figure 8.3 shows the convergence

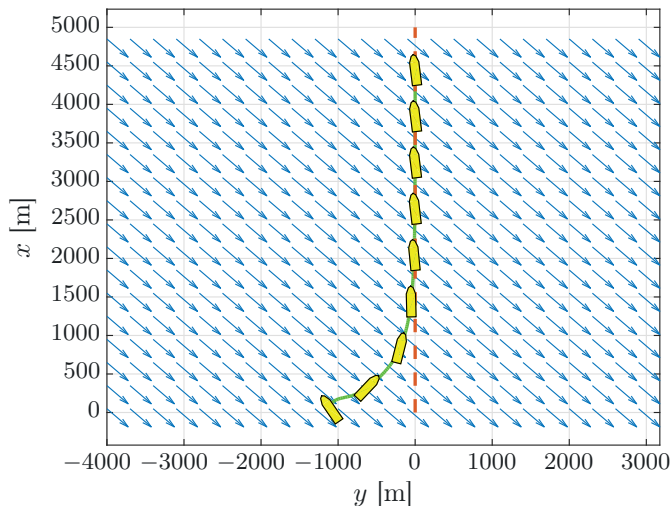


Figure 8.2: Motion of the vessel. The arrows indicates the direction of the ocean current, but they are not in scale.

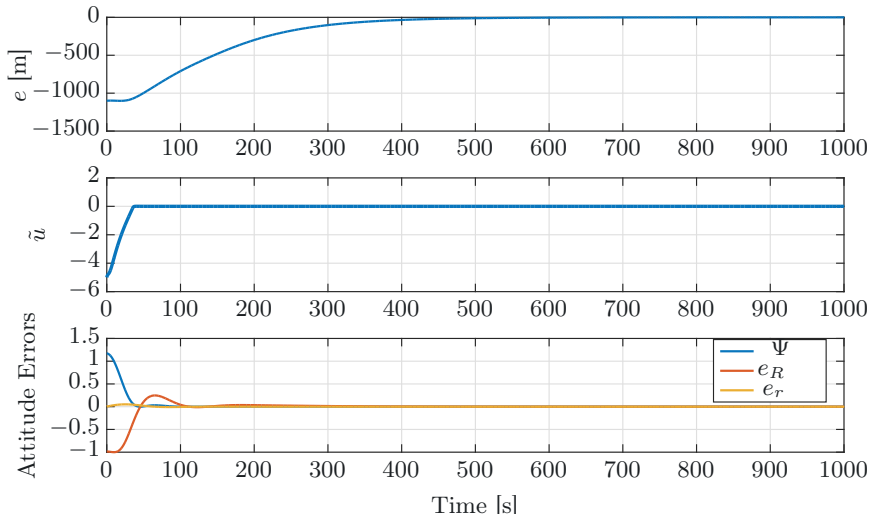


Figure 8.3: Cross-track error.

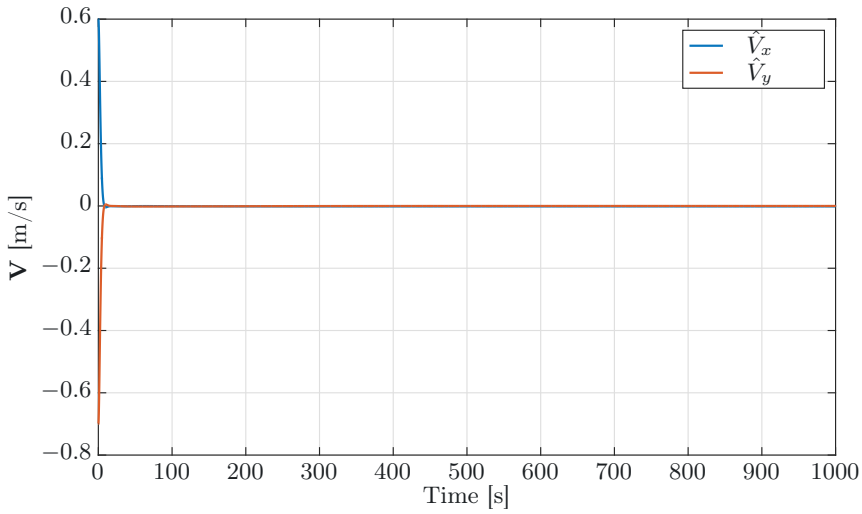


Figure 8.4: Ocean current estimate errors.

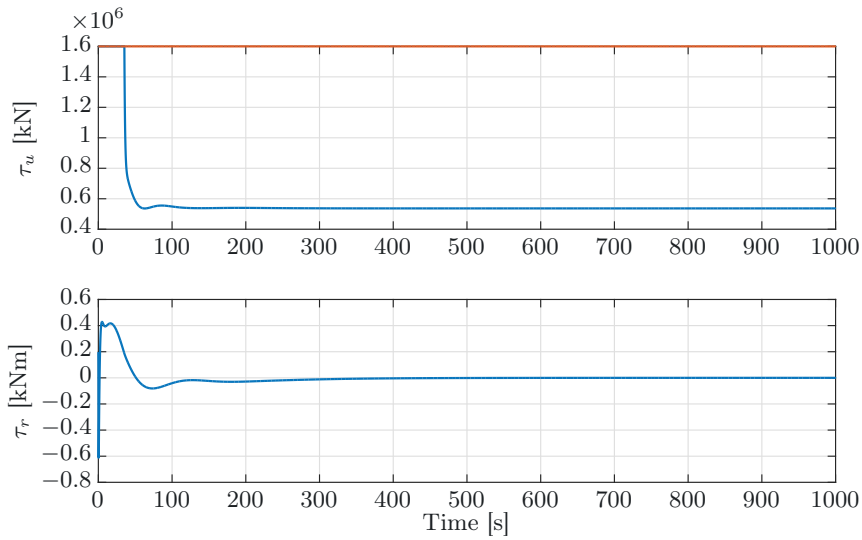


Figure 8.5: Top: surge propeller force; bottom: rudder torque

to zero of the cross track error e , the surge velocity error \tilde{u} and the attitude errors $\Psi(\mathbf{R}, \mathbf{R}_d)$, e_R and \tilde{r} . In Figure 8.4 we can see that the error estimates of the ocean current converge to zero without overshooting. This means that during the transient we have $\|\hat{\mathbf{V}}\| \leq \mathbf{V}$. Finally, in Figure 8.5 we can see the surge propeller force is saturated. and the rudder torque. We see that at the beginning of the motion, the surge propeller force is saturated.

8.7 Conclusions

In this chapter we have presented a guidance control approach for ASVs and AUVs moving in the horizontal plane, based on geometric considerations. The method has been inspired by the control strategies used in [84] for UAVs, and further extended to handle environmental disturbances. Our method uses an observer in order to estimate the ocean current and counteract it during the motion. Based on a model including both the kinematics and dynamics of the vehicle, and using cascaded systems theory, *almost*-GAS for the closed-loop system has been proved. Finally, simulation results from a case study have been reported in order to validate the theoretical results.

8.A Perturbation terms

The nonlinear terms appearing in (8.1) are reported here

$$F_{u_r} \triangleq \frac{1}{m_{11}}(m_{22}v_r + m_{23}r)r, \quad (8.55)$$

$$X(u_r) \triangleq \frac{m_{23}^2 - m_{11}m_{33}}{m_{22}m_{33} - m_{23}^2}u_r + \frac{d_{33}m_{23} - d_{23}m_{33}}{m_{22}m_{33} - m_{23}^2}, \quad (8.56)$$

$$Y(u_r) \triangleq \frac{(m_{22} - m_{11})m_{23}}{m_{22}m_{33} - m_{23}^2}u_r - \frac{d_{22}m_{33} - d_{32}m_{23}}{m_{22}m_{33} - m_{23}^2}, \quad (8.57)$$

$$F_r \triangleq \frac{m_{23}d_{22} - m_{22}(d_{32} + (m_{22} - m_{11})u_r)}{m_{22}m_{33} - m_{23}^2}v_r + \frac{m_{23}(d_{23} + m_{11}u_r) - m_{22}(d_{33} + m_{23}u_r)}{m_{22}m_{33} - m_{23}^2}r \quad (8.58)$$

$$(8.59)$$

The nonlinear terms representing the perturbation terms in (8.32) are reported here

$$g_e = z_2^T \left(\mathbf{I} - \tilde{\mathbf{R}} \right) \mathbf{R}_d u_{r_d} + z_2^T \left(\mathbf{I} - \tilde{\mathbf{R}} \right) + \left(\frac{-ke - V_y}{\hat{N}} \right) \tilde{u}_r + \left(\frac{1 - \sqrt{1 + \frac{g}{(u_x - V_x)^2 + (ke - V_y)^2}}}{\sqrt{(u_x - V_x)^2 + (ke - V_y)^2 + g}} \right) \left(\frac{ke + V_y}{N} u_{r_d} \frac{(u_x - V_x)}{N} v_r \right) \quad (8.60)$$

$$g_{v_r} = X g_r + X \tilde{r} \quad (8.61)$$

$$g = \tilde{V}_x^2 + \tilde{V}_y^2 - 2u_x \tilde{V}_x + k^2 \tilde{y}^2 + 2k^2 e \tilde{y} + 2k \tilde{y} \hat{V}_y + 2\tilde{y} \tilde{V}_y + 2ke \tilde{V}_y + k V_y \tilde{V}_y \quad (8.62)$$

$$g_r = -\frac{k(u_x - V_x)}{\hat{N}} g_e - \frac{(u_x - V_x)}{\hat{N}} k_{y_1} \tilde{y} - \frac{(ke + \hat{V}_y)}{\hat{N}} k_{x_1} \tilde{x} + \frac{\tilde{V}_x}{\hat{N}} \left(-\frac{ke u_{r_d}}{N} + \left(1 - \frac{u_{r_d}}{N} \right) V_y + \frac{(u_x - V_x)}{N} v_r + g_e \right) + \frac{\tilde{V}_y}{\hat{N}} \left(-\frac{k u_{r_d}}{N} + \frac{u_x - V_x}{N} v_r + \left(1 - \frac{u_{r_d}}{N} \right) V_y + g_e \right). \quad (8.63)$$

It is possible to verify that g_e, g_{v_r} are made of additive terms which are all at the most linear in e, v_r or bounded with respect to e, v_r . Recall that

$$G(\xi_1, \xi_2, z) = \begin{bmatrix} g_e(\xi_1, \xi_2, z) \\ g_{v_r}(\xi_1, \xi_2, z) \end{bmatrix} \quad (8.64)$$

then it holds

$$G(\xi) \leq G_1(\|\xi\|)\|z\| + G_2(\|z\|) \leq \bar{G}_1\|z\| + \bar{G}_2. \quad (8.65)$$

Chapter 9

Observer based path following for generic paths: a local approach

In this chapter a solution to the problem of following a curved path in the presence of a constant unknown ocean current disturbance is presented. The path is parametrized by a path variable that is used to propagate a path-tangential reference frame. The update law for the path variable is chosen such that the motion of the path-tangential frame ensures that the vessel remains on the normal of the path-tangential reference frame. As shown in the seminal work [124] such a parametrization is only possible locally. A tube is defined in which the aforementioned parametrization is valid and the path following problem is solved within this tube. The size of the tube is proportional to the maximum curvature of the path.

The control strategy presented in this chapter differs from the one in Chapter 6 in the control approach. In fact, in Chapter 6, a change of inputs was performed using the input-output feedback linearization method and defining the motion of the hand position point as output. Here, we control the vehicle with respect to the pivot point. Furthermore, in this chapter, we consider parametrized curved paths, while in Chapter 8 we considered unparametrized straight-line paths only.

It is shown that within the tube, the closed-loop system of the proposed controller, guidance law, and the ocean current observer provides exponential stability of the path following error dynamics. The sway velocity dynamics are analyzed taking into account couplings previously overlooked in the literature, and is shown to remain bounded. Simulation results are presented.

The work in this chapter is based on [99].

The chapter is organized as follows: in Section 9.1 the vessel model and the problem definition are presented. The path parametrization is introduced in Section 9.2. Section 9.3 presents the ocean current observer, the guidance law, and controllers. The closed-loop system is then formulated and analyzed in Section 9.4. A simulation case study is presented in Section 9.5 and conclusions are given in Section 9.6.

9.1 Vessel model

In this section we consider the model for a surface vessel given in Chapter 2. This model can be used to describe an autonomous surface vessel or an autonomous underwater vehicle moving in a plane. We consider vehicles satisfying Assumptions 2.1-2.3. Thus, their model can be expressed in component form as:

$$\dot{x} = u_r \cos(\psi) - v_r \sin(\psi) + V_x, \quad (9.1a)$$

$$\dot{y} = u_r \sin(\psi) + v_r \cos(\psi) + V_y, \quad (9.1b)$$

$$\dot{\psi} = r, \quad (9.1c)$$

$$\dot{u}_r = F_{u_r}(v_r, r) - \frac{d_{11}}{m_{11}} u_r + \tau_u, \quad (9.1d)$$

$$\dot{v}_r = X(u_r)r + Y(u_r)v_r, \quad (9.1e)$$

$$\dot{r} = F_r(u_r, v_r, r) + \tau_r, \quad (9.1f)$$

The functions $X(u_r)$, $Y(u_r)$, F_u , and F_r are given in Chapter 2. The kinematic variables are illustrated in Figure 9.1. We consider the ocean current to satisfy the following assumption.

Assumption 9.1. *The ocean current is assumed to be constant and irrotational with respect to the inertial frame, i.e. $\mathbf{V}_c \triangleq [V_x, V_y, 0]^T$. Furthermore, it is bounded by $V_{\max} > 0$ such that $\|\mathbf{V}_c\| = \sqrt{V_x^2 + V_y^2} \leq V_{\max}$.*

Additionally, we assume that the following assumption holds

Assumption 9.2. *It is assumed that $2V_{\max} < u_{rd}(t) \forall t$, i.e. the desired relative velocity of the vessel is larger than the maximum value of the ocean current.*

Assumption 9.2 assures that the vessel has enough propulsion power to overcome the ocean current affecting it. The factor two in Assumption 9.2 adds some extra conservativeness to bound the solutions of the ocean current observer. This is discussed further in Section 9.6.

9.2 Problem definition

The goal is to follow a smooth path P , parametrised by a path variable θ , by appropriately controlling the ship's surge velocity and yaw rate. For an underactuated vessel, path following can be achieved by positioning the vessel on the path with the total velocity $u_t \triangleq \sqrt{u_r^2 + v_r^2}$ (see Figure 9.1) tangential to the path. To express the path following error we propagate a path-tangential frame along P such that the vessel will be on the normal of the path-tangential frame at all time. This is illustrated in Figure 9.2. The preceding implies that the progression of the path-tangential frame is controlled such that the path following error takes the form:

$$\begin{bmatrix} x_{b/p} \\ y_{b/p} \end{bmatrix} = \begin{bmatrix} \cos(\gamma_p(\theta)) & \sin(\gamma_p(\theta)) \\ -\sin(\gamma_p(\theta)) & \cos(\gamma_p(\theta)) \end{bmatrix} \begin{bmatrix} x - x_P(\theta) \\ y - y_P(\theta) \end{bmatrix} \quad (9.2a)$$

$$= \begin{bmatrix} 0 \\ y_{b/p} \end{bmatrix}, \quad (9.2b)$$

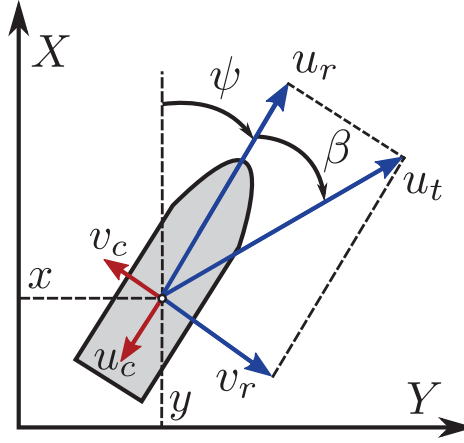


Figure 9.1: Definition of the ship's kinematic variables.

where $\gamma(\theta)$ is the angle of the path with respect to the X -axis, $x_{b/p}$ is the deviation from the normal in tangential direction, and $y_{b/p}$ is the deviation from the tangent in normal direction. The time derivative of the angle $\gamma(\theta)$ is given by $\dot{\gamma}(\theta) = \kappa(\theta)\dot{\theta}$ where $\kappa(\theta)$ is the curvature of P at θ . The goal is to regulate $x_{b/p}$ and $y_{b/p}$ to zero.

9.2.1 Locally valid parametrization

The error in the tangential direction $x_{b/p}$ will be kept at zero by the choice of the update law for the path variable θ , i.e. the vehicle is kept on the normal. It is well known that such a parametrization will only be unique locally [124]. In particular, such a unique expression exists when the vehicle is closer to the path than the inverse of the maximum curvature of the path, i.e. when $y_{b/p} < 1/\kappa_{\max}$ where κ_{\max} is the maximum curvature of the path. Note that this is equivalent to being closer than the radius of the smallest inscribed circle of the path. To design such a parametrization we first consider the error dynamics of the vessel with respect to the path frame, which is given by:

$$\dot{x}_{b/p} = -\dot{\theta}(1 - \kappa(\theta)y_{b/p}) + u_t \cos(\chi - \gamma_p(\theta)) + V_T, \quad (9.3a)$$

$$\dot{y}_{b/p} = u_t \sin(\chi - \gamma_p(\theta)) + V_N - \kappa(\theta)\dot{\theta}x_{b/p}, \quad (9.3b)$$

where $\chi \triangleq \psi + \beta$ is the course angle (see Figure 9.1) and $V_T \triangleq V_x \cos(\gamma_p(\theta)) + V_y \sin(\gamma_p(\theta))$ and $V_N \triangleq V_y \cos(\gamma_p(\theta)) - V_x \sin(\gamma_p(\theta))$ are the ocean current component in the tangential direction and normal direction of the path-tangential reference frame, respectively. Consequently, if the path variable θ is updated according to

$$\dot{\theta} = \frac{u_t \cos(\chi - \gamma_p(\theta)) + V_T}{1 - \kappa(\theta)y_{b/p}}, \quad (9.4)$$

the vessel stays on the normal when it starts on the normal. In particular, substitution of (9.4) in (9.3a) results in $\dot{x}_{b/p} = 0$. To make sure that the update law (9.4) is well defined the following condition should be satisfied

Condition 9.1. *To have a well defined update law for the path variable θ it should hold that*

$$1 - \kappa(\theta)y_{b/p} \neq 0 \quad (9.5)$$

for all time.

Note that Condition 9.1 implies that the update law is well defined within the tube of radius $y_{b/p} < 1/\kappa_{\max}$ which results in the parametrization being only locally valid.

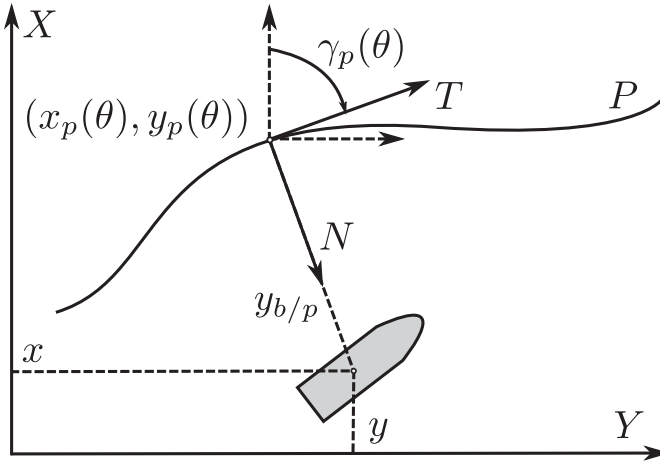


Figure 9.2: Definition of the path.

The update law (9.4) depends on the current component V_T . However, since the current is assumed unknown we have to replace V_T by its estimate $\hat{V}_T \triangleq \hat{V}_x \cos(\gamma(\theta)) + \hat{V}_y \sin(\gamma(\theta))$. Consequently, (9.2b) does not hold until the current is estimated correctly. Therefore, (9.2) takes the form

$$\begin{bmatrix} x_{b/p} \\ y_{b/p} \end{bmatrix} = \begin{bmatrix} \cos(\gamma(\theta)) & \sin(\gamma(\theta)) \\ -\sin(\gamma(\theta)) & \cos(\gamma(\theta)) \end{bmatrix} \begin{bmatrix} x - x_P(\theta) \\ y - y_P(\theta) \end{bmatrix}. \quad (9.6)$$

To force (9.6) to become equal to (9.2) once the ocean current is estimated correctly we augment (9.4) to be

$$\dot{\theta} = \frac{u_t \cos(\chi - \gamma_p(\theta)) + \hat{V}_T + k_\delta x_{b/p}}{1 - \kappa(\theta)y_{b/p}}, \quad (9.7)$$

such that the path-tangential reference frame propagates based on an estimate of the ocean current and has a restoring term to drive $x_{b/p}$ to zero. Hence, substituting (9.7) in (9.3a) gives

$$\dot{x}_{b/p} = -k_\delta x_{b/p} + \tilde{V}_T, \quad (9.8)$$

which shows that if the estimate of the current has converged the restoring term $k_\delta x_{b/p}$ remains to drive $x_{b/p}$ to zero after which the vessel remains on the normal of the path-tangential frame.

The dynamics of the error along the normal are given by

$$\dot{y}_{b/p} = u_t \sin(\chi - \gamma_p(\theta)) + V_N - x_{b/p} \kappa(\theta) \dot{\theta}. \quad (9.9)$$

In the next section a guidance law is chosen to stabilise the origin of the dynamics (9.8)-(9.9) and achieve the goal of path following.

Note that since the path parametrization is only local, we can only utilise it within a tube around the path with radius $1/\kappa_{\max}$. To achieve global results this tube needs to be made attractive and invariant, such that the vehicle first converges to the tube after which the unique parametrization to achieve path following can be used. The disadvantage of this is that a two-step approach is needed to solve the path following problem, which complicates the analysis. There is, however, also a big advantage to this approach, since extra design freedom is available when making the tube attractive. This allows one to design the approach behaviour and convergence when far from the path, while for a global one-step approach this is in general not possible to do independently of the behaviour close to the path. Hence, for the one-step approach the global behaviour will be a compromise between the desired behaviour far away from the path and the desired behaviour close to the path. For the two-step approach, the behaviour far away from the path and close to the path can be optimised independently. This, for instance, allows strategies where the vehicle moves along the normal of the path to reach the path as fast as possible. Moreover, in cluttered environments this allows the vessel to converge to the path along a clearly defined approach path, after which it can switch to the guidance strategy that allows it to follow the desired path P .

9.3 Controller, observer, and guidance

In this section we design the two control laws τ_u and τ_r , and the ocean current estimator that are used to achieve path following. In the first subsection we present the velocity control law τ_u . The second subsection presents the ocean current estimator. The third subsection first presents the guidance to be used within the tube.

9.3.1 Surge velocity control

The velocity control law is a feedback-linearising P-controller that is used to drive the relative surge velocity to a desired u_{rd} and is given by

$$\tau_u = -F_{u_r}(v_r, r) + \dot{u}_{rd} + \frac{d_{11}}{m_{11}} u_{rd} - k_u (u_r - u_{rd}), \quad (9.10)$$

where $k_u > 0$ is a constant controller gain. It is straightforward to verify that (9.10) ensures global exponential tracking of the desired velocity. In particular, when (9.10) is substituted in (9.1d) we obtain

$$\dot{\tilde{u}}_r = -k_u (u_r - u_{rd}) = -k_u \tilde{u}_r, \quad (9.11)$$

where $\tilde{u}_r \triangleq u_r - u_{rd}$. Consequently, the velocity error dynamics are described by a stable linear systems, which assures exponential tracking of the desired velocity u_{rd} .

9.3.2 Ocean current estimator

This subsection presents the ocean current estimator introduced in [2]. This observer provides the estimate of the ocean current needed to implement (9.7) and the guidance law developed in the next subsection. Rather than estimating the time-varying current components in the path frame V_T and V_N the observer is used to estimate the constant ocean current components in the inertial frame V_x and V_y . The observer from [2] is based on the kinematic equations of the vehicle, i.e. (9.1a) and (9.1b), and requires measurements of the vehicle's x and y position in the inertial frame. The observer is formulated as

$$\dot{\hat{x}} = u_r \cos(\psi) - v_r \sin(\psi) + \hat{V}_x + k_{x_1} \tilde{x} \quad (9.12a)$$

$$\dot{\hat{y}} = u_r \sin(\psi) + v_r \cos(\psi) + \hat{V}_y + k_{y_1} \tilde{y} \quad (9.12b)$$

$$\dot{\hat{V}}_x = k_{x_2} \tilde{x} \quad (9.12c)$$

$$\dot{\hat{V}}_y = k_{y_2} \tilde{y} \quad (9.12d)$$

where $\tilde{x} \triangleq x - \hat{x}$ and $\tilde{y} = y - \hat{y}$ are the positional errors and k_{x_1} , k_{x_2} , k_{y_1} , and k_{y_2} are constant positive gains. Consequently, the estimation error dynamics are given by

$$\dot{\tilde{x}} = \tilde{V}_x - k_{x_1} \tilde{x} \quad (9.13a)$$

$$\dot{\tilde{y}} = \tilde{V}_y - k_{y_1} \tilde{y} \quad (9.13b)$$

$$\dot{\tilde{V}}_x = -k_{x_2} \tilde{x} \quad (9.13c)$$

$$\dot{\tilde{V}}_y = -k_{y_2} \tilde{y} \quad (9.13d)$$

which can be written in vector form as

$$\begin{bmatrix} \dot{\tilde{x}} \\ \dot{\tilde{y}} \\ \dot{\tilde{V}}_x \\ \dot{\tilde{V}}_y \end{bmatrix} = \begin{bmatrix} -k_{x_1} & 0 & 1 & 0 \\ 0 & -k_{y_1} & 0 & 1 \\ -k_{x_2} & 0 & 0 & 0 \\ 0 & -k_{y_2} & 0 & 0 \end{bmatrix} \begin{bmatrix} \tilde{x} \\ \tilde{y} \\ \tilde{V}_x \\ \tilde{V}_y \end{bmatrix}. \quad (9.14)$$

which is a linear system with negative eigenvalues. Hence, the observer error dynamics are globally exponentially stable at the origin. Note that this implies that also \hat{V}_T and \hat{V}_N go to V_T and V_N respectively with exponential convergence since it holds that

$$\hat{V}_T = \hat{V}_x \cos(\gamma(\theta)) + \hat{V}_y \sin(\gamma(\theta)), \quad (9.15a)$$

$$\hat{V}_N = -\hat{V}_x \sin(\gamma(\theta)) + \hat{V}_y \cos(\gamma(\theta)). \quad (9.15b)$$

For implementation of the controllers it is desired that $\|\hat{V}_N(t)\| < u_{rd}(t) \forall t$. To achieve this we first choose the initial conditions of the estimator as

$$[\hat{x}(t_0), \hat{y}(t_0), \hat{V}_x(t_0), \hat{V}_y(t_0)]^T = [x(t_0), y(t_0), 0, 0]^T. \quad (9.16)$$

Consequently, the initial estimation error is given by

$$[\tilde{x}(t_0), \tilde{y}(t_0), \tilde{V}_x(t_0), \tilde{V}_y(t_0)]^T = [0, 0, V_x, V_y]^T, \quad (9.17)$$

which has a norm smaller than or equal to V_{\max} according to Assumption 9.1. Now consider the function

$$W(t) = \tilde{x}^2 + \tilde{y}^2 + \frac{1}{k_{x_2}} \tilde{V}_x^2 + \frac{1}{k_{y_2}} \tilde{V}_y^2, \quad (9.18)$$

which has the following time derivative

$$\begin{aligned} \dot{W}(t) &= 2\tilde{x}\dot{\tilde{x}} + 2\tilde{y}\dot{\tilde{y}} + \frac{2}{k_{x_2}} \tilde{V}_x \dot{\tilde{V}}_x + \frac{2}{k_{y_2}} \tilde{V}_y \dot{\tilde{V}}_y \\ &= 2\tilde{x}(\tilde{V}_x - k_{x_1}\tilde{x}) + 2\tilde{y}(\tilde{V}_y - k_{y_1}\tilde{y}) - 2\tilde{V}_y\dot{\tilde{y}} - 2\tilde{V}_x\dot{\tilde{x}} \\ &= -2k_{x_1}\tilde{x}^2 - 2k_{y_1}\tilde{y}^2 \leq 0. \end{aligned} \quad (9.19)$$

This implies that $W(t) \leq \|W(t_0)\|$. From our choice of initial conditions we know that

$$\|W(t_0)\| = \frac{1}{k_{x_2}} V_x^2 + \frac{1}{k_{y_2}} V_y^2 \leq \frac{1}{\min(k_{x_2}, k_{y_2})} V_{\max}^2. \quad (9.20)$$

Moreover, it is straightforward to verify

$$\frac{1}{\max(k_{x_2}, k_{y_2})} \|\tilde{V}_c(t)\|^2 W(t). \quad (9.21)$$

Combining the observations given above we obtain

$$\frac{1}{\max(k_{x_2}, k_{y_2})} \|\tilde{V}_c(t)\|^2 \leq \frac{1}{\min(k_{x_2}, k_{y_2})} V_{\max}^2. \quad (9.22)$$

Consequently, we obtain

$$\|\tilde{V}_c(t)\| \leq \sqrt{\frac{\max(k_{x_2}, k_{y_2})}{\min(k_{x_2}, k_{y_2})}} V_{\max} < \sqrt{\frac{\max(k_{x_2}, k_{y_2})}{\min(k_{x_2}, k_{y_2})}} u_{rd}(t), \quad \forall t, \quad (9.23)$$

which implies that if the gains are chosen as $k_{x_2} = k_{y_2}$ we have

$$\|\hat{V}_N\| \leq 2V_{\max} \leq u_{rd}(t), \quad \forall t. \quad (9.24)$$

Hence, $\|\hat{V}_N\| < u_{rd}(t)$, $\forall t$ if $2V_{\max} < u_{rd}(t)$, $\forall t$.

Remark 9.1. *The bound $2V_{\max} < u_{rd}$, $\forall t$, is only required when deriving the bound on the solutions of the observer. In particular, it is required to guarantee that $\|\hat{V}_N\| < u_{rd}(t)$, $\forall t$. For the rest of the analysis it suffices that $V_{\max} < u_{rd}$, $\forall t$.*

Therefore, if the more conservative bound $2V_{\max} < u_{rd}$, $\forall t$, is not satisfied the observer can be changed to an observer that allows explicit bounds on the estimate \hat{V}_N , e.g. the observer developed Narendra and Annaswamy [104], rather than an observer that only provides a bound on the error \hat{V}_c as is the case here. For practical purposes the estimate can also be saturated such that $\|\hat{V}_N\| < u_{rd}$, $\forall t$, which is the approach taken in Moe et al. [103]. However, in the theoretical analysis of the yaw controller we use derivatives of \hat{V}_N which will be discontinuous when saturation is applied.

9.3.3 Guidance

This subsection presents the guidance that is used in combination with the local parametrization. Since, the chosen parametrization is only valid in a tube around the path, the proposed guidance is designed for operation in the tube. Inside the tube we propose the following guidance law

$$\psi_d = \gamma(\theta) - \operatorname{atan}\left(\frac{v_r}{u_{rd}}\right) - \operatorname{atan}\left(\frac{y_{b/p} + g}{\Delta}\right). \quad (9.25)$$

The guidance law consists of three terms. The first term is a feedforward of the angle of the path with respect to the inertial frame. The second part is the desired side-slip angle, i.e. the angle between the surge velocity and the total speed when $u_r \equiv u_{rd}$. This side-slip angle is used to make the vehicle's total speed tangential to the path when the sway velocity is non-zero. The third term is a line-of-sight (LOS) term that is intended to steer the vessel to the path, where g is a term dependent on the ocean current. The choice of g provides extra design freedom to compensate for the component of the ocean current along the normal axis V_N . To analyse the effect of this guidance law and to design g we consider the error dynamics along the normal (9.9). To do this we substitute (9.25) in (9.9) and obtain

$$\dot{y}_{b/p} = u_{td} \sin\left(\psi_d + \tilde{\psi} + \beta_d - \gamma_p(\theta)\right) + V_N - x_{b/p} \kappa(\theta) \dot{\theta} + \tilde{u}_r \sin(\psi - \gamma_p(\theta)) \quad (9.26a)$$

$$= -u_{td} \frac{y_{b/p} + g}{\sqrt{(y_{b/p} + g)^2 + \Delta^2}} + V_N + G_1(\tilde{\psi}, \tilde{u}_r, x_{b/p}, \psi_d, y_{b/p}, u_{td}, \dot{\gamma}_p(\theta)) \quad (9.26b)$$

where $G_1(\cdot)$ is a perturbing term given by

$$\begin{aligned} G_1(\cdot) &= u_{td} \left[1 - \cos(\tilde{\psi}) \right] \sin\left(\arctan\left(\frac{y_{b/p} + g}{\Delta}\right)\right) + \tilde{u}_r \sin(\psi - \gamma_p(\theta)) \\ &+ u_{td} \cos\left(\arctan\left(\frac{y_{b/p} + g}{\Delta}\right)\right) \sin(\tilde{\psi}) - x_{b/p} \dot{\gamma}_p(\theta) \end{aligned} \quad (9.27)$$

and $u_{td} \triangleq \sqrt{u_{rd}^2 + v_r^2}$ is the desired total velocity. Note that $G_1(\cdot)$ satisfies

$$G_1(0, 0, 0, \psi_d, y_{b/p}, u_{td}, \dot{\gamma}_p(\theta)) = 0 \quad (9.28a)$$

$$\|G_1(\tilde{\psi}, \tilde{u}_r, x_{b/p}, \psi_d, y_{b/p}, u_{td}, \dot{\gamma}_p(\theta))\| \leq \zeta(\dot{\gamma}_p(\theta), u_{td}) \|(\tilde{\psi}, \tilde{u}, x_{b/p})\|, \quad (9.28b)$$

where $\zeta(\dot{\gamma}_p(\theta), u_{td}) > 0$, which shows that $G_1(\cdot)$ is zero when the perturbing variables are zero and that it has maximal linear growth in the perturbing variables.

To compensate for the ocean current component V_N the variable g is now chosen to satisfy the equality

$$u_{td} \frac{g}{\sqrt{\Delta^2 + (y_{b/p} + g)^2}} = \hat{V}_N. \quad (9.29)$$

which is a choice inspired by [103]. In order for g to satisfy the equality above, g should be the solution of the following second order equality

$$\underbrace{(u_{td}^2 - \hat{V}_N^2)}_{-a} \left(\frac{g}{\hat{V}_N} \right)^2 = \underbrace{\Delta^2 + y_{b/p}^2}_c + \underbrace{2y_{b/p}\hat{V}_N}_b \left(\frac{g}{\hat{V}_N} \right), \quad (9.30)$$

hence we choose g to be

$$g = \hat{V}_N \frac{b + \sqrt{b^2 - ac}}{-a}, \quad (9.31)$$

which has the same sign as \hat{V}_N and is well defined for $(u_{rd}^2 - \hat{V}_N^2) > 0$. Moreover, since

$$\sqrt{b^2 - ac} = \sqrt{\Delta^2(u_{td}^2 - \hat{V}_N^2) + y_{b/p}^2 u_{td}^2} \quad (9.32)$$

solutions are real for $(u_{rd}^2 - \hat{V}_N^2) > 0$.

Consequently, if we substitute this choice for g in (9.26) we obtain

$$\dot{y}_{b/p} = -u_{td} \frac{y_{b/p}}{\sqrt{(y_{b/p} + g)^2 + \Delta^2}} + \tilde{V}_N + G_1(\tilde{\psi}, \tilde{u}, x_{b/p}, \psi_d, y_{b/p}, u_{td}, \dot{\gamma}_p(\theta)). \quad (9.33)$$

The desired yaw rate can be found by taking the time derivative of (9.25) resulting in

$$\dot{\psi}_d = \kappa(\theta)\dot{\theta} + \frac{\dot{v}_r u_{rd} - \dot{u}_{rd} v_r}{u_{rd}^2 + v_r^2} + \frac{\Delta(\dot{y}_{b/p} + \dot{g})}{\Delta^2 + (y_{b/p} + g)^2}, \quad (9.34)$$

where \dot{v}_r as given in (9.1e), $\dot{y}_{b/p}$ in (9.33), and \dot{g} is given by

$$\dot{g} = \dot{\hat{V}}_N \frac{b + \sqrt{b^2 - ac}}{-a} + \frac{\partial g}{\partial a} \dot{a} + \frac{\partial g}{\partial b} \dot{b} + \frac{\partial g}{\partial c} \dot{c}, \quad (9.35)$$

where

$$\frac{\partial g}{\partial a} = \hat{V}_N \frac{c}{2a\sqrt{b^2 - ac}} + \hat{V}_N \frac{b + \sqrt{b^2 - ac}}{a^2}, \quad (9.36a)$$

$$\dot{a} = 2\hat{V}_N \dot{\hat{V}}_N - 2u_{rd} \dot{u}_{rd} - 2v_r [X(u_r)r + Y(u_r)v_r], \quad (9.36b)$$

$$\frac{\partial g}{\partial b} = \hat{V}_N \frac{b + \sqrt{b^2 - ac}}{a\sqrt{b^2 - ac}}, \quad (9.36c)$$

$$\dot{b} = 2\hat{V}_N \dot{y}_{b/p} + 2\dot{\hat{V}}_N y_{b/p}, \quad \frac{\partial g}{\partial c} = \hat{V}_N \frac{1}{2\sqrt{b^2 - ac}}, \quad \dot{c} = 2y_{b/p} \dot{y}_{b/p}. \quad (9.36d)$$

Note that $\dot{y}_{b/p}$ appears a number of times in the expression for $\dot{\psi}_d$ and that $\dot{y}_{b/p}$ depends on \tilde{V}_N . Consequently, $\dot{\psi}_d$ depends on an unknown variable and cannot be

used to control the yaw rate. This was not considered in [103] where the proposed controller contained both $\dot{\psi}_d$ and $\dot{\psi}_d$.

Moreover, since $\dot{\psi}_d$ contains \dot{v}_r , which depends on $r = \dot{\psi}$, the yaw rate error $\dot{\psi} \triangleq \dot{\psi} - \dot{\psi}_d$ grows with $\dot{\psi}$ which leads to a necessary condition for a well defined yaw rate error. The yaw rate error dynamics are given by

$$\begin{aligned}
 \dot{\psi} = r & \left[1 + \frac{X(u_r)u_{rd}}{u_{rd}^2 + v_r^2} - \frac{\Delta}{\Delta^2 + (y_{b/p} + g)^2} \frac{\partial g}{\partial a} (2v_r X(u_r)) \right] \\
 & - \kappa(\theta)\dot{\theta} + \frac{Y(u_r)v_r u_{rd} - \dot{u}_{rd}v_r}{u_{rd}^2 + v_r^2} \\
 & + \frac{\Delta}{\Delta^2 + (y_{b/p} + g)^2} \hat{V}_N \frac{b + \sqrt{b^2 - ac}}{-a} \\
 & + \frac{\Delta}{\Delta^2 + (y_{b/p} + g)^2} \frac{\partial g}{\partial a} \left(2\hat{V}_N \dot{\hat{V}}_N - 2u_{rd}\dot{u}_{rd} - 2v_r Y(u_r)v_r \right) \\
 & + \frac{\Delta}{\Delta^2 + (y_{b/p} + g)^2} \frac{\partial g}{\partial b} \left(2\hat{V}_N y_{b/p} \right) \\
 & + \left[1 + \frac{\partial g}{\partial c} 2y_{b/p} + \frac{\partial g}{\partial b} \left(2\hat{V}_N \right) \right] \frac{\Delta \dot{y}_{b/p}}{\Delta^2 + (y_{b/p} + g)^2}
 \end{aligned} \tag{9.37}$$

which leads to the following necessary condition for a well defined yaw rate, i.e. existence of the yaw controller,

Condition 9.2. *To have a well defined yaw controller it should hold that*

$$C_r \triangleq 1 + \frac{X(u_r)u_{rd}}{u_{rd}^2 + v_r^2} - \frac{\partial g}{\partial a} \frac{2v_r X(u_r)\Delta}{\Delta^2 + (y_{b/p} + g)^2} \neq 0. \tag{9.38}$$

for all time after entering the tube.

Remark 9.2. *The condition above can be verified for any positive velocity, for the vehicles considered in this thesis. Note that for most vessels this condition is verifiable since standard ship design practices will result in similar properties of the function $X(u_r)$. Besides having a lower bound greater than zero C_r is also upper-bounded since the term between brackets can be verified to be bounded in its arguments.*

Since $\dot{\psi}_d$ depends on the unknown signal \tilde{V}_N we cannot take $\dot{\psi}_d = r_d$. To define

an expression for r_d without requiring the knowledge of \tilde{V}_N we use (9.37) to define

$$\begin{aligned}
 r_d \triangleq & -\frac{1}{C_r} \left[\kappa(\theta) \left(\frac{u_t \cos(\psi + \beta - \gamma_p(\theta)) + k_\delta x_{b/p} + \hat{V}_T}{1 - \kappa(\theta) y_{b/p}} \right) \right. \\
 & + \frac{Y(u_r) v_r u_{rd} - \dot{u}_{rd} v_r}{u_{rd}^2 + v_r^2} + \frac{\Delta}{\Delta^2 + (y_{b/p} + g)^2} \left[\dot{\hat{V}}_N \frac{b + \sqrt{b^2 - ac}}{-a} \right. \\
 & + \frac{\partial g}{\partial a} \left(2\hat{V}_N \dot{\hat{V}}_N - 2u_{rd} \dot{u}_{rd} - 2v_r Y(u_r) v_r \right) + \frac{\partial g}{\partial b} \left(2\dot{\hat{V}}_N y_{b/p} \right) \\
 & \left. + \left[1 + \frac{\partial g}{\partial c} 2y_{b/p} + \frac{\partial g}{\partial b} 2\hat{V}_N \right] \left(\frac{-u_{td} y_{b/p}}{\sqrt{\Delta^2 + (y_{b/p} + g)^2}} + G_1(\cdot) \right) \right] \quad (9.39)
 \end{aligned}$$

which results in the following yaw angle error dynamics

$$\dot{\psi} = C_r \tilde{r} + \left[1 + \frac{\partial g}{\partial c} 2y_{b/p} + \frac{\partial g}{\partial b} \left(2\hat{V}_N \right) \right] \frac{\Delta \tilde{V}_N}{\Delta^2 + (y_{b/p} + g)^2} \quad (9.40)$$

where $\tilde{r} \triangleq r - r_d$ is the yaw rate error. From (9.40) it can be seen that choosing r_d as in (9.39) results in yaw angle error dynamics that have a term dependent on the yaw rate error \tilde{r} and a perturbing term that vanishes when the estimation error \tilde{V}_N goes to zero.

To add acceleration feedforward to the yaw rate controller, the derivative of r_d needs to be calculated. However, when we analyse the dependencies of r_d we obtain

$$r_d = r_d(h, y_{b/p}, x_{b/p}, \tilde{\psi}, \tilde{x}, \tilde{y}), \quad (9.41)$$

where $h = [\theta, v_r, u_r, u_{rd}, \dot{u}_{rd}, \hat{V}_T, \hat{V}_N]^T$ is introduced for the sake of brevity and represents all the variables whose derivatives do not contain \tilde{V}_N or \tilde{V}_T . Consequently, the acceleration feedforward cannot be taken as \dot{r}_d since using (9.41), (9.8), and (9.9) it is straightforward to verify this signal contains the unknowns \tilde{V}_T and \tilde{V}_N . Therefore we define the yaw rate controller in terms of only known signals as:

$$\begin{aligned}
 \tau_r = & -F(u_r, v_r, r) + \frac{\partial r_d}{\partial h^T} \dot{h} + \frac{\partial r_d}{\partial y_{b/p}} \left(-u_{td} \frac{y_{b/p}}{\sqrt{\Delta^2 + (y_{b/p} + g)^2}} + G_1(\cdot) \right) \\
 & + \frac{\partial r_d}{\partial x_{b/p}} (-k_\delta x_{b/p}) + \frac{\partial r_d}{\partial \tilde{\psi}} C_r \tilde{r} - \frac{\partial r_d}{\partial \tilde{x}} k_x \tilde{x} - \frac{\partial r_d}{\partial \tilde{y}} k_y \tilde{y} - k_1 \tilde{r} - k_2 \tilde{\psi} \quad (9.42)
 \end{aligned}$$

Using (9.42) in (9.1f) we then obtain the yaw rate error dynamics

$$\begin{aligned}
 \dot{\tilde{r}} = & -k_1 \tilde{r} - k_2 C_r \tilde{\psi} - \frac{\partial r_d}{\partial \tilde{\psi}} \left[1 + \frac{\partial g}{\partial c} 2y_{b/p} + \frac{\partial g}{\partial b} \left(2\hat{V}_N \right) \right] \frac{\Delta \tilde{V}_N}{\Delta^2 + (y_{b/p} + g)^2} \\
 & - \frac{\partial r_d}{\partial y_{b/p}} \tilde{V}_N - \frac{\partial r_d}{\partial x_{b/p}} \tilde{V}_T + \frac{\partial r_d}{\partial \tilde{x}} \tilde{V}_x + \frac{\partial r_d}{\partial \tilde{y}} \tilde{V}_y \quad (9.43)
 \end{aligned}$$

which has a term depending on the yaw angle error, a term depending on the yaw rate error, and perturbing terms depending on the unknown ocean current estimation error.

Remark 9.3. *It is straightforward to verify that all the terms in (9.34) are smooth fractionals that are bounded with respect to $(y_{b/p}, x_{b/p}, \tilde{x}, \tilde{y}, \tilde{\psi})$ or are periodic functions with linear arguments and consequently the partial derivatives (9.42) and (9.43) are all bounded. This is something that is used when showing closed-loop stability in the next section.*

9.4 Closed-loop analysis

In this section we analyse the closed-loop system of the model (9.1) with controllers (9.10) and (9.42) and observer (9.12) when the frame propagates with (9.7) along the path P . To show that path following is achieved we have to show that the following error dynamics converge to zero

$$\dot{x}_{b/p} = -k_\delta x_{b/p} + \tilde{V}_T \quad (9.44a)$$

$$\dot{y}_{b/p} = -u_{td} \frac{y_{b/p}}{\sqrt{\Delta^2 + (y_{b/p} + g)^2}} + G_1(\cdot) + \tilde{V}_N \quad (9.44b)$$

$$\dot{\tilde{\psi}} = C_r \tilde{r} + \left[1 + \frac{\partial g}{\partial c} 2y_{b/p} + \frac{\partial g}{\partial b} (2\hat{V}_N) \right] \frac{\Delta \tilde{V}_N}{\Delta^2 + (y_{b/p} + g)^2} \quad (9.44c)$$

$$\begin{aligned} \dot{\tilde{r}} = & -k_1 \tilde{r} - k_2 C_r \tilde{\psi} - \frac{\partial r_d}{\partial y_{b/p}} \tilde{V}_N - \frac{\partial r_d}{\partial x_{b/p}} \tilde{V}_T + \frac{\partial r_d}{\partial \tilde{x}} \tilde{V}_x + \frac{\partial r_d}{\partial \tilde{y}} \tilde{V}_y \\ & - \frac{\partial r_d}{\partial \tilde{\psi}} \left[1 + \frac{\partial g}{\partial c} 2y_{b/p} + \frac{\partial g}{\partial b} (2\hat{V}_N) \right] \frac{\Delta \tilde{V}_N}{\Delta^2 + (y_{b/p} + g)^2} \end{aligned} \quad (9.44d)$$

$$\dot{\tilde{u}} = - \left(k_u + \frac{d_{11}}{m_{11}} \right) \tilde{u} \quad (9.44e)$$

The system (9.44) has the following perturbed form:

$$\begin{aligned} \dot{\tilde{X}} \triangleq \begin{bmatrix} \dot{x}_{b/p} \\ \dot{y}_{b/p} \\ \dot{\tilde{\psi}} \\ \dot{\tilde{r}} \\ \dot{\tilde{u}} \end{bmatrix} &= \begin{bmatrix} -k_\delta x_{b/p} \\ -u_{td} \frac{y_{b/p}}{\sqrt{\Delta^2 + (y_{b/p} + g)^2}} + G_1(\cdot) \\ C_r \tilde{r} \\ -k_1 \tilde{r} - k_2 C_r \tilde{\psi} \\ -k_3 \tilde{u} \end{bmatrix} + \\ &\begin{bmatrix} \tilde{V}_T \\ \tilde{V}_N \\ \left[1 + \frac{\partial g}{\partial c} 2y_{b/p} + \frac{\partial g}{\partial b} (2\hat{V}_N) \right] \frac{\Delta \tilde{V}_N}{\Delta^2 + (y_{b/p} + g)^2} \\ - \frac{\partial r_d}{\partial \mathbf{p}_{b/p}} \begin{bmatrix} \tilde{V}_T \\ \tilde{V}_N \end{bmatrix} - \frac{\partial r_d}{\partial \tilde{\psi}} \left[1 + \frac{\partial g}{\partial c} 2y_{b/p} + \frac{\partial g}{\partial b} 2\hat{V}_N \right] \frac{\Delta \tilde{V}_N}{\Delta^2 + (y_{b/p} + g)^2} - \frac{\partial r_d}{\partial \mathbf{p}_{b/p}} \tilde{V}_c \\ 0 \end{bmatrix} \end{aligned} \quad (9.45)$$

where $\mathbf{p}_{b/p} \triangleq [x_{b/p}, y_{b/p}]^T$ and all the perturbing terms disappear as the current estimates converge to zero. In particular, we cannot apply our desired control action whilst the current estimates have not converged yet, since the current cannot be compensated for until it is estimated correctly.

The full closed-loop system of the model (9.1) with controllers (9.10) and (9.42) and observer (9.12) is given by

$$\dot{\tilde{X}}_1 \triangleq \begin{bmatrix} \dot{y}_{b/p} \\ \dot{\tilde{\psi}} \\ \dot{\tilde{r}} \end{bmatrix} = \begin{bmatrix} -u_{td} \frac{y_{b/p}}{\sqrt{\Delta^2 + (y_{b/p} + g)^2}} + G_1(\cdot) \\ C_r \tilde{r} \\ -k_1 \tilde{r} - k_2 C_r \tilde{\psi} \end{bmatrix} + \begin{bmatrix} \frac{\tilde{V}_N}{\Delta^2 + (y_{b/p} + g)^2} \left[1 + \frac{\partial g}{\partial c} 2y_{b/p} + \frac{\partial g}{\partial b} (2\hat{V}_N) \right] \\ -\frac{\partial r_d}{\partial \mathbf{p}_{b/p}} \begin{bmatrix} \tilde{V}_T \\ \tilde{V}_N \end{bmatrix} - \frac{\partial r_d}{\partial \tilde{\psi}} \left[1 + \frac{\partial g}{\partial c} 2y_{b/p} + \frac{\partial g}{\partial b} 2\hat{V}_N \right] \frac{\Delta \tilde{V}_N}{\Delta^2 + (y_{b/p} + g)^2} - \frac{\partial r_d}{\partial \mathbf{p}} \tilde{\mathbf{V}}_c \end{bmatrix} \quad (9.46a)$$

$$\dot{\tilde{X}}_2 \triangleq \begin{bmatrix} \dot{x}_{b/p} \\ \dot{\tilde{x}} \\ \dot{\tilde{y}} \\ \dot{\tilde{V}}_x \\ \dot{\tilde{V}}_y \\ \dot{\tilde{u}} \end{bmatrix} = \begin{bmatrix} -k_\delta x_{b/p} + \tilde{V}_T \\ -k_x \tilde{x} - \tilde{V}_x \\ -k_y \tilde{y} - \tilde{V}_y \\ -k_{x1} \tilde{x} \\ -k_{y1} \tilde{y} \\ -k_u \tilde{u} \end{bmatrix} \quad (9.46b)$$

$$\dot{v}_r = X(u_{rd} + \tilde{u})r_d(h, y_{b/p}, x_{b/p}, \tilde{\psi}, \tilde{x}, \tilde{y}) + X(u_{rd} + \tilde{u})\tilde{r} + Y(u_{rd} + \tilde{u})v_r \quad (9.46c)$$

Before starting with the stability analysis of (9.46), we first establish GES of (9.46b) by using the following lemma.

Lemma 9.1. *The system (9.46b) is GES.*

Proof. Note that (9.46b) is a cascaded system of the form

$$\dot{x}_{b/p} = -k_\delta x_{b/p} + \tilde{V}_T, \quad (9.47a)$$

$$\begin{bmatrix} \dot{\tilde{x}} \\ \dot{\tilde{y}} \\ \dot{\tilde{V}}_x \\ \dot{\tilde{V}}_y \\ \dot{\tilde{u}} \end{bmatrix} = \begin{bmatrix} -k_x \tilde{x} - \tilde{V}_x \\ -k_y \tilde{y} - \tilde{V}_y \\ -k_{x1} \tilde{x} \\ -k_{y1} \tilde{y} \\ -k_u \tilde{u} \end{bmatrix}. \quad (9.47b)$$

The nominal dynamics of (9.47) are given by $\dot{x}_{b/p} = -k_\delta x_{b/p}$ from (9.47a), which is a stable linear system and thus GES. The perturbing dynamics are given by (9.47b) and where shown to be GES in Section 9.3. The interconnection term is the term \tilde{V}_T from (9.47a). The growth of the interconnection term can be bounded by $\|\tilde{V}_T\| \leq \|[\tilde{V}_x, \tilde{V}_y]^T\|$, which satisfies the condition for the interconnection term from Theorem A.1. Note that it is trivial to shown the nominal dynamics admit the quadratic Lyapunov function $V_{x_{b/p}} = 1/2x_{b/p}^2$. Consequently, all the conditions of Theorem A.1 and Proposition A.1 are satisfied. Therefore, the cascaded system (9.47) is GES, which implies that (9.46b) is GES. \square

Note that although we show that the system (9.46b) is GES, the dynamics of $x_{b/p}$ are only defined in the tube to avoid the singularity in the parametrization. Hence, the stability result is only valid in the tube.

The first step in the stability analysis of (9.46) is to assure that the closed-loop system is forward complete and that the sway velocity v_r remains bounded. Therefore, under the assumption that Condition 9.1-9.2 are satisfied, i.e. $1 - \kappa(\theta)y_{b/p} \neq 0$ and $C_r \neq 0$, we take the following three steps:

1. First, we prove that the trajectories of the closed-loop system are forward complete.
2. Then, we derive a necessary condition such that v_r is locally bounded with respect to $(\tilde{X}_1, \tilde{X}_2)$.
3. Finally, we establish that for a sufficiently big value of Δ , v_r is locally bounded only with respect to \tilde{X}_2 .

The above three steps are taken by formulation and proving three lemmas. For the sake of brevity in the main body of this chapter the proofs of the following lemmas are replaced by a sketch of each proof in the main body. The full proofs can be found in the Appendices 9.A-9.C.

Lemma 9.2 (Forward completeness). *The trajectories of the global closed-loop system (9.46) are forward complete.*

The proof of this lemma is given in Appendix 9.A. The general idea is as follows. Forward completeness for (9.46b) is evident since this part of the closed-loop system consists of GES error dynamics. Using the forward completeness and in fact boundedness of (9.46b) we can show forward completeness of (9.46c), $\dot{\psi}$, and \dot{r} . Hence, forward completeness of (9.46) depends on forward completeness of $\dot{y}_{b/p}$. To show forward completeness of $\dot{y}_{b/p}$, we consider the $y_{b/p}$ dynamics with \tilde{X}_2 , $\tilde{\psi}$, \tilde{r} , and v_r as input, which allows us to claim forward completeness of $\dot{y}_{b/p}$ according to Theorem A.3. Consequently, all the states of the closed-loop system are forward complete and hence the closed-loop system (9.46) is forward complete

Lemma 9.3 (Boundedness near $(\tilde{X}_1, \tilde{X}_2) = 0$). *The system (9.46c) is bounded near $(\tilde{X}_1, \tilde{X}_2) = 0$ if and only if the curvature of P satisfies the following condition:*

$$\kappa_{\max} \triangleq \max_{\theta \in P} |\kappa(\theta)| < \frac{Y_{\min}}{X_{\max}}. \quad (9.48)$$

The proof of this lemma is given in Appendix 9.B. A sketch of the proof is as follows. The sway velocity dynamics (9.46c) are analyzed using a quadratic Lyapunov function $V = 1/2v_r^2$. It can be shown that the derivative of this Lyapunov function satisfies the conditions for boundedness when the solutions are on or close to the manifold where $(\tilde{X}_1, \tilde{X}_2) = 0$. Consequently, (9.46c) satisfies the conditions of boundedness near $(\tilde{X}_1, \tilde{X}_2) = 0$ as long as (9.48) is satisfied.

In Lemma 9.3 we show boundedness of v_r for small values of $(\tilde{X}_1, \tilde{X}_2)$ to derive the bound on the curvature. However, locality with respect to \tilde{X}_1 , i.e. the path following errors and yaw angle and yaw rate errors, is not desired and in the next lemma boundedness independent of \tilde{X}_1 is shown under an extra condition on the look-ahead distance Δ .

Lemma 9.4 (Boundedness near $\tilde{X}_2 = 0$). *If the following additional assumption is satisfied:*

$$\exists \sigma > 0 \text{ s.t. } 1 - \kappa(\theta)y_{b/p} \geq \sigma > 0 \quad \wedge \quad \left[Y_{\min} - X_{\max}\kappa_{\max}\frac{1}{\sigma} \right] > 0 \quad (9.49)$$

the system (9.46c) is bounded only near $\tilde{X}_2 = 0$ if we have

$$\Delta > \frac{4X_{\max}}{\left[Y_{\min} - X_{\max}\kappa_{\max}\frac{1}{\sigma} \right]} \quad (9.50)$$

$$\kappa_{\max} < \sigma \frac{Y_{\min}}{X_{\max}} \quad (9.51)$$

Remark 9.4. *The size of σ can be calculated by using the following tuning procedure.*

1. Start by calculating the absolute bound on the curvature from Lemma 9.3. This is a bound that is necessary for feasibility of the trajectories.
2. Now choose a positive Δ and using the maximum curvature of the path, solve (9.50) to obtain a possible value for σ .
3. Using the value for σ obtained in the previous step and the maximum value of the curvature we can use the inequality $1 - \kappa(\theta)y_{b/p} \geq \sigma$ from (9.49) to calculate the size of the tube as

$$y_{b/p}^{\text{tube}} = \frac{1 - \sigma}{\kappa_{\max}}. \quad (9.52)$$

If initial conditions are within the tube $y_{b/p}^{\text{tube}}$, and are chosen such that the transient caused by the unknown current does not force the vessel out of the tube. Then the sway velocity is bounded for all time. Note that the choice of Δ in step two given above determines how large the tube will be. More specifically, a larger choice for Δ will result in a smaller value for σ which will lead to a larger tube in step three. However, due to the nature of the guidance a larger Δ will mean slower steering and consequently slower convergence to the path.

The proof of Lemma 9.4 is given in Appendix 9.C, the general idea is given as follows. The proof follows along the same lines of that of Lemma 9.3 but solutions are considered close to the manifold $\tilde{X}_2 = 0$ rather than $(\tilde{X}_1, \tilde{X}_2) = 0$. It is shown that boundedness can still be shown if (9.50) is satisfied additionally to the conditions of Lemma 9.3.

Theorem 9.1. *Consider a θ -parametrised path denoted by $P(\theta) \triangleq (x_p(\theta), y_p(\theta))$. Then under Conditions 9.1-9.2 and the conditions of Lemma 9.2-9.4, the system (9.1) with control laws (9.10) and (9.42) and observer (9.12) follows the path P , while maintaining v_r , τ_r and τ_u bounded. In particular, the origin of the system (9.46a)-(9.46b) is exponentially stable in the tube.*

Proof. From the fact that the origin of (9.46b) is GES, the fact that the closed-loop system (9.46) is forward complete according to Lemma 9.2, and the fact that

solutions of (9.46c) are locally bounded near $\tilde{X}_2 = 0$ according to Lemma 9.4, we can conclude that there is a finite time $T > t$ after which solutions of (9.46b) will be sufficiently close to $\tilde{X}_2 = 0$ to guarantee boundedness of v_r .

Having established that v_r is bounded we first analyse the cascade

$$\begin{bmatrix} \dot{\tilde{\psi}} \\ \dot{\tilde{r}} \end{bmatrix} = \begin{bmatrix} C_r \tilde{r} \\ -k_1 \tilde{r} - k_2 C_r \tilde{\psi} \end{bmatrix} + \begin{bmatrix} G_2(\cdot) \\ -\frac{\partial r_d}{\partial \tilde{\psi}} G_2(\cdot) - \frac{\partial r_d}{\partial \mathbf{p}_{b/p}} [\tilde{V}_T, \tilde{V}_N]^T + \frac{\partial r_d}{\partial [\tilde{x}, \tilde{y}]^T} \tilde{\mathbf{V}}_c \end{bmatrix} \quad (9.53a)$$

$$\begin{bmatrix} \dot{x}_{b/p} \\ \dot{\tilde{x}} \\ \dot{\tilde{y}} \\ \dot{\tilde{V}}_x \\ \dot{\tilde{V}}_y \\ \dot{\tilde{u}} \end{bmatrix} = \begin{bmatrix} -k_\delta x_{b/p} + \tilde{V}_T \\ -k_x \tilde{x} - \tilde{V}_x \\ -k_y \tilde{y} - \tilde{V}_y \\ -k_{x1} \tilde{x} \\ -k_{y1} \tilde{y} \\ -k_u \tilde{u} \end{bmatrix} \quad (9.53b)$$

The perturbing system (9.53b) is GES as shown in Lemma 9.1. The interconnection term, i.e. the second and third term in (9.53a), satisfies the linear growth criteria from Theorem A.1. More specifically, it does not grow with the $\tilde{\psi}$ and \tilde{r} since all the partial derivatives of r_d and g can be bounded by constants. The nominal dynamics, i.e. the first matrix in (9.53a), can be analyzed with the following quadratic Lyapunov function

$$V_{(\tilde{r}, \tilde{\psi})} = \frac{1}{2} \tilde{r}^2 + \frac{1}{2} k_2 \tilde{\psi}^2 \quad (9.54)$$

whose derivative along the solutions of the nominal system is given by

$$\dot{V}_{(\tilde{r}, \tilde{\psi})} = -k_1 \tilde{r}^2 - k_2 C_r \tilde{\psi} \tilde{r} + k_2 C_r \tilde{r} \tilde{\psi} = -k_2 \tilde{r}^2 \leq 0 \quad (9.55)$$

which implies that \tilde{r} and $\tilde{\psi}$ are bounded. The derivative of (9.55) is given by

$$\ddot{V}_{(\tilde{r}, \tilde{\psi})} = -2k_1^2 \tilde{r}^2 - 2k_1 k_2 C_r \tilde{\psi} \tilde{r} \quad (9.56)$$

which is bounded since \tilde{r} and $\tilde{\psi}$ are bounded. This implies that (9.55) is a uniformly continuous function. Consequently, by applying Barbalat's lemma (see Lemma A.5) we have that

$$\lim_{t \rightarrow \infty} \dot{V}_{(\tilde{r}, \tilde{\psi})} = \lim_{t \rightarrow \infty} -k_1 \tilde{r}^2 = 0 \Rightarrow \lim_{t \rightarrow \infty} \tilde{r} = 0. \quad (9.57)$$

Since C_r is persistently exciting, which follows from the fact that C_r is upper bounded and lower bounded by a constant larger than zero, it follows from the expression of the nominal dynamics that

$$\lim_{t \rightarrow \infty} \tilde{r} = 0 \Rightarrow \lim_{t \rightarrow \infty} \tilde{\psi} = 0. \quad (9.58)$$

This implies that the system is globally asymptotically stable according to Definition A.3 and since the nominal dynamics are linear it follows that the nominal dynamics are globally exponentially stable. Consequently, from the above it follows that the cascade (9.53) is GES using Theorem A.1 and Proposition A.1.

We now consider the following dynamics

$$\dot{y}_{b/p} = -u_{td} \frac{y_{b/p}}{\sqrt{\Delta^2 + (y_{b/p} + g)^2}} + \tilde{V}_N + G_1(\cdot). \quad (9.59)$$

Note that we can view the systems (9.53) and (9.59) as a cascaded system where the nominal dynamics are formed by the first term of (9.59), the interconnection term is given by second matrix of (9.59), and the perturbing dynamics are given by (9.53). As we have just shown the perturbing dynamics are GES. Using the bound on $G_1(\cdot)$ from (9.28) it is straightforward to verify that the interconnection term satisfies the conditions of Theorem A.1. We now consider the following Lyapunov function for the nominal system

$$V_{y_{b/p}} = \frac{1}{2} y_{b/p}^2. \quad (9.60)$$

whose derivative along the solutions of the nominal system is given by

$$\dot{V}_{y_{b/p}} = -u_{td} \frac{y_{b/p}^2}{\sqrt{\Delta^2 + (y_{b/p} + g)^2}} \leq 0, \quad (9.61)$$

which implies that the nominal system is GAS. Moreover, since it is straightforward to verify that $\dot{V}_{y_{b/p}} \leq \alpha V_{y_{b/p}}$ for some constant α dependent on initial conditions, it follows from the comparison lemma (Lemma A.4) that the nominal dynamics are also LES. Consequently, the cascaded system satisfies the conditions of Theorem A.1 and Lemma A.3, and therefore the cascaded system is GAS and LES. This implies that the origin of the error dynamics, i.e. $(\tilde{X}_1, \tilde{X}_2) = (0, 0)$, is globally asymptotically stable and locally exponentially stable. However, since the parametrization is only valid locally we can only claim exponential stability in the tube. \square

9.5 Case study

This section presents a case study to verify the theoretical results presented in this chapter. The case study under consideration is following of a circular path using the model of an underactuated surface vessel from Fredriksen and Pettersen [57], the parameters of which are given in Section B.1. The ocean current components are given by $V_x = -1$ m/s and $V_y = 1.2$ m/s and consequently $V_{\max} \approx 1.562$ m/s. The desired relative surge velocity is chosen to be constant and set to $u_{rd} = 5$ m/s such that Assumption 9.2 is verified. Now recall the expression for $X(u_r)$, $Y(u_r)$ given by Equations (2.12b-2.12c):

$$X(u_r) \triangleq -X_1 u_r + X_2, \quad (9.62a)$$

$$Y(u_r) \triangleq -Y_1 u_r - Y_2. \quad (9.62b)$$

Using the ship's model parameters from Section B.1 and the expressions (9.62a) and (9.62b) it is straightforward to see that the curvature bound from Lemma 9.3 is given by $\kappa_{\max} < (Y_{\min})/(X_{\max}) \approx 0.1333$. The observer is initialised as

suggested in Subsection 9.3.2 and the observer gains are selected as $k_{x_1} = k_{y_1} = 1$ and $k_{x_2} = k_{y_2} = 0.1$. The controller gains are selected as $k_{u_r} = 0.1$ for the surge velocity controller and $k_1 = 1000$ and $k_2 = 400$ for the yaw rate controller.

In this case study the vessel is required to follow a circle with a radius of 400 m that is centred around the origin. Consequently, the curvature of the path is given by $\kappa_p = 1/400 = 0.0025$. To choose the parameters of the guidance law we will now follow the tuning procedure lined out in Remark 9.4. In the first step we verify that the feasibility constraint on the curvature is satisfied for the path under consideration, which is clearly the case since $\kappa_p < (Y_{\min})/(X_{\max}) \approx 0.133$. In the second step we fix our Δ as $\Delta = 40$ m, which results in $\sigma \approx 0.0268$. In the third step we use the value for σ to calculate the size of the tube as $y_{b/p}^{\text{tube}} \approx 369.983$ m. Note that this is only slightly smaller than the size of the tube where the parametrization is valid, i.e. 400 m. To stay within this tube we choose the initial conditions as

$$[u_r(t_0), v_r(t_0), r(t_0), x(t_0), y(t_0), \psi(t_0)]^T = [0, 0, 0, 700, 10, \pi/2]^T. \quad (9.63)$$

The resulting trajectory for the vessel can be seen in Figure 9.3. The blue dashed line is the trajectory of the vessel and the red circle is the reference path. The yellow vessels represent the orientation of the vessel at certain instances. From the plot in Figure 9.3 it can be seen that the vessel converges to the circle and starts to follow the path. Moreover, it can be seen from the yellow vessels that the orientation of the ship is not tangential to the circle which is necessary to compensate for the ocean current.

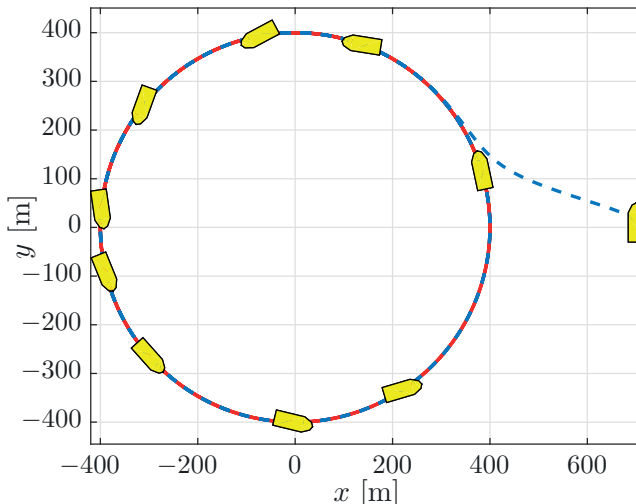


Figure 9.3: Path of the vessel in the $x - y$ -plane. The dashed blue line is the trajectory of the path and the red line is the reference. The yellow ships denote the orientation of the vessel at certain times.

The path following errors can be seen in the top plot of Figure 9.4 which confirm that the path following errors converge to zero. A detail of the steady-state is

given to show the reduction of the error. Moreover, note that because of the choice of parametrization the error in tangential direction $x_{b/p}$ is zero throughout the motion except from a very small transient at the beginning caused by the transient of the observer. The estimates obtained from the ocean current observer can be seen in the second plot from the top in Figure 9.4. From this plot it can be seen that the estimates converge exponentially with no overshoot. This underlines the conservativeness of the bound from Assumption 9.2 that is required for the error bound for the observer as explained in Subsection 9.3.2. The third plot in Figure 9.4 depicts the yaw rate and the sway velocity induced by the motion. It can be seen that these do not converge to zero but converge to a periodic motion. Note that for circular motion in the absence of current the yaw rate would converge to zero. However, when current is present the vessel needs to change its turning rate depending on if it goes with or against the current. The relative surge velocity is given in the fourth plot from the top in Figure 9.4 and shows that the surge velocity converges exponentially to the desired value. This plot is especially interesting in combination with the plot of the magnitude of C_r given at the bottom of Figure 9.4. From this plot it can clearly be seen that Condition 9.2 is verified both in steady-state and during the transient of the velocity controller.

9.6 Conclusion

This chapter considered curved-path following for underactuated marine vessels in the presence of constant ocean currents. In this approach the path is parametrized by a path variable with an update law that is designed to keep the vessel on the normal of a path-tangential reference frame. This assures that the path following error is defined as the shortest distance to the path. However, the disadvantage is that this type of update law has a singularity which only allows for local results. The vessel is steered using a line-of-sight guidance law, which to compensate for the unknown ocean currents is aided by an ocean current observer. The closed-loop system with the controllers and observer was analyzed. This was done by first showing boundedness of the underactuated sway velocity dynamics under certain conditions. It was then shown that if these conditions are satisfied and the sway velocity is bounded, the path following errors are exponentially stable within the tube in which the parametrization is well defined. Due to the singularity of the update law, the feasibility of this problem depends on the initial conditions, the curvature of the path, and the magnitude of the ocean current. More specifically, the size of the tube in which the parametrization is well defined was shown to be a function of the maximal curvature of the path. This implies that the combination of curvature and ocean current should be such that a suitable set of initial conditions exists for which the transient of the ocean current observer does not bring the vessel out of the tube.

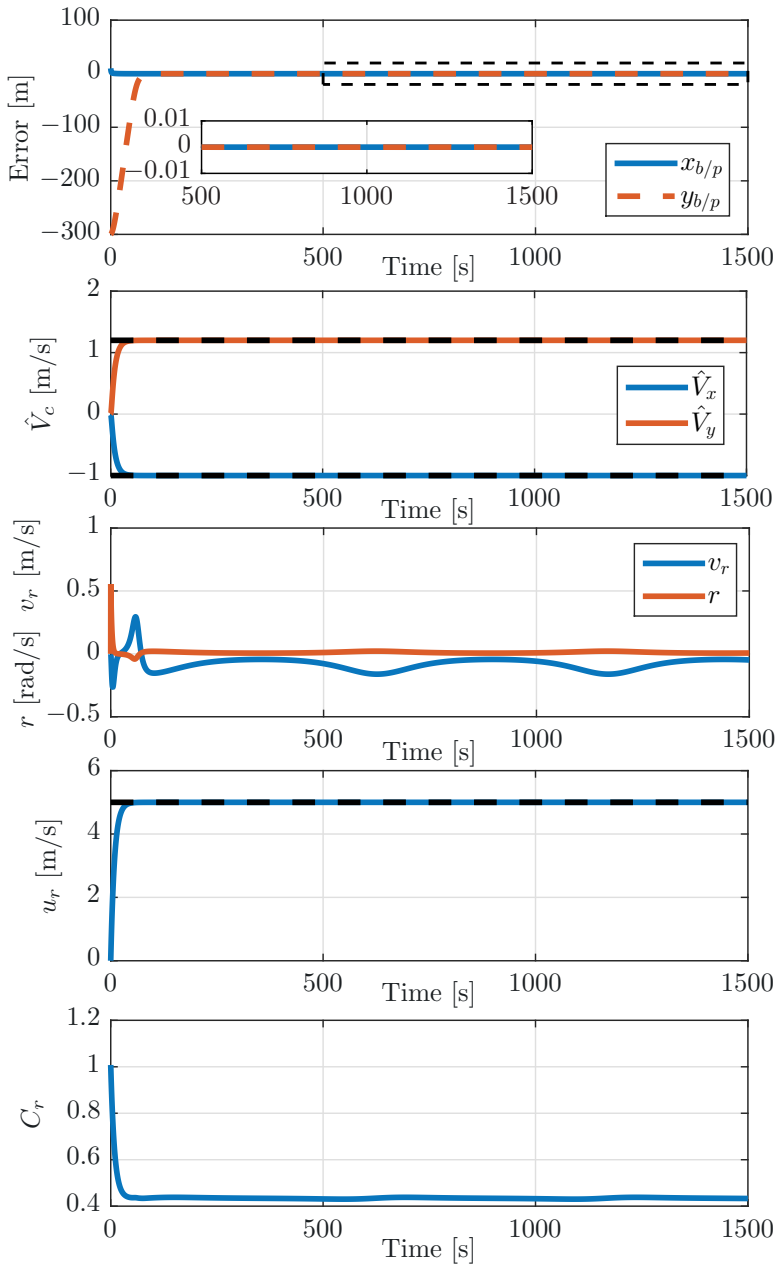


Figure 9.4: Path following errors plotted against time (top), current estimates against time (second), sway velocity and yaw rate against time (third), surge velocity against time (fourth), and size of C_r over time (bottom).

9.A Proof of Lemma 9.2

Consider the following part of the global closed-loop system:

$$\begin{aligned} \begin{bmatrix} \dot{\tilde{\psi}} \\ \dot{\tilde{r}} \end{bmatrix} &= \begin{bmatrix} C_r \tilde{r} \\ -k_1 \tilde{r} - k_2 C_r \tilde{\psi} \end{bmatrix} \\ &+ \underbrace{\begin{bmatrix} \left[1 + \frac{\partial g}{\partial c} 2y_{b/p} + \frac{\partial g}{\partial b} (2\hat{V}_N) \right] \frac{\Delta \tilde{V}_N}{\Delta^2 + (y_{b/p} + g)^2} \\ -\frac{\partial r_d}{\partial \mathbf{p}_{b/p}} \left[\frac{\tilde{V}_T}{\tilde{V}_N} \right] - \frac{\partial r_d}{\partial \tilde{\psi}} \left[1 + \frac{\partial g}{\partial c} 2y_{b/p} + \frac{\partial g}{\partial b} 2\hat{V}_N \right] \frac{\Delta \tilde{V}_N}{\Delta^2 + (y_{b/p} + g)^2} - \frac{\partial r_d}{\partial \mathbf{p}_{b/p}} \tilde{V}_c \end{bmatrix}}_{R(h, y_{b/p}, x_{b/p}, \tilde{\psi}, \tilde{x}, \tilde{y})} \end{aligned} \quad (9.64a)$$

$$\dot{v}_r = X(u_{rd} + \tilde{u})r_d(h, y_{b/p}, x_{b/p}, \tilde{\psi}, \tilde{x}, \tilde{y}) + X(u_{rd} + \tilde{u})\tilde{r} + Y(u_{rd} + \tilde{u})v_r \quad (9.64b)$$

From the boundedness of the vector $[\tilde{X}_2^T, \kappa(\theta), u_{rd}, \dot{u}_{rd}, V_T, V_N]^T$ we know that $\|[\tilde{X}_2^T, \kappa(\theta), u_{rd}, \dot{u}_{rd}, V_T, V_N]^T\| \leq \beta_0$, and from (9.39) we can conclude the existence of positive functions $a_{r_d}(\cdot)$, $b_{r_d}(\cdot)$, $a_R(\cdot)$, and $b_R(\cdot)$ which are all continuous in their arguments and are such that the following inequalities hold:

$$|r_d(\cdot)| \leq a_{r_d}(\Delta, \beta_0) |v_r| + b_{r_d}(\Delta, \beta_0) \quad (9.65)$$

and,

$$\|R(\cdot)\| \leq a_R(\Delta, \beta_0) |v_r| + b_R(\Delta, \beta_0) \quad (9.66)$$

Then taking the following Lyapunov function candidate:

$$V_1(\tilde{\psi}, \tilde{r}, v_r) = \frac{1}{2} \left(k_2 \tilde{\psi}^2 + \tilde{r}^2 + v_r^2 \right) \quad (9.67)$$

whose time derivative along the solutions of (9.64) is

$$\begin{aligned} \dot{V}_1(\cdot) &= k_2 C_r \tilde{r} \tilde{\psi} - k_1 \tilde{r}^2 - k_2 C_r \tilde{r} \tilde{\psi} + [\tilde{\psi} \ \tilde{r}] R(\cdot) + Y(u_{rd} + \tilde{u}) v_r^2 \\ &\quad + X(u_{rd} + \tilde{u}) \tilde{r} v_r + X(u_{rd} + \tilde{u}) r_d(\cdot) v_r \end{aligned} \quad (9.68)$$

Using Young's inequality we note that

$$\begin{aligned} \dot{V}_1(\cdot) &\leq k_1 \tilde{r}^2 + \tilde{\psi}^2 + \tilde{r}^2 + R^2(\cdot) + Y(u_{rd} + \tilde{u}) v_r^2 \\ &\quad + |X(u_{rd} + \beta_0)| (\tilde{r}^2 + v_r^2) + |X(u_{rd} + \beta_0)| (r_d^2(\cdot) + v_r^2) \\ &\leq \alpha V + \beta, \quad \alpha \geq 0, \beta \geq 0 \end{aligned} \quad (9.69)$$

Note that since the differential inequality (9.69) is scalar we can invoke the comparison lemma Khalil [77, Lemma 3.4] given as Lemma A.4 in Appendix A.1. From Lemma A.4 we know that the solutions of differential inequality (9.69) are bounded by the solutions of the linear system:

$$\dot{x} = \alpha x + \beta \quad (9.70)$$

which has solutions

$$x(t) = \frac{\|x(t_0)\| \alpha + \beta}{\alpha} e^{\alpha(t-t_0)} - \frac{\beta}{\alpha} \quad (9.71)$$

Hence, from Lemma A.4 we have that

$$V_1(\cdot) \leq \frac{\|V_1(t_0)\| \alpha + \beta}{\alpha} e^{\alpha(t-t_0)} - \frac{\beta}{\alpha} \quad (9.72)$$

which shows the solutions of $V_1(\cdot)$ are defined up to $t_{\max} = \infty$ and consequently from (9.67) it follows that the solutions of $\tilde{\psi}$, \tilde{r} , and v_r must be defined up to $t_{\max} = \infty$. Hence, the solutions of (9.64) satisfy Definition A.5 and we can conclude forward completeness of trajectories of (9.64).

The forward completeness of trajectories of the global closed-loop system now depends on forward completeness of $\dot{y}_{b/p}$ from (9.46a). We can conclude forward completeness of $\dot{y}_{b/p}$ by considering the Lyapunov function

$$V_2 = \frac{1}{2} y_{b/p}^2. \quad (9.73)$$

The time derivative of (9.73) is given by

$$\begin{aligned} \dot{V}_2 &= y_{b/p} \dot{y}_{b/p} \\ &\leq -u_{td} \frac{y_{b/p}}{\sqrt{\Delta^2 + (y_{b/p} + g)^2}} + (G_1(\cdot) + \tilde{V}_N) y_{b/p} \\ &\leq (G_1(\cdot) + \tilde{V}_N) y_{b/p} \end{aligned} \quad (9.74)$$

where using the bound on $G_1(\cdot)$ from (10.23) and Young's inequality we obtain

$$\dot{V}_2 \leq V_2 + \frac{1}{2} \left(\zeta^2 (\dot{\gamma}_p(\theta), u_{td}) \|\tilde{\psi}, \tilde{r}, x_{b/p}\|^2 + \tilde{V}_N^2 \right) \quad (9.75)$$

$$\leq V_2 + \sigma_2(v_r, \tilde{\psi}, \tilde{r}, \tilde{V}_N, \tilde{V}_T, x_{b/p}) \quad (9.76)$$

with $\sigma_2(\cdot) \in \mathcal{K}_\infty$. Consequently, if we view the arguments of $\sigma_2(\cdot)$ as input to the $y_{b/p}$ dynamics, then (9.75) satisfies Theorem A.3 and hence $\dot{x}_{b/p}$ and $\dot{y}_{b/p}$ are forward complete. Note that the arguments of $\sigma_2(\cdot)$ are all forward complete and therefore fit the definition of an input signal given in Definition A.5. We have now shown forward completeness of (9.46a) and (9.46c) and since (9.46b) is GES is trivially forward complete. We can therefore claim forward completeness of the entire closed-loop system (9.46) and the proof of Lemma 9.2 is complete.

9.B Proof of Lemma 9.3

Recall the sway velocity dynamics (9.46c):

$$\dot{v}_r = X(\tilde{u} + u_{rd})(r_d + \tilde{r}) + Y(u_{rd} + \tilde{u})v_r, \quad Y(u_{rd}) < 0$$

Consider the following Lyapunov function candidate:

$$V_3(v_r) = \frac{1}{2} v_r^2 \quad (9.77)$$

The derivative of (9.77) along the solutions of (9.46c) is given by

$$\begin{aligned}\dot{V}_3 &= v_r \dot{v}_r = v_r X(u_{rd} + \tilde{u})r_d + X(u_{rd} + \tilde{u})v_r \tilde{r} + Y(u_{rd} + \tilde{u})v_r^2 \\ &\leq X(u_{rd})r_d v_r + a_x \tilde{u} r_d v_r + X(u_{rd})v_r \tilde{r} + a_x \tilde{u} v_r \tilde{r} + a_y \tilde{u} v_r^2 + Y(u_{rd})v_r^2\end{aligned}\quad (9.78)$$

where we used the fact that:

$$Y(u_r) = a_y u_r + b_y \quad (9.79)$$

$$X(u_r) = a_x u_r + b_x \quad (9.80)$$

The term $r_d v_r$ can be bounded as a function of v_r as follows

$$\begin{aligned}r_d v_r &= -\frac{v_r}{C_r} \left[\kappa(\theta) \left(\frac{u_t \cos(\psi + \beta - \gamma_p(\theta)) + k_\delta x_{b/p} + \hat{V}_T}{1 - \kappa(\theta) y_{b/p}} \right) \right. \\ &\quad + \frac{Y(u_r) v_r u_{rd} - \dot{u}_{rd} v_r}{u_{rd}^2 + v_r^2} + \frac{\Delta}{\Delta^2 + (y_{b/p} + g)^2} \left[\dot{V}_N \frac{b + \sqrt{b^2 - ac}}{-a} \right. \\ &\quad + \frac{\partial g}{\partial a} \left(2\hat{V}_N \dot{V}_N - 2u_{rd} \dot{u}_{rd} - 2v_r Y(u_r) v_r \right) + \frac{\partial g}{\partial b} \left(2\dot{V}_N y_{b/p} \right) \\ &\quad \left. \left. + \left[1 + \frac{\partial g}{\partial c} 2y_{b/p} + \frac{\partial g}{\partial b} 2\hat{V}_N \right] \left(\frac{-u_{td} y_{b/p}}{\sqrt{\Delta^2 + (y_{b/p} + g)^2}} + G_1(\cdot) \right) \right] \right] \\ &\leq \frac{1}{C_r} |\kappa(\theta)| v_r^2 \frac{1}{1 - \kappa(\theta) y_{b/p}} + F_2(\tilde{X}_1, \tilde{X}_2, \Delta, V_T, V_N, u_{rd}) v_r^2 \\ &\quad + F_1(\tilde{X}_1, \tilde{X}_2, \Delta, V_T, V_N, u_{rd}) v_r \\ &\quad - \frac{1}{C_r} \left(\frac{u_{rd}}{u_{rd}^2 + v_r^2} - \frac{2\Delta v_r}{\Delta^2 + (y_{b/p} + g)^2} \frac{\partial g}{\partial a} \right) Y(u_r) v_r^2\end{aligned}\quad (9.81)$$

where $F_{1,2}(\cdot)$ are continuous functions in their arguments with:

$$F_2(0, 0, \Delta, V_T, V_N, u_{rd}) = 0. \quad (9.82)$$

When substituting (9.81) in (9.78) we obtain

$$\begin{aligned}\dot{V}_3 &\leq X(u_{rd}) F_2(\tilde{X}_1, \tilde{X}_2, \Delta, V_T, V_N, u_{rd}) v_r^2 + \left| \frac{C_r^* - C_r}{C_r C_r^*} \right| (|X(u_{rd}) \kappa(\theta)| - |Y(u_{rd})|) v_r^2 \\ &\quad + \frac{1}{C_r^*} \left[|X(u_{rd})| |\kappa(\theta)| \left(1 + \frac{y_{b/p}}{1 - \kappa(\theta) y_{b/p}} \right) - |Y(u_{rd})| + a_y \tilde{u} \right] v_r^2 \\ &\quad + \left(X(u_{rd}) F_1(\tilde{X}_1, \tilde{X}_2, \Delta, V_T, V_N, u_{rd}) + a_x \tilde{u} (r_d + \tilde{r}) + X(u_{rd}) \tilde{r} \right) v_r\end{aligned}\quad (9.83)$$

where $C_r^*(v_r, y_{b/p}, \Delta, V_N, u_{rd}) = C_r(v_r, y_{b/p}, \Delta, \hat{V}_N = V_N, u_r = u_{rd})$. When substituting (9.81) in (9.78) we have used the fact that

$$\frac{1}{C_r} \left(\frac{u_{rd}}{u_{rd}^2 + v_r^2} - \frac{2\Delta v_r}{\Delta^2 + (y_{b/p} + g)^2} \frac{\partial g}{\partial a} \right) X(u_r) Y(u_r) v_r^2 = \frac{C_r - 1}{C_r} Y(u_r) v_r^2. \quad (9.84)$$

Remark 9.5. Note that $C_r^*(v_r, y_{b/p}, \Delta, V_N, u_{rd})$ can be found independently of $y_{b/p}$ and $x_{b/p}$ since the terms in C_r are bounded with respect to these variables.

Consequently, on the manifold where $(\tilde{X}_1, \tilde{X}_2) = 0$ we have

$$\dot{V}_3 \leq \frac{1}{C_r^*} (X_{\max} |\kappa(\theta)| - Y_{\min}) v_r^2 + X(u_{rd}) F_1(0, 0, \Delta, V_T, V_N, u_{rd}) |v_r| \quad (9.85)$$

which is bounded as long as

$$X_{\max} |\kappa(\theta)| - Y_{\min} < 0. \quad (9.86)$$

Hence, satisfaction of (9.86) renders the quadratic term in (9.85) negative and since the quadratic term is dominant for sufficiently large v_r , (9.85) is negative definite for sufficiently large v_r . If \dot{V}_3 is negative for sufficiently large v_r this implies that V_3 decreases for sufficiently large v_r . Since $V_3 = 1/2v_r^2$, a decrease in V_3 implies a decrease in v_r^2 and by extension in v_r . Therefore, v_r cannot increase above a certain value and v_r is bounded near the manifold where $(\tilde{X}_1, \tilde{X}_2) = 0$.

Consequently, close to the manifold where $(\tilde{X}_1, \tilde{X}_2) = 0$ the sufficient and necessary condition for local boundedness of (9.46c) is the following:

$$X_{\max} |\kappa(\theta)| - Y_{\min} < 0. \quad (9.87)$$

which is satisfied if and only if the condition in Lemma 9.3 is satisfied.

9.C Proof of Lemma 9.4

Recall the sway velocity dynamics (9.46c):

$$\dot{v}_r = X(\tilde{u} + u_{rd})(r_d + \tilde{r}) + Y(u_{rd} + \tilde{u})v_r, \quad Y(u_{rd}) < 0$$

Consider the following Lyapunov function candidate:

$$V_3(v_r) = \frac{1}{2} v_r^2 \quad (9.88)$$

The derivative of (9.88) along the solutions of (9.46c) is given by

$$\begin{aligned} \dot{V}_3 &= v_r \dot{v}_r = v_r X(u_{rd} + \tilde{u})r_d + X(u_{rd} + \tilde{u})v_r \tilde{r} + Y(u_{rd} + \tilde{u})v_r^2 \\ &\leq X(u_{rd})r_d v_r + a_x \tilde{u} r_d v_r + X(u_{rd})v_r \tilde{r} + a_x \tilde{u} v_r \tilde{r} + a_y \tilde{u} v_r^2 + Y(u_{rd})v_r^2 \end{aligned} \quad (9.89)$$

where we used the fact that:

$$Y(u_r) = a_y u_r + b_y \quad (9.90)$$

$$X(u_r) = a_x u_r + b_x \quad (9.91)$$

The term $r_d v_r$ is given by:

$$\begin{aligned}
 r_d v_r = & -\frac{1}{C_r} v_r \left[\kappa(\theta) \frac{u_t \cos(\psi + \beta - \gamma_p(\theta))}{1 - \kappa(\theta) y_{b/p}} + \kappa(\theta) \frac{k_\delta x_{b/p} + \hat{V}_T}{1 - \kappa(\theta) y_{b/p}} \right. \\
 & + \frac{\Delta (b + \sqrt{b^2 - ac})}{a\Delta^2 + a(y_{b/p} + g)^2} (-k_{x_1} \tilde{x} \sin(\gamma_p(\theta)) + k_{y_1} \tilde{y} \cos(\gamma_p(\theta))) \\
 & + \frac{\Delta \kappa(\theta) \hat{V}_T (b + \sqrt{b^2 - ac})}{a\Delta^2 + a(y_{b/p} + g)^2} \left(\frac{u_t \cos(\psi + \beta - \gamma_p(\theta))}{1 - \kappa(\theta) y_{b/p}} + \frac{k_\delta x_{b/p} - \hat{V}_T}{1 - \kappa(\theta) y_{b/p}} \right) \\
 & + \frac{\Delta \frac{\partial g}{\partial a} 2\hat{V}_N}{\Delta^2 + (y_{b/p} + g)^2} (k_{x_1} \tilde{x} \sin(\gamma_p(\theta)) - k_{y_1} \tilde{y} \cos(\gamma_p(\theta))) \\
 & - \frac{\Delta \kappa(\theta) \frac{\partial g}{\partial a} 2\hat{V}_N \hat{V}_T}{\Delta^2 + (y_{b/p} + g)^2} \left(\frac{u_t \cos(\psi + \beta - \gamma_p(\theta))}{1 - \kappa(\theta) y_{b/p}} + \frac{k_\delta x_{b/p} + \hat{V}_T}{1 - \kappa(\theta) y_{b/p}} \right) \\
 & - \frac{\Delta \frac{\partial g}{\partial a}}{\Delta^2 + (y_{b/p} + g)^2} (2u_{rd} \dot{u}_{rd} - 2v_r Y(u_r) v_r) + \frac{Y(u_r) v_r u_{rd} - \dot{u}_{rd} v_r}{u_{rd}^2 + v_r^2} \\
 & + \frac{\Delta \frac{\partial g}{\partial b} 2y_{b/p}}{\Delta^2 + (y_{b/p} + g)^2} (k_{x_1} \tilde{x} \sin(\gamma_p(\theta)) - k_{y_1} \tilde{y} \cos(\gamma_p(\theta))) \\
 & - \frac{\Delta \kappa(\theta) \frac{\partial g}{\partial b} 2y_{b/p} \hat{V}_T}{\Delta^2 + (y_{b/p} + g)^2} \left(\frac{u_t \cos(\psi + \beta - \gamma_p(\theta))}{1 - \kappa(\theta) y_{b/p}} + \frac{k_\delta x_{b/p} + \hat{V}_T}{1 - \kappa(\theta) y_{b/p}} \right) \\
 & - \phi(\cdot) u_{td} \frac{y_{b/p}}{\sqrt{\Delta^2 + (y_{b/p} + g)^2}} + \phi(\cdot) \tilde{u} \sin(\psi - \gamma_p) \\
 & + \phi(\cdot) \left[1 - \cos(\tilde{\psi}) \right] u_{td} \sin \left(\arctan \left(\frac{y_{b/p} + g}{\Delta} \right) \right) \\
 & + \phi(\cdot) \cos \left(\arctan \left(\frac{y_{b/p} + g}{\Delta} \right) \right) \sin(\tilde{\psi}) u_{td} \\
 & \left. - 2\phi(\cdot) x_{b/p} \kappa(\theta) \left(\frac{u_t \cos(\psi + \beta - \gamma_p(\theta))}{1 - \kappa(\theta) y_{b/p}} + \frac{k_\delta x_{b/p} + \hat{V}_T}{1 - \kappa(\theta) y_{b/p}} \right) \right]
 \end{aligned} \tag{9.92}$$

where the function $\phi(y_{b/p}, v_r, u_{rd}, \hat{V}_N, \Delta)$ is bounded by a constant with respect to v_r and defined as

$$\phi(\cdot) \triangleq \underbrace{\frac{2\Delta y_{b/p}}{\Delta^2 + (y_{b/p} + g)^2} \frac{\partial g}{\partial c}}_{\phi_1(\cdot)} + \underbrace{\frac{\Delta}{\Delta^2 + (y_{b/p} + g)^2}}_{\phi_2(\cdot)} + \underbrace{\frac{2\Delta \hat{V}_N}{\Delta^2 + (y_{b/p} + g)^2} \frac{\partial g}{\partial b}}_{\phi_3(\cdot)} \tag{9.93}$$

We can rewrite $r_d v_r$ to obtain

$$\begin{aligned}
 r_d v_r = & -\frac{1}{C_r} v_r \left[\kappa(\theta) \frac{u_t \cos(\psi + \beta - \gamma_p(\theta))}{1 - \kappa(\theta) y_{b/p}} \right. \\
 & - \phi_2(\cdot) u_{td} \frac{y_{b/p} + g}{\sqrt{\Delta^2 + (y_{b/p} + g)^2}} + \phi_2(\cdot) \hat{V}_N \\
 & + \phi_2(\cdot) \left[1 - \cos(\tilde{\psi}) \right] u_{td} \sin \left(\arctan \left(\frac{y_{b/p} + g}{\Delta} \right) \right) \\
 & + \phi_2(\cdot) \cos \left(\arctan \left(\frac{y_{b/p} + g}{\Delta} \right) \right) \sin(\tilde{\psi}) u_{td} \left. \right] - \frac{1}{C_r} v_r \Phi_1(\cdot) \\
 & - \frac{1}{C_r} \left(\frac{u_{rd}}{u_{rd}^2 + v_r^2} - \frac{2\Delta v_r}{\Delta^2 + (y_{b/p} + g)^2} \frac{\partial g}{\partial a} \right) Y(u_r) v_r^2
 \end{aligned} \tag{9.94}$$

where $\Phi_1(\cdot)$ collects terms that are bounded with respect to v_r and terms that grow linearly with v_r , but vanish when $\tilde{X}_2 = 0$. The function $\Phi_1(\cdot)$ is defined as

$$\begin{aligned}
 \Phi_1(\cdot) \triangleq & \kappa(\theta) \frac{k_\delta x_{b/p} - \hat{V}_T}{1 - \kappa(\theta) y_{b/p}} - \frac{\dot{u}_{rd} v_r}{u_{rd}^2 + v_r^2} + \frac{2u_{rd} \dot{u}_{rd} \Delta}{\Delta^2 + (y_{b/p} + g)^2} \frac{\partial g}{\partial a} \\
 & + \frac{\Delta (b + \sqrt{b^2 - ac})}{a\Delta^2 + a(y_{b/p} + g)^2} (-k_{x_1} \tilde{x} \sin(\gamma_p(\theta)) + k_{y_1} \tilde{y} \cos(\gamma_p(\theta))) \\
 & + \frac{\Delta \kappa(\theta) \hat{V}_T (b + \sqrt{b^2 - ac})}{a\Delta^2 + a(y_{b/p} + g)^2} \left(\frac{u_t \cos(\psi + \beta - \gamma_p(\theta))}{1 - \kappa(\theta) y_{b/p}} + \frac{k_\delta x_{b/p} + \hat{V}_T}{1 - \kappa(\theta) y_{b/p}} \right) \\
 & + \frac{\Delta \frac{\partial g}{\partial a} 2\hat{V}_N}{\Delta^2 + (y_{b/p} + g)^2} (k_{x_1} \tilde{x} \sin(\gamma_p(\theta)) - k_{y_1} \tilde{y} \cos(\gamma_p(\theta))) \\
 & - \frac{\Delta \frac{\partial g}{\partial a} 2\kappa(\theta) \hat{V}_N \hat{V}_T}{\Delta^2 + (y_{b/p} + g)^2} \left(\frac{u_t \cos(\psi + \beta - \gamma_p(\theta))}{1 - \kappa(\theta) y_{b/p}} + \frac{k_\delta x_{b/p} + \hat{V}_T}{1 - \kappa(\theta) y_{b/p}} \right) \\
 & + \frac{\Delta \frac{\partial g}{\partial b} 2y_{b/p}}{\Delta^2 + (y_{b/p} + g)^2} (k_{x_1} \tilde{x} \sin(\gamma_p(\theta)) - k_{y_1} \tilde{y} \cos(\gamma_p(\theta))) \\
 & - \frac{\Delta \frac{\partial g}{\partial b} 2y_{b/p} \kappa(\theta) \hat{V}_T}{\Delta^2 + (y_{b/p} + g)^2} \left(\frac{u_t \cos(\psi + \beta - \gamma_p(\theta))}{1 - \kappa(\theta) y_{b/p}} + \frac{k_\delta x_{b/p} + \hat{V}_T}{1 - \kappa(\theta) y_{b/p}} \right) \\
 & - (\phi_1(\cdot) + \phi_3(\cdot)) u_{td} \frac{y_{b/p}}{\sqrt{\Delta^2 + (y_{b/p} + g)^2}} + \phi(\cdot) \tilde{u} \sin(\psi - \gamma_p) \\
 & + (\phi_1(\cdot) + \phi_3(\cdot)) \left[1 - \cos(\tilde{\psi}) \right] u_{td} \sin \left(\arctan \left(\frac{y_{b/p} + g}{\Delta} \right) \right) \\
 & + (\phi_1(\cdot) + \phi_3(\cdot)) \cos \left(\arctan \left(\frac{y_{b/p} + g}{\Delta} \right) \right) \sin(\tilde{\psi}) u_{td} \\
 & - 2\phi(\cdot) x_{b/p} \kappa(\theta) \left(\frac{u_t \cos(\psi + \beta - \gamma_p(\theta))}{1 - \kappa(\theta) y_{b/p}} + \frac{k_\delta x_{b/p} + \hat{V}_T}{1 - \kappa(\theta) y_{b/p}} \right)
 \end{aligned} \tag{9.95}$$

We now introduce $C_r^*(\cdot)$ as defined in the proof of Lemma 9.3, so we can rewrite $r_d v_r$ to obtain:

$$\begin{aligned}
 r_d v_r = & -\frac{1}{C_r^*} v_r \left[\frac{\kappa(\theta) u_t \cos(\psi + \beta - \gamma_p(\theta))}{1 - \kappa(\theta) y_{b/p}} - \right. \\
 & \left. \phi_2(\cdot) u_{td} \frac{y_{b/p} + g}{\sqrt{\Delta^2 + (y_{b/p} + g)^2}} + \right. \\
 & \left. \phi_2(\cdot) \left[1 - \cos(\tilde{\psi}) \right] u_{td} \sin \left(\arctan \left(\frac{y_{b/p} + g}{\Delta} \right) \right) + \right. \\
 & \left. \phi_2(\cdot) \cos \left(\arctan \left(\frac{y_{b/p} + g}{\Delta} \right) \right) \sin(\tilde{\psi}) u_{td} \right] - \frac{1}{C_r} v_r \Phi_2(\cdot) \\
 & - \frac{1}{C_r} \left(\frac{u_{rd}}{u_{rd}^2 + v_r^2} - \frac{2\Delta v_r}{\Delta^2 + (y_{b/p} + g)^2} \frac{\partial g}{\partial a} \right) Y(u_r) v_r^2
 \end{aligned} \tag{9.96}$$

where $\Phi_2(\cdot)$ collects terms that are bounded with respect to v_r and terms that grow linearly with v_r but vanish when $\tilde{X}_2 = 0$. The function $\Phi_2(\cdot)$ is defined as

$$\begin{aligned}
 \Phi_2(\cdot) \triangleq & \Phi_1(\cdot) + \frac{C_r^* - C_r}{C_r^*} \left[\phi_2(\cdot) \left[1 - \cos(\tilde{\psi}) \right] u_{td} \sin \left(\arctan \left(\frac{y_{b/p} + g}{\Delta} \right) \right) \right. \\
 & + \frac{\kappa(\theta) u_t \cos(\psi + \beta - \gamma_p(\theta))}{1 - \kappa(\theta) y_{b/p}} - \frac{\phi_2(\cdot) u_{td} (y_{b/p} + g)}{\sqrt{\Delta^2 + (y_{b/p} + g)^2}} \\
 & + \phi_2(\cdot) \cos \left(\arctan \left(\frac{y_{b/p} + g}{\Delta} \right) \right) \sin(\tilde{\psi}) u_{td} \\
 & \left. - \left(\frac{u_{rd}}{u_{rd}^2 + v_r^2} - \frac{2\Delta v_r}{\Delta^2 + (y_{b/p} + g)^2} \frac{\partial g}{\partial a} \right) Y(u_r) v_r \right] + \phi_2(\cdot) \hat{V}_N
 \end{aligned} \tag{9.97}$$

Considering the above we derive the following upper bound for $r_d v_r$:

$$r_d v_r \leq \left| \frac{1}{C_r^*} v_r \right| \left[\frac{|\kappa(\theta)| u_t}{1 - \kappa(\theta) y_{b/p}} + 4 |\phi_2(\cdot)| u_{td} \right] - \frac{1}{C_r} v_r \Phi_2(\cdot) \tag{9.98}$$

$$- \frac{1}{C_r} \left(\frac{u_{rd}}{u_{rd}^2 + v_r^2} - \frac{2\Delta v_r}{\Delta^2 + (y_{b/p} + g)^2} \frac{\partial g}{\partial a} \right) Y(u_r) v_r^2 \tag{9.99}$$

Using the fact that: $u_t \leq |u_r| + |v_r|$, we obtain:

$$\begin{aligned}
 r_d v_r \leq & \left| \frac{v_r}{C_r^*} \right| \left[\frac{|\kappa(\theta)| (|u_r| + |v_r|)}{1 - \kappa(\theta) y_{b/p}} + 4 |\phi_2(\cdot)| |u_{rd}| + 4 |\phi_2(\cdot)| |v_r| \right] - \frac{v_r}{C_r} \Phi_2(\cdot) \\
 & - \frac{1}{C_r} \left(\frac{u_{rd}}{u_{rd}^2 + v_r^2} - \frac{2\Delta v_r}{\Delta^2 + (y_{b/p} + g)^2} \frac{\partial g}{\partial a} \right) Y(u_r) v_r^2 \\
 \leq & \left| \frac{1}{C_r^*} \right| \frac{|\kappa(\theta)| v_r^2}{1 - \kappa(\theta) y_{b/p}} + 4 \left| \frac{1}{C_r^*} \right| |\phi_2(\cdot)| v_r^2 + \Phi_3(\cdot) \\
 & - \frac{1}{C_r} \left(\frac{u_{rd}}{u_{rd}^2 + v_r^2} - \frac{2\Delta v_r}{\Delta^2 + (y_{b/p} + g)^2} \frac{\partial g}{\partial a} \right) Y(u_r) v_r^2
 \end{aligned} \tag{9.100}$$

where Φ_3 collects the terms that grow linear in v_r and terms that grow quadratically in v_r but vanish when $\tilde{X}_2 = 0$. The function Φ_3 is defined as

$$\Phi_3(\cdot) \triangleq \left| \frac{1}{C_r^*} \right| \frac{|\kappa(\theta)| |v_r u_r|}{1 - \kappa(\theta) y_{b/p}} + \left| \frac{1}{C_r^*} \right| |v_r u_{rd}| |\phi_2(\cdot)| - \frac{1}{C_r} v_r \Phi_2(\cdot) \quad (9.101)$$

Observing the definition of $\Phi_3(\cdot)$ one can easily conclude the existence of three continuous positive functions $F_{0,2}(\tilde{X}_1, \tilde{X}_2, u_{rd}, \dot{u}_{rd}, V_T, V_N, \Delta)$ which are bounded since the vector $[\tilde{X}_2^T, u_{rd}, \dot{u}_{rd}, V_T, V_N, \Delta]^T$ is bounded, and where

$$F_2(\tilde{X}_1, \tilde{X}_2 = 0, u_{rd}, \dot{u}_{rd}, V_T, V_N, \Delta) = 0,$$

such that:

$$\Phi_3(\cdot) \leq F_2(\cdot) v_r^2 + F_1(\cdot) v_r + F_0(\cdot) \quad (9.102)$$

Consequently, when we substitute (9.100) in (9.89) obtain:

$$\begin{aligned} \dot{V}_3 = v_r \dot{v}_r &\leq |X(u_{rd})| \left[\left| \frac{1}{C_r^*} \right| \frac{|\kappa(\theta)| v_r^2}{1 - \kappa(\theta) y_{b/p}} + 4 \left| \frac{1}{C_r^*} \right| |\phi_2(\cdot)| v_r^2 + \Phi_3(\cdot) \right] \\ &\quad + a_x \tilde{u}_{rd} v_r + X(u_{rd}) v_r \tilde{r} + a_x \tilde{u} v_r \tilde{r} + a_y \tilde{u} v_r^2 + Y(u_{rd}) v_r^2 \\ &\quad - \frac{1}{C_r} \left(\frac{u_{rd}}{u_{rd}^2 + v_r^2} - \frac{2\Delta v_r}{\Delta^2 + (y_{b/p} + g)^2} \frac{\partial g}{\partial a} \right) X(u_{rd}) Y(u_{rd}) v_r^2 \quad (9.103) \\ &\leq \left| \frac{1}{C_r^*} \right| \left[\frac{X_{\max} \kappa_{\max}}{1 - \kappa(\theta) y_{b/p}} + 4X_{\max} |\phi_2(\cdot)| - Y_{\min} \right] v_r^2 \\ &\quad + |X(u_{rd})| |\Phi_3(\cdot)| + a_x \tilde{u}_{rd} v_r + X(u_{rd}) v_r \tilde{r} + a_x \tilde{u} v_r \tilde{r} + a_y \tilde{u} v_r^2 \end{aligned}$$

To have boundedness of v_r for small values of \tilde{X}_2 we have to satisfy the following inequality:

$$\frac{X_{\max} \kappa_{\max}}{1 - \kappa(\theta) y_{b/p}} + 4X_{\max} |\phi_2(\cdot)| - Y_{\min} < 0 \quad (9.104)$$

such that the quadratic term in (9.103) is negative. Using (9.49) we need to choose Δ , such that:

$$|\phi_2(\cdot)| < \frac{[Y_{\min} - X_{\max} \kappa_{\max} \frac{1}{\sigma}]}{4X_{\max}} > 0, \quad (9.105)$$

since $|\phi_2(\cdot)| \leq \frac{1}{\Delta}$, we can take $\Delta > \frac{4X_{\max}}{[Y_{\min} - X_{\max} \kappa_{\max} \frac{1}{\sigma}]}$ such that (9.104) holds.

Consequently, near the manifold $\tilde{X}_2 = 0$ it holds that (9.103) is negative definite for sufficiently large v_r . If \dot{V}_3 is negative for sufficiently large v_r this implies that V_3 decreases for sufficiently large v_r . Since $V_3 = 1/2v_r^2$, a decrease in V_3 implies a decrease in v_r^2 and by extension in v_r . Consequently, v_r cannot increase above a certain value and v_r is bounded near $\tilde{X}_2 = 0$.

Chapter 10

Observer based path following for generic paths: a global approach

This chapter considers path following of generic paths for under-actuated marine vessels in the presence of constant ocean currents. The path is parametrized by a parameter s . We assume that a Serret-Frenet frame moves along the path and its motion is described by a certain time update law for the parameter s . The update law for s is a design parameter and we design it in order to achieve the path following task. The parametrization that we use was first introduced in [80]. The work presented in this chapter is an extension of the results in Chapter 9, where the time update law for s was valid only locally.

We use a line-of-sight-like (LOS-like) guidance strategy together with an observer for the ocean current estimation. The look-ahead distance of the guidance law depends on the distance from the path and it is therefore time-varying. The observer is used to estimate the unknown ocean current in order to compensate for it. A thorough analysis of the closed-loop system is done and it shows boundedness of the sway velocity and global asymptotic stability of the path following errors. We want also to remark that the control strategy presented in this chapter is similar to the one presented in [103]. In particular, we add stabilizing term for the tangential error dynamics. This approach is needed in order to achieve boundedness of the zero dynamics which were not analyzed in [103].

The work in this chapter is based on [16].

The outline of the chapter is as follows. In Section 10.1 the vessel model is given. The path-following problem and the chosen path parametrization are introduced in Section 10.2. Section 10.3 presents the ocean current observer that is used together with the guidance law and controllers. The closed-loop system is then formulated and analyzed in Section 10.4. A simulation case study is presented in Section 10.5 and conclusions are given in Section 10.6.

10.1 Vessel model

In this section we consider the model for a surface vessel given in Chapter 2. This model can be used to describe an autonomous surface vessel or an autonomous

underwater vehicle moving in a plane. We consider vehicles satisfying Assumptions 2.1-2.3. Thus, their model can be expressed in component form as:

$$\dot{x} = u_r \cos(\psi) - v_r \sin(\psi) + V_x, \quad (10.1a)$$

$$\dot{y} = u_r \sin(\psi) + v_r \cos(\psi) + V_y, \quad (10.1b)$$

$$\dot{\psi} = r, \quad (10.1c)$$

$$\dot{u}_r = F_{u_r}(v_r, r) - \frac{d_{11}}{m_{11}} u_r + \tau_u, \quad (10.1d)$$

$$\dot{v}_r = X(u_r)r + Y(u_r)v_r, \quad (10.1e)$$

$$\dot{r} = F_r(u_r, v_r, r) + \tau_r, \quad (10.1f)$$

The functions $X(u_r)$, $Y(u_r)$, F_u , and F_r are given in Chapter 2. The kinematic variables are illustrated in Figure 10.1. We consider the ocean current to satisfy the following assumption.

Assumption 10.1. *The ocean current is assumed to be constant and irrotational with respect to the inertial frame, i.e. $\mathbf{V}_c \triangleq [V_x, V_y, 0]^T$. Furthermore, it is bounded by $V_{\max} > 0$ such that $\|\mathbf{V}_c\| = \sqrt{V_x^2 + V_y^2} \leq V_{\max}$.*

Additionally, we assume that the following assumption holds

Assumption 10.2. *It is assumed that $2V_{\max} < u_{rd}(t) \forall t$, i.e. the desired relative velocity of the vessel is larger than the maximum value of the ocean current.*

Assumption 10.2 assures that the vessel has enough propulsion power to overcome the ocean current affecting it. The factor two in Assumption 10.2 adds some extra conservativeness to bound the solutions of the ocean current observer. This is discussed further in Section 10.6.

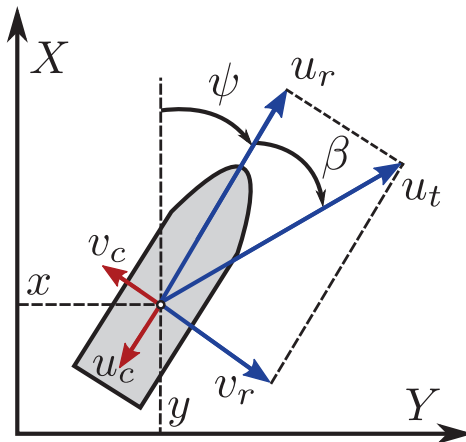


Figure 10.1: Definition of the ship's kinematic variables.

10.2 Problem definition

The goal is to follow a smooth path P , parametrised by a path variable θ , by appropriately controlling the ship's surge velocity and yaw rate. For an underactuated vessel path following can be achieved by positioning the vessel on the path with the total velocity $u_t \triangleq \sqrt{u_r^2 + v_r^2}$ (see Figure 10.1) tangential to the path. To express the path-following errors we propagate a path-tangential frame along P . This is illustrated in Figure 10.2. The path-following errors, $\mathbf{p}_{b/p} \triangleq [x_{b/p}, y_{b/p}]^T$, take the following form:

$$\begin{bmatrix} x_{b/p} \\ y_{b/p} \end{bmatrix} = \begin{bmatrix} \cos(\gamma_p(\theta)) & \sin(\gamma_p(\theta)) \\ -\sin(\gamma_p(\theta)) & \cos(\gamma_p(\theta)) \end{bmatrix} \begin{bmatrix} x - x_p(\theta) \\ y - y_p(\theta) \end{bmatrix}$$

where $\gamma(\theta)$ is the angle of the path with respect to the X -axis. The time derivative of the angle $\gamma(\theta)$ is given by $\dot{\gamma}(\theta) = \kappa(\theta)\dot{\theta}$ where $\kappa(\theta)$ is the curvature of P at θ . The path-following error is expressed in $x_{b/p}$ and $y_{b/p}$ which are the relative positions between the path frame and body frame expressed along the axes of the path frame. Hence, $x_{b/p}$ is the position of the vehicle along the path-frame tangential axis and $y_{b/p}$ is the position of the vehicle along the path-frame normal axis. The goal is to regulate both $x_{b/p}$ and $y_{b/p}$ to zero.

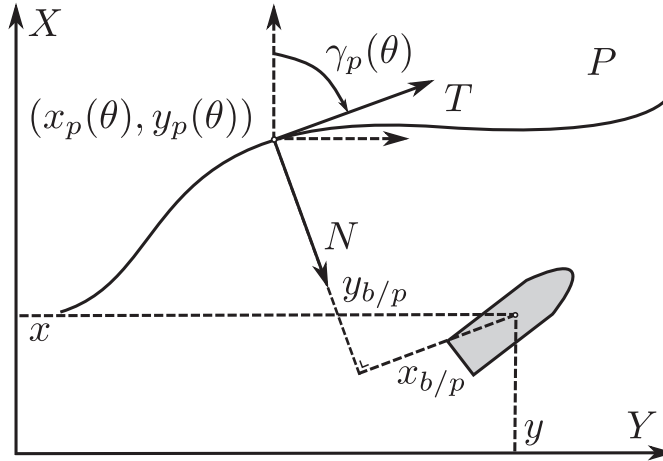


Figure 10.2: Definition of the path.

The error dynamics of a vessel with respect to the path frame are given by:

$$\dot{x}_{b/p} = u_t \cos(\chi - \gamma_p(\theta)) - \dot{\theta}(1 - \kappa(\theta)y_{b/p}) + V_T \quad (10.2a)$$

$$\dot{y}_{b/p} = u_t \sin(\chi - \gamma_p(\theta)) + V_N - \kappa(\theta)\dot{\theta}x_{b/p} \quad (10.2b)$$

where $\chi \triangleq \psi + \beta$ is the course angle (see Figure 10.1) and $V_T \triangleq V_x \cos(\gamma_p(\theta)) + V_y \sin(\gamma_p(\theta))$ and $V_N \triangleq V_y \cos(\gamma_p(\theta)) - V_x \sin(\gamma_p(\theta))$ are the ocean current component in the tangential direction and normal direction of the path-tangential reference frame respectively.

As proposed in [80] we can use the update law of the path variable as an extra degree of freedom in the controller design. In particular, the propagation speed of the frame is used to get the desired behaviour of the $x_{b/p}$ dynamics. This is achieved by setting

$$\dot{\theta} = u_t \cos(\chi - \gamma_p(\theta)) + k_x f_\theta(x_{b/p}, y_{b/p}) + V_T \quad (10.3)$$

where $k_x > 0$ is a control gain for the convergence of $x_{b/p}$ and $f_\theta(x_{b/p}, y_{b/p})$ is a function to be designed later satisfying $f_\theta(x_{b/p}, y_{b/p})x_{b/p} > 0$. Consequently, when substituting (10.3) in (10.2a) we obtain

$$\dot{x}_{b/p} = -k_x f_\theta(x_{b/p}, y_{b/p}) + \dot{\theta} \kappa(\theta) y_{b/p} \quad (10.4)$$

For the case where the current is unknown we need to replace V_T by its estimate \hat{V}_T , and the update law becomes

$$\dot{\theta} = u_t \cos(\chi - \gamma(\theta)) + k_x f_\theta(x_{b/p}, y_{b/p}) + \hat{V}_T \quad (10.5)$$

Substituting this revised update law into (10.2) results in

$$\dot{x}_{b/p} = -k_x f_\theta(x_{b/p}, y_{b/p}) + \dot{\theta} \kappa(\theta) y_{b/p} + \tilde{V}_T \quad (10.6)$$

$$\dot{y}_{b/p} = u_t \sin(\chi - \gamma_p(\theta)) + V_N - x_{b/p} \kappa(\theta) \dot{\theta}. \quad (10.7)$$

Note that the parametrization (10.5) does not decouple (10.6) from (10.7). Consequently, since (10.6) depends on $y_{b/p}$ the $x_{b/p}$ it does not converge independently from those of $y_{b/p}$ and both $x_{b/p}$ and $y_{b/p}$ will have to be regulated to zero using the surge and yaw rate controllers. Moreover, note that although this parametrization has the advantage that the update law can be well defined on the entire state space the path-following error is no longer defined as the shortest distance to the path since the vessel is not on the normal.

10.3 Controllers, Observer, and Guidance

In this section we design the two control laws τ_u and τ_r , and the ocean current estimator that are used to achieve path-following. In the first subsection we present the velocity control law τ_u . The second subsection presents the ocean current observer. The third subsection presents the guidance to be used.

10.3.1 Surge velocity control

The velocity control law is a feedback-linearising P-controller that is used to drive the relative surge velocity to a desired u_{rd} and is given by

$$\tau_u = -F_{u_r}(v_r, r) + \dot{u}_{rd} + \frac{d_{11}}{m_{11}} u_{rd} - k_u (u_r - u_{rd}) \quad (10.8)$$

where $k_u > 0$ is a constant controller gain. It is straightforward to verify that (10.8) ensures global exponential tracking of the desired velocity. In particular, when (10.8) is substituted in (10.1d) we obtain

$$\dot{\tilde{u}}_r = -k_u (u_r - u_{rd}) = -k_u \tilde{u}_r \quad (10.9)$$

where $\tilde{u}_r \triangleq u_r - u_{rd}$. Consequently, the velocity error dynamics are described by a stable linear systems, which assures exponential tracking of the desired velocity u_{rd} .

10.3.2 Ocean current estimator

This subsection presents the ocean current estimator introduced in [2]. This observer provides the estimate of the ocean current needed to implement (10.5) and the guidance law developed in the next subsection. Rather than estimating the time-varying current components in the path frame V_T and V_N the observer is used to estimate the constant ocean current components in the inertial frame V_x and V_y . The observer from [2] is based on the kinematic equations of the vehicle, i.e. (10.1a) and (10.1b), and requires measurements of the vehicle's x and y position in the inertial frame. The observer is formulated as

$$\dot{\hat{x}} = u_r \cos(\psi) - v_r \sin(\psi) + \hat{V}_x + k_{x_1} \tilde{x} \quad (10.10a)$$

$$\dot{\hat{y}} = u_r \sin(\psi) + v_r \cos(\psi) + \hat{V}_y + k_{y_1} \tilde{y} \quad (10.10b)$$

$$\dot{\hat{V}}_x = k_{x_2} \tilde{x} \quad (10.10c)$$

$$\dot{\hat{V}}_y = k_{y_2} \tilde{y} \quad (10.10d)$$

where $\tilde{x} \triangleq x - \hat{x}$ and $\tilde{y} \triangleq y - \hat{y}$ are the positional errors and k_{x_1} , k_{x_2} , k_{y_1} , and k_{y_2} are constant positive gains. Consequently, the estimation error dynamics are given by

$$\begin{bmatrix} \dot{\tilde{x}} \\ \dot{\tilde{y}} \\ \dot{\tilde{V}}_x \\ \dot{\tilde{V}}_y \end{bmatrix} = \begin{bmatrix} -k_{x_1} & 0 & 1 & 0 \\ 0 & -k_{y_1} & 0 & 1 \\ -k_{x_2} & 0 & 0 & 0 \\ 0 & -k_{y_2} & 0 & 0 \end{bmatrix} \begin{bmatrix} \tilde{x} \\ \tilde{y} \\ \tilde{V}_x \\ \tilde{V}_y \end{bmatrix} \quad (10.11)$$

which is a linear system with negative eigenvalues. Hence, the observer error dynamics are globally exponentially stable at the origin. Note that this implies that also \hat{V}_T and \hat{V}_N go to V_T and V_N respectively with exponential convergence since it holds that

$$\hat{V}_T = \hat{V}_x \cos(\gamma(\theta)) + \hat{V}_y \sin(\gamma(\theta)) \quad (10.12a)$$

$$\hat{V}_N = -\hat{V}_x \sin(\gamma(\theta)) + \hat{V}_y \cos(\gamma(\theta)) \quad (10.12b)$$

For implementation of the controllers it is desired that $\|\hat{V}_N(t)\| < u_{rd}(t) \forall t$. To achieve this we first choose the initial conditions of the estimator as

$$[\hat{x}(t_0), \hat{y}(t_0), \hat{V}_x(t_0), \hat{V}_y(t_0)]^T = [x(t_0), y(t_0), 0, 0]^T.$$

Consequently, the initial estimation error is given by

$$[\tilde{x}(t_0), \tilde{y}(t_0), \tilde{V}_x(t_0), \tilde{V}_y(t_0)]^T = [0, 0, V_x, V_y]^T \quad (10.13)$$

which has a norm smaller than or equal to V_{\max} according to Assumption 10.1. Now consider the function

$$W(t) = \tilde{x}^2 + \tilde{y}^2 + \frac{1}{k_{x_2}} \tilde{V}_x^2 + \frac{1}{k_{y_2}} \tilde{V}_y^2 \quad (10.14)$$

which has the following time derivative

$$\dot{W}(t) = -2k_{x_1}\tilde{x}^2 - 2k_{y_1}\tilde{y}^2 \leq 0. \quad (10.15)$$

This implies that $W(t) \leq \|W(t_0)\|$. From our choice of initial conditions we know that

$$\|W(t_0)\| = \frac{V_x^2}{k_{x_2}} + \frac{V_y^2}{k_{y_2}} \leq \frac{1}{\min(k_{x_2}, k_{y_2})} V_{\max}^2. \quad (10.16)$$

Moreover, it is straightforward to verify

$$\frac{1}{\max(k_{x_2}, k_{y_2})} \|\tilde{V}_c(t)\|^2 \leq W(t). \quad (10.17)$$

Combining the observations given above we obtain

$$\frac{1}{\max(k_{x_2}, k_{y_2})} \|\tilde{V}_c(t)\|^2 \leq \frac{1}{\min(k_{x_2}, k_{y_2})} V_{\max}^2. \quad (10.18)$$

Consequently, we obtain

$$\begin{aligned} \|\tilde{V}_c(t)\| &\leq \sqrt{\frac{\max(k_{x_2}, k_{y_2})}{\min(k_{x_2}, k_{y_2})}} V_{\max} \\ &< \sqrt{\frac{\max(k_{x_2}, k_{y_2})}{\min(k_{x_2}, k_{y_2})}} u_{rd}(t), \quad \forall t, \end{aligned} \quad (10.19)$$

which implies that if the gains are chosen as $k_{x_2} = k_{y_2}$ we have

$$\|\hat{V}_N\| \leq 2V_{\max} \leq u_{rd}(t), \quad \forall t. \quad (10.20)$$

Hence, $\|\hat{V}_N\| < u_{rd}(t)$, $\forall t$ if $2V_{\max} < u_{rd}(t)$, $\forall t$.

Remark 10.1. *The bound $2V_{\max} < u_{rd}$, $\forall t$, is only required when deriving the bound on the solutions of the observer. In particular, it is required to guarantee that $\|\hat{V}_N\| < u_{rd}(t)$, $\forall t$. For the rest of the analysis it suffices that $V_{\max} < u_{rd}$, $\forall t$. Therefore, if the more conservative bound $2V_{\max} < u_{rd}$, $\forall t$, is not satisfied the observer can be changed to an observer that allows explicit bounds on the estimate \hat{V}_N , e.g. the observer developed Narendra and Annaswamy [104], rather than an observer that only provides a bound on the error \tilde{V}_c as is the case here. For practical purposes the estimate can also be saturated such that $\|\hat{V}_N\| < u_{rd}$, $\forall t$, which is the approach taken in Moe et al. [103]. However, in the theoretical analysis of the yaw controller we use derivatives of \hat{V}_N which will be discontinuous when saturation is applied.*

10.3.3 Guidance for global parametrization

When using the global parametrization we can define one guidance law that can be used everywhere. As in Moe et al. [103] we choose a guidance law of the form:

$$\psi_d = \gamma(\theta) - \operatorname{atan}\left(\frac{v_r}{u_{rd}}\right) - \operatorname{atan}\left(\frac{y_{b/p} + g}{\Delta(\mathbf{p}_{b/p})}\right) \quad (10.21)$$

The guidance law consists of three terms. The first term is a feedforward of the angle of the path with respect to the inertial frame. The second part is the desired side-slip angle, i.e. the angle between the surge velocity and the total speed when $u_r \equiv u_{rd}$. This side-slip angle is used to make the vehicle's total speed tangential to the path when the sway velocity is non-zero. The third term is a line-of-sight (LOS) term that is intended to steer the vessel to the path, where g is a term dependent on the ocean current. The choice of g provides extra design freedom to compensate for the component of the ocean current along the normal axis V_N .

Remark 10.2. *The guidance law (10.21) with the choice $\Delta(x_{b/p}, y_{b/p}) = \sqrt{\mu^2 + x_{b/p}^2}$ was utilised in Moe et al. [103]. However, as will be shown this leads to a desired yaw rate that goes to infinity as $y_{b/p}$ goes to infinity. Consequently, no finite value of the constant μ can be found that stabilises the system globally, i.e. for any $y_{b/p}$.*

When we substitute (10.21) in (10.7) we obtain

$$\begin{aligned} \dot{y}_{b/p} &= u_{td} \sin\left(\psi_d + \tilde{\psi} + \beta_d - \gamma_p(\theta)\right) + V_N \\ &\quad - x_{b/p} \kappa(\theta) \dot{\theta} + \tilde{u}_r \sin(\psi - \gamma_p(\theta)) \\ &= -\frac{u_{td}(y_{b/p} + g)}{\sqrt{(y_{b/p} + g)^2 + \Delta^2}} - x_{b/p} \dot{\gamma}_p(\theta) \\ &\quad + V_N + G_1(\tilde{\psi}, \tilde{u}_r, g, \psi_d, y_{b/p}, u_{td}) \end{aligned} \quad (10.22)$$

where $G_1(\cdot)$ is a perturbing term given by

$$\begin{aligned} G_1(\cdot) &= u_{td} \left[1 - \cos(\tilde{\psi})\right] \sin\left(\arctan\left(\frac{y_{b/p} + g}{\Delta}\right)\right) \\ &\quad + \tilde{u}_r \sin(\psi - \gamma_p(\theta)) \\ &\quad + u_{td} \cos\left(\arctan\left(\frac{y_{b/p} + g}{\Delta}\right)\right) \sin(\tilde{\psi}) \end{aligned}$$

Note that $G_1(\cdot)$ satisfies

$$G_1(0, 0, g, \psi_d, y_{b/p}, u_{td}) = 0 \quad (10.23a)$$

$$\|G_1(\tilde{\psi}, \tilde{u}_r, \psi_d, y_{b/p}, u_{td})\| \leq \zeta(u_{td}) \|\tilde{\psi}, \tilde{u}_r\|^T, \quad (10.23b)$$

where $\zeta(u_{td}) > 0$, which shows that $G_1(\cdot)$ is zero when the perturbing variables are zero and that it has maximal linear growth in the perturbing variables.

To compensate for the ocean current component V_N the variable g is now chosen to satisfy the equality

$$u_{td} \frac{g}{\sqrt{\Delta^2 + (y_{b/p} + g)^2}} = \hat{V}_N. \quad (10.24)$$

which is a choice inspired by [103]. In order for g to satisfy the equality above, it should be the solution of the following second order equality

$$\underbrace{(u_{td}^2 - \hat{V}_N^2)}_{-a} \left(\frac{g}{\hat{V}_N}\right)^2 = \underbrace{\Delta^2 + y_{b/p}^2}_c + 2 \underbrace{y_{b/p} \hat{V}_N}_b \left(\frac{g}{\hat{V}_N}\right)$$

hence we choose g to be

$$g = \hat{V}_N \frac{b + \sqrt{b^2 - ac}}{-a} \quad (10.25)$$

which has the same sign as \hat{V}_N and is well defined for $(u_{rd}^2 - \hat{V}_N^2) = -a > 0$. Substituting this in (10.22) gives

$$\begin{aligned} \dot{y}_{b/p} = & -u_{td} \frac{y_{b/p}}{\sqrt{(y_{b/p} + g)^2 + \Delta^2}} - x_{b/p} \dot{\gamma}_p(\theta) \\ & + \tilde{V}_N + G_1(\tilde{\psi}, \tilde{u}, \psi_d, y_{b/p}, u_{td}) \end{aligned} \quad (10.26)$$

Recall that the error in tangential direction is given by :

$$\dot{x}_{b/p} = \dot{\theta}(1 - \kappa(\theta)y_{b/p}) + u_t \cos(\psi + \beta - \gamma_p(\theta)) + V_T \quad (10.27)$$

where $\kappa(\theta)$ is the curvature of the path at the point $(x_p(\theta), y_p(\theta))$. We now choose $\dot{\theta}$ to be:

$$\dot{\theta} = u_t \cos(\psi + \beta - \gamma_p(\theta)) + \frac{k_\delta x_{b/p}}{\sqrt{1 + x_{b/p}^2}} + \hat{V}_T \quad (10.28)$$

such that we obtain:

$$\dot{x}_{b/p} = -k_\delta \frac{x_{b/p}}{\sqrt{1 + x_{b/p}^2}} + \dot{\theta} \kappa(\theta) y_{b/p} + \tilde{V}_T. \quad (10.29)$$

where $k_\delta > 0$. In this way we introduce a stabilising term to the tangential error dynamics by appropriately controlling the propagation of our path-tangential frame.

The derivative of (10.21) is given by

$$\begin{aligned} \dot{\psi}_d = & \kappa(\theta) \dot{\theta} - \frac{\dot{v}_r u_{rd} - \dot{u}_{rd} v_r}{u_{rd}^2 + v_r^2} - \frac{\Delta(\dot{y}_{b/p} + \dot{g})}{\Delta^2 + (y_{b/p} + g)^2} \\ & + \frac{y_{b/p} + g}{\Delta^2 + (y_{b/p} + g)^2} \left[\frac{\partial \Delta}{\partial x_{b/p}} \dot{x}_{b/p} + \frac{\partial \Delta}{\partial y_{b/p}} \dot{y}_{b/p} \right] \end{aligned} \quad (10.30)$$

with

$$\dot{g} = \dot{V}_N \frac{b + \sqrt{b^2 - ac}}{-a} + \frac{\partial g}{\partial a} \dot{a} + \frac{\partial g}{\partial b} \dot{b} + \frac{\partial g}{\partial c} \dot{c} \quad (10.31)$$

where

$$\frac{\partial g}{\partial a} = \hat{V}_N \frac{c}{2a\sqrt{b^2 - ac}} + \hat{V}_N \frac{b + \sqrt{b^2 - ac}}{a^2} \quad (10.32a)$$

$$\frac{\partial g}{\partial b} = \hat{V}_N \frac{b + \sqrt{b^2 - ac}}{a\sqrt{b^2 - ac}} \quad (10.32b)$$

$$\frac{\partial g}{\partial c} = \hat{V}_N \frac{1}{2\sqrt{b^2 - ac}} \quad (10.32c)$$

$$\dot{a} = 2\hat{V}_N \dot{\hat{V}}_N - 2u_{rd}\dot{u}_{rd} - 2v_r [X(u_r)r + Y(u_r)v_r] \quad (10.32d)$$

$$\dot{b} = \hat{V}_N \dot{y}_{b/p} + \dot{\hat{V}}_N y_{b/p} \quad (10.32e)$$

$$\dot{c} = 2y_{b/p}\dot{y}_{b/p} + 2\Delta(x_{b/p}, y_{b/p}) \left[\frac{\partial \Delta}{\partial x_{b/p}} \dot{x}_{b/p} + \frac{\partial \Delta}{\partial y_{b/p}} \dot{y}_{b/p} \right] \quad (10.32f)$$

The expression for $\dot{\psi}_d$ contains terms depending on $\dot{y}_{b/p}$ and $\dot{x}_{b/p}$ which depend on \tilde{V}_N and \tilde{V}_T respectively. Consequently, $\dot{\psi}_d$ depends on unknown variables and cannot be used to control the yaw rate. This was not considered in [103] where the proposed controller contained both $\dot{\psi}_d$ and $\ddot{\psi}_d$.

Moreover, from (10.21) we see that $\dot{\psi}_d$ contains \dot{v}_r , which depends on $r = \dot{\psi}$. Therefore, the yaw rate error $\dot{\tilde{\psi}} \triangleq \dot{\psi} - \dot{\psi}_d$ grows with $\dot{\psi}$ which leads to a necessary condition for a well defined yaw rate error. The yaw rate error dynamics are given by

$$\begin{aligned} \dot{\tilde{\psi}} = & r \left[1 + \frac{X(u_r)u_{rd}}{u_{rd}^2 + v_r^2} - \frac{\Delta}{\Delta^2 + (y_{b/p} + g)^2} \frac{\partial g}{\partial a} (2v_r X(u_r)) \right] \\ & - \kappa(\theta)\dot{\theta} + \frac{Y(u_r)v_r u_{rd} - \dot{u}_{rd}v_r}{u_{rd}^2 + v_r^2} \\ & + \frac{\Delta}{\Delta^2 + (y_{b/p} + g)^2} \left[\dot{\hat{V}}_N \frac{b + \sqrt{b^2 - ac}}{-a} + \frac{\partial g}{\partial b} (2\dot{\hat{V}}_N y_{b/p}) \right] \\ & + \frac{\partial g}{\partial a} (2\hat{V}_N \dot{\hat{V}}_N - 2u_{rd}\dot{u}_{rd} - 2v_r Y(u_r)v_r) \\ & + \left[1 + \frac{\partial g}{\partial c} 2y_{b/p} + \frac{\partial g}{\partial b} (2\hat{V}_N) \right] \dot{y}_e \\ & + \frac{\partial g}{\partial c} 2\Delta \left[\frac{\partial \Delta}{\partial x_{b/p}} \dot{x}_{b/p} + \frac{\partial \Delta}{\partial y_{b/p}} \dot{y}_{b/p} \right] \\ & - \frac{y_{b/p} + g}{\Delta^2 + (y_{b/p} + g)^2} \left[\frac{\partial \Delta}{\partial x_{b/p}} \dot{x}_{b/p} + \frac{\partial \Delta}{\partial y_{b/p}} \dot{y}_{b/p} \right] \end{aligned} \quad (10.33)$$

which shows we have the following necessary condition for the existence of our controller:

Condition 10.1. *If it holds that*

$$C_r \triangleq 1 + \left[\frac{u_{rd}}{u_{rd}^2 + v_r^2} - \frac{2v_r \Delta}{\Delta^2 + (y_{b/p} + g)^2} \frac{\partial g}{\partial a} \right] X(u_r) > 0. \quad (10.34)$$

then the yaw rate controller is well defined for all time.

Remark 10.3. *The condition above can be verified for any positive velocity, for the vehicles considered in this thesis. Note that for most vessels this condition is verifiable since standard ship design practices will result in similar properties of the function $X(u_r)$. Besides having a lower bound greater than zero C_r is also upper-bounded since the term between brackets can be verified to be bounded in its arguments.*

Since $\dot{\psi}_d$ depends on the unknown signal \tilde{V}_N we cannot take $\dot{\psi}_d = r_d$. To define an expression for r_d without requiring the knowledge of \tilde{V}_N we use (10.34) to define

$$\begin{aligned}
 r_d = & -\frac{1}{C_r} \left[\kappa(\theta) \left(u_t \cos(\psi + \beta - \gamma_p) + k_\delta \frac{x_{b/p}}{\sqrt{1 + x_{b/p}^2}} + \hat{V}_T \right) \right. \\
 & + \frac{Y(u_r)v_r u_{rd} - \dot{u}_{rd}v_r}{u_{rd}^2 + v_r^2} + \frac{\Delta}{\Delta^2 + (y_{b/p} + g)^2} \left[\dot{\tilde{V}}_N \frac{b + \sqrt{b^2 - ac}}{-a} \right. \\
 & + \frac{\partial g}{\partial b} (2\dot{\tilde{V}}_N y_{b/p}) + \frac{\partial g}{\partial a} (2\hat{V}_N \dot{\tilde{V}}_N - 2u_{rd} \dot{u}_{rd} \\
 & - 2v_r Y(u_r)v_r) + \left[1 + \frac{\partial g}{\partial c} 2y_{b/p} + \frac{\partial g}{\partial b} 2\hat{V}_N \right] * \\
 & * \left(\frac{-u_{td} y_{b/p}}{\sqrt{\Delta^2 + (y_{b/p} + g)^2}} + G_1(\cdot) - x_{b/p} \kappa(\theta) \dot{\theta} \right) \\
 & + \frac{\partial g}{\partial c} 2\Delta \left[\frac{\partial \Delta}{\partial x_{b/p}} \left(-k_\delta \frac{x_{b/p}}{\sqrt{1 + x_{b/p}^2}} + y_{b/p} \kappa(\theta) \dot{\theta} \right) \right. \\
 & + \left. \left. \frac{\partial \Delta}{\partial y_{b/p}} \left(-u_{td} \frac{y_{b/p}}{\sqrt{\Delta^2 + (y_{b/p} + g)^2}} + G_1(\cdot) - x_{b/p} \kappa(\theta) \dot{\theta} \right) \right] \right] \\
 & - \frac{y_{b/p} + g}{\Delta^2 + (y_{b/p} + g)^2} \left[\frac{\partial \Delta}{\partial x_{b/p}} \left(-k_\delta \frac{x_{b/p}}{\sqrt{1 + x_{b/p}^2}} + y_{b/p} \kappa(\theta) \dot{\theta} \right) \right. \\
 & + \left. \left. \frac{\partial \Delta}{\partial y_{b/p}} \left(-u_{td} \frac{y_{b/p}}{\sqrt{\Delta^2 + (y_{b/p} + g)^2}} + G_1(\cdot) - x_{b/p} \kappa(\theta) \dot{\theta} \right) \right] \right]
 \end{aligned} \tag{10.35}$$

with,

$$\begin{aligned}
 \dot{\tilde{V}}_N = & -\dot{\tilde{V}}_x \sin(\gamma_p(\theta)) + \dot{\tilde{V}}_y \cos(\gamma_p(\theta)) \\
 & - \kappa(\theta) \left(u_t \cos(\psi + \beta - \gamma_p(\theta)) + \frac{k_\delta x_{b/p}}{\sqrt{1 + x_{b/p}^2}} - \hat{V}_T \right) \hat{V}_T
 \end{aligned} \tag{10.36}$$

Notice that (10.35) is equivalent to (10.30), but without the terms depending on the unknowns \tilde{V}_x and \tilde{V}_y that cannot be used in the input functions. If we substitute

(10.35) in (10.33) and use $\tilde{r} \triangleq r - r_d$ we obtain

$$\begin{aligned} \dot{\tilde{\psi}} = & C_r \tilde{r} + \frac{\Delta}{\Delta^2 + (y_{b/p} + g)^2} \left[1 + \frac{\partial g}{\partial c} 2y_{b/p} + \frac{\partial g}{\partial b} 2\hat{V}_N \right] \tilde{V}_N \\ & + \left(\frac{2\Delta^2}{\Delta^2 + (y_{b/p} + g)^2} \frac{\partial g}{\partial c} - \frac{y_{b/p} + g}{\Delta^2 + (y_{b/p} + g)^2} \right) \frac{\partial \Delta}{\partial \mathbf{p}_{b/p}} [\tilde{V}_T, \tilde{V}_N]^T \end{aligned} \quad (10.37)$$

Note that we have used the notation

$$\frac{\partial \Delta}{\partial \mathbf{p}_{b/p}} [\tilde{V}_T, \tilde{V}_N]^T = \frac{\partial \Delta}{\partial x_{b/p}} \tilde{V}_T + \frac{\partial \Delta}{\partial y_{b/p}} \tilde{V}_N. \quad (10.38)$$

From (10.37) it can be seen that choosing r_d as in (10.35) results in yaw angle error dynamics that have a term dependent on the yaw rate error \tilde{r} and a perturbing term that vanishes when the estimation errors \tilde{V}_T and \tilde{V}_N go to zero. To add acceleration feedforward to the yaw rate controller, the derivative of r_d should be calculated. Using the expression of r_d in (10.35) with (10.10), (10.11) and (10.12) it can be seen that r_d has the following dependencies

$$r_d = r_d(h^T, y_{b/p}, x_{b/p}, \tilde{\psi}, \tilde{x}, \tilde{y}), \quad h \triangleq [\theta, v_r, u_r, u_{rd}, \dot{u}_{rd}, \hat{V}_T, \hat{V}_N]^T. \quad (10.39)$$

where h is a vector that contains all the variable whose time derivative do not depend on \tilde{V}_N and \tilde{V}_T . However, the other dependencies of r_d do introduce new terms depending on \tilde{V}_N and \tilde{V}_T when the acceleration feedforward is calculated. Consequently, we define our yaw rate controller instead with an acceleration feedforward that contains only the known terms from \dot{r}_d

$$\begin{aligned} \tau_r = & -F(u_r, v_r, r) + \frac{\partial r_d}{\partial h^T} \dot{h} + \frac{\partial r_d}{\partial x_{b/p}} \left(-k_\delta \frac{x_{b/p}}{\sqrt{1 + x_{b/p}^2}} + y_{b/p} \kappa(\theta) \dot{\theta} \right) \\ & + \frac{\partial r_d}{\partial \tilde{\psi}} C_r \tilde{r} - \frac{\partial r_d}{\partial \tilde{x}} k_x \tilde{x} - \frac{\partial r_d}{\partial \tilde{y}} k_y \tilde{y} - k_1 \tilde{r} - k_2 C_r \tilde{\psi} \\ & + \frac{\partial r_d}{\partial y_{b/p}} \left(-u_{td} \frac{y_{b/p}}{\sqrt{\Delta^2 + (y_{b/p} + g)^2}} + G_1(\cdot) - x_{b/p} \kappa(\theta) \dot{\theta} \right). \end{aligned} \quad (10.40)$$

where $k_1 > 0$ and $k_2 > 0$ are constant controller gains.

Using the controller (10.40) in (10.1f) the yaw rate error dynamics become

$$\begin{aligned} \dot{\tilde{r}} = & -k_1 \tilde{r} - k_2 C_r \tilde{\psi} - \frac{\partial r_d}{\partial y_{b/p}} \tilde{V}_N - \frac{\partial r_d}{\partial x_{b/p}} \tilde{V}_T + \frac{\partial r_d}{\partial \tilde{x}} \tilde{V}_x + \frac{\partial r_d}{\partial \tilde{y}} \tilde{V}_y \\ & - \frac{\partial r_d}{\partial \tilde{\psi}} \left[\frac{\Delta}{\Delta^2 + (y_{b/p} + g)^2} \left[1 + \frac{\partial g}{\partial c} 2y_{b/p} + \frac{\partial g}{\partial b} 2\hat{V}_N \right] \tilde{V}_N \right. \\ & \left. + \left(\frac{2\Delta^2}{\Delta^2 + (y_{b/p} + g)^2} \frac{\partial g}{\partial c} - \frac{y_{b/p} + g}{\Delta^2 + (y_{b/p} + g)^2} \right) \frac{\partial \Delta}{\partial \mathbf{p}_{b/p}} [\tilde{V}_T, \tilde{V}_N]^T \right] \end{aligned} \quad (10.41)$$

which contains two stabilising terms $-k_1 \tilde{r}$ and $-k_2 C_r \tilde{\psi}$, and perturbing terms depending on \tilde{V}_T and \tilde{V}_N that cannot be cancelled by the controller.

Remark 10.4. *It is straightforward to verify that all the terms in (10.30) are smooth fractionals that are bounded with respect to $(y_{b/p}, x_{b/p}, \tilde{x}, \tilde{y}, \tilde{\psi})$ or are periodic functions with linear arguments and consequently the partial derivatives in (10.40) and (10.41) are all bounded. This is something that is used when showing closed-loop stability in the next section.*

10.4 Closed-Loop Analysis

In this section we analyse the closed-loop system of the model (10.1) with controllers (10.8) and (10.40) and observer (10.10), when the frame propagates along the path P with update law (10.5). To show that path following is achieved we have to show that the following error dynamics converge to zero

$$\dot{y}_{b/p} = -u_{td} \frac{y_{b/p}}{\sqrt{\Delta^2 + (y_{b/p} + g)^2}} + G_1(\cdot) - x_{b/p} \kappa(\theta) \dot{\theta} + \tilde{V}_N \quad (10.42a)$$

$$\dot{x}_{b/p} = -k_\delta \frac{x_{b/p}}{\sqrt{1 + x_{b/p}^2}} + y_{b/p} \kappa(\theta) \dot{\theta} + \tilde{V}_T \quad (10.42b)$$

$$\dot{\tilde{\psi}} = C_r \tilde{r} + \frac{\Delta}{\Delta^2 + (y_{b/p} + g)^2} \left[1 + \frac{\partial g}{\partial c} 2y_{b/p} + \frac{\partial g}{\partial b} 2\hat{V}_N \right] \tilde{V}_N \quad (10.42c)$$

$$+ \left(\frac{2\Delta^2}{\Delta^2 + (y_{b/p} + g)^2} \frac{\partial g}{\partial c} - \frac{y_{b/p} + g}{\Delta^2 + (y_{b/p} + g)^2} \right) \frac{\partial \Delta}{\partial \mathbf{p}_{b/p}} \left[\tilde{V}_T, \tilde{V}_N \right]^T$$

$$\dot{\tilde{r}} = -k_1 \tilde{r} - k_2 C_r \tilde{\psi} - \frac{\partial r_d}{\partial y_{b/p}} \tilde{V}_N - \frac{\partial r_d}{\partial x_{b/p}} \tilde{V}_T + \frac{\partial r_d}{\partial \tilde{x}} \tilde{V}_x + \frac{\partial r_d}{\partial \tilde{y}} \tilde{V}_y$$

$$- \frac{\partial r_d}{\partial \tilde{\psi}} \left[\frac{\Delta}{\Delta^2 + (y_{b/p} + g)^2} \left[1 + \frac{\partial g}{\partial c} 2y_{b/p} + \frac{\partial g}{\partial b} 2\hat{V}_N \right] \tilde{V}_N \right. \\ \left. + \left(\frac{2\Delta^2}{\Delta^2 + (y_{b/p} + g)^2} \frac{\partial g}{\partial c} - \frac{y_{b/p} + g}{\Delta^2 + (y_{b/p} + g)^2} \right) \frac{\partial \Delta}{\partial \mathbf{p}_{b/p}} \left[\tilde{V}_T, \tilde{V}_N \right]^T \right] \quad (10.42d)$$

$$\dot{\tilde{u}} = -k_u \tilde{u} \quad (10.42e)$$

To show that the error variables in (10.42) converge to zero, we formulate the following total closed-loop system that also contains all variables that converge to

zero independently of the variables in (10.42)

$$\dot{\tilde{X}}_1 = \begin{bmatrix} \dot{y}_{b/p} \\ \dot{x}_{b/p} \\ \dot{\psi} \\ \dot{\tilde{r}} \end{bmatrix} = \begin{bmatrix} -u_{td} \frac{y_{b/p}}{\sqrt{\Delta^2 + (y_{b/p} + g)^2}} - x_{b/p} \kappa(\theta) \dot{\theta} + G_1(\cdot) \\ -k_\delta \frac{x_{b/p}}{\sqrt{1 + x_{b/p}^2}} + y_{b/p} \kappa(\theta) \dot{\theta} \\ C_r \tilde{r} \\ -k_1 \tilde{r} - k_2 C_r \tilde{\psi} \end{bmatrix} \quad (10.43a)$$

$$+ \begin{bmatrix} \tilde{V}_N \\ \tilde{V}_T \\ G_2(\Delta, y_{b/p}, x_{b/p}, g, \hat{V}_N, \hat{V}_T, \tilde{V}_N, \tilde{V}_T) \\ -\frac{\partial r_d}{\partial \psi} G_2(\cdot) - \frac{\partial r_d}{\partial y_{b/p}} \tilde{V}_N - \frac{\partial r_d}{\partial x_{b/p}} \tilde{V}_T + \frac{\partial r_d}{\partial \tilde{x}} \tilde{V}_x + \frac{\partial r_d}{\partial \tilde{y}} \tilde{V}_y \end{bmatrix}$$

$$\dot{\tilde{X}}_2 = \begin{bmatrix} \dot{\tilde{x}} \\ \dot{\tilde{y}} \\ \dot{\tilde{V}}_x \\ \dot{\tilde{V}}_y \\ \dot{\tilde{u}} \end{bmatrix} = \begin{bmatrix} -k_{x_1} \tilde{x} - \tilde{V}_x \\ -k_{y_1} \tilde{y} - \tilde{V}_y \\ -k_{x_2} \tilde{x} \\ -k_{y_2} \tilde{y} \\ -k_u \tilde{u} \end{bmatrix} \quad (10.43b)$$

$$\dot{v}_r = X(u_{rd} + \tilde{u})r_d(h, y_{b/p}, x_{b/p}, \tilde{\psi}, \tilde{x}, \tilde{y}) + X(u_{rd} + \tilde{u})\tilde{r} + Y(u_{rd} + \tilde{u})v_r \quad (10.43c)$$

where

$$G_2(\cdot) = \frac{\Delta}{\Delta^2 + (y_{b/p} + g)^2} \left[1 + \frac{\partial g}{\partial c} 2y_{b/p} + \frac{\partial g}{\partial b} 2\hat{V}_N \right] \tilde{V}_N$$

$$+ \left(\frac{2\Delta^2}{\Delta^2 + (y_{b/p} + g)^2} \frac{\partial g}{\partial c} - \frac{y_{b/p} + g}{\Delta^2 + (y_{b/p} + g)^2} \right) \frac{\partial \Delta}{\partial \mathbf{p}_{b/p}} [\tilde{V}_T, \tilde{V}_N]^T \quad (10.44)$$

Note that $G_2(\Delta, y_{b/p}, x_{b/p}, g, \hat{V}_N, \hat{V}_T, \tilde{V}_N, \tilde{V}_T)$ satisfies

$$G_2(\Delta, y_{b/p}, x_{b/p}, g, \hat{V}_N, \hat{V}_T, 0, 0) = 0 \quad (10.45)$$

$$\|G_2(\Delta, y_{b/p}, x_{b/p}, g, \hat{V}_N, \hat{V}_T, \tilde{V}_N, \tilde{V}_T)\| \leq \zeta_2(\Delta) \|\tilde{V}_T, \tilde{V}_N\|, \quad (10.46)$$

where $\zeta_2(\Delta) > 0$, which shows that $G_2(\cdot)$ is zero when the perturbing variables, i.e. \tilde{V}_T and \tilde{V}_N , are zero and that it has at most linear growth in the perturbing variables. Note that by an appropriate choice of Δ we will assure that $\zeta_2(\Delta) > 0$ is a constant independent of $x_{b/p}$ and $y_{b/p}$.

The first step in the stability analysis of (10.43) is to assure that the closed-loop system is forward complete and that the sway velocity v_r remains bounded. Therefore, under the assumption that Condition 10.1 is satisfied, i.e. $C_r > 0$, we take the following three steps:

1. First, we prove that the trajectories of the closed-loop system are forward complete.
2. Then, we derive a necessary condition such that v_r is locally bounded with respect to $(\tilde{X}_1, \tilde{X}_2)$.
3. Finally, we establish that for a sufficiently big value of Δ , v_r is locally bounded only with respect to \tilde{X}_2 , i.e. independently of \tilde{X}_1 .

Furthermore we design the time-varying look-ahead distance as

$$\Delta(x_{b/p}, y_{b/p}) = \sqrt{\mu + x_{b/p}^2 + y_{b/p}^2}, \quad (10.47)$$

where $\mu > 0$ is a constant. The choice of (10.47) depending on $x_{b/p}$ and $y_{b/p}$ is necessary to find a bounded value of μ to assure local boundedness of v_r with respect to \tilde{X}_2 independently of \tilde{X}_1 .

The above three steps are taken by formulating and proving three lemmas. For the sake of brevity in the main body of this chapter, the proofs of the following lemmas are replaced by a sketch of each proof in the main body. The full proofs can be found in the Appendices 10.A-10.C.

Remark 10.5. *In the proof of Lemma 10.2 it is shown that by choosing (10.47) the skew symmetric terms $-x_{b/p}\kappa(\theta)\dot{\theta}$ and $y_{b/p}\kappa(\theta)\dot{\theta}$ do not affect the boundedness of the sway velocity. The choice of Δ proposed in Moe et al. [103], i.e. $\Delta(x_{b/p}) = \sqrt{\mu + x_{b/p}^2}$ is impossible since the terms that cancel due to skew-symmetry in the case presented here will not vanish. The terms that remain have no upper bound independent of $y_{b/p}$ and g , and therefore a lower bound on μ necessary for boundedness of v_r independent on $x_{b/p}$ and $y_{b/p}$ cannot be found.*

Lemma 10.1 (Forward completeness). *The trajectories of the closed-loop system (10.43) are forward complete.*

The proof of this lemma is given in Appendix 10.A. The general idea is as follows. Forward completeness for (10.43b) is evident since this part of the closed-loop system consists of GES error dynamics. Using the forward completeness and in fact boundedness of (10.43b) we can show forward completeness of (10.43c), $\dot{\psi}$, and \dot{r} . Hence, forward completeness of (10.43) depends on forward completeness of $\dot{x}_{b/p}$ and $\dot{y}_{b/p}$. To show forward completeness of $\dot{x}_{b/p}$ and $\dot{y}_{b/p}$, we consider the $x_{b/p}$ and $y_{b/p}$ dynamics with \tilde{X}_2 , $\tilde{\psi}$, \tilde{r} , and v_r as input which allows us to claim forward completeness of $\dot{x}_{b/p}$ and $\dot{y}_{b/p}$ according to Theorem A.3. Consequently, all the states of the closed-loop system are forward complete and hence the closed-loop system (10.43) is forward complete

Lemma 10.2 (Boundedness near $(\tilde{X}_1, \tilde{X}_2) = 0$). *The system (10.43c) is bounded near $(\tilde{X}_1, \tilde{X}_2) = 0$ if and only if the curvature of P satisfies the following condition:*

$$\kappa_{\max} \triangleq \max_{\theta \in P} |\kappa(\theta)| < \frac{Y_{\min}}{2X_{\max}}. \quad (10.48)$$

The proof of this lemma is given in Appendix 10.B. A sketch of the proof is as follows. The sway velocity dynamics (10.43c) are analyzed using a quadratic Lyapunov function $V = 1/2v_r^2$. It can be shown that the derivative of this Lyapunov function satisfies the conditions for boundedness when the solutions are on or close to the manifold where $(\tilde{X}_1, \tilde{X}_2) = 0$. Consequently, (10.43c) satisfies the conditions of boundedness near $(\tilde{X}_1, \tilde{X}_2) = 0$ as long as (10.48) is satisfied.

In Lemma 10.2 we show boundedness of v_r for small values of $(\tilde{X}_1, \tilde{X}_2)$ to derive the bound on the curvature. However, locality with respect to \tilde{X}_1 , i.e. the path-following errors and yaw angle and yaw rate errors, is not desirable and in the next

lemma boundedness independent of \tilde{X}_1 is shown under an extra condition on the constant μ from the definition (10.47) of the look-ahead distance Δ .

Lemma 10.3 (Boundedness near $\tilde{X}_2 = 0$). *The system (10.43c) is bounded near $\tilde{X}_2 = 0$, independent of \tilde{X}_1 , if we choose*

$$\mu > \frac{8X_{\max}}{Y_{\min} - 2X_{\max}\kappa_{\max}}. \quad (10.49)$$

The proof of this lemma is given in Appendix 10.C. The general idea is given as follows. The proof follows along the same lines of that of Lemma 10.2 but solutions are considered close to the manifold $\tilde{X}_2 = 0$ rather than $(\tilde{X}_1, \tilde{X}_2) = 0$. It is shown that boundedness can still be shown if (10.49) is satisfied additionally to the conditions of Lemma 10.2.

Theorem 10.1. *Consider a θ -parametrized path denoted by $P(\theta) \triangleq (x_p(\theta), y_p(\theta))$. Then under Condition 10.1 and the conditions of Lemma 10.1-10.3, the system (10.1) with control laws (10.8) and (10.40) and observer (10.10) follows the path P , while maintaining v_r , τ_r and τ_u bounded. In particular, the origin of the system (10.43a)-(10.43b) is GAS and LES.*

Proof. From the fact that the origin of (10.43b) is GES, the fact that the closed-loop system (10.43) is forward complete according to Lemma 10.1, and the fact that solutions of (10.43c) are locally bounded near $\tilde{X}_2 = 0$ according to Lemma 10.3, we can conclude that there is a finite time $T > t$ after which solutions of (10.43b) will be sufficiently close to $\tilde{X}_2 = 0$ to guarantee boundedness of v_r .

Having established that v_r is bounded we first analyse the cascade

$$\begin{bmatrix} \dot{\tilde{\psi}} \\ \dot{\tilde{r}} \end{bmatrix} = \begin{bmatrix} C_r \tilde{r} \\ -k_1 \tilde{r} - k_2 C_r \tilde{\psi} \end{bmatrix} + \begin{bmatrix} G_2(\cdot) \\ -\frac{\partial r_d}{\partial \psi} G_2(\cdot) - \frac{\partial r_d}{\partial \mathbf{p}_{v/p}} [\tilde{V}_T, \tilde{V}_N]^T + \frac{\partial r_d}{\partial [\tilde{x}, \tilde{y}]^T} \tilde{V}_c \end{bmatrix} \quad (10.50a)$$

$$\begin{bmatrix} \dot{\tilde{x}} \\ \dot{\tilde{y}} \\ \dot{\tilde{V}}_x \\ \dot{\tilde{V}}_y \\ \dot{\tilde{u}} \end{bmatrix} = \begin{bmatrix} -k_{x_1} \tilde{x} - \tilde{V}_x \\ -k_{y_1} \tilde{y} - \tilde{V}_y \\ -k_{x_2} \tilde{x} \\ -k_{y_2} \tilde{y} \\ -k_u \tilde{u} \end{bmatrix} \quad (10.50b)$$

The perturbing system (10.50b) is GES as shown in Section 10.3. The interconnection term, i.e. the second matrix in (10.50a), satisfies the linear growth criteria from Theorem A.1. More specifically, it does not grow with the $\tilde{\psi}$ and \tilde{r} since all the partial derivatives of r_d and $G_2(\cdot)$ can respectively be bounded by constants and linear functions of \tilde{V}_x and \tilde{V}_y . The nominal dynamics, i.e. the first matrix in (10.50a), can be analyzed with the following quadratic Lyapunov function

$$V_{(\tilde{r}, \tilde{\psi})} = \frac{1}{2} \tilde{r}^2 + \frac{1}{2} k_2 \tilde{\psi}^2 \quad (10.51)$$

whose derivative along the solutions of the nominal system is given by

$$\dot{V}_{(\tilde{r}, \tilde{\psi})} = -k_1 \tilde{r}^2 - k_2 C_r \tilde{\psi} \tilde{r} + k_2 C_r \tilde{r} \tilde{\psi} = -k_2 \tilde{r}^2 \leq 0 \quad (10.52)$$

which implies that \tilde{r} and $\tilde{\psi}$ are bounded. The derivative of (10.52) is given by

$$\dot{V}_{(\tilde{r}, \tilde{\psi})} = -2k_1^2 \tilde{r}^2 - 2k_1 k_2 C_r \tilde{\psi} \tilde{r} \quad (10.53)$$

which is bounded since \tilde{r} and $\tilde{\psi}$ are bounded. This implies that (10.52) is a uniformly continuous function. Consequently, by applying Barbalat's lemma (see Lemma A.5) we have that

$$\lim_{t \rightarrow \infty} \dot{V}_{(\tilde{r}, \tilde{\psi})} = \lim_{t \rightarrow \infty} -k_1 \tilde{r}^2 = 0 \Rightarrow \lim_{t \rightarrow \infty} \tilde{r} = 0. \quad (10.54)$$

Since C_r is persistently exciting, which follows from the fact that C_r is upper bounded and lower bounded by a constant larger than zero, it follows from the expression of the nominal dynamics that

$$\lim_{t \rightarrow \infty} \tilde{r} = 0 \Rightarrow \lim_{t \rightarrow \infty} \tilde{\psi} = 0. \quad (10.55)$$

This implies that the system is globally asymptotically stable according to Definition A.3 and since the nominal dynamics are linear it follows that the nominal dynamics are globally exponentially stable. Consequently, from the above it follows that the cascade (10.50) is GES using Theorem A.1 and Proposition A.1.

We now consider the following dynamics

$$\begin{bmatrix} \dot{y}_{b/p} \\ \dot{x}_{b/p} \end{bmatrix} = \begin{bmatrix} -u_{td} \frac{y_{b/p}}{\sqrt{\Delta^2 + (y_{b/p} + g)^2}} - x_{b/p} \kappa(\theta) \dot{\theta} \\ -k_\delta \frac{x_{b/p}}{\sqrt{1 + x_{b/p}^2}} + y_{b/p} \kappa(\theta) \dot{\theta} \end{bmatrix} + \begin{bmatrix} \tilde{V}_N + G_1(\cdot) \\ \tilde{V}_T \end{bmatrix}. \quad (10.56)$$

Note that we can view the systems (10.50) and (10.56) as a cascaded system where the nominal dynamics are formed by the first matrix of (10.56), the interconnection term is given by second matrix of (10.56), and the perturbing dynamics are given by (10.50). As we have just shown the perturbing dynamics are GES. Using (10.23) it is straightforward to verify that the interconnection term satisfies the conditions of Theorem A.1. We now consider the following Lyapunov function for the nominal system

$$V_{(x_{b/p}, y_{b/p})} = \frac{1}{2} x_{b/p}^2 + \frac{1}{2} y_{b/p}^2. \quad (10.57)$$

whose derivative along the solutions of the nominal system is given by

$$\dot{V}_{(x_{b/p}, y_{b/p})} = -u_{td} \frac{y_{b/p}^2}{\sqrt{\Delta^2 + (y_{b/p} + g)^2}} - k_\delta \frac{x_{b/p}^2}{\sqrt{1 + x_{b/p}^2}} \leq 0, \quad (10.58)$$

which implies that the nominal system is GAS. Moreover, since it is straightforward to verify that $\dot{V}_{(x_{b/p}, y_{b/p})} \leq \alpha V_{(x_{b/p}, y_{b/p})}$ for some constant α dependent on initial conditions, it follows from the comparison lemma (Lemma A.4) that the nominal dynamics are also LES. Consequently, the cascaded system satisfies the conditions of Theorem A.1 and Lemma A.3, and therefore the cascaded system is GAS and LES. This implies that the origin of the error dynamics, i.e. $(\tilde{X}_1, \tilde{X}_2) = (0, 0)$, is globally asymptotically stable and locally exponentially stable. \square

10.5 Case Study

This section presents a case study for the theoretical results presented in this chapter. We will apply the path-following approach to the case of following a circular path. The ocean current components are given by $V_x = -1$ m/s and $V_y = 1.2$ m/s and consequently $V_{\max} \approx 1.562$ m/s. The desired relative surge velocity is chosen to be constant and set to $u_{rd} = 5$ m/s such that Assumption 10.2 is verified. We recall here the expression for $X(u_r)$, $Y(u_r)$ given by Equations (2.12b-2.12c):

$$X(u_r) \triangleq -X_1 u_r + X_2, \quad (10.59a)$$

$$Y(u_r) \triangleq -Y_1 u_r - Y_2, \quad (10.59b)$$

The simulation uses the ship model parameters from Fredriksen and Pettersen [57] and reported in Section B.1. Using these parameters and expressions (10.59a) and (10.59b) it is straightforward to verify that the curvature bound from Lemma 10.2 is given by $\kappa_{\max} < (Y_{\min})/(2X_{\max}) \approx 0.0667$. The observer is initialised as suggested in Subsection 10.3.2 and the observer gains are selected as $k_{x_1} = k_{y_1} = 1$ and $k_{x_2} = k_{y_2} = 0.1$. The controller gains are selected as $k_{u_r} = 0.1$ for the surge velocity controller and $k_1 = 1000$ and $k_2 = 400$ for the yaw rate controller.

In this case study the vessel is required to follow a circle with a radius of 400 m. Consequently, the curvature of the path is given by $\kappa_p = 1/400 = 0.0025$. This implies we satisfy our constraint on the curvature $\kappa_p < (Y_{\min})/(2X_{\max}) \approx 0.0667$. The required value for μ can be calculated as suggested in Lemma 10.3 to obtain $\mu > 62.3468$ m, which can be satisfied by taking $\mu = 70$ m. The initial conditions are taken as

$$[u_r(t_0), v_r(t_0), r(t_0), x(t_0), y(t_0), \psi(t_0)]^T = [0, 0, 0, 700, 10, \pi/2]^T. \quad (10.60)$$

The resulting trajectory of the ship can be seen in Figure 10.3. The dashed blue line is the trajectory of the vessel and the red circle is the reference. The yellow ships represent the orientation of the ship at certain times. From Figure 10.3 it can clearly be seen that the orientation of the ship is not tangent to the circle, which is indeed what is needed to compensate for the ocean current.

The path-following errors in tangential direction, $x_{b/p}$, and in normal direction, $y_{b/p}$ can be seen in the top plot of Figure 10.4 from which it can clearly be seen that the path-following error converge to zero after a transient period. A detail of the last portion of the simulation is given to illustrate the errors converge to zero. The estimates for the ocean current components obtained from the ocean current observer are given in the second plot from the top in Figure 10.4. From this plot it can clearly be seen that the estimates converge to the desired values without overshoot, which illustrates the conservativeness of the bound $2V_{\max} < u_{rd}(t)$, $\forall t$, derived in the analysis of the observer-error dynamics in Subsection 10.3.2. The yaw rate r and sway velocity v_r are plotted together in the third plot of Figure 10.4. These plots show that due to the curvature of the path the yaw rate and sway velocity do not converge to zero but follow a periodic motion induced by the motion along the circle. The periodic signals are not symmetric due to the ocean current affecting the ship's motion, i.e. on part of the circle the ship moves against the current and on part of the circle it moves with the current. The relative surge

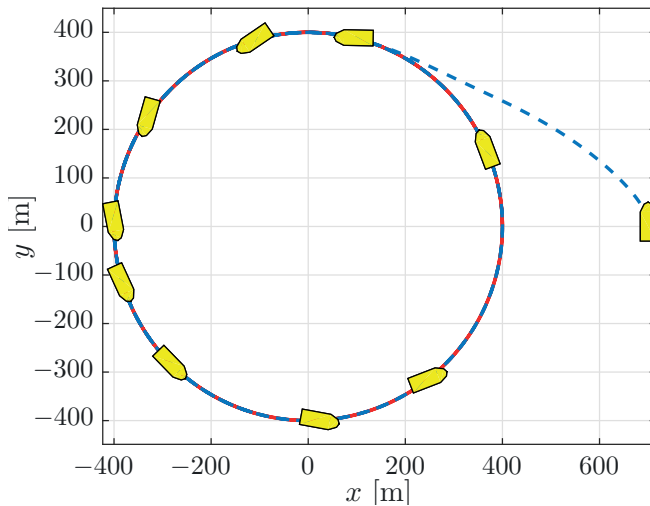


Figure 10.3: Path of the vessel in the $x - y$ -plane. The dashed blue line is the trajectory of the path and the red line is the reference. The yellow ships denote the orientation of the vessel at certain times.

velocity is plotted in the fourth plot from the top of Figure 10.4. This plot clearly shows the exponential convergence of the velocity as it moves to the desired value of $u_{rd} = 5$ m/s. Especially interesting is the coupling of the relative surge velocity with the value of C_r from Condition 10.1, which is plotted in the bottom plot of Figure 10.4. From this plot it can clearly be seen that C_r is bounded away from zero throughout the motion.

10.6 Conclusion

In this chapter the path following control problem of generic paths has been considered for ASVs and AUVs moving in the horizontal plane. An unknown ocean current has been considered to affect the system. The path has been considered to be parametrized by a parameter s . Then a Serret-Frenet frame has been considered to propagate along the path according to a specified update law for s . In order to solve the path following control problem, a LOS-like guidance control strategy has been proposed together with a certain update law for s and an observer for the ocean current. The guidance law has been characterized by a time-varying look-ahead distance which is dependent on the distance from the path. The parametrization s has been chosen to allow the fulfillment of the control objectives for all the initial conditions. The observer was necessary in order to estimate and compensate for the ocean current.

The closed-loop system has been thoroughly analyzed. Boundedness of the zero dynamics under certain conditions has been proven. Finally, if these conditions are

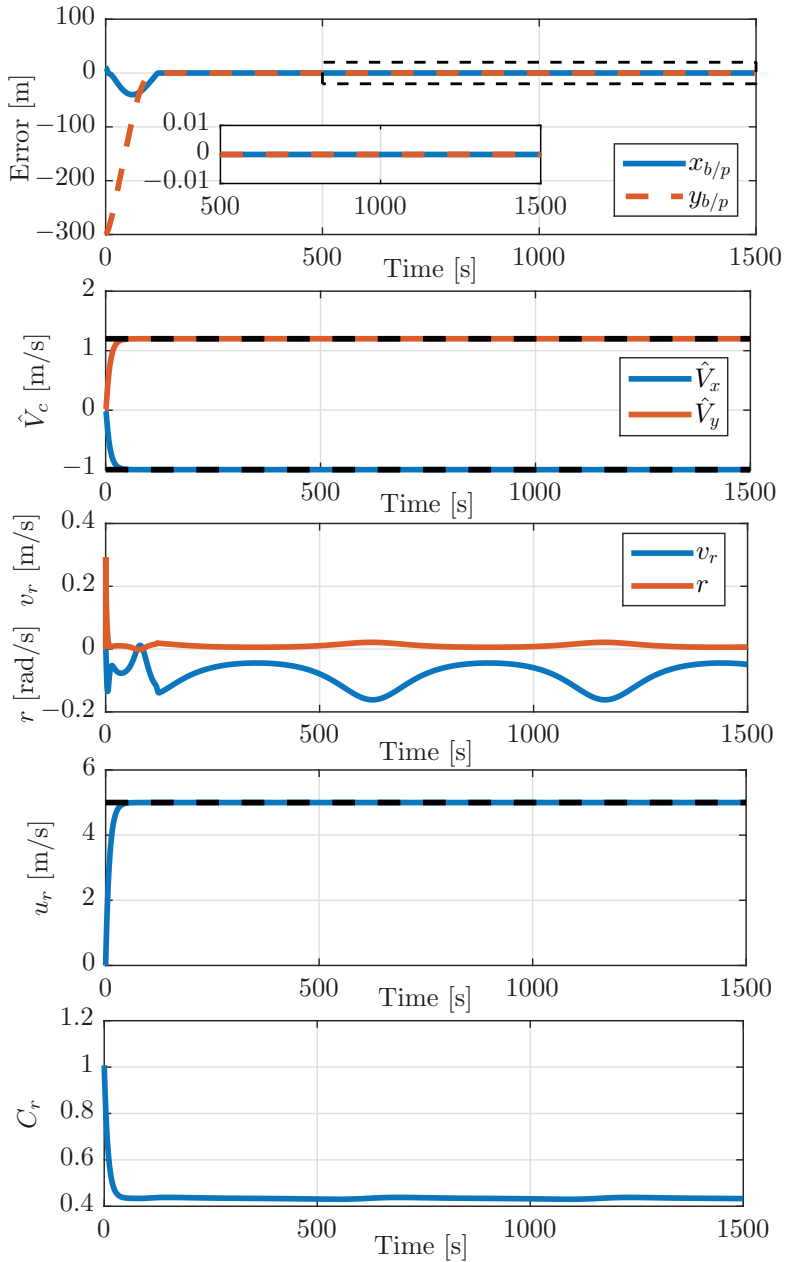


Figure 10.4: Path following errors plotted against time (top), current estimates against time (second), sway velocity and yaw rate against time (third), surge velocity against time (fourth), and size of C_r over time (bottom).

verified, the path following control errors are proved to be globally asymptotically stable.

10.A Proof of Lemma 10.1

Consider the following part of the global closed-loop system:

$$\begin{aligned} \begin{bmatrix} \dot{\tilde{\psi}} \\ \dot{\tilde{r}} \end{bmatrix} &= \begin{bmatrix} C_r \tilde{r} \\ -k_1 \tilde{r} - k_2 C_r \tilde{\psi} \end{bmatrix} \\ &+ \underbrace{\begin{bmatrix} G_2(\Delta, y_{b/p}, x_{b/p}, g, \hat{V}_N, \hat{V}_T, \tilde{V}_N, \tilde{V}_T) \\ -\frac{\partial r_d}{\partial \tilde{\psi}} G_2(\cdot) - \frac{\partial r_d}{\partial y_{b/p}} \tilde{V}_N - \frac{\partial r_d}{\partial x_{b/p}} \tilde{V}_T + \frac{\partial r_d}{\partial \tilde{x}} \tilde{V}_x + \frac{\partial r_d}{\partial \tilde{y}} \tilde{V}_y \end{bmatrix}}_{R(h, y_{b/p}, \delta_x, \tilde{\psi}, \tilde{x}, \tilde{y})} \end{aligned} \quad (10.61a)$$

$$\dot{v}_r = X(u_{rd} + \tilde{u})r_d(h, y_{b/p}, \delta_x, \tilde{\psi}, \tilde{x}, \tilde{y}) + X(u_{rd} + \tilde{u})\tilde{r} + Y(u_{rd} + \tilde{u})v_r \quad (10.61b)$$

where

$$\begin{aligned} G_2(\cdot) &= \frac{\Delta}{\Delta^2 + (y_{b/p} + g)^2} \left[1 + \frac{\partial g}{\partial c} 2y_{b/p} + \frac{\partial g}{\partial b} 2\hat{V}_N \right] \tilde{V}_N \\ &+ \left(\frac{2\Delta^2}{\Delta^2 + (y_{b/p} + g)^2} \frac{\partial g}{\partial c} - \frac{y_{b/p} + g}{\Delta^2 + (y_{b/p} + g)^2} \right) \frac{\partial \Delta}{\partial \mathbf{p}_{b/p}} \left[\tilde{V}_T, \tilde{V}_N \right]^T \end{aligned} \quad (10.62)$$

From the boundedness of the vector $[\tilde{X}_2^T, \kappa(\theta), u_{rd}, \dot{u}_{rd}, V_T, V_N]^T$ we know that $\|[\tilde{X}_2^T, \kappa(\theta), u_{rd}, \dot{u}_{rd}, V_T, V_N]^T\| \leq \beta_0$, and from (10.35) we can conclude the existence of positive functions $a_{r_d}(\cdot)$, $b_{r_d}(\cdot)$, $a_R(\cdot)$, and $b_R(\cdot)$ which are all continuous in their arguments and are such that such the following inequalities hold:

$$|r_d(\cdot)| \leq a_{r_d}(\mu, \beta_0) |v_r| + b_{r_d}(\mu, \beta_0) \quad (10.63)$$

and,

$$\|R(\cdot)\| \leq a_R(\mu, \beta_0) |v_r| + b_R(\mu, \beta_0) \quad (10.64)$$

Then we choose the following Lyapunov function candidate:

$$V_1(\tilde{\psi}, \tilde{r}, v_r) = \frac{1}{2} \left(k_2 \tilde{\psi}^2 + \tilde{r}^2 + v_r^2 \right) \quad (10.65)$$

whose time derivative along the solutions of (10.61) is

$$\begin{aligned} \dot{V}_1(\cdot) &= k_2 C_r \tilde{r} \tilde{\psi} - k_1 \tilde{r}^2 - k_2 C_r \tilde{r} \tilde{\psi} + [\tilde{\psi} \quad \tilde{r}] R(\cdot) \\ &+ Y(u_{rd} + \tilde{u})v_r^2 + X(u_{rd} + \tilde{u})\tilde{r}v_r + X(u_{rd} + \tilde{u})r_d(\cdot)v_r \end{aligned} \quad (10.66)$$

Using Young's inequality we note that

$$\begin{aligned} \dot{V}_1(\cdot) &\leq k_1 \tilde{r}^2 + \tilde{\psi}^2 + \tilde{r}^2 + R^2(\cdot) + Y(u_{rd} + \tilde{u})v_r^2 \\ &+ |X(u_{rd} + \beta_0)| (\tilde{r}^2 + v_r^2) + |X(u_{rd} + \beta_0)| (r_d^2(\cdot) + v_r^2) \\ &\leq \alpha V_1 + \beta, \quad \alpha \geq 0, \quad \beta \geq 0 \end{aligned} \quad (10.67)$$

Note that since the differential inequality (10.67) is scalar we can invoke the comparison lemma Khalil [77, Lemma 3.4] given as Lemma A.4 in Appendix A.1. From Lemma A.4 we know that the solutions of differential inequality (10.67) are bounded by the solutions of the linear system:

$$\dot{x} = \alpha x + \beta \quad (10.68)$$

which has solutions

$$x(t) = \frac{\|x(t_0)\|\alpha + \beta}{\alpha} e^{\alpha(t-t_0)} - \frac{\beta}{\alpha} \quad (10.69)$$

Hence, from Lemma A.4 we have that

$$V_1(\cdot) \leq \frac{\|V_1(t_0)\|\alpha + \beta}{\alpha} e^{\alpha(t-t_0)} - \frac{\beta}{\alpha} \quad (10.70)$$

which shows the solutions of $V_1(\cdot)$ are defined up to $t_{\max} = \infty$ and consequently from (10.65) it follows that the solutions of $\tilde{\psi}$, \tilde{r} , and v_r must be defined up to $t_{\max} = \infty$. Hence, the solutions of (10.61) satisfy Definition A.5 and we can conclude forward completeness of trajectories of (10.61).

The forward completeness of trajectories of the global closed-loop system now depends on forward completeness of $\dot{y}_{b/p}$ and $\dot{x}_{b/p}$ from (10.43a). We can conclude forward completeness of $\dot{y}_{b/p}$ and $\dot{x}_{b/p}$ by considering the Lyapunov function

$$V_2 = \frac{1}{2}x_{b/p}^2 + \frac{1}{2}y_{b/p}^2. \quad (10.71)$$

The time derivative of (10.71) is given by

$$\begin{aligned} \dot{V}_2 &= x_{b/p}\dot{x}_{b/p} + y_{b/p}\dot{y}_{b/p} \\ &\leq -u_{td} \frac{y_{b/p}^2}{\sqrt{\Delta^2 + (y_{b/p} + g)^2}} - \frac{k_\delta x_{b/p}^2}{\sqrt{1 + x_{b/p}^2}} + (G_1(\cdot) + \tilde{V}_N)y_{b/p} + \tilde{V}_T x_{b/p} \quad (10.72) \\ &\leq (G_1 + \tilde{V}_N)y_{b/p} + \tilde{V}_T x_{b/p} \end{aligned}$$

where using the bound on $G_1(\cdot)$ from (10.23) and Young's inequality we obtain

$$\dot{V}_2 \leq V_2 + \frac{1}{2} \left(\zeta^2(u_{td}) \|\tilde{\psi}, \tilde{r}\|^2 + \tilde{V}_N^2 + \tilde{V}_T^2 \right) \quad (10.73)$$

$$\leq V_2 + \sigma_2(v_r, \tilde{\psi}, \tilde{r}, \tilde{V}_N, \tilde{V}_T) \quad (10.74)$$

with $\sigma_2(\cdot) \in \mathcal{K}_\infty$. Consequently, if we view the arguments of $\sigma_2(\cdot)$ as input to the $x_{b/p}$ and $y_{b/p}$ dynamics, then (10.73) satisfies Theorem A.3 and hence $\dot{x}_{b/p}$ and $\dot{y}_{b/p}$ are forward complete. Note that the arguments of $\sigma_2(\cdot)$ are all forward complete and therefore fit the definition of an input signal given in Definition A.5. We have now shown forward completeness of (10.43a) and (10.43c) and since (10.43b) is GES is trivially forward complete. We can therefore claim forward completeness of the entire closed-loop system (10.43) and the proof of Lemma 10.1 is complete.

10.B Proof of Lemma 10.2

Recall the sway velocity dynamics (10.43c):

$$\dot{v}_r = X(\tilde{u} + u_{rd})(r_d + \tilde{r}) + Y(u_{rd} + \tilde{u})v_r, \quad Y(u_{rd}) < 0$$

Consider the following Lyapunov function candidate:

$$V_3(v_r) = \frac{1}{2}v_r^2 \quad (10.75)$$

The derivative of (10.75) along the solutions of (10.43c) is given by

$$\begin{aligned} \dot{V}_3 &= v_r \dot{v}_r = v_r X(u_{rd} + \tilde{u})r_d + X(u_{rd} + \tilde{u})v_r \tilde{r} + Y(u_{rd} + \tilde{u})v_r^2 \\ &\leq X(u_{rd})r_d v_r + a_x \tilde{u} r_d v_r + X(u_{rd})v_r \tilde{r} + a_x \tilde{u} v_r \tilde{r} + a_y \tilde{u} v_r^2 + Y(u_{rd})v_r^2 \end{aligned} \quad (10.76)$$

where we used the fact that:

$$Y(u_r) = a_y u_r + b_y \quad (10.77)$$

$$X(u_r) = a_x u_r + b_x \quad (10.78)$$

The term $r_d v_r$ is given by

$$\begin{aligned} r_d v_r &= -\frac{v_r}{C_r} \left[\kappa(\theta) \left(u_t \cos(\psi + \beta - \gamma_p(\theta)) + k_\delta \frac{x_{b/p}}{\sqrt{1 + x_{b/p}^2}} + \hat{V}_T \right) \right. \\ &\quad + \frac{Y(u_r)v_r u_{rd} - \dot{u}_{rd}v_r}{u_{rd}^2 + v_r^2} + \frac{\Delta}{\Delta^2 + (y_{b/p} + g)^2} \left[\dot{\hat{V}}_N \frac{b + \sqrt{b^2 - ac}}{-a} \right. \\ &\quad + \frac{\partial g}{\partial b} \left(2\dot{\hat{V}}_N y_{b/p} \right) + \frac{\partial g}{\partial a} \left(2\hat{V}_N \dot{\hat{V}}_N - 2u_{rd}\dot{u}_{rd} - 2v_r Y(u_r)v_r \right) \\ &\quad + \left[1 + \frac{\partial g}{\partial c} 2y_{b/p} + \frac{\partial g}{\partial b} 2\hat{V}_N \right] \left(\frac{-u_{td}y_{b/p}}{\sqrt{\Delta^2 + (y_{b/p} + g)^2}} + G_1(\cdot) - x_{b/p}\kappa(\theta)\dot{\theta} \right) \\ &\quad + \frac{\partial g}{\partial c} 2\Delta \left[\frac{\partial \Delta}{\partial x_{b/p}} \left(-k_\delta \frac{x_{b/p}}{\sqrt{1 + x_{b/p}^2}} + y_{b/p}\kappa(\theta)\dot{\theta} \right) \right. \\ &\quad + \left. \left. \frac{\partial \Delta}{\partial y_{b/p}} \left(-u_{td} \frac{y_{b/p}}{\sqrt{\Delta^2 + (y_{b/p} + g)^2}} + G_1(\cdot) - x_{b/p}\kappa(\theta)\dot{\theta} \right) \right] \right] \\ &\quad - \frac{y_{b/p} + g}{\Delta^2 + (y_{b/p} + g)^2} \left[\frac{\partial \Delta}{\partial x_{b/p}} \left(-k_\delta \frac{x_{b/p}}{\sqrt{1 + x_{b/p}^2}} + y_{b/p}\kappa(\theta)\dot{\theta} \right) \right. \\ &\quad + \left. \left. \frac{\partial \Delta}{\partial y_{b/p}} \left(-u_{td} \frac{y_{b/p}}{\sqrt{\Delta^2 + (y_{b/p} + g)^2}} + G_1(\cdot) - x_{b/p}\kappa(\theta)\dot{\theta} \right) \right] \right] \end{aligned} \quad (10.79)$$

We now introduce a term $F(\tilde{X}_1, \tilde{X}_2, \Delta, V_T, V_T, u_{rd}, v_r)$ to collect all the terms that grow linearly with v_r and the terms that grow quadratically with v_r but vanish when \tilde{X}_1 and \tilde{X}_2 are zero. Consequently we rewrite (10.79) to obtain

$$\begin{aligned} r_d v_r = & -\frac{v_r}{C_r} \left[1 + \frac{\Delta x_{b/p}}{\Delta^2 + (y_{b/p} + g)^2} \right] \kappa(\theta) (u_t \cos(\psi + \beta - \gamma_p(\theta))) \\ & - \frac{1}{C_r} \left(\frac{u_{rd}}{u_{rd}^2 + v_r^2} - \frac{2\Delta v_r}{\Delta^2 + (y_{b/p} + g)^2} \frac{\partial g}{\partial a} \right) Y(u_r) v_r^2 \\ & + F(\tilde{X}_1, \tilde{X}_2, \Delta, V_T, V_T, u_{rd}, v_r) \end{aligned} \quad (10.80)$$

where

$$\begin{aligned} F(\cdot) = & -\frac{v_r}{C_r} \left[\kappa(\theta) \left(k_\delta \frac{x_{b/p}}{\sqrt{1 + x_{b/p}^2}} + \hat{V}_T \right) - \frac{\dot{u}_{rd} v_r}{u_{rd}^2 + v_r^2} \right. \\ & + \frac{\Delta}{\Delta^2 + (y_{b/p} + g)^2} \left[\dot{\hat{V}}_N \frac{b + \sqrt{b^2 - ac}}{-a} + \frac{\partial g}{\partial b} (2\dot{\hat{V}}_N y_{b/p}) \right. \\ & + 2 \frac{\partial g}{\partial a} (\hat{V}_N \dot{\hat{V}}_N - u_{rd} \dot{u}_{rd}) - x_{b/p} \kappa(\theta) \left(\frac{k_\delta x_{b/p}}{\sqrt{1 + x_{b/p}^2}} + \hat{V}_T \right) \\ & + \left. \left[\frac{\partial g}{\partial c} 2y_{b/p} + \frac{\partial g}{\partial b} (2\hat{V}_N) \right] \left(\frac{-u_{td} y_{b/p}}{\sqrt{\Delta^2 + (y_{b/p} + g)^2}} + G_1(\cdot) - x_{b/p} \kappa(\theta) \dot{\theta} \right) \right. \\ & - \left. \frac{\partial g}{\partial c} 2\Delta \left[\frac{\partial \Delta}{\partial x_{b/p}} \frac{k_\delta x_{b/p}}{\sqrt{1 + x_{b/p}^2}} + \frac{\partial \Delta}{\partial y_{b/p}} \left(\frac{u_{td} y_{b/p}}{\sqrt{\Delta^2 + (y_{b/p} + g)^2}} + G_1(\cdot) \right) \right] \right] \\ & + \frac{y_{b/p} + g}{\Delta^2 + (y_{b/p} + g)^2} \left[\frac{\partial \Delta}{\partial x_{b/p}} \frac{k_\delta x_{b/p}}{\sqrt{1 + x_{b/p}^2}} \right. \\ & \quad \left. + \frac{\partial \Delta}{\partial y_{b/p}} \left(\frac{u_{td} y_{b/p}}{\sqrt{\Delta^2 + (y_{b/p} + g)^2}} + G_1(\cdot) \right) \right] \end{aligned} \quad (10.81)$$

Note here that using our definition of Δ in (10.47) all the terms in $r_d v_r$ with partial derivatives of Δ multiplied by $\dot{\theta}$ are cancelled due to skew-symmetry. It is straightforward to verify that the function $F(\cdot)$ satisfies the following inequality:

$$|F(\cdot)| \leq F_2(\tilde{X}_1, \tilde{X}_2, \Delta, V_T, V_N, u_{rd}) v_r^2 + F_1(\tilde{X}_1, \tilde{X}_2, \Delta, V_T, V_N, u_{rd}) |v_r| \quad (10.82)$$

where $F_{1,2}(\cdot)$ are positive functions continuous in their arguments with:

$$F_2(0, 0, \Delta, V_T, V_N, u_{rd}) = 0. \quad (10.83)$$

Consequently, using (10.80) the term $r_d v_r$ can be bounded as a function of v_r as follows

$$\begin{aligned}
 r_d v_r &\leq \sqrt{u_r^2 + v_r^2} \left| \frac{v_r}{C_r} \right| |\kappa(\theta)| \left| \left[-1 + \frac{\Delta x_{b/p}}{\Delta^2 + (y_{b/p} + g)^2} \right] \right| + |F(\cdot)| \\
 &\quad - \frac{1}{C_r} \left(\frac{u_{rd}}{u_{rd}^2 + v_r^2} - \frac{2\Delta v_r}{\Delta^2 + (y_{b/p} + g)^2} \frac{\partial g}{\partial a} \right) Y(u_r) v_r^2 \\
 &\leq \left| \frac{v_r^2}{C_r} \right| |\kappa(\theta)| \left| \left[-1 + \frac{\Delta x_{b/p}}{\Delta^2 + (y_{b/p} + g)^2} \right] \right| + |F(\cdot)| \\
 &\quad + \left| \frac{v_r}{C_r} \right| |\kappa(\theta)| |u_r| \left| \left[-1 + \frac{\Delta x_{b/p}}{\Delta^2 + (y_{b/p} + g)^2} \right] \right| \\
 &\quad - \frac{1}{C_r} \left(\frac{u_{rd}}{u_{rd}^2 + v_r^2} - \frac{2\Delta v_r}{\Delta^2 + (y_{b/p} + g)^2} \frac{\partial g}{\partial a} \right) Y(u_r) v_r^2
 \end{aligned} \tag{10.84}$$

Remark 10.6. *The necessity for the choice of Δ as in (10.47) becomes evident from (10.80). The choice of Δ constant would make all partial derivatives of Δ equal to zero. However, from $v_r/C_r x_{b/p} \kappa(\theta) \theta$ we obtain a term of the form*

$$\frac{v_r^2}{C_r} \kappa(\theta) \frac{\Delta^2 x_{b/p}}{(\Delta^2 + (y_{b/f} + g)^2)^{3/2}} \tag{10.85}$$

which grows quadratically in v_r with a gain that cannot be bounded independent of $x_{b/f}$ if Δ is independent of $x_{b/f}$. Therefore, boundedness of v_r cannot be shown independently of $x_{b/f}$. With the choice of $\Delta = \sqrt{\mu^2 + x_{b/p}^2}$ as proposed in Moe et al. [103], the partial derivatives with respect to $y_{b/p}$ would be zero. The term in (10.85) would now be upper-bounded by one. However, a new term would then be introduced from the partial derivative of Δ

$$\frac{v_r^2}{C_r} \frac{\partial \Delta}{\partial x_{b/p}} \kappa(\theta) \frac{\Delta y_{b/p} (y_{b/p} + g)}{(\Delta^2 + (y_{b/f} + g)^2)^{3/2}} \tag{10.86}$$

where it should be noted that this term can grow unbounded in $y_{b/p}$ near the manifold where $g = -(y_{b/p} + 1)$. Hence, the growth of this quadratic term in v_r cannot be upper-bounded independent of $y_{b/p}$.

To avoid the issues describe in Remark 10.6, we choose Δ as defined in (10.47). Using the definition of $\Delta(x_{b/p}, y_{b/p})$ given in (10.47) it is straightforward to verify

that

$$\begin{aligned}
 r_d v_r &\leq \left| \frac{v_r^2}{C_r} \right| |\kappa(\theta)| \left| \left[-1 + \frac{\Delta x_{b/p}}{\Delta^2 + (y_{b/p} + g)^2} \right] \right| + |F(\cdot)| \\
 &\quad + \left| \frac{v_r}{C_r} \right| |\kappa(\theta)| |u_r| \left| \left[-1 + \frac{\Delta x_{b/p}}{\Delta^2 + (y_{b/p} + g)^2} \right] \right| \\
 &\quad - \frac{1}{C_r} \left(\frac{u_{rd}}{u_{rd}^2 + v_r^2} - \frac{2\Delta v_r}{\Delta^2 + (y_{b/p} + g)^2} \frac{\partial g}{\partial a} \right) Y(u_r) v_r^2 \\
 &\leq 2 \left| \frac{v_r^2}{C_r} \right| |\kappa(\theta)| + 2 |u_r| \left| \frac{v_r}{C_r} \right| |\kappa(\theta)| + |F(\cdot)| \\
 &\quad - \frac{1}{C_r} \left(\frac{u_{rd}}{u_{rd}^2 + v_r^2} - \frac{2\Delta v_r}{\Delta^2 + (y_{b/p} + g)^2} \frac{\partial g}{\partial a} \right) Y(u_r) v_r^2
 \end{aligned} \tag{10.87}$$

When substituting (10.87) in (10.76) we obtain

$$\begin{aligned}
 \dot{V}_3 = v_r \dot{v}_r &\leq \frac{1}{C_r} \left[2 |X(u_{rd})| |\kappa(\theta)| + Y(u_{rd}) \right] v_r^2 + a_y \tilde{u} v_r^2 + a_x \tilde{u} v_r \tilde{r} \\
 &\quad + X(u_{rd}) \left(F(\cdot) + 2 |u_r| \left| \frac{v_r}{C_r} \right| \right) + a_x \tilde{u} r_d v_r + X(u_{rd}) v_r \tilde{r}
 \end{aligned} \tag{10.88}$$

Consequently, on the manifold where $(\tilde{X}_1, \tilde{X}_2) = 0$ we have

$$\dot{V}_3 \leq \frac{1}{C_r^*} \left(2X_{\max} |\kappa(\theta)| + Y_{\min} \right) v_r^2 + X(u_{rd}) F_1(0, 0, \Delta, V_T, V_N, u_{rd}) |v_r| \tag{10.89}$$

where $C_r^*(v_r, x_{b/p}, y_{b/p}, \Delta, V_N, u_{rd}) = C_r(v_r, x_{b/p}, y_{b/p}, \Delta, \hat{V}_N = V_N, u_r = u_{rd})$. Boundedness of (10.89) is guaranteed as long as

$$2X_{\max} |\kappa(\theta)| + Y_{\min} < 0 \tag{10.90}$$

Hence, satisfaction of (10.48) renders the quadratic term in (10.89) negative and since the quadratic term is dominant for sufficiently large v_r , (10.89) is negative definite for sufficiently large v_r . If \dot{V}_3 is negative for sufficiently large v_r this implies that V_3 decreases for sufficiently large v_r . Since $V_3 = 1/2v_r^2$, a decrease in V_3 implies a decrease in v_r^2 and by extension in v_r . Therefore, v_r cannot increase above a certain value and v_r is bounded near the manifold where $(\tilde{X}_1, \tilde{X}_2) = 0$.

Remark 10.7. Note that $C_r^*(v_r, y_{b/p}, \Delta, V_N, u_{rd})$ can be found independently of $y_{b/p}$ and $x_{b/p}$ since the terms in C_r are bounded with respect to these variables.

Consequently, close to the manifold where $(\tilde{X}_1, \tilde{X}_2) = 0$ the sufficient and necessary condition for local boundedness of (10.43c) is the following:

$$2X_{\max} |\kappa(\theta)| + Y_{\min} < 0 \tag{10.91}$$

which is satisfied if and only if the condition in Lemma 10.2 is satisfied. This completes the proof of Lemma 10.2.

10.C Proof of Lemma 10.3

Recall the sway velocity dynamics (10.43c):

$$\dot{v}_r = X(\tilde{u} + u_{rd})(r_d + \tilde{r}) + Y(u_{rd} + \tilde{u})v_r, \quad Y(u_{rd}) < 0$$

Consider the following Lyapunov function candidate:

$$V_3(v_r) = \frac{1}{2}v_r^2 \quad (10.92)$$

The derivative of (10.92) along the solutions of (10.43c) is given by

$$\begin{aligned} \dot{V}_3 &= v_r \dot{v}_r = v_r X(u_{rd} + \tilde{u})r_d + X(u_{rd} + \tilde{u})v_r \tilde{r} + Y(u_{rd} + \tilde{u})v_r^2 \\ &\leq X(u_{rd})r_d v_r + a_x \tilde{u} r_d v_r + X(u_{rd})v_r \tilde{r} + a_x \tilde{u} v_r \tilde{r} + a_y \tilde{u} v_r^2 + Y(u_{rd})v_r^2 \end{aligned} \quad (10.93)$$

where we used the fact that:

$$Y(u_r) = a_y u_r + b_y \quad (10.94)$$

$$X(u_r) = a_x u_r + b_x \quad (10.95)$$

The term $r_d v_r$ is given by:

$$\begin{aligned} r_d v_r &= -\frac{v_r}{C_r} \left[\kappa(\theta) \left(u_t \cos(\psi + \beta - \gamma_p(\theta)) + k_\delta \frac{x_{b/p}}{\sqrt{1 + x_{b/p}^2}} + \hat{V}_T \right) \right. \\ &\quad + \frac{Y(u_r)v_r u_{rd} - \dot{u}_{rd} v_r}{u_{rd}^2 + v_r^2} + \frac{\Delta}{\Delta^2 + (y_{b/p} + g)^2} \left[\dot{\hat{V}}_N \frac{b + \sqrt{b^2 - ac}}{-a} \right. \\ &\quad + \frac{\partial g}{\partial b} (2\dot{\hat{V}}_N y_{b/p}) + \frac{\partial g}{\partial a} (2\hat{V}_N \dot{\hat{V}}_N - 2u_{rd} \dot{u}_{rd} - 2v_r Y(u_r)v_r) \\ &\quad + \left[1 + \frac{\partial g}{\partial c} 2y_{b/p} + \frac{\partial g}{\partial b} 2\hat{V}_N \right] \left(\frac{-u_{td} y_{b/p}}{\sqrt{\Delta^2 + (y_{b/p} + g)^2}} + G_1(\cdot) - x_{b/p} \kappa(\theta) \dot{\theta} \right) \\ &\quad + \frac{\partial g}{\partial c} 2\Delta \left[\frac{\partial \Delta}{\partial x_{b/p}} \left(-k_\delta \frac{x_{b/p}}{\sqrt{1 + x_{b/p}^2}} + y_{b/p} \kappa(\theta) \dot{\theta} \right) \right. \\ &\quad + \left. \left. \frac{\partial \Delta}{\partial y_{b/p}} \left(-u_{td} \frac{y_{b/p}}{\sqrt{\Delta^2 + (y_{b/p} + g)^2}} + G_1(\cdot) - x_{b/p} \kappa(\theta) \dot{\theta} \right) \right] \right] \\ &\quad - \frac{y_{b/p} + g}{\Delta^2 + (y_{b/p} + g)^2} \left[\frac{\partial \Delta}{\partial x_{b/p}} \left(-k_\delta \frac{x_{b/p}}{\sqrt{1 + x_{b/p}^2}} + y_{b/p} \kappa(\theta) \dot{\theta} \right) \right. \\ &\quad + \left. \left. \frac{\partial \Delta}{\partial y_{b/p}} \left(-u_{td} \frac{y_{b/p}}{\sqrt{\Delta^2 + (y_{b/p} + g)^2}} + G_1(\cdot) - x_{b/p} \kappa(\theta) \dot{\theta} \right) \right] \right] \end{aligned} \quad (10.96)$$

We can now collect the terms that have less than quadratic growth in v_r and/or vanish when $\tilde{X}_2 = 0$.

$$\begin{aligned}
 r_d v_r = & -\frac{v_r}{C_r} \kappa(\theta) \left(\sqrt{u_r^2 + v_r^2} \cos(\psi + \beta - \gamma_p(\theta)) \right) \\
 & + \frac{v_r}{C_r} \frac{\Delta x_{b/p}}{\Delta^2 + (y_{b/p} + g)^2} \left(\kappa(\theta) \sqrt{u_r^2 + v_r^2} \cos(\psi + \beta - \gamma_p) \right) \\
 & - \frac{v_r}{C_r} \frac{\Delta}{\Delta^2 + (y_{b/p} + g)^2} \left(-u_{td} \frac{y_{b/p}}{\sqrt{\Delta^2 + (y_{b/p} + g)^2}} + G_1(\cdot) \right) \\
 & + \frac{v_r}{C_r} \frac{y_{b/p} + g}{\Delta^2 + (y_{b/p} + g)^2} \frac{\partial \Delta}{\partial y_{b/p}} \left(-u_{td} \frac{y_{b/p}}{\sqrt{\Delta^2 + (y_{b/p} + g)^2}} + G_1(\cdot) \right) \\
 & - \frac{1}{C_r} \left(\frac{u_{rd}}{u_{rd}^2 + v_r^2} - \frac{2\Delta v_r}{\Delta^2 + (y_{b/p} + g)^2} \frac{\partial g}{\partial a} \right) Y(u_r) v_r^2 \\
 & + G(\tilde{X}_1, \tilde{X}_2, \Delta, V_T, V_N, u_{rd}, v_r)
 \end{aligned} \tag{10.97}$$

where,

$$\begin{aligned}
 G(\cdot) \triangleq & -\frac{v_r}{C_r} \left[\kappa(\theta) \left(k_\delta \frac{x_{b/p}}{\sqrt{1 + x_{b/p}^2}} + \hat{V}_T \right) - \frac{k_\delta x_{b/p}}{\sqrt{1 + x_{b/p}^2}} \right. \\
 & - \frac{\dot{u}_{rd} v_r}{u_{rd}^2 + v_r^2} - \frac{y_{b/p} + g}{\Delta^2 + (y_{b/p} + g)^2} \frac{\partial \Delta}{\partial x_{b/p}} \\
 & + \frac{\Delta}{\Delta^2 + (y_{b/p} + g)^2} \left[\dot{V}_N \frac{b + \sqrt{b^2 - ac}}{-a} + \frac{\partial g}{\partial b} (2\dot{V}_N y_{b/p}) \right. \\
 & \left. \left. - \frac{\partial g}{\partial c} 2\Delta \left[\frac{\partial \Delta}{\partial x_{b/p}} \frac{k_\delta x_{b/p}}{\sqrt{1 + x_{b/p}^2}} + \frac{\partial \Delta}{\partial y_{b/p}} \left(\frac{u_{td} y_{b/p}}{\sqrt{\Delta^2 + (y_{b/p} + g)^2}} + G_1(\cdot) \right) \right] \right] \right. \\
 & + 2 \left[\frac{\partial g}{\partial c} y_{b/p} + \frac{\partial g}{\partial b} \hat{V}_N \right] \left(\frac{-u_{td} y_{b/p}}{\sqrt{\Delta^2 + (y_{b/p} + g)^2}} + G_1(\cdot) - x_{b/p} \kappa(\theta) \dot{\theta} \right) \\
 & \left. + 2 \frac{\partial g}{\partial a} \left(\hat{V}_N \dot{V}_N - u_{rd} \dot{u}_{rd} \right) - x_{b/p} \kappa(\theta) \left(\frac{k_\delta x_{b/p}}{\sqrt{1 + x_{b/p}^2}} + \hat{V}_T \right) \right] \tag{10.98}
 \end{aligned}$$

where $G(\cdot)$ is the function introduced to collect the terms that have less than quadratic growth in v_r and/or vanish when $\tilde{X}_2 = 0$. Note here that using our definition of Δ in (10.47) all the terms in $r_d v_r$ with partial derivatives of Δ multiplied by $\dot{\theta}$ are cancelled due to skew-symmetry. We can now find the following bound on

(10.96)

$$\begin{aligned}
 r_d v_r &\leq \left| \frac{v_r}{C_r} \right| |\kappa(\theta)| \sqrt{u_r^2 + v_r^2} \left| \frac{\Delta x_{b/p}}{\Delta^2 + (y_{b/p} + g)^2} - 1 \right| \\
 &\quad + \left| \frac{v_r}{C_r} \right| \left| \frac{1}{\Delta} \right| \left(4\sqrt{u_r^2 + v_r^2} + |\tilde{u}| \right) \\
 &\quad + \left| \frac{v_r}{C_r} \right| \left| \frac{y_{b/p} + g}{\Delta^2 + (y_{b/p} + g)^2} \right| \left(4\sqrt{u_r^2 + v_r^2} + |\tilde{u}| \right) + |G(\cdot)| \\
 &\quad - \frac{1}{C_r} \left(\frac{u_{rd}}{u_{rd}^2 + v_r^2} - \frac{2\Delta v_r}{\Delta^2 + (y_{b/p} + g)^2} \frac{\partial g}{\partial a} \right) Y(u_r) v_r^2 \\
 &\leq \left| \frac{v_r^2}{C_r} \right| \left[|\kappa(\theta)| \left| \frac{\Delta x_{b/p}}{\Delta^2 + (y_{b/p} + g)^2} - 1 \right| + \frac{8}{\Delta} \right] + |G(\cdot)| \\
 &\quad + \left| \frac{v_r}{C_r} \right| |\kappa(\theta)| |u_r| \left| \frac{\Delta x_{b/p}}{\Delta^2 + (y_{b/p} + g)^2} - 1 \right| + \left| \frac{v_r}{C_r} \right| \left| \frac{2}{\Delta} \right| (4|u_r| + |\tilde{u}|) \quad (10.99) \\
 &\quad - \frac{1}{C_r} \left(\frac{u_{rd}}{u_{rd}^2 + v_r^2} - \frac{2\Delta v_r}{\Delta^2 + (y_{b/p} + g)^2} \frac{\partial g}{\partial a} \right) Y(u_r) v_r^2 \\
 &\leq \left| \frac{v_r^2}{C_r} \right| \left[|\kappa(\theta)| \left| \frac{\Delta x_{b/p}}{\Delta^2 + (y_{b/p} + g)^2} - 1 \right| + \frac{8}{\Delta} \right] + \Phi(\cdot) \\
 &\quad - \frac{1}{C_r} \left(\frac{u_{rd}}{u_{rd}^2 + v_r^2} - \frac{2\Delta v_r}{\Delta^2 + (y_{b/p} + g)^2} \frac{\partial g}{\partial a} \right) Y(u_r) v_r^2 \\
 &\leq \left| \frac{v_r^2}{C_r} \right| \left[2|\kappa(\theta)| + \frac{8}{\Delta} \right] + \Phi(\cdot) \\
 &\quad - \frac{1}{C_r} \left(\frac{u_{rd}}{u_{rd}^2 + v_r^2} - \frac{2\Delta v_r}{\Delta^2 + (y_{b/p} + g)^2} \frac{\partial g}{\partial a} \right) Y(u_r) v_r^2
 \end{aligned}$$

where,

$$\Phi(\cdot) \triangleq |G(\cdot)| + 2 \left| \frac{v_r}{C_r} \right| |\kappa(\theta)| |u_r| + 2 \left| \frac{v_r}{C_r} \right| \left| \frac{1}{\Delta} \right| (4|u_r| + |\tilde{u}_r|) \quad (10.100)$$

The function $\Phi(\cdot)$ is introduced to collect the remaining terms that have less than quadratic growth in v_r and/or vanish when $\tilde{X}_2 = 0$. Note also the terms in $G(\cdot)$ with partial derivatives of g that appear to have quadratic growth. Although the overall terms appear to have quadratic growth, the partial derivatives of g actually decrease for increasing v_r giving the entire term less than quadratic growth. From the definitions of $\Phi(\cdot)$ and $G(\cdot)$ one can easily conclude the existence of three continuous positive functions $F_{0,2}(\tilde{X}_1, \tilde{X}_2, u_{rd}, \dot{u}_{rd}, V_T, V_N, \Delta)$ which are bounded under the boundedness of the vector $[\tilde{X}_2^T, u_{rd}, \dot{u}_{rd}, V_T, V_N, \Delta]^T$, with

$$F_2(\tilde{X}_1, \tilde{X}_2 = 0, u_{rd}, \dot{u}_{rd}, V_{x_e}, V_{y_e}, \Delta) = 0,$$

such that:

$$\Phi(\cdot) \leq F_2(\cdot) v_r^2 + F_1(\cdot) v_r + F_0(\cdot). \quad (10.101)$$

When we substitute the bound on $r_d v_r$ from (10.99) in (10.93) we obtain:

$$\begin{aligned}
 \dot{V}_3 = v_r \dot{v}_r &\leq |X(u_{rd})| \left(\left| \frac{v_r^2}{C_r} \right| \left[2|\kappa(\theta)| + \frac{8}{\Delta} \right] + \Phi(\cdot) \right) + a_x \tilde{u} r_d v_r \\
 &\quad + X(u_{rd}) v_r \tilde{r} + a_x \tilde{u} v_r \tilde{r} + a_y \tilde{u} v_r^2 + Y(u_{rd}) v_r^2 \\
 &\quad - \frac{1}{C_r} \left(\frac{u_{rd}}{u_{rd}^2 + v_r^2} - \frac{2\Delta v_r}{\Delta^2 + (y_{b/p} + g)^2} \frac{\partial g}{\partial a} \right) Y(u_r) v_r^2 \\
 &\leq \left| \frac{1}{C_r} \right| \left[|X(u_{rd})| \left[2|\kappa(\theta)| + \frac{8}{\Delta} \right] - |Y(u_{rd})| \right] v_r^2 \\
 &\quad + a_x \tilde{u} r_d v_r + X(u_{rd})(v_r \tilde{r} + \Phi(\cdot)) + a_x \tilde{u} v_r \tilde{r} + a_y \tilde{u} v_r^2
 \end{aligned} \tag{10.102}$$

Consequently, on the manifold where $\tilde{X}_2 = 0$ we obtain

$$\begin{aligned}
 \dot{V}_3 &\leq \left| \frac{1}{C_r} \right| \left[X_{\max} \left[2\kappa_{\max} + \frac{8}{\Delta} \right] - Y_{\min} \right] v_r^2 \\
 &\quad + X(u_{rd})(F_1(\tilde{X}_1, 0, u_{rd}, \dot{u}_{rd}, V_T, V_N, \Delta) |v_r| \\
 &\quad + F_0(\tilde{X}_1, 0, u_{rd}, \dot{u}_{rd}, V_T, V_N, \Delta))
 \end{aligned} \tag{10.103}$$

To have boundedness of v_r for small values of \tilde{X}_2 we have to satisfy the following inequality:

$$X_{\max} \left[2\kappa_{\max} + \frac{8}{\Delta} \right] - Y_{\min} < 0 \tag{10.104}$$

such that the quadratic term in (10.103) is negative. Using (10.47) we need to choose μ , such that:

$$\mu > \frac{8X_{\max}}{Y_{\min} - 2\kappa_{\max}X_{\max}} \tag{10.105}$$

which is the condition given in Lemma 10.3. Note that the denominator of μ is nonzero and positive as long of the conditions of Lemma 10.2 are satisfied. Consequently, near the manifold $\tilde{X}_2 = 0$ it holds that (10.103) is negative definite for sufficiently large v_r . Consequently, near the manifold $\tilde{X}_2 = 0$ it holds that (10.102) is negative definite for sufficiently large v_r . If \dot{V}_3 is negative for sufficiently large v_r this implies that V_3 decreases for sufficiently large v_r . Since $V_3 = 1/2v_r^2$, a decrease in V_3 implies a decrease in v_r^2 and by extension in v_r . Consequently, v_r cannot increase above a certain value and v_r is bounded near $\tilde{X}_2 = 0$ if μ is chosen such that (10.49) holds, which completes the proof of Lemma 10.3.

Chapter 11

Path following of unparametrized paths

This chapter addresses the path following control problem of unparametrized curved paths for ASVs and AUVs. In particular, we consider that the path is identified by an implicit expression and we do not use an explicit parametrization for control purposes. That is, we do not define a path parameter s which uniquely identifies a point on the path. The control objective is to make the vehicle converge to the path and move along it with a specified constant forward velocity. We consider that a constant and irrotational ocean current affects the vehicle. However, differently from the previous chapters, the disturbance is not considered to act as a disturbance at the level of the kinematics, but rather as a disturbance at the level of the accelerations. For this reason, a different model for ASVs and AUVs is introduced in this chapter.

The path following control problem has already been considered in Chapters 6, 8-10. However, in Chapters 6, 8-10 we considered parametrized paths. In that case the proposed solution consisted of finding a control law which made the vehicle track a virtual frame propagating along the curve according to the motion of the vehicle. Since here we do not use any parametrization, such an approach cannot be used. The approach presented in this chapter is based on the hierarchical control approach presented in [47]. In particular, the control design is divided into two main steps. We first solve the path following control problem for a kinematic point-mass. We then use the feedback designed for the point-mass in order to obtain a desired yaw angle to assign to the marine vehicle. The desired yaw angle is assigned using a feedback linearizing controller together with an adaptive control law in order to reject the constant disturbance. These two steps are equivalent to defining and stabilizing two nested subsets of the state space. Using the hierarchical control methodology in [47] we show that under certain conditions on the curvature of the path, the path following control problem is solved and the sway velocity of the vehicle stays bounded.

Note that the problem of unparametrized straight line paths was already presented in Chapters 6, 8, where we showed that the control approach presented in Chapters 6, 8 can solve the path following control problem for unparametrized

straight line paths. Note also that the path following of straight line unparametrized paths has already been dealt with in the past, for instance in [20, 32, 56]. Furthermore, the path following problem for curves parametrized by a path variable has also been dealt with in the past, see for instance [80, 103]. However, to the best of our knowledge, for marine vehicles, the path following control problem of unparametrized curved paths is an open problem. A preliminary solution for the case of no disturbance affecting the vehicle was given in [15]. In this chapter a solution for the case of non-zero ocean current is also presented.

The work presented in this chapter is an extension of the work presented in [15].

The chapter is organized as follows: Section 11.1 gives some preliminaries and the notations used in the chapter; in Section 11.2 the control problem is described and the dynamic model used for the vehicle is introduced; Section 11.3 describes our hierarchical approach; Section 11.4 presents our approach to the control design and stability analysis for the case of zero ocean current; in Section 11.5 the considerations given in the previous section are extended to the case of non-zero ocean current; Section 11.6 presents the simulation results both for the case of zero and non-zero ocean current; Finally, Section 11.7 gives the conclusions.

11.1 Preliminaries and notation

In this chapter we adopt the following notation. We denote by \mathbb{S}^1 the set of real numbers modulo 2π , with the differentiable manifold structure making it diffeomorphic to the unit circle. If $\psi \in \mathbb{S}^1$, R_ψ is the rotation matrix

$$R_\psi = \begin{bmatrix} \cos(\psi) & -\sin(\psi) \\ \sin(\psi) & \cos(\psi) \end{bmatrix}.$$

If $f(x, y)$ is a differentiable function of two scalar variables, we denote by $\partial_x f$, $\partial_y f$ the partial derivatives with respect to x and y , respectively. Similarly, we define $\partial_{xy}^2 f := \partial_x \partial_y f$, and similarly for the other second-order partial derivatives. If $f : \mathbb{R}^n \rightarrow \mathbb{R}^m$ is a differentiable vector function and $p \in \mathbb{R}^n$, df_p is the $m \times n$ Jacobian matrix of f at p . If Γ is a closed subset of a metric space (M, d) and $x \in M$, then we denote by $\|x\|_M$ the point-to-set distance of x to M , $\|x\|_M = \inf_{y \in M} d(x - y)$.

The following stability definitions are taken from [47]. Let $\Sigma : \dot{\chi} = f(\chi)$ be a smooth dynamical system with state space a Riemannian manifold \mathcal{X} with associated metric d . Let $\phi(t, \chi_0)$ denote the local phase flow generated by Σ , and let $B_\delta(x)$ denote the ball of radius δ centred at $x \in M$.

Consider a closed set $\Gamma \subset \mathcal{X}$ which is positively invariant for Σ , i.e., for all $\chi_0 \in \Gamma$, $\phi(t, \chi_0) \in \Gamma$ for all $t > 0$ for which $\phi(t, \chi_0)$ is defined. Then we have the following stability definitions taken from [47].

Definition 11.1. *The set Γ is stable for Σ if for any $\varepsilon > 0$, there exists a neighborhood $\mathcal{N}(\Gamma) \subset \mathcal{X}$ such that, for all $\chi_0 \in \mathcal{N}(\Gamma)$, $\phi(t, \chi_0) \in B_\varepsilon(\Gamma)$, for all $t > 0$ for which $\phi(t, \chi_0)$ is defined. The set Γ is attractive for Σ if there exists a neighborhood $\mathcal{N}(\Gamma) \subset \mathcal{X}$ such that for all $\chi_0 \in \mathcal{N}(\Gamma)$, $\lim_{t \rightarrow \infty} \|\phi(t, \chi_0)\|_\Gamma = 0$. The domain of attraction of Γ is the set $\{\chi_0 \in \mathcal{X} : \lim_{t \rightarrow \infty} \|\phi(t, \chi_0)\|_\Gamma = 0\}$. The set Γ is globally*

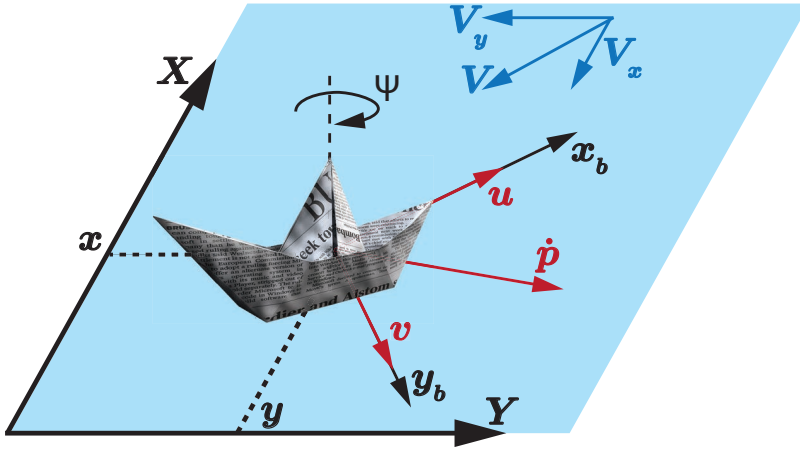


Figure 11.1: Illustration of the ship's kinematic variables.

attractive for Σ if it is attractive with domain of attraction \mathcal{X} . The set Γ is locally asymptotically stable (LAS) for Σ if it is stable and attractive. The set Γ is globally asymptotically stable for Σ if it is stable and globally attractive. If $\Gamma_1 \subset \Gamma_2$ are two closed positively invariant sets, then Γ_1 is asymptotically stable relative to Γ_2 if Γ_1 is asymptotically stable for the restriction of Σ to Γ_2 . System Σ is locally uniformly bounded (LUB) near Γ if for each $x \in \Gamma$ there exist positive scalars λ and m such that $\phi(\mathbb{R}_+, B_\lambda(x)) \subset B_m(x)$. \triangle

The following result is key in the development of this chapter.

Theorem 11.1 ([47]). *Let $\Gamma_1, \Gamma_2, \Gamma_1 \subset \Gamma_2 \subset \mathcal{X}$, be two closed sets that are positively invariant for Σ and suppose that Γ_1 is not compact. If*

- (i) Γ_1 is asymptotically stable relative to Γ_2 ,
- (ii) Γ_2 is asymptotically stable, and
- (iii) Σ is LUB near Γ_1 ,

then Γ_1 is asymptotically stable for Σ .

11.2 The problem

Consider the 3-degrees-of-freedom vessel depicted in Figure 11.1, which may describe an autonomous surface vessel (ASV) or an autonomous underwater vehicle (AUV) moving in the horizontal plane. We denote by $p \in \mathbb{R}^2$ the position of the vessel on the plane and $\psi \in \mathbb{S}^1$ its heading (or yaw) angle. The yaw rate $\dot{\psi}$ is denoted by r .

We attach at the point p of the vessel a body frame aligned with the main axes of the vessel, as depicted in the figure, with the standard convention that the z -axis points into the plane (towards the sea bottom). We represent the velocity vector \dot{p} in body frame coordinates as (u, v) , where u , the longitudinal component of the

velocity vector, is called the surge speed, while v , the lateral component, is called the sway speed. Finally, the control inputs of the vessel are the surge thrust T_u and the rudder angle T_r . In terms of these variables, the model derived in [54] is

$$\dot{\boldsymbol{\eta}} = \begin{bmatrix} R_\psi & 0 \\ 0 & 1 \end{bmatrix} \boldsymbol{\nu} \quad (11.1)$$

$$\mathbf{M}_{RB}\dot{\boldsymbol{\nu}} + \mathbf{C}_{RB}(\boldsymbol{\nu})\boldsymbol{\nu} = -\mathbf{M}_A\dot{\boldsymbol{\nu}}_r - \mathbf{C}_A(\boldsymbol{\nu}_r)\boldsymbol{\nu}_r - \mathbf{D}\boldsymbol{\nu}_r + \mathbf{B}\mathbf{f}.$$

with $\boldsymbol{\eta} \triangleq [p, \psi]^\top$, $\boldsymbol{\nu} \triangleq [u, v, r]^\top$, where $\boldsymbol{\nu}_r \triangleq \boldsymbol{\nu} - \boldsymbol{\nu}_c$ with $\boldsymbol{\nu}_c = \mathbf{R}^\top(\psi)\mathbf{V}_c \triangleq [u_c, v_c, 0]^\top$, and $\mathbf{V}_c \triangleq [V_x, V_y, 0]^\top$ is the constant ocean current affecting the system. Finally, $\mathbf{f} \triangleq [T_u, T_r]^\top$. The matrices \mathbf{M}_{RB} , \mathbf{M}_A , \mathbf{D} and \mathbf{B} are given by

$$\mathbf{M}_i \triangleq \begin{bmatrix} m_{11}^i & 0 & 0 \\ 0 & m_{22}^i & m_{23}^i \\ 0 & m_{23}^i & m_{33}^i \end{bmatrix}, \mathbf{D} \triangleq \begin{bmatrix} d_{11} & 0 & 0 \\ 0 & d_{22} & d_{23} \\ 0 & d_{32} & d_{33} \end{bmatrix}, \mathbf{B} \triangleq \begin{bmatrix} b_{11} & 0 \\ 0 & b_{22} \\ 0 & b_{32} \end{bmatrix}.$$

with $i \in \{RB, A\}$ and $\mathbf{M}_i = \mathbf{M}_i^\top > 0$. The matrices \mathbf{M}_{RB} and \mathbf{M}_A are the inertia and added mass matrix, respectively. $\mathbf{D} > 0$ is the hydrodynamic damping matrix, and \mathbf{B} is the actuator configuration matrix. Moreover, $\mathbf{C}_{RB}(\boldsymbol{\nu})$ is the matrix of centripetal forces and $\mathbf{C}_A(\boldsymbol{\nu}_r)$ is the matrix of the centripetal forces due to the added mass \mathbf{M}_A . The matrices $\mathbf{C}_{RB}(\boldsymbol{\nu})$ and $\mathbf{C}_A(\boldsymbol{\nu}_r)$ can be obtained from \mathbf{M}_{RB} and \mathbf{M}_A (see [54]). We place the origin of the body frame at a point on the center-line of the vessel with distance ϵ from the centre of mass. Following [58], assuming that the vessel is starboard symmetric, there exists ϵ such that the resulting dynamics have mass and damping matrices satisfying this relation: $\mathbf{M}^{-1}\mathbf{B}\mathbf{f} = [\tau_u, 0, \tau_r]^\top$. Thus, with this choice of origin of the body frame, the sway dynamics become decoupled from the rudder control input, making it easier to analyze the stability properties of the sway dynamics. Using this convention, the model of the marine vessel (11.1) can be represented as

$$\begin{aligned} \dot{p} &= R_\psi \begin{bmatrix} u \\ v \end{bmatrix} \\ \dot{u} &= -\frac{d_{11}}{m_{11}}u + \frac{(m_{22}v + m_{23}r)}{m_{11}} + \boldsymbol{\phi}_u^\top(\psi, r)\boldsymbol{\theta}_u + \tau_u \\ \dot{v} &= X(u)r + Y(u)v + \boldsymbol{\phi}_{v1}^\top(u, v, \psi)\boldsymbol{\theta}_v + \boldsymbol{\phi}_{v2}^\top(\psi)\boldsymbol{\theta}_u r \\ \dot{\psi} &= r \\ \dot{r} &= F_r(u, v, r) + \boldsymbol{\phi}_r^\top(u, v, r, \psi)\boldsymbol{\theta}_r + \tau_r. \end{aligned} \quad (11.2)$$

The functions $X(u)$ and $Y(u)$ are linear. Their expressions are given in Appendix 11.A together with those of F_u , F_r , $\boldsymbol{\phi}_u$, $\boldsymbol{\phi}_{v1}$, $\boldsymbol{\phi}_{v2}$, $\boldsymbol{\phi}_r$. Moreover, $\boldsymbol{\theta}_u \triangleq [V_x, V_y]^\top$, and $\boldsymbol{\theta}_v \triangleq \boldsymbol{\theta}_r \triangleq [V_x, V_y, V_x^2, V_y^2, V_x V_y]^\top$. Denoting by $\chi \triangleq (p, u, v, \psi, r)$ the state of the vessel, the state space is $\mathcal{X} := \mathbb{R}^2 \times \mathbb{R} \times \mathbb{R} \times \mathbb{S}^1 \times \mathbb{R}$.

Assumption 11.1. *We assume that $Y(u) < 0$ for all $u \in [0, U_{\max}]$.*

This is a realistic assumption, since $Y(\bar{u}) \geq 0$ would imply that the sway dynamics are undamped or unstable when the yaw rate r is zero.

Assumption 11.2. *The ocean current is assumed to be constant and irrotational with respect to the inertial frame, i.e. $\mathbf{V}_c \triangleq [V_x, V_y, 0]^T$. Furthermore, it is bounded by $V_{\max} > 0$ such that $\|\mathbf{V}_c\| = \sqrt{V_x^2 + V_y^2} \leq V_{\max}$.*

Consider a planar Jordan¹ curve γ expressed in implicit form as $\gamma = \{p : h(p) = 0\}$, where h is a C^1 function whose gradient never vanishes on γ . We assume that $h : \mathbb{R}^2 \rightarrow \mathbb{R}$ is a proper function, i.e., all its sublevel sets $\{p : h(p) \leq c\}$, $c \in \mathbb{R}$, are compact. Since γ is assumed to be compact, there is no loss of generality in this assumption.

Path Following Problem (PFP). Design a smooth time-invariant feedback such that, for suitable initial conditions, the position vector $p(t) \rightarrow \{p : h(p) = 0\}$, and the speed $\|\dot{p}(t)\|$ satisfies $0 < \|\dot{p}(t)\| \leq \sup_t \|\dot{p}(t)\| < \infty$. In other words, we want to make the position of the ship converge to the path, travel along it without stopping, while guaranteeing that its speed is bounded.

Geometric objects. Associated with the implicit representation $h(p) = 0$ of γ there are three geometric objects: the unit tangent and normal vectors, and the signed curvature. The unit normal vector at p is

$$N(p) := dh_p^\top / \|dh_p\|.$$

The unit tangent vector at p is the counterclockwise rotation of $N(p)$ by $\pi/2$,

$$T(p) := R_{\pi/2} N(p).$$

Finally, the signed curvature $\kappa(p)$ is defined as

$$\kappa(p) = -\frac{(\partial_y h)^2 \partial_{xx}^2 h - 2\partial_{xy}^2 h \partial_x h \partial_y h + \partial_{yy}^2 h (\partial_x h)^2}{((\partial_x h)^2 + (\partial_y h)^2)^{(3/2)}}. \quad (11.3)$$

The quantities $N(p), T(p), \kappa(p)$ are defined not just on γ , but at all points p such that $dh_p \neq [0 \ 0]$. If $p_0 \notin \gamma$, then $N(p_0), T(p_0), \kappa(p_0)$ are the normal vector, tangent vector, and curvature at p_0 of the curve $\{p : h(p) = p_0\}$.

11.3 Hierarchical control approach

The idea of the proposed solution is hierarchical in nature.

1. We regulate the surge speed u to a desired constant $\bar{u} > 0$.
2. We consider the kinematic point-mass system

$$\dot{p} = \mu,$$

and we solve the PFP with the constraint that $\|\mu\| = (\bar{u}^2 + v^2)^{(1/2)}$. The result of this design is a function $\mu(p, v)$.

¹A curve is said to be Jordan if it is closed and has no self-intersections.

3. Having found $\mu(p, v)$, we find the desired heading angle $\psi_d(p, v)$ such that

$$R_{\psi_d} \begin{bmatrix} \bar{u} \\ v \end{bmatrix} = \mu.$$

This equation has a solution because, by construction, $\|\mu\| = (\bar{u}^2 + v^2)^{(1/2)}$. Intuitively, when $\psi = \psi_d$ and $u = \bar{u}$, the marine vessel behaves like a kinematic point-mass subject to a path following control law.

4. Having found $\psi_d(p, v)$, we define the output function $e = \psi - \psi_d$ and we show that, under certain conditions on \bar{u} (possibly any $\bar{u} > 0$), the system with input τ_r and output e has relative degree 2. We thus define a controller $\tau_r(\chi)$ that stabilizes the set where $e = \dot{e} = 0$.
5. We show that, if the curvature of the path is not too large, then the sway speed v remains bounded. We use Theorem 11.1 to prove that the hierarchical approach described above does indeed solve the PFP if the curvature of the path is not too large.

In the remainder of this chapter we solve the PFP for system (11.2). However, for the sake of clarity we first consider the special case where the current is zero in the next section. In Section 11.5 we will then extend our to the general case where the ocean current is non-zero.

11.4 The case of zero ocean current

When the ocean current is zero, i.e. $\mathbf{V}_c = \mathbf{0}$, the model (11.2) reduces to

$$\begin{aligned} \dot{p} &= R_\psi \begin{bmatrix} u \\ v \end{bmatrix} \\ \dot{u} &= F_u(v, r) - \frac{d_{11}}{m_{11}}u + \tau_u \\ \dot{v} &= X(u)r + Y(u)v \\ \dot{\psi} &= r \\ \dot{r} &= F_r(u, v, r) + \tau_r. \end{aligned} \tag{11.4}$$

In this section we first carry out the design steps 1-4 outlined above, then we deal with the stability analysis of step 5 for the special case $\mathbf{V}_c = \mathbf{0}$.

11.4.1 Control design

Step 1: regulation of surge speed. This step is trivial, we choose the feedback linearizing control law

$$\tau_u = -F_u(v, r) + \frac{d_{11}}{m_{11}}u - K_u(u - \bar{u}), \quad K_u > 0. \tag{11.5}$$

Step 2: solution of the PFP for a kinematic point-mass. Consider the kinematic point-mass system

$$\dot{p} = \mu, \tag{11.6}$$

where the velocity vector $\mu \in \mathbb{R}^2$ is the control input. We are to design μ such that $\|\mu\| = (\bar{u}^2 + v^2)^{(1/2)}$ and the set $\{h(p)\}$ is asymptotically stable. To this end, consider the output $z = h(p)$. The derivative is

$$\dot{z} = dh_p \mu = \|dh_p\| N(p)^\top \mu. \quad (11.7)$$

Define

$$\mu(p, v) := -\left[\bar{u}\sigma(h(p))\right] N(p) + w(p, v)T(p). \quad (11.8)$$

This control input is composed of two terms. The first term is orthogonal to all level sets of h (in particular, to γ) and is responsible for making $z \rightarrow 0$, as we shall see in a moment. The second term is tangent to the level sets of h and it will be designed to guarantee that $\|\mu\| = (\bar{u}^2 + v^2)^{(1/2)}$. The function $\sigma : \mathbb{R} \rightarrow (-a, a)$, $a \in (0, 1)$, is a saturation function, chosen to be smooth, monotonically increasing, zero in zero, and such that $\lim_{|z| \rightarrow \infty} |\sigma(z)| = a$. The positive scalar a is a design parameter.

Since $\{T(p), N(p)\}$ is an orthonormal frame, substitution of (11.8) into (11.7) gives

$$\dot{z} = -\|dh_p\| \bar{u}\sigma(z).$$

Since, by assumption, $\|dh_p\| \neq 0$ on γ , by continuity of h we have that $\|dh_p\| \neq 0$ in a neighborhood of γ . Therefore, for any $\bar{u} > 0$, the set $\{p : h(p) = 0\}$ is asymptotically stable.

Next we design $w(p, v)$ such that $\|\mu(p, v)\| = (\bar{u}^2 + v^2)^{(1/2)}$. Referring to the identity (11.8), since $\{T(p), N(p)\}$ form an orthonormal frame, we have

$$\|\mu\|^2 = \bar{u}^2 \sigma^2(h(p)) + w^2(p, v).$$

Setting

$$w(p, v) := (\bar{u}^2(1 - \sigma^2(h(p))) + v^2)^{(1/2)}, \quad (11.9)$$

we have $\|\mu(p, v)\| = (\bar{u}^2 + v^2)^{(1/2)}$, as required. Note that the above expression of $w(p, v)$ is well-defined and smooth because, by construction, $|\sigma| < a \leq 1$.

In conclusion, we have the following result.

Lemma 11.1. *The feedback $\mu(p, v)$ defined in (11.8) and (11.9) makes the set $\{p \in \mathbb{R}^2 : h(p) = 0\}$ asymptotically stable for the kinematic point-mass system (11.6).*

Step 3: definition of ψ_d . We need to find a smooth function $\psi_d(p, v)$ such that

$$R_{\psi_d} \begin{bmatrix} \bar{u} \\ v \end{bmatrix} = \mu(p, v).$$

The vector on the left-hand side of the identity above has norm $(\bar{u}^2 + v^2)^{(1/2)}$ and, by construction, so does the vector on the right-hand side. Thus ψ_d is just the phase of the vector μ ,

$$\psi_d(p, v) := \text{atan2}(\mu_2(p, v), \mu_1(p, v)), \quad (11.10)$$

where atan2 is the four-quadrant arctangent function such that $\text{atan2}(\sin(\theta), \cos(\theta)) = \theta \bmod{2\pi}$.

Step 4: regulation of ψ to ψ_d . We define the output function $e = \psi - \psi_d$. Consequently

$$\dot{e} = g(p, u, v)r + f(p, u, v, \psi), \quad (11.11)$$

where

$$\begin{aligned} g(p, u, v) &= 1 - (\partial_v \psi_d(p, v))X(u), \\ f(p, u, v, \psi) &= -(\partial_p \psi_d(p, v))R_\psi \begin{bmatrix} u \\ v \end{bmatrix} - \partial_v \psi_d Y(u)v. \end{aligned}$$

Taking one more time derivative along (11.4) we get

$$\ddot{e} = g(p, u, v)(F_r(v, r) + \tau_r) + \dot{g}(\chi)r + \dot{f}(\chi).$$

Lemma 11.2. *The following identity holds:*

$$\partial_v \psi_d = -\frac{\bar{u}}{\bar{u}^2 + v^2} \left[1 + \frac{\sigma(h(p))v}{w(p, v)} \right], \quad (11.12)$$

where $w(p, v)$ is given in (11.9). Suppose that

$$1 - \frac{\bar{u}|X(\bar{u})|}{\bar{u}^2 + v^2} > 0 \quad (11.13)$$

for all $v \in \mathbb{R}$. Then, the parameter $a \in (0, 1]$ in the saturation σ can be chosen small enough that system (11.4) with input τ_r and output $e = \psi - \psi_d(p, v)$ has relative degree 2 at any point $\chi = (p, u, v, \psi, r)$ such that $u = \bar{u}$.

Remark 11.1. Condition (11.13) is met for all \bar{u} , for the ship parameters listed in Appendix 11.A and used in our simulations.

Proof. Recall that, by definition, ψ_d satisfies the following identity

$$R_{\psi_d} \begin{bmatrix} \bar{u} \\ v \end{bmatrix} = \mu,$$

from which we deduce that

$$\begin{bmatrix} \cos(\psi_d) \\ \sin(\psi_d) \end{bmatrix} = \frac{1}{\bar{u}^2 + v^2} \begin{bmatrix} \bar{u} & v \\ -v & \bar{u} \end{bmatrix} \mu.$$

Now using the identity

$$\partial_v \psi_d = \begin{bmatrix} -\sin(\psi_d) & \cos(\psi_d) \end{bmatrix} \begin{bmatrix} \partial_v \cos(\psi_d) \\ \partial_v \sin(\psi_d) \end{bmatrix},$$

and the expressions for $\cos(\psi_d)$, $\sin(\psi_d)$ found above, after some manipulation one gets

$$\partial_v \psi_d = -\frac{\bar{u}}{\bar{u}^2 + v^2} + \frac{1}{\bar{u}^2 + v^2} \mu^\top \begin{bmatrix} 0 & 1 \\ -1 & 0 \end{bmatrix} \partial_v \mu.$$

Substituting in the above the expression for μ given in (11.8), after some algebra one obtains identity (11.12).

Now we turn to the relative degree property. System (11.4) with input τ_r and output e has relative degree 2 when $u = \bar{u}$ if $1 - \partial_v \psi_d(p, v)X(\bar{u}) > 0$, or

$$1 + \frac{X(\bar{u})\bar{u}}{\bar{u}^2 + v^2} \left[1 + \frac{\sigma(h(p))v}{w(p, v)} \right] > 0.$$

Using the fact that $|\sigma(\cdot)| < a \leq 1$ and $|v/w(p, v)| < 1$, we have the inequality

$$1 + \frac{X(\bar{u})\bar{u}}{\bar{u}^2 + v^2} \left[1 + \frac{\sigma(h(p))v}{w(p, v)} \right] > 1 - \frac{|X(\bar{u})|(1+a)\bar{u}}{\bar{u}^2 + v^2}.$$

If condition (11.13) holds, there exists $a \in (0, 1]$, such that the lower bound above is greater than zero, implying that the system (11.4) with output e has relative degree 2. \square \square

Assuming that (11.13) holds, we define the smooth feedback linearizing control law

$$\begin{aligned} \tau_r = & -F_r(v, r) + \frac{1}{g(p, u, v)} \left(-\dot{f}(\chi) - \dot{g}(\chi)r \right. \\ & \left. - K_p \sin(\psi - \psi_d(p, v)) - K_d(r - \dot{\psi}_d(\chi)) \right), \end{aligned} \quad (11.14)$$

where dot on a function denotes the time derivative of the function along the vector field (11.4) with τ_u as in (11.5). With the feedback above, we obtain

$$\ddot{e} + K_p \sin(e) + K_d \dot{e} = 0.$$

This is the equation of a pendulum with friction. Thus the equilibrium $(e, \dot{e}) = (0, 0)$ is almost globally asymptotically stable. This implies that the set $\{\chi \in \mathcal{X} : \psi = \psi_d(p, v), r = \dot{\psi}_d(\chi)\}$ is stable. Moreover, this set is also asymptotically stable if the original system (11.4) with the chosen feedbacks τ_u and τ_r has no finite escape times. The absence of finite escape times will be proved in the next section.

Summary of feedback design. We have designed the following feedback control law

$$\begin{aligned} \tau_u = & -F_u(v, r) + \frac{d_{11}}{m_{11}}u - K_u(u - \bar{u}), \\ \tau_r = & -F_r(v, r) + \frac{1}{g(p, u, v)} \left(-\dot{f}(\chi) - \dot{g}(\chi)r \right. \\ & \left. - K_p \sin(\psi - \psi_d(p, v)) - K_d(r - \dot{\psi}_d(\chi)) \right), \end{aligned} \quad (11.15)$$

where $\bar{u}, K_u, K_p, K_d > 0$ are design parameters and

$$\begin{aligned} \psi_d(p, v) &= \text{atan2}(\mu_2(p, v), \mu_1(p, v)), \\ \mu(p, v) &= - \left[\bar{u}\sigma(h(p)) \right] N(p) + (\bar{u}^2(1 - \sigma^2(h(p))) + v^2)^{(1/2)} T(p). \end{aligned}$$

Finally, $\sigma(z)$ is any smooth, monotonically increasing function such that $\sigma(0) = 0$ and $\lim_{|z| \rightarrow \infty} |\sigma(z)| = a$, where $a \in (0, 1]$ is sufficiently small as in Lemma 11.2. For instance, $\sigma(z) = a \tanh(Kz)$, $K > 0$, has the desired properties.

As we discussed, in the absence of finite escape times the feedback above asymptotically stabilizes the set $\Gamma_2 := \{\chi \in \mathcal{X} : u = \bar{u}, \psi = \psi_d(p, v), r - \dot{\psi}_d(p, u, v, r) = 0\}$. In Theorem 11.2 below we show that it solves the PFP.

11.4.2 Stability analysis

As we shall see in a moment, the control design procedure developed in the previous section amounts to the simultaneous stabilization of the two nested closed sets $\Gamma_1 \subset \Gamma_2$

$$\begin{aligned}\Gamma_2 &= \{\chi \in \mathcal{X} : u = \bar{u}, \psi = \psi_d(p, v), r = \dot{\psi}_d(\chi)\}, \\ \Gamma_1 &= \{\chi \in \Gamma_2 : h(p) = 0\}.\end{aligned}$$

On Γ_2 , the ship behaves like a kinematic point-mass subject to a path following control law. On Γ_1 , the ship is on the path with a desired surge speed \bar{u} . Showing that the feedback (11.15) solves the PFP amounts to showing that Γ_1 is asymptotically stable. To prove this property, we will use Theorem 11.1.

To begin, we observe that, by design, Γ_2 is stable, and asymptotically stable if solutions starting in a neighborhood of Γ_2 have no finite escape times. Assume for a moment that this is the case. On Γ_2 , we have

$$\dot{p} = R_{\psi_d} \begin{bmatrix} \bar{u} \\ v \end{bmatrix}.$$

By the construction in step 2,

$$R_{\psi_d} \begin{bmatrix} \bar{u} \\ v \end{bmatrix} = \mu(p, v),$$

and thus

$$\dot{p} = \mu(p, v).$$

By Lemma 11.1, the set $\{h(p) = 0\}$ is asymptotically stable for the above dynamics. In the absence of finite escape times, this implies that Γ_1 is asymptotically stable relative to Γ_2 . Therefore, in order to prove asymptotic stability of Γ_1 , we will prove that the closed-loop system has no finite escape times near Γ_2 and, in addition, property (iii) of Theorem 11.1 holds. This is done in the next lemma.

Lemma 11.3. *Consider system (11.4) with the feedbacks defined in (11.15), and suppose Assumptions 11.1 and 11.2 hold. Suppose further that the desired surge speed $\bar{u} \in [0, U_{\max}]$ is such that $1 + \bar{u}X(\bar{u})/(\bar{u}^2 + v^2) \neq 0$. Then for any initial condition in a neighborhood of Γ_2 , the solution is defined for all $t \geq 0$. Moreover, if the curvature κ of γ satisfies the bound*

$$\max_{p \in \gamma} |\kappa(p)| < \frac{|Y(\bar{u})|}{|X(\bar{u})|},$$

then the closed-loop system is LUB near Γ_1 .

Proof. We first show that the closed-loop system has no finite escape times near Γ_2 . Since Γ_2 is stable, for any $\delta > 0$ there exists a positively invariant neighborhood of Γ_2 , $\mathcal{N}(\Gamma_2)$, such that all solutions originating in $\mathcal{N}(\Gamma_2)$ satisfy $|u(t) - \bar{u}| < \delta$, $|\psi(t) - \psi_d(p(t), v(t))| < \delta$, $|\dot{r}(t) - \dot{\psi}_d(\chi(t))| < \delta$. From now on, consider an arbitrary solution $\chi(t)$ originating in $\mathcal{N}(\Gamma_2)$. Since $u - \bar{u}$ is bounded, u has no finite escape

times. Since $\psi \in \mathbb{S}^1$, a compact set, the same holds for ψ . Recalling that on Γ_2 we have $\dot{p} = \mu(p, v)$, we may write

$$\begin{aligned} \dot{p} &= \mu(p, v) + \left(R_\psi \begin{bmatrix} u \\ v \end{bmatrix} - R_{\psi_d} \begin{bmatrix} \bar{u} \\ v \end{bmatrix} \right) \\ &= R_{\psi - \psi_d} \mu(p, v) + R_\psi \begin{bmatrix} u - \bar{u} \\ 0 \end{bmatrix}. \end{aligned}$$

Letting, as in the previous section, $z = h(p)$, we have

$$\begin{aligned} \dot{z} &= -\|dh_p\| \left(\bar{u}\sigma(z)N^\top R_{\psi - \psi_d}N - N^\top R_\psi \begin{bmatrix} u - \bar{u} \\ 0 \end{bmatrix} \right) \\ &= -\|dh_p\| \left(\bar{u}\sigma(z)\cos(\psi - \psi_d) - N^\top R_\psi \begin{bmatrix} u - \bar{u} \\ 0 \end{bmatrix} \right). \end{aligned}$$

Using the fact that $z\sigma(z) \geq 0$, $\cos(\psi - \psi_d) > \cos(\delta)$, and $|u - \bar{u}| < \delta$, we deduce the following inequality

$$z\dot{z} \leq -\|dh_p\||z|(\bar{u}\sigma(z)\cos(\delta) - \delta). \quad (11.16)$$

Pick δ small enough that $\delta/(\bar{u}\cos(\delta)) < 1$, then we see that $z\dot{z} \leq 0$ whenever $z > \rho(\delta) := \sigma^{-1}(\delta/\bar{u}\cos(\delta))$. This implies that all trajectories of the z -dynamics are bounded and, moreover, the interval $\{z : |z| < \rho(\delta)\}$ is positively invariant for the z -dynamics. Recalling that $z = h(p)$ and that h is proper, we deduce that all trajectories of the p subsystem are bounded and hence have no finite escape times. Moreover, the neighborhood of Γ_1 defined as $\{\chi \in \mathcal{N}(\Gamma_2) : |h(p)| < \rho(\delta)\}$, is positively invariant. Since $\rho(\cdot)$ is a class- \mathcal{K} function, Γ_1 is stable. In the rest of the proof we denote

$$\mathcal{N}(\Gamma_1) = \{\chi \in \Gamma_2 : |h(p)| < \rho(\delta)\}.$$

By the construction above, for any $\delta > 0$ this set is a neighborhood of Γ_1 and trajectories originating in it satisfy the bounds

$$|u - \bar{u}| < \delta, |\psi - \psi_d(p, v)| < \delta, |\dot{r} - \dot{\psi}_d(\chi)| < \delta, |h(p)| < \rho(\delta).$$

We now turn our attention to the v -subsystem. For convenience, denote $\alpha(p, v) := \partial_v \psi_d$, whose expression is given in Lemma 11.2. On $\mathcal{N}(\Gamma_2)$, \dot{e} is bounded. Using (11.11) and Lemma 11.2, we have

$$r = \frac{1}{1 - \alpha(p, v)X(u)} \left(\alpha(p, v)Y(u)v + (\partial_p \psi_d)R_\psi \begin{bmatrix} u \\ v \end{bmatrix} + \dot{e} \right),$$

where \dot{e} is bounded. Since condition (11.13) is assumed to hold, the quantity $1 - \alpha(p, v)X(\bar{u}) > 0$. Therefore, for small enough $\delta > 0$, the quantity $1 - \alpha(p, v)X(u) > 0$ as well, implying that r above is well defined. Substituting the expression for r in the \dot{v} equation in (11.4) and rearranging terms, we get

$$\dot{v} = \frac{1}{1 - \alpha(p, v)X(u)} \left(Y(u)v + X(u) \left((\partial_p \psi_d)R_\psi \begin{bmatrix} u \\ v \end{bmatrix} + \dot{e} \right) \right).$$

We argue that $|\dot{v}| \leq C_1 + C_2|v|$, for suitable $C_1, C_2 > 0$. Indeed, on $\mathcal{N}(\Gamma_2)$ the coefficient in front of the parenthesis is upper bounded by a constant. The term $Y(u)v$ is linear in v and u is bounded. The term $\partial_p\psi_d$ is a continuous function of (p, v) . Since we have established that $p(t)$ is bounded, $\partial_p\psi_d$ is bounded with respect to p . Moreover, using the definition of ψ_d and μ it is possible to show that $\sup_v |\partial_p\psi_d| < \infty$. Thus the term $X(u)\partial_p\psi_d R_\psi[u \ v]^\top$ grows linearly with v , proving the claim. Since $|\dot{v}|$ grows linearly with v , the v subsystem has no finite escape times. Finally, concerning $r(t)$, we have expressed it as function of $(p(t), u(t), v(t), \psi(t), \dot{e}(t))$, signals that are defined for all $t \geq 0$, and therefore $r(t)$ has no finite escape times. In conclusion, all solutions originating on $\mathcal{N}(\Gamma_2)$ are defined for all $t \geq 0$.

Now we prove that the closed-loop system is LUB near Γ_1 . Consider a generic solution $\chi(t)$ originating in $\mathcal{N}(\Gamma_1)$. Since $|h(p(t))| < \rho(\delta)$, and since h is proper, $\|p(t)\|$ has a bound independent of the initial condition in $\mathcal{N}(\Gamma_1)$. Consider now the \dot{v} equation above, and in particular the term $(\partial_p\psi_d)R_\psi[u \ v]^\top$. On Γ_2 , this term reduces to

$$(\partial_p\psi_d)R_{\psi_d} \begin{bmatrix} \bar{u} \\ v \end{bmatrix} = (\partial_p\psi_d)\mu(p, v).$$

We show in Appendix 11.B that

$$(\partial_p\psi_d)\mu(p, v) = -\kappa(p)w(p, v) + \Delta_1(p, v),$$

where $\kappa(p)$ is the curvature at p of the level set of h through p , $w(p, v)$ is defined in (11.9), and $\Delta_1(p, v)$ is a smooth function that vanishes on γ and is bounded with respect to v . Since $p(t)$ has a uniform bound over initial conditions in $\mathcal{N}(\Gamma_1)$, so does $\Delta_1(p(t), v(t))$. Back to the \dot{v} equation, using the identity

$$R_\psi \begin{bmatrix} u \\ v \end{bmatrix} = R_{\psi_d} \begin{bmatrix} \bar{u} \\ v \end{bmatrix} + (R_{\psi-\psi_d} - I) \begin{bmatrix} \bar{u} \\ v \end{bmatrix} + R_\psi \begin{bmatrix} u - \bar{u} \\ 0 \end{bmatrix},$$

we have

$$\begin{aligned} \dot{v} = & \frac{1}{1 - \alpha X} \left(Y(u)v - w(p, v)X(u)\kappa(p) \right. \\ & \left. + X(u)(\partial_p\psi_d)(R_{\psi-\psi_d} - I) \begin{bmatrix} \bar{u} \\ v \end{bmatrix} + \Delta_2(\chi) \right), \end{aligned}$$

where $\Delta_2(\chi) = X(u)(\Delta_1(p, v) + \partial_p\psi_d(R_\psi[u - \bar{u} \ 0]^\top) + \dot{e})$ is uniformly bounded along solutions originating in $\mathcal{N}(\Gamma_1)$. We now derive two bounds valid on the positively invariant set $\mathcal{N}(\Gamma_1)$. First, the boundedness of p yields

$$|w(p, v)X(u)\kappa(p)| \leq C_1 + |X(u)||\kappa||v|$$

for some $C_1 > 0$. Also, it is possible to show that $\|\partial_p\psi_d(p, v)\|$ is bounded. Then, since $|\psi - \psi_d| < \delta$, we have the second bound

$$|X(u)(\partial_p\psi_d)(R_{\psi-\psi_d} - I)[\bar{u} \ v]^\top| \leq |X(u)|\delta|v| + C_2,$$

for some $C_2 > 0$. Recall that, by Assumption 11.1, $\bar{u} \in [0, U_{\max}]$, so that $Y(\bar{u}) < 0$ and for sufficiently small δ , $Y(u) < 0$ as well. Define the Lyapunov function $V =$

$v^2/2$, then

$$\begin{aligned} \dot{V} \leq & \frac{-1}{1-\alpha X} \left(|Y(u)| - |X(u)|(|\kappa| + \delta) \right) v^2 \\ & + \left((C_1 + C_2) + \sup_{x \in \mathcal{N}(\Gamma_1)} \Delta_2(x) \right) |v|. \end{aligned}$$

By assumption, $|Y(\bar{u})| - |X(\bar{u})|\kappa(p) > 0$ for all $p \in \gamma$. Since κ is a continuous function and since, on $\mathcal{N}(\Gamma_1)$, $|u - \bar{u}| < \delta$ and $|h(p)| < \rho(\delta)$, we have that for small enough δ ,

$$|Y(u)| - |X(u)|(|\kappa(p)| + \delta) > 0.$$

Thus $v(t)$ is uniformly bounded. Since r is a continuous function of (p, u, v, ψ, \dot{e}) , r is uniformly bounded as well. This proves the LUB property near Γ_1 . \square

Application of Theorem 11.1 gives the following result.

Theorem 11.2. *Consider system (11.4) with the feedbacks defined in (11.15), suppose that Assumptions 11.1 and 11.2 hold, and assume that the desired surge speed $\bar{u} \in [0, U_{\max}]$ is chosen such that condition (11.13) holds. If the curvature κ of γ satisfies the bound*

$$\max_{p \in \gamma} |\kappa(p)| < \frac{|Y(\bar{u})|}{|X(\bar{u})|},$$

then Γ_1 and Γ_2 are asymptotically stable, implying that feedback (11.15) solves the PFP.

Remark 11.2. *It is interesting to note that in [103, Theorem 1], the authors present a stability result for a path following control law with a similar, but more restrictive, curvature bound, $\max |\kappa| < (1/3)|Y(\bar{u})/X(\bar{u})|$ compared to that in Theorem 11.2.*

11.5 The case of non-zero ocean current

The model of the system in this case is given by (11.2). In this section we first carry out the control design of steps 1-4 and then the stability analysis for $\mathbf{V}_c \neq \mathbf{0}$.

11.5.1 Control design

Step 1: regulation of surge speed. The dynamics of u in (11.2) is affected by the unknown disturbance $\boldsymbol{\theta}_u$. We choose to reject the disturbance using an adaptive controller. Define $\hat{\boldsymbol{\theta}}_u$ to be the adaptive state and $e_u \triangleq u - \bar{u}$. We choose the following feedback linearizing controller and adaptive law

$$\begin{aligned} \tau_u &= F_u(\cdot) - \boldsymbol{\phi}(\psi, r)^T \boldsymbol{\theta}_u - K_u (u - \bar{u}) \\ \dot{\hat{\boldsymbol{\theta}}}_u &= \Lambda K_u e_u \boldsymbol{\phi}_u^T(\psi, r) \end{aligned} \tag{11.17}$$

where $\Lambda = \Lambda^T > 0$. The following result is straightforward.

Lemma 11.4. *The feedback controller and adaptive law (11.17) make $u = \bar{u}$ and $\hat{\boldsymbol{\theta}}_u = \boldsymbol{\theta}_u$ globally stable and in particular $u \rightarrow \bar{u}$ asymptotically.*

Step 2: solution of the PFP for a kinematic point-mass. This step is the same as for the case with $\mathbf{V}_c = \mathbf{0}$. We can choose μ as in (11.8).

Step 3: definition of ψ_d . This step is the same as for the case with $\mathbf{V}_c = \mathbf{0}$. We can choose ψ_d as in (11.10).

Step 4: regulation of ψ to ψ_d . Consider the yaw dynamics

$$\begin{aligned}\dot{\psi} &= r \\ \dot{r} &= F_r(u, v, r) + \phi_r^T(u, v, r, \psi)\boldsymbol{\theta}_r + \tau_r.\end{aligned}\tag{11.18}$$

Consider also the expression of ψ_d in (11.10). Since ψ_d depends on ψ, u, v, r , it is easy to verify that $\dot{\psi}_d, \ddot{\psi}_d$ depend on $\boldsymbol{\theta}_u, \boldsymbol{\theta}_r, \boldsymbol{\theta}_{v_1}, \boldsymbol{\theta}_{v_2}$. Then the same approach as in Step 4 in Section 11.4.1, i.e., defining $e \triangleq \psi - \psi_d$, leads to a complicated control design phase due to the coupling of several unknown terms in the error dynamics \ddot{e} . Therefore, we take a different approach and we start defining $e_\psi \triangleq \psi - \psi_d$. Then

$$\begin{aligned}\dot{e}_\psi &= r - \dot{\psi}_d \\ &= \frac{r}{C(p, u, v, \psi)} - r_d + \delta_{\psi_d}(p, u, v, \psi, r)\tilde{\boldsymbol{\theta}}_r\end{aligned}\tag{11.19}$$

where

$$\begin{aligned}r_d &= \frac{1}{C(\cdot)} \left(\frac{\partial \psi_d}{\partial v} \left(Y(u)v + \phi_{v_1}^T(u, v, \psi)\hat{\boldsymbol{\theta}}_r \right) + \frac{\partial \psi_d}{\partial p} \dot{p} \right) \\ C(\cdot) &= 1 - \frac{\partial \psi_d}{\partial v} \left(X(u) + S\phi_{v_1}^T(\psi)\hat{\boldsymbol{\theta}}_r \right) \\ \delta_{\psi_d}(\cdot) &= - \frac{\partial \psi_d}{\partial v} \left(\phi_{v_1}^T(\cdot) + \phi_{v_2}^T(\cdot)S \right)\end{aligned}\tag{11.20}$$

and $S = [I_{2 \times 2}, \mathbf{0}_{2 \times 3}]$. The term r_d depends only on known terms and it is well defined only if $C(\cdot) \neq 0$. We consider the following assumption to hold

Assumption 11.3. For the term $C(\cdot)$ it holds that

$$C(\cdot) = 1 - \frac{\partial \psi_d}{\partial v} \left(X(u) + S\phi_{v_1}^T(\psi)\hat{\boldsymbol{\theta}}_r \right) > 0.\tag{11.21}$$

Remark 11.3. Condition (11.21) depends on the ship parameters and it is met for the ship parameters listed in Appendix 11.A.

Now define $e_r = r - r_d$, its derivative is

$$\begin{aligned}\dot{e}_r &= \frac{\partial r_d}{\partial p} \dot{p} + \frac{\partial r_d}{\partial \psi} r - K_u \frac{\partial r_d}{\partial u} (u - \bar{u}) \\ &\quad + \frac{\partial r_d}{\partial v} \left(X(u)r + Y(u)v + \phi_{v_1}^T(\cdot)\hat{\boldsymbol{\theta}}_r + \phi_{v_2}^T(\cdot)\hat{\boldsymbol{\theta}}_r S \right) \\ &\quad + \delta_r(p, \psi, u, v, r)\end{aligned}$$

where

$$\delta_r(\cdot) = \frac{\partial r_d}{\partial u} \phi_u^T(\cdot)S + \frac{\partial r_d}{\partial v} \left(\phi_{v_1}^T(\cdot) + \phi_{v_2}^T(\cdot)S \right) + \phi_r^T(\cdot).$$

In order to stabilize e_ψ and e_r to the origin, we define a feedback linearizing controller using r_d and the known terms of \dot{r}_d together with an adaptive law for the state $\hat{\theta}_r$. Choose

$$\begin{aligned} \tau_r = & -F_r(\cdot) - \phi_r^T(\cdot)\hat{\theta}_r - K_\psi C(\cdot)\sin(e_\psi) - K_r e_r \\ & \frac{\partial r_d}{\partial p}\dot{p} + \frac{\partial r_d}{\partial \psi}r - K_u \frac{\partial r_d}{\partial u}(u - \bar{u}) \\ & + \frac{\partial r_d}{\partial v}\left(X(u)r + Y(u)v + \phi_{v_1}^T(\cdot)\hat{\theta}_r + \phi_{v_2}^T(\cdot)\hat{\theta}_r S r\right) \\ \dot{\hat{\theta}}_r = & -\Gamma \delta P e \end{aligned} \quad (11.22)$$

where $e = [e_\psi, e_r]^T$, $\delta = [\delta_\psi(\cdot), \delta_r(\cdot)]^T$ and $\Gamma = \Gamma^T > 0$. The following result holds

Lemma 11.5. *Consider the yaw dynamics (11.18). The feedback linearizing controller together with the adaptive law (11.22) make e_ψ, e_r asymptotically stable at the origin and the state $\tilde{\theta}_r$ is bounded.*

A sketch of the proof of Lemma 11.5 is presented here.

Proof. Substituting (11.22) in (11.18) we obtain

$$\underbrace{\begin{bmatrix} \dot{e}_\psi \\ \dot{e}_r \end{bmatrix}}_e = \begin{bmatrix} 0 & C(\cdot) \\ -K_\psi C(\cdot)\frac{\sin(e_\psi)}{e_\psi} & -K_r \end{bmatrix} \begin{bmatrix} e_\psi \\ e_r \end{bmatrix} + \underbrace{\begin{bmatrix} \delta_{\psi_d}(\cdot) \\ \delta_r(\cdot) \end{bmatrix}}_\delta \tilde{\theta}_r. \quad (11.23)$$

Note that for $e_\psi \in (-\pi/2, \pi/2)$ we have $\frac{\sin(e_\psi)}{e_\psi} > 0$. Since $\psi_d \in (-\pi/2, \pi/2)$ by design, assume $\psi|_{t=0} \in (-\pi/2, \pi/2)$. Now consider the case $\tilde{\theta}_r = \mathbf{0}$. Choose

$$P = \begin{bmatrix} \frac{k_\psi(\bar{C} + \epsilon)}{k_r} & \frac{1}{2} \\ \frac{1}{2} & \frac{\bar{C} + \epsilon}{k_r} \end{bmatrix}$$

where $\bar{C} > C(\cdot)$ and $\epsilon > 0$. Then defining

$$V = \frac{1}{2} e^T P e$$

we obtain

$$\dot{V} = -e^T Q e \leq 0$$

where

$$Q = \begin{bmatrix} k_\psi \frac{\bar{C}}{2} & \frac{k_r}{2} \\ \frac{k_r}{2} & \epsilon \end{bmatrix}.$$

Then choose

$$W = V + \tilde{\theta}_r^T \gamma^{-1} \tilde{\theta}_r. \quad (11.24)$$

The choice for $\dot{\hat{\theta}}_r$ implies

$$\dot{W} \leq -\lambda_Q^{\min} \|e\|^2 \leq 0 \quad \psi|_{t=0} \in (-\pi/2, \pi/2)$$

where $\lambda_Q^{\min} > 0$ is the smallest eigenvalue of Q . □

Remark 11.4. Lemma 11.5 proves that for any $|\psi|_{t_0} < \pi/2$ we have $|\psi(t)| < \pi/2 \forall t > 0$. Since the set $(-\pi/2, \pi/2)$ almost cover the unit sphere \mathbb{S} , we can say that the feedback linearizing controlelr together with the adaptive law (11.22) almost globally stabilizes $\psi = \psi_d$ and $r = r_d$.

Summary of feedback design. We have designed the following feedback control laws and adaptive laws

$$\begin{aligned}
 \tau_u &= F_u(\cdot) - \phi(\psi, r)^T \hat{\theta}_u - K_u(u - \bar{u}) \\
 \dot{\hat{\theta}}_u &= \Lambda K_u e_u \phi_u^T(\psi, r) \\
 \tau_r &= -F_r(\cdot) - \phi_r^T(\cdot) \hat{\theta}_r - K_\psi C(\cdot) \sin(e_\psi) - K_r e_r \\
 &\quad + \frac{\partial r_d}{\partial p} \dot{p} + \frac{\partial r_d}{\partial \psi} r - K_u \frac{\partial r_d}{\partial u} (u - \bar{u}) \\
 &\quad + \frac{\partial r_d}{\partial v} \left(X(u)r + Y(u)v + \phi_{v_1}^T(\cdot) \hat{\theta}_r + \phi_{v_2}^T(\cdot) \hat{\theta}_r S r \right) \\
 \dot{\hat{\theta}}_r &= -\Gamma \delta P e
 \end{aligned} \tag{11.25}$$

where $e_u = u - \bar{u}$, $e_\psi = \psi - \psi_d$, $e_r = r - r_d$, ψ_d is given in (11.10) and r_d in (11.20).

From the discussion above, we have that the feedback and the adaptive law (11.25) asymptotically stabilizes the set $\Gamma_2 := \{\chi \in \mathcal{X} : u = \bar{u}, \psi = \psi_d(p, v), r - r_d(p, u, v, r) = 0\}$. In Theorem 11.3 below, we show that (11.25) solves the PFP for the marine vehicle described by (11.1) when $\mathbf{V}_c \neq \mathbf{0}$.

11.5.2 Stability analysis

As in Section 11.4.2, the control procedure presented above aims to stabilize the two nested sets $\Gamma_1 \subset \Gamma_2$ simultaneously. Thus, showing that Γ_1 is asymptotically stable is equivalent to showing that the feedback (11.25) solves the PFP.

The proof follows along the lines of the stability analysis presented in Section 11.4.2. Consequently, we have to prove that the closed-loop system has no finite escape time and that property (iii) of Theorem 11.1 holds. Due to the presence of the unknown disturbances $\theta_u, \theta_r, \theta_{v_1}, \theta_{v_2}$ we cannot apply Lemma 11.3. However, we can modify Lemma 11.3 as follows

Lemma 11.6. Consider system (11.2) with the feedbacks and the adaptive laws defined in (11.25), and suppose Assumptions 11.1 and 11.3 hold. Consider the sublevel set $\Gamma_W \triangleq \{\mathcal{X} | W \leq c\}$, where W is given in (11.24). Then for any initial condition in $\mathcal{N}(\Gamma_2) \cap \Gamma_W$, the solution is defined for all $t \geq 0$. Moreover, assume that the curvature κ of γ satisfies the bound

$$\max_{p \in \gamma} |\kappa(p)| < \frac{|Y(\bar{u}) + K_3 V_{\max}|}{|(X(\bar{u}) + \phi_{v_2} V_{\max})|},$$

where K_3 is given in the Appendix 11.A. Then the closed-loop system is LUB near Γ_1 .

Proof. The proof of Lemma 11.6 follows along the lines of the proof of Lemma 11.3. However, it presents some differences due to the presence of the unknown disturbances $\theta_u, \theta_r, \theta_{v_1}, \theta_{v_2}$. The boundedness of the states u, ψ, r originating in $\mathcal{N}(\Gamma_1)$ follows in the same way as in Lemma 11.6. Now we draw our attention on v . First rewrite

$$r = \frac{1}{1 - \partial_v \psi_d (X(u) + \phi_{v_2}^T(\psi)\theta_u)} [\partial_v \psi_d Y(u)v + \partial_v \psi_d \phi_{v_1}^T(u, v, \psi)\theta_r + \partial_p \psi_d R_\psi \begin{bmatrix} u \\ v \end{bmatrix} + \dot{e}_\psi].$$

The state r is always well defined according to Assumption 11.3. Substituting in the expression for \dot{v} we obtain

$$\dot{v} = \frac{1}{1 - \partial_v \psi_d (X(u) + \phi_{v_2}^T(\psi)\theta_u)} \left(Y(u)v + \phi_{v_1}^T(\cdot)\theta_r + (X(u) + \phi_{v_2}^T(\psi)\theta_u) \left[\partial_p \psi_d R_\psi \begin{bmatrix} u \\ v \end{bmatrix} + \dot{e}_\psi \right] \right).$$

The coefficients of v are bounded in $\mathcal{N}(\Gamma_2)$. Furthermore, also the terms which do not contain v are bounded. Attention has to be paid on the state \dot{e}_r which, according to Lemma 11.5, is bounded bounded for any $\mathcal{X} \in \mathcal{N}(\Gamma_2) \cap \Gamma_W$. In fact, from Lemma 11.5 we have that $e_\psi, e_r \rightarrow 0$, while $\hat{\theta}_r$ is bounded. Then, it is easy to check that $W(t) \leq W(t_0) \leq c$ and that $\hat{\theta}_r \in \mathcal{N}(\Gamma_2) \cap \Gamma_W$. Thus, using the same approach as in the proof for Lemma 11.3, it is easy to check that $|\dot{v} \leq C_1 + C_2|v|$ and that the closed-loop system is LUB in $\mathcal{N}(\Gamma_1)$. Note that now the uniformly boundedness of v follow on the new condition for the curvature

$$\max_{p \in \gamma} |\kappa(p)| < \frac{|Y(\bar{u}) + K_3 V_{\max}|}{|(X(\bar{u}) + \bar{\phi}_{v_2} V_{\max})|},$$

which depends also on the ocean current. □

Applying Theorem 11.1 gives the following result

Theorem 11.3. *Consider system (11.2) with the feedbacks and the adaptive laws defined in (11.25), and suppose Assumptions 11.1 and 11.3 hold. Consider the sublevel set $\Gamma_W = \{\mathcal{X} | W \leq c\}$, where W is given in (11.24). Then for any initial condition in $\mathcal{N}(\Gamma_2) \cap \Gamma_W$, the solution is defined for all $t \geq 0$. Moreover, assume that the curvature κ of γ satisfies the bound*

$$\max_{p \in \gamma} |\kappa(p)| < \frac{|Y(\bar{u}) + K_3 V_{\max}|}{|(X(\bar{u}) + \bar{\phi}_{v_2} V_{\max})|},$$

where K_3 is given in the Appendix 11.A. Then Γ_1 and Γ_2 are asymptotically stable, implying that feedback (11.25) solves the PFP.

11.6 Simulation results

In this section two case studies are presented to verify the proposed path following strategy. We first consider the case where there is no disturbance affecting the system. We then consider a non-zero ocean current affecting the motion of the vessel. For this purpose we consider a supply vessel described by the model (11.4) with the function descriptions and model parameters given in Appendix 11.A.

11.6.1 The case of zero ocean current

In this case study the goal is to follow a Cassini oval. This implies that $h(p) \triangleq (p_x^2 + p_y^2)^2 - 2a^2(p_x^2 - p_y^2) + a^4 - b^4$ and that the path is implicitly described by

$$\gamma = \{p : (p_x^2 + p_y^2)^2 - 2a^2(p_x^2 - p_y^2) + a^4 - b^4 = 0\}.$$

where in this case study $a = 22.5$ [m] and $b = 24.9$ [m]. This results in a curve for which the maximum curvature $\max_{p \in \gamma} |\kappa(p)| = 0.0785$ and with a desired velocity $\bar{u} = 2$ [m/s] the ratio $|Y(\bar{u})|/|X(\bar{u})| = 0.2483$. Note that this curve satisfies the curvature condition of Theorem 11.2 showing that this is not a very restrictive condition, since it allows a ship with a length of approximately 83 meters to follow a curve whose diameter (the maximum distance between any two of its points) is approximately 70 metres. The saturation function is set to $\sigma(h(p)) = 2/\pi \tan^{-1}(\alpha h(p))$, where α is a parameter that can be used to tune the slope of the saturation function. In this case the magnitude of $h(p)$ is large, therefore α needs to be small to make the saturation effective close to the path and we choose $\alpha = 10^{-4}$. The initial conditions are given by $\chi_0 := ([15, 45], 0, 0, -2/3\pi, 0)$ and the controller gains from (11.15) are given by $K_u = 1$, $K_p = 30$, and $K_d = 5$. The trajectory of the ship and the desired oval can be seen in Figure 11.2. From Figure 11.2 we can clearly see convergence to the desired oval and from the superimposed ships it can be seen that the heading of the vessel is not tangent to the oval. Its velocity vector, on the other hand, is tangent to the path. From the plot of the sway velocity in Figure 11.3 it can be seen that this motion induces quite large sway velocities relative to the desired surge velocity $\bar{u} = 2$ [m/s]. The value of $h(p)$ is plotted in Figure 11.4 which shows that $h(p)$ is driven to zero as the ship converges to the path, showing that the ship is able to track the specified Cassini oval in accordance with the theoretical analysis.

11.6.2 The case of non-zero ocean current

In this case study we consider the same Cassini oval as in the previous section. The maximum curvature is again $\max_{p \in \gamma} |\kappa(p)| = 0.0785$. Given a desired velocity $\bar{u} = 2$ [m/s] the ratio

$$\max_{p \in \gamma} |\kappa(p)| < \frac{|Y(\bar{u}) + K_3 V_{\max}|}{|(X(\bar{u}) + \bar{\phi}_{v_2} V_{\max})|} = 0.3287.$$

The condition required by Theorem 11.3 is thus respected. Note that also in this case this condition is not restrictive since the dimensions of the path are

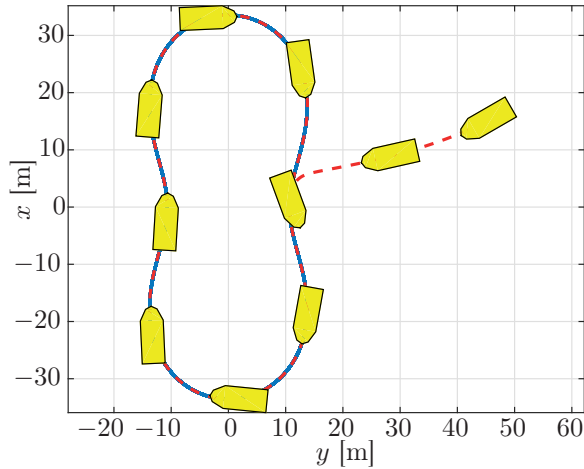


Figure 11.2: Path of the ship and the Cassini oval (the ship is not to scale).

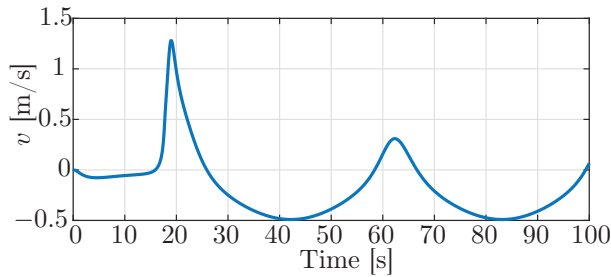


Figure 11.3: Sway velocity of the ship.

the same as the section above and they are very small compared to a path that a real vehicle would follow in a real application. We consider an ocean current $\mathbf{V}_c = [0.1, -0.2]$ [m/s] affecting the system. Therefore, we consider the model (11.2) together with the feedback law and the adaptive law given in (11.25). The saturation function is set to $\sigma(h(p)) = 2/\pi \tan^{-1}(\alpha h(p))$, where $\alpha = 10^{-4}$. The controller gains from (11.25) are given by $K_u = 1$, $K_p = 30$, $K_d = 5$. The initial conditions are given by $\chi_0 := ([15, 45], 0, 0, -2/3\pi, 0)$.

The trajectory of the ship and the desired oval can be seen in Figure 11.5. The vectors in the figure give an idea of the direction of the ocean current. Figure 11.5 shows that the vehicle converges to the path. Note that the heading of the vehicle is not tangent to the oval. This is normal since the vehicle is under-actuated and there is also a disturbance affecting its motion. Figure 11.6 gives the plot of the sway velocity. Also in this case we see that this motion induces quite large sway velocities relative to the desired surge velocity $\bar{u} = 2$ [m/s]. Figure 11.7 shows that $h(p)$ is driven to zero. This implies that the vehicle converges and constraints its

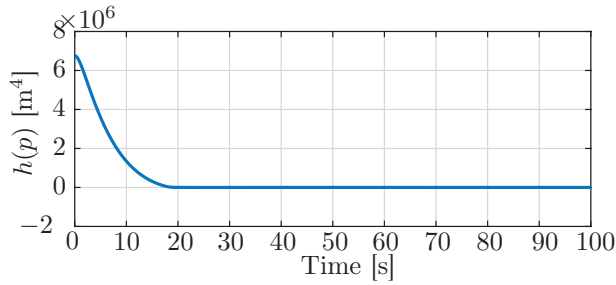


Figure 11.4: Magnitude of $h(p)$ as the vessel converges to the path.

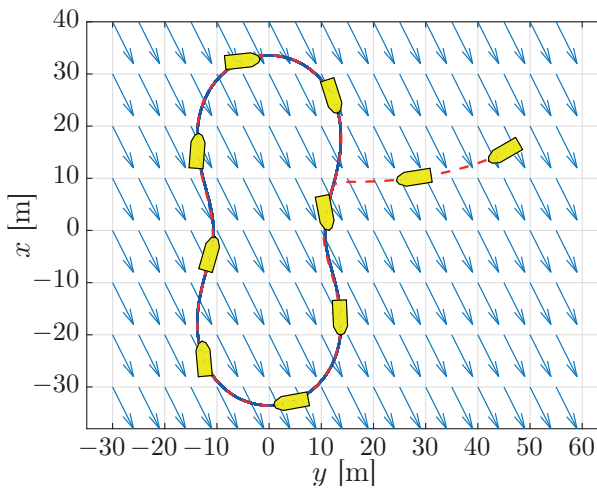


Figure 11.5: Case of non-zero ocean current. The path of the ship and the Cassini oval (the ship and the ocean current vectors are not to scale).

motion along the Cassini oval. This is in accordance with the theoretical analysis.

11.7 Conclusions

In this chapter we presented a methodology to design path following controllers for a class of under-actuated marine vessels. The methodology allows one to migrate a path following controller designed for a point-mass to one that is guaranteed to work for the under-actuated vessel. Both the cases of zero and non-zero ocean current have been considered. For simplicity, we assumed the curve to be Jordan.

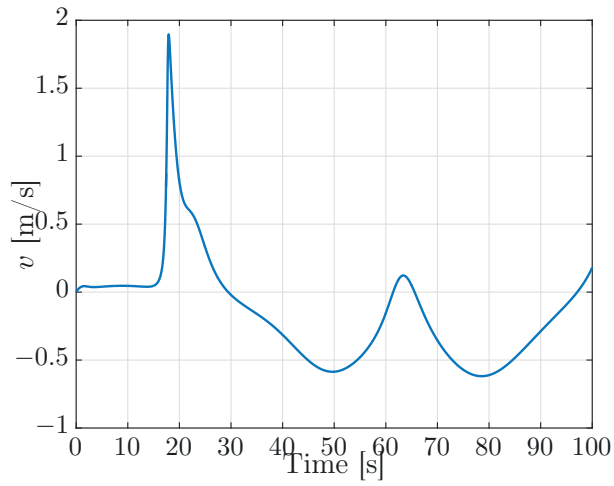


Figure 11.6: Case of non-zero ocean current. Sway velocity of the ship.

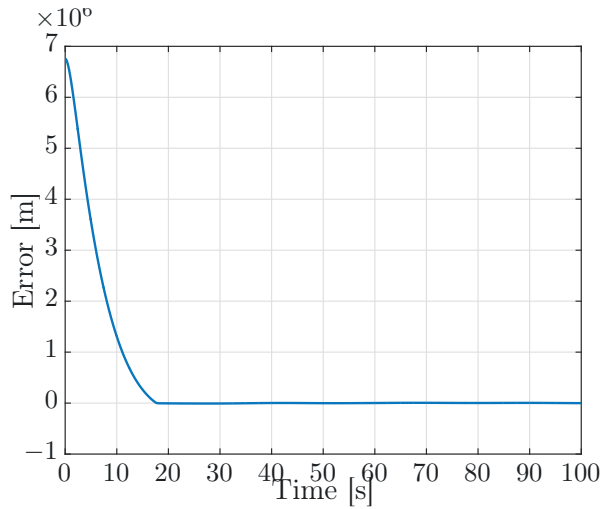


Figure 11.7: Case of non-zero ocean current. Magnitude of $h(p)$ as the vessel converges to the path.

11.A Functions used in the model

The functions F_u , $X(u)$, $Y(u)$, and F_r are given by: The functions $X(u_r, u_c)$, $Y(u_r)$, F_u , $F_r(u, v, r)$, $\phi_u(\psi, r)$, $\phi_v(u, v, r, \psi)$, and $\phi_r(u, v, r, \psi)$ are given by:

$$\begin{aligned}
 X(u) &\triangleq \frac{m_{33}(-d_{23} - m_{11}u) + m_{23}(d_{33} + m_{23}u)}{m_{22}m_{33} - m_{23}^2} \\
 Y(u) &\triangleq \frac{m_{23}d_{32} - m_{33}d_{22} + m_{23}(m_{22}^A - m_{11}^A)u}{m_{22}m_{33} - m_{23}^2} \\
 F_u &\triangleq \frac{1}{m_{11}}(m_{22}v + m_{23}r)r, \\
 F_r(u, v, r) &\triangleq \frac{m_{22}(m_{11}uv - (m_{22}v - m_{23}r)u - d_{32}v - d_{33}r)}{m_{22}m_{33} - m_{23}^2} - \frac{m_{23}(-m_{11}ur - d_{22}v - d_{23}r)}{m_{22}m_{33} - m_{23}^2} \\
 \phi_u(\psi, r) &\triangleq \begin{bmatrix} \frac{d_{11}}{m_{11}} \cos(\psi) - \frac{m_{11}^A - m_{22}^A}{m_{11}} r \sin(\psi) \\ \frac{d_{11}}{m_{11}} \sin(\psi) + \frac{m_{11}^A - m_{22}^A}{m_{11}} r \cos(\psi) \end{bmatrix} \\
 \phi_r(u, v, \psi, r) &\triangleq \begin{bmatrix} a_1 \cos(\psi) - a_2 \sin(\psi) \\ a_1 \sin(\psi) + a_2 \cos(\psi) \\ -\frac{m_{22}(m_{11}^A - m_{22}^A)}{m_{22}m_{33} - m_{23}^2} \sin(\psi) \cos(\psi) \\ \frac{m_{22}(m_{11}^A - m_{22}^A)}{m_{22}m_{33} - m_{23}^2} \sin(\psi) \cos(\psi) \\ \frac{m_{22}(m_{11}^A - m_{22}^A)}{m_{22}m_{33} - m_{23}^2} (1 - 2 \sin^2(\psi)) \end{bmatrix} \\
 \phi_{v1}(u, v, \psi) &\triangleq \begin{bmatrix} b_1 \cos(\psi) - b_2 \sin(\psi) \\ b_1 \sin(\psi) + b_2 \cos(\psi) \\ \frac{m_{23}(m_{11}^A - m_{22}^A)}{m_{22}m_{33} - m_{23}^2} \sin(\psi) \cos(\psi) \\ -\frac{m_{23}(m_{11}^A - m_{22}^A)}{m_{22}m_{33} - m_{23}^2} \sin(\psi) \cos(\psi) \\ -\frac{m_{23}(m_{11}^A - m_{22}^A)}{m_{22}m_{33} - m_{23}^2} (1 - 2 \sin^2(\psi)) \end{bmatrix} \\
 \phi_{v2} &\triangleq \frac{(m_{33}m_{11}^A + m_{23}(m_{22}^A - m_{23}^A))}{m_{22}m_{33} - m_{23}^2} \begin{bmatrix} \cos(\psi) \\ \sin(\psi) \end{bmatrix}
 \end{aligned}$$

where

$$\begin{aligned}
 a_1 &\triangleq -\frac{m_{22}((m_{11}^A - m_{22}^A)v + (m_{23}^A - m_{22}^A)r) + m_{23}m_{11}^A r}{m_{22}m_{33} - m_{23}^2} \\
 a_2 &\triangleq \frac{m_{22}(d_{32} - (m_{11}^A - m_{22}^A)u) - m_{23}d_{22}}{m_{22}m_{33} - m_{23}^2} \\
 b_1 &\triangleq -\frac{m_{23}(m_{22}^A - m_{11}^A)v}{m_{22}m_{33} - m_{23}^2} \\
 b_2 &\triangleq \frac{m_{33}d_{22} - m_{23}d_{32} - m_{23}(m_{22}^A - m_{11}^A)u}{m_{22}m_{33} - m_{23}^2}
 \end{aligned}$$

The numerical expressions for the matrices \mathbf{M} , \mathbf{D} , and \mathbf{B} used in the simulations are

$$\mathbf{M} \triangleq \begin{bmatrix} 7.22e6 & 0 & 0 \\ 0 & 1.21e7 & -5.6446e7 \\ 0 & -5.6446e7 & 4.9044e9 \end{bmatrix},$$

$$\mathbf{D} \triangleq \begin{bmatrix} 9.507e4 & 0 & 0 \\ 0 & 4.34e6 & -9.6961e6 \\ 0 & -2.6026e7 & 8.0445e8 \end{bmatrix} \quad \mathbf{B} \triangleq \begin{bmatrix} 1 & 0 \\ 0 & -1.13e6 \\ 0 & 9.8181e9 \end{bmatrix}$$

which are the model parameters from [57] translated from the center of gravity to the point ϵ , where $\epsilon = 1.6650$ m.

The constant K_3 used in Lemma 11.6 is

$$K_3 = -\frac{m_{23}(m_{22}^A - m_{11}^A)}{m_{22}m_{33} - m_{23}^2}.$$

11.B Curvature computation for Lemma 11.3

We need to find an expression for $(\partial_p \psi_d)\mu(p, v)$. We begin by recalling the expressions for $\cos(\psi_d)$ and $\sin(\psi_d)$ from the proof of Lemma 11.2:

$$\begin{bmatrix} \cos(\psi_d) \\ \sin(\psi_d) \end{bmatrix} = \frac{1}{\bar{u}^2 + v^2} \begin{bmatrix} \bar{u} & v \\ -v & \bar{u} \end{bmatrix} \mu.$$

Then we write

$$\begin{aligned} \partial_p \psi_d &= \begin{bmatrix} -\sin(\psi_d) & \cos(\psi_d) \end{bmatrix} \begin{bmatrix} \partial_p \cos(\psi_d) \\ \partial_p \sin(\psi_d) \end{bmatrix} \\ &= \frac{1}{(\bar{u}^2 + v^2)^2} \mu^\top \begin{bmatrix} v & \bar{u} \\ -\bar{u} & v \end{bmatrix} \begin{bmatrix} \bar{u} & v \\ -v & \bar{u} \end{bmatrix} \partial_p \mu \\ &= \frac{1}{(\bar{u}^2 + v^2)} \mu^\top \begin{bmatrix} 0 & 1 \\ -1 & 0 \end{bmatrix} \partial_p \mu. \end{aligned}$$

Thus

$$(\partial_p \psi_d)\mu(p, v) = \frac{1}{(\bar{u}^2 + v^2)} \mu^\top \begin{bmatrix} 0 & 1 \\ -1 & 0 \end{bmatrix} (\partial_p \mu)\mu.$$

At this point we substitute in the expression for $\mu(p, v)$ in (11.8), using $w(p, v)$ in (11.9) and the fact that

$$N(p) = \frac{1}{((\partial_x h)^2 + (\partial_y h)^2)^{(1/2)}, \quad T(p) = \begin{bmatrix} 0 & -1 \\ 1 & 0 \end{bmatrix} N(p).$$

After some algebra we obtain

$$(\partial_p \psi_d)\mu = -\kappa(p)w(p, v) + \Delta_1(p, v),$$

where κ is given in (11.3) and

$$\begin{aligned} \Delta_1(p, v) = & -\frac{\bar{u}\sigma(h(p))}{((\partial_x h)^2 + (\partial_y h)^2)^{3/2}} \left[\partial_{xy}^2 h ((\partial_x h)^2 - (\partial_y h)^2) \right. \\ & \left. + (\partial_x h)(\partial_y h)(\partial_{yy}^2 h - \partial_{xx}^2 h) \right] - \frac{\bar{u}^2 \sigma(h(p)) \sigma'(h(p))}{w(p, v)((\partial_x h)^2 + (\partial_y h)^2)^{3/2}} \\ & \cdot [(\partial_x h)^4 + (\partial_y h)^4 + 2(\partial_x h)^2(\partial_y h)^2]. \end{aligned}$$

We see that $\Delta_1(p, v)$ vanishes when $h(p) = 0$. Moreover, its dependence on v arises in the term $w(p, v)$ in one denominator. Since the function $1/w(p, v)$ is bounded with respect to v , so is Δ_1 .

Chapter 12

Conclusions and future work

This thesis considered several topics in the field of marine robotics and it was divided into three main parts. This chapter gives some concluding remarks and some suggestions for future works.

12.1 Conclusions

In this section the concluding remarks for each chapter are given.

12.1.1 Source seeking strategies for marine vehicles

Part I of the thesis was divided into two chapters.

Chapter 3 - Source seeking strategies for marine vehicles

Chapter 3 dealt with the source seeking problem for agents modeled as kinematic unicycles. We considered a leader-follower scheme with a variable leader. Inspired by the biological model of schools of birds given in Couzin et al. [37] and studied in Leonard [88], we extended the definition of the investment parameter to artificial networks. In particular, we defined the investment parameter as a function of the intensity of the measurements from the scalar field surrounding the source. Only two agents in the group, the initial leader and the active follower, were considered able to exchange the leadership during the motion. The initial leader steered the agents towards an assigned direction of motion if the measurements from the source were below a certain threshold. If instead the measurements from the source crossed a certain level, then the active follower took on the role as a leader and steered the agents towards the source. It was assumed that only the active follower got distributed measurements of the scalar field surrounding the source. The other followers had a passive role with respect to the source-seeking, that is, they could carry other sensors, for instance, cameras, but they were not considered to take an active part in the localization of the source. The main scientific contribution of the chapter was the design of a controlled agreement protocol with exchange of the leadership between two agents.

Chapter 4 - Adaptive source seeking with marine vehicles

Chapter 4 considered the source-seeking problem more specifically for multi-agent systems consisting of marine vehicles. It was considered that the agents are organized in a leader-follower scheme. The synchronization controller in [13] was used in order to obtain motion in formation of the vehicles. It was assumed that the each agent got scalar measurements of the field and communicated the value of the measurement to the leader. Then the leader computed the approximated gradient of the source and from this it computed the direction pointing towards the source. The leader computed the direction of motion using an adaptive law based on the concept of the investment parameter introduced in Chapter 3. However, the result in Chapter 4 was based on a different approach with respect to the one in Chapter 3. In fact, no change in the leadership was used in Chapter 4.

12.1.2 Control of marine vehicles using the hand position approach

Part II of this dissertation focused on a novel approach to control of marine vehicles and it was divided into three chapters.

Chapter 5 - Trajectory tracking of marine vehicles

This chapter focused on the trajectory tracking control problem for under-actuated marine vehicles in presence of unknown disturbances. Generic paths were considered and the problem was approached using a method introduced for ground vehicles in Lawton et al. [82] and based on the definition of the so called hand position point as output of the system. In particular, we extended the definition of the hand position point to marine vehicles. We then applied an input-output feedback linearizing controller choosing the hand position point as output. As common for feedback linearized systems we obtained a linear external dynamics for control purposes and a nonlinear internal dynamics. We designed a simple PID for the external dynamics in order to fulfill the trajectory tracking objectives. We then showed that, under certain conditions on the desired trajectory, the external dynamics is GES and that the states of the internal dynamics are ultimately bounded. Finally, we considered also the special case of straight-straight trajectories and we showed that the closed-loop system is AGAS in this case.

Chapter 6 - Path following of marine vehicles

In this chapter the path following control problem for under-actuated marine vehicles affected by an unknown ocean current was considered. We used the same approach as in Chapter 5, that is, we used an input-output feedback linearizing controller choosing the hand position point as output. The path following strategy was based on a parametrization of the path where the path parameter was used to propagate a path-tangential frame along the curve. The path following error was defined with respect to the propagating frame. The time update law for the path parameter, which defines the propagation of the path-tangential frame, was chosen dependent on the path following error. Under certain conditions on the curvature

of the path, the external dynamics was proven to be GES and the internal dynamics to have bounded states. The special case of parametrized straight-line paths was also considered and the closed-loop system was proven to be AGAS. In this chapter, we also considered the case of unparametrized straight-line paths. In this special case, the closed-loop system was proven to be AGAS. Finally, simulation and experimental results were presented in order to validate the theoretical results.

Chapter 7 - Multi-agent formation with disturbance rejection

This chapter focused on the development of a leader-follower synchronization law for LTI systems. The proposed control law was based on a diffusive coupling approach and it included an integral action in order to reject constant disturbances affecting the system. We showed that this diffusive coupling law may be applied to marine vehicles. In fact, considering a group of marine vehicles, it was possible to apply to each vehicle an input-output feedback linearizing controller using the hand position point as output. Each vehicle was then characterized by a linear external dynamics. Consequently, it was possible to apply to each agent the diffusive coupling law designed for LTIs. We showed that this approach solves the synchronization control problem for marine vehicles. In particular, we showed that the synchronization error between the leader and the followers is globally asymptotically stable, while the states of the internal dynamics of each vehicle are bounded. A simulation case study was presented in order to validate the theoretical results.

12.1.3 Path following for marine vehicles

Part III of the thesis focused on the path following problem for under-actuated marine vehicles. This part was divided into four chapters.

Chapter 8 - Geometric guidance for path following of marine vehicles

In this chapter the path following control problems of unparametrized straight-line paths for under-actuated marine vehicles was considered. A guidance law based on geometric control considerations was proposed. The method was based on the definition of the direction pointing towards the desired path using information about the cross-track error, the ocean current and the desired along path speed. The ocean current was supposed to be unknown, and, therefore, we used an observer to estimate it. The method was inspired by [84], where a similar strategy for UAVs in absence of disturbances was presented. Almost-GAS of the closed-loop system was proven using Lyapunov theory and cascaded systems theory. Simulation results from a case study were reported in order to validate the theoretical results.

Chapter 9 - Observer based path following for generic paths: A local approach

The path following control problem for curved paths was dealt with in this chapter. A control strategy for under-actuated marine vehicles described by the relative velocity model presented in Chapter 2 was considered. The effect of a constant and irrotational ocean current was also taken into account. The presented approach is

valid for paths parametrized via a path parameter. A path-tangential frame was propagated along the curve using a designed time update law for the path variable. The path following error was defined with respect to the path-tangential frame. The guidance law was a line-of-sight like strategy which was combined with an ocean current observer in order to counteract the ocean current effect. In this approach, the path following error was defined as the shortest distance with respect to the path. This resulted in a parametrization which was valid only locally, that is, inside a tube around the path. It was shown that the path following error is exponentially stable when the initial position of the vehicle is inside the tube. The sway velocity was shown to be bounded under certain conditions.

Chapter 10 - Observer based path following for generic paths: A global approach

In this chapter the path following control problem for under-actuated marine vehicles was dealt with using a similar approach to the one presented in Chapter 9. We considered curved paths, parametrized by a path parameter whose time update law was chosen in order to propagate a path-tangential frame. The guidance approach is also a line-of-sight like law used together with an ocean current observer in order to counteract the ocean current disturbance. The main difference with respect to Chapter 9 is given by the parameterization of the path. In particular, in Chapter 10 we relaxed the requirement that the vehicle has to move along the normal direction of the path-tangential frame. This gives extra freedom in the design of the time update law for the path variable and avoids that the parametrization is valid only locally. The path following error was shown to be globally asymptotically stable while the sway velocity was proven to be bounded.

Chapter 11 - Path following of unparametrized paths

In this chapter a novel approach to path following of curved paths was proposed. Ocean current disturbances were also considered. The approach in this chapter differs from all the others presented in the rest of this dissertation since it dealt with unparametrized curved paths. In this sense this strategy represented a *pure* approach to the path following control problem since it aimed to stabilize the curve seen as a manifold in the state space. The control law was based on geometric control and hierarchical principles. Furthermore, considerations from adaptive control were used in order to counteract the effect of the ocean current. We showed that under certain conditions for the curvature of the path the closed-loop system is asymptotically stable.

12.2 Future work

In this section some suggestions for future work are given.

The method designed in Chapter 3 may be improved by including also a formation controller for the agents. Furthermore, the extension to the case of agents modeled with a more realistic model for ASVs and AUVs is also a possible direction of improvement.

The approach presented in Chapter 4 may be extended taking into account noisy measurements from the source.

The investigation of 3D trajectories and 3D paths may be a possible future step for the results in Chapters 5, 6. Also the considerations of other environmental disturbances, like wind or waves effect, may be of interest for practical applications.

In Chapter 7 it was considered continuous time communication among the agents. This assumption is easily violated in real applications, and especially in underwater environment, because of practical restrictions on the bandwidth of the communication. This implies that the information exchanged among the agents may present some delays. Therefore, a possible future step is the development of a leader-follower synchronization law which takes into account communication delays.

A possible development of the results in Chapter 8 is the extension to the 3D case. In fact, the method used in Chapter 8, and based on the definition of an attitude error function defined in the $SO(2)$ group, would solve the problem of the singularities arising in the attitude control.

The control strategies presented in Chapters 9, 10 might be extended to the 3D case. Furthermore, these two path following control approaches may be used also for coordinated path following of multi-vehicle systems. That is, defining a path for each agent in a multi-vehicle system, these strategies may be used to make each vehicle converge to its own path. It is then possible to design a certain law for the tangential speed in order to reach motion in formation of the vehicles.

Finally, the results presented in Chapter 11 are limited to the case of Jordan curves, that is, closed curves with no self-intersections. Future work may aim to the relaxation of this condition.

Appendix A

Mathematical references

A.1 Mathematical References

This section contains some of the mathematical definitions and notations that are used in the thesis.

A.1.1 Notation

We denote by \mathbb{R}^n the n -dimensional Euclidean space and by \mathbb{R}^+ the set of all non-negative real numbers. The absolute value of a scalar x is denoted by $|x|$. The p -norm of a vector $x \in \mathbb{R}^n$ is denoted by $\|x\|_p$, for $p \in [1, \infty]$, when no subscript is given, i.e. $\|x\|$, the Euclidean norm is implied. The following definitions of comparison functions, known as class \mathcal{K} and \mathcal{KL} functions, are used throughout the thesis.

Definition A.1 (Khalil [77, Definition 4.2]). *A continuous function $\alpha : [0, a) \rightarrow [0, \infty)$ is said to belong to class \mathcal{K} if it is strictly increasing and $\alpha(0) = 0$. It is said to belong to class \mathcal{K}_∞ if $a = \infty$ and $\alpha(r) \rightarrow \infty$ as $r \rightarrow \infty$.*

Definition A.2 (Khalil [77, Definition 4.3]). *A continuous function $\beta : [0, a) \times [0, \infty) \rightarrow [0, \infty)$ is said to belong to class \mathcal{KL} if, for each fixed s , the mapping $\beta(r, s)$ belongs to class \mathcal{K} with respect to r and, for each fixed r , the mapping $\beta(r, s)$ is decreasing with respect to s and $\beta(r, s) \rightarrow 0$ as $s \rightarrow \infty$.*

Lemma A.1 (Khalil [77, Lemma 4.2]). *Let α_3 and α_4 be class \mathcal{K} functions on $[0, a)$, α_1 and α_2 be class \mathcal{K}_∞ functions on $[0, a)$, and β be a class \mathcal{KL} function. Denote the inverse of α_i by α_i^{-1} . Then,*

- α_1^{-1} is defined on $[0, \alpha_1(a))$ and belongs to class \mathcal{K} .
- α_3^{-1} is defined on $[0, \infty)$ and belongs to class \mathcal{K}_∞ .
- $\alpha_1 \circ \alpha_2$ belongs to class \mathcal{K} .
- $\alpha_3 \circ \alpha_4$ belongs to class \mathcal{K}_∞ .
- $\sigma(r, s) = \alpha_1(\beta(\alpha_2(r), s))$ belongs to class \mathcal{KL} .

A.1.2 Stability definitions

We now presents some notions of stability for a nonautonomous system

$$\dot{x} = f(t, x) \tag{A.1}$$

where $f : [0, \infty) \times D \rightarrow \mathbb{R}^n$ is piecewise continuous in t and locally Lipschitz in x on $[0, \infty) \times D$, with $D \subset \mathbb{R}^n$ a domain that contains the origin $x = 0$. The following definitions are obtained from Khalil [77]

Definition A.3. *The equilibrium point $x = 0$ of (A.1) is*

- *uniformly stable (US) if and only if there exist a class \mathcal{K} function α and a positive constant c , independent of t_0 , such that*

$$\|x(t)\| \leq \alpha(\|x(t_0)\|), \forall t \geq t_0 \geq 0, \forall \|x(t_0)\| < c \tag{A.2}$$

- *globally uniformly stable (UGS) if and only if inequality (A.2) is satisfied for any initial state $x(t_0)$.*
- *uniformly asymptotically stable (UAS) if and only if there exist a class \mathcal{KL} function β and a positive constant c , independent of t_0 , such that*

$$\|x(t)\| \leq \beta(\|x(t_0)\|, t - t_0), \forall t \geq t_0 \geq 0, \forall \|x(t_0)\| < c \tag{A.3}$$

- *globally uniformly asymptotically stable (UGAS) if and only if inequality (A.3) is satisfied for any initial state $x(t_0)$*
- *almost-globally asymptotically stable (AGAS) if and only if inequality (A.3) is satisfied for almost all the initial conditions, e.g.,*

$$x(t_0) \in \mathbb{R}^n / \mathcal{W}$$

where \mathcal{W} has zero Lebesgue measure.

Definition A.4 (Khalil [77, Definition 4.5]). *The equilibrium point $x = 0$ of (A.1) is locally exponentially stable (LES) if there exist positive constants c, k , and λ such that*

$$\|x(t)\| \leq k\|x(t_0)\|e^{-\lambda(t-t_0)}, \forall \|x(t_0)\| < c \tag{A.4}$$

and globally exponentially stable (GES) if (A.4) is satisfied for any initial state $x(t_0)$.

A.1.3 Cascaded systems

Consider the following nonlinear time-varying cascaded system:

$$\dot{x} = f_1(t, x) + g(t, x, y) \tag{A.5a}$$

$$y = f_2(t, y) \tag{A.5b}$$

where $x \in \mathbb{R}^n$, $y \in \mathbb{R}^m$, and $f_1(t, x)$ and $f_2(t, x)$ continuously differentiable in their arguments. The following results characterise the stability properties of the system (A.5).

Lemma A.2 (Panteley and Loria [114, Lemma 2]). *Consider the cascaded system (A.5). If both $\dot{x} = f_1(t, x)$ and $\dot{y} = f_2(t, y)$ are UGAS and the solutions of (A.5a) and (A.5b) are globally uniformly bounded, then the cascaded system (A.5) is UGAS.*

Theorem A.1 (Panteley and Loria [113, Theorem 2]). *Consider the cascaded system (A.5). Assume that the system $\dot{x} = f_1(t, x)$ is UGAS with a Lyapunov function $V(t, x)$ satisfying*

$$\left\| \frac{\partial V}{\partial x} \right\| \|x\| \leq c_1 V(t, x), \quad \forall \|x\| \geq \eta > 0, \quad (\text{A.6})$$

and that Assumptions (A1)-(A2) below are satisfied. Then the cascaded system (A.5) is UGAS.

(A1) *The function $g(t, x, y)$ satisfies*

$$\|g(t, x, y)\| \leq \theta_1(\|y\|) + \theta_2(\|y\|)\|x\|, \quad (\text{A.7})$$

where $\theta_1, \theta_2 : \mathbb{R}^+ \rightarrow \mathbb{R}^+$ are continuous.

(A2) *The system $\dot{y} = f_2(t, y)$ is UGAS and for all $t \geq t_0$,*

$$\int_{t_0}^t \|x(s)\| ds \leq \phi(\|x(t_0)\|), \quad (\text{A.8})$$

where $\phi(\cdot) \in \mathcal{K}$.

Remark A.1. *If the nominal system $\dot{x} = f_1(t, x)$ is UGAS with a quadratic Lyapunov function, then the condition (A.6) is satisfied trivially.*

Remark A.2. *If the perturbing system $\dot{y} = f_2(t, y)$ is UGAS and ULES (or equivalently exponentially stable in any ball of initial conditions), then the integrability condition (A.8) is satisfied trivially*

Lemma A.3 (Panteley et al. [115, Lemma 8]). *If in addition to the assumptions in Theorem A.1, both $\dot{x} = f_1(t, x)$ and $\dot{y} = f_2(t, y)$ are UGAS and ULES then the cascaded system (A.5) is UGAS and ULES.*

Proposition A.1 (Loria and Panteley [97, Proposition 2.3]). *If in addition to the assumptions in Theorem A.1, both $\dot{x} = f_1(t, x)$ and $\dot{y} = f_2(t, y)$ are UGES then the cascaded system (A.5) is UGES.*

A.1.4 Additional tools

Lemma A.4 (Comparison Lemma, Khalil [77, Lemma 3.4]). *Consider the scalar differential equation*

$$\dot{u} = f(t, u), \quad u(t_0) = u_0$$

where $f(t, u)$ is continuous in t and locally Lipschitz in u , for all $t \geq 0$ and all $u \in J \subset \mathbb{R}$. Let $[t_0, T)$ (T could be infinity) be the maximal interval of existence of the solution $u(t) \in J$ for all $t \in [t_0, T)$. Let $v(t)$ be a continuous function whose upper right-hand derivative $D^+v(t)$ satisfies the differential inequality

$$D^+v(t) \leq f(t, v(t)), \quad v(t_0) \leq u_0$$

with $v(t) \in J$ for all $t \in [t_0, T)$. Then, $v(t) \leq u(t)$ for all $t \in [t_0, T)$.

Theorem A.2 (Theorem 1.3.2 [61] - Stable Manifold Theorem for a Fixed Point)).
 Consider the system

$$\dot{x} = f(x) \quad x \in \mathbb{R}^n \quad (\text{A.9})$$

where $f = [f_1(x), \dots, f_n(x)]^T$. The linearized system around the fixed point \bar{x} is

$$\dot{\xi} = Df(\bar{x}), \quad \xi \in \mathbb{R}^n, \quad (\text{A.10})$$

where $Df = [\partial f_i / \partial x_j]$. Suppose that $\dot{x} = f(x)$ has a hyperbolic fixed point \bar{x} . Then there exist local stable and unstable manifolds $\mathcal{W}_{loc}^s(\bar{x})$ and $\mathcal{W}_{loc}^u(\bar{x})$, of the same dimensions n_s, n_u as those of the eigenspaces E^s, E^u of the linearized system A.10, and tangent to E^s, E^u at \bar{x} . $\mathcal{W}_{loc}^s(\bar{x}), \mathcal{W}_{loc}^u(\bar{x})$ are as smooth as the function f .

Definition A.5 (Angeli and Sontag [7]). Consider a general nonlinear system of the form

$$\dot{x} = f(x, u), \quad y = h(x) \quad (\text{A.11})$$

with states $x \in \mathbb{R}^n$, inputs $u \in \mathbb{R}^m$, and outputs $y \in \mathbb{R}^p$. The maps $f : \mathbb{R}^n \times \mathbb{R}^m \rightarrow \mathbb{R}^n$ and $h : \mathbb{R}^n \rightarrow \mathbb{R}^p$ are locally Lipschitz continuous. By an input signal for (A.11) we mean any measurable locally essentially bounded function of time, $u(\cdot) : \mathbb{R} \rightarrow \mathbb{R}^m$. The system (A.11) is called forward complete if for every initial condition and every input signal u , the corresponding solution is defined for all $t \geq 0$.

Theorem A.3 (Angeli and Sontag [7, Corollary 2.11]). System (A.11) is forward complete if and only if there exists a smooth and proper function $V : \mathbb{R}^n \rightarrow \mathbb{R}_{\geq 0}$ and such that

$$\frac{\partial V(x)}{\partial x} f(x, u) \leq V(x) + \sigma(\|u\|), \quad \forall x \in \mathbb{R}^n, \forall u \in \mathbb{R}^m \quad (\text{A.12})$$

holds for some $\sigma \in \mathcal{K}_\infty$.

Lemma A.5 (Khalil [77, Lemma 8.2]). Let $\phi : \mathbb{R} \rightarrow \mathbb{R}$ be a uniformly continuous function on $[0, \infty)$. Suppose that $\lim_{t \rightarrow \infty} \int_0^t \phi(\tau) d\tau$ exists and is finite. Then,

$$\phi(t) \rightarrow 0 \quad (\text{A.13})$$

as $t \rightarrow \infty$.

A.2 Graph theory tools

This section provides some notions from graph theory which will be used throughout this dissertation. Further information about graph theory can be found in [101].

Consider a network of $N + 1$ agents, where we have N follower agents and one leader agent. Assume that the communication scheme among the N follower agents is described by a directed graph \mathcal{G} . A directed graph, or digraph, \mathcal{G} is defined by the pair of sets $(\mathcal{V}, \mathcal{E})$, where \mathcal{V} , addressed as the vertex set, is the set of N vertices $v_i, i = 1 \dots, N$, while \mathcal{E} , addressed as the edge set, is the set of ordered pair of vertices $\varepsilon_{ij} = (v_i, v_j) \in \mathcal{E} \subseteq \mathcal{V} \times \mathcal{V}$. In particular, in the ordered pair of vertices

$\varepsilon_{ij} = (v_i, v_j) \in \mathcal{E}$, $i \neq j$, $i, j = 1, \dots, N$, the vertex v_i is said to be the tail and v_j is said to be the head of the edge ε_{ij} . This means that ε_{ij} tells that it is possible to go from v_i to v_j , but not vice versa. We will consider that the edge $\varepsilon_{ii} \notin \mathcal{E}$, i.e. we consider that there are no self-loop in the digraph. If $\varepsilon_{ij} \in \mathcal{E}$, then v_j is said to be a neighbor of v_i . The set of the neighbors of the agent v_i is defined as $\mathcal{N}_i = \{v_j | (v_i, v_j) \in \mathcal{E}\}$. A directed path of length r in a digraph is a sequence of $r + 1$ neighbor vertices. A digraph is said to have a spanning tree if there is a node v_r (called the root), such that there is a directed path from the root to every other node in the graph. The adjacency matrix \mathcal{A} is a $N \times N$ matrix with elements a_{ij} , $i, j = 1, \dots, N$. The elements $a_{ij} > 0$ if $\varepsilon_{ij} \in \mathcal{E}$, while $a_{ij} = 0$ otherwise. Notice that $a_{ii} = 0$ since there are no self-loops in the digraph. The value a_{ij} gives the weight of the edge ε_{ij} . For convenience and without loss of generality we will assume that if $a_{ij} > 0$, then $a_{ij} = 1$. That is, we assume that the weight of all the edges is the same. The in-degree matrix Δ is the diagonal $N \times N$ matrix where the i -th element on the diagonal, Δ_i , is such that

$$\Delta = \begin{bmatrix} \Delta_1 & \dots & \dots & 0 \\ \vdots & \ddots & & \vdots \\ \vdots & & \ddots & \vdots \\ 0 & \dots & \dots & \Delta_N \end{bmatrix}, \tag{A.14}$$

where $\Delta_i = \sum_{j \in \mathcal{N}_i} a_{ij} \forall i \in \{1, \dots, n\}$. The Laplacian matrix L is defined as $L = \Delta - \mathcal{A}$. By definition we have $L\mathbf{1}_N = 0$, where $\mathbf{1}_N$ is the N -dimensional column vector where all the entries are equal to 1. Without loss of generality we assume that the leader agent is addressed as the agent v_0 . We define the pinning matrix G as the diagonal $N \times N$ matrix where the i -th element on the diagonal is defined as $g_i = 1$ if the follower agent v_i can communicate with the leader agent v_0 , or $g_i = 0$ otherwise. The matrix G captures the interaction between the leader and the group of the followers.

Appendix B

Numerical simulation models

This appendix presents the 3DOF models used for numerical simulations in the thesis.

B.1 Numerical model for a supply vessel

Several simulations presented in this dissertation have used the numerical model of the under-actuated supply vessel used in Fredriksen and Pettersen [58]. Note that in Chapters 4-10 a dynamic model based on relative velocities has been used. While in Chapter 11 a model based on absolute velocities has been used. A picture of a supply vessel is given in Figure B.1. The physical parameters of both the models are reported here.



Figure B.1: A supply vessel. [36]

B.1.1 Relative velocities model

Recall the dynamic model based on relative velocities given in [54], and introduced in Chapter 2

$$\mathbf{M}\dot{\boldsymbol{\nu}}_r + \mathbf{C}(\boldsymbol{\nu}_r) + \mathbf{D}(\boldsymbol{\nu}_r)\boldsymbol{\nu}_r = \mathbf{B}\mathbf{f}. \quad (\text{B.1})$$

The mass of the vehicle is $m = 6.4 \cdot 10^6$ [kg]. The numerical values for \mathbf{M} , \mathbf{B} , $\mathbf{C}(\boldsymbol{\nu}_r)$ are given by

$$\begin{aligned} \mathbf{M} &= \begin{bmatrix} 7.22 \cdot 10^6 & 0 & 0 \\ 0 & 1.21 \cdot 10^7 & -3.63 \cdot 10^7 \\ 0 & -3.63 \cdot 10^7 & 4.75 \cdot 10^9 \end{bmatrix}, \\ \mathbf{C}(\boldsymbol{\nu}_r) &= \begin{bmatrix} 0 & 0 & -1.21 \cdot 10^7 v_r + 3.63 \cdot 10^7 r \\ 0 & 0 & 7.22 \cdot 10^6 u_r \\ 1.21 \cdot 10^7 v_r - 3.63 \cdot 10^7 r & -7.22 \cdot 10^6 u_r & 0 \end{bmatrix} \\ \mathbf{B} &= \begin{bmatrix} 1 & 0 \\ 0 & -1.13 \cdot 10^6 \\ 0 & 9.63 \cdot 10^7 \end{bmatrix}. \end{aligned} \quad (\text{B.2})$$

The linear damping matrix from Fredriksen and Pettersen [58] is given by

$$\mathbf{D} = \begin{bmatrix} 95070 & 0 & 0 \\ 0 & 4.34 \cdot 10^6 & -2.47 \cdot 10^6 \\ 0 & -1.88 \cdot 10^7 & 7.57 \cdot 10^8 \end{bmatrix}. \quad (\text{B.3})$$

B.1.2 Absolute velocities model

Recall the dynamic model based on relative velocities given in [54], and introduced in Chapter 11

$$\mathbf{M}_{RB}\dot{\boldsymbol{\nu}} + \mathbf{C}_{RB}(\boldsymbol{\nu})\boldsymbol{\nu} = -\mathbf{M}_A\dot{\boldsymbol{\nu}}_r - \mathbf{C}_A(\boldsymbol{\nu}_r)\boldsymbol{\nu}_r - \mathbf{D}\boldsymbol{\nu}_r + \mathbf{B}\mathbf{f}. \quad (\text{B.4})$$

The numerical values for \mathbf{M}_{RB} , \mathbf{M}_A , \mathbf{B} , $\mathbf{C}_{RB}(\boldsymbol{\nu}_r)$, $\mathbf{C}_A(\boldsymbol{\nu}_r)$ are given by

$$\begin{aligned}
 \mathbf{M}_{RB} &= \begin{bmatrix} 6.4 \cdot 10^6 & 0 & 0 \\ 0 & 6.4 \cdot 10^6 & 1.07 \cdot 10^7 \\ 0 & 1.07 \cdot 10^7 & m_{RB33} \end{bmatrix}, \\
 \mathbf{M}_A &= \begin{bmatrix} 8.2 \cdot 10^5 & 0 & 0 \\ 0 & 5.70 \cdot 10^6 & -4.696 \cdot 10^7 \\ 0 & -4.696 \cdot 10^7 & m_{A33} \end{bmatrix}, \\
 \mathbf{C}_{RB}(\boldsymbol{\nu}_r) &= \begin{bmatrix} 0 & 0 & 4.696 \cdot 10^7 \cdot r - 5.70 \cdot 10^6 \cdot v \\ 0 & 0 & 8.2 \cdot 10^5 \cdot u \\ -4.696 \cdot 10^7 \cdot r + 5.70 \cdot 10^6 \cdot v & -8.2 \cdot 10^5 \cdot u & 0 \end{bmatrix}, \\
 \mathbf{C}_A(\boldsymbol{\nu}_r) &= \begin{bmatrix} 0 & 0 & 4.696 \cdot 10^7 \cdot r - 5.70 \cdot 10^6 \cdot v \\ 0 & 0 & 8.2 \cdot 10^5 \cdot u \\ -4.696 \cdot 10^7 \cdot r + 5.70 \cdot 10^6 \cdot v & -8.2 \cdot 10^5 \cdot u & 0 \end{bmatrix}, \\
 \mathbf{B} &= \begin{bmatrix} 1 & 0 \\ 0 & -1.13 \cdot 10^6 \\ 0 & 9.63 \cdot 10^7 \end{bmatrix}.
 \end{aligned} \tag{B.5}$$

The linear damping matrix from Fredriksen and Pettersen [58] is given by

$$\mathbf{D} = \begin{bmatrix} 95070 & 0 & 0 \\ 0 & 4.34 \cdot 10^6 & -2.47 \cdot 10^6 \\ 0 & -1.88 \cdot 10^7 & 7.57 \cdot 10^8 \end{bmatrix}. \tag{B.6}$$

B.2 Numerical model for the light autonomous under-water vehicle (LAUV)

The simulation results presented in Chapters 5-6 are based on the model of the LAUV. The LAUV was developed by the Laboratório de Sistemas e Tecnologia Subaquática of the LSTS at the University of Porto. A picture of the LAUV is given in Figure B.2. The physical parameter of the vehicle are reported here and taken from da Silva et al. [38].

Recall the dynamic model based on relative velocities given in [54], and introduced in Chapter 2

$$\mathbf{M}\dot{\boldsymbol{\nu}}_r + \mathbf{C}(\boldsymbol{\nu}_r) + \mathbf{D}(\boldsymbol{\nu}_r)\boldsymbol{\nu}_r = \mathbf{B}\mathbf{f}. \tag{B.7}$$

The mass of the vehicle is $m = 6.4 \cdot 10^6$ [kg]. The numerical values for \mathbf{M} , \mathbf{B} ,



Figure B.2: The LAUV.

$C(\nu_r)$ are given by

$$\begin{aligned}
 \mathbf{M} &= \begin{bmatrix} 19 & 0 & 0 \\ 0 & 2.1 & 0 \\ 0 & 0 & 2.1 \end{bmatrix}, \\
 \mathbf{C}(\nu_r) &= \begin{bmatrix} 0 & 0 & -34 \cdot v_r \\ 0 & 0 & 19 \cdot u_r \\ 34 \cdot v_r & -19 \cdot u_r & 0 \end{bmatrix} \\
 \mathbf{B} &= \begin{bmatrix} 1 & 0 \\ 0 & -39.8783 \\ 0 & 18.1446 \end{bmatrix}.
 \end{aligned} \tag{B.8}$$

The linear damping matrix from da Silva et al. [38] is given by

$$\mathbf{D} = \begin{bmatrix} 2.4 & 0 & 0 \\ 0 & 9.7 & -11.5 \\ 0 & 3.1 & 9.7 \end{bmatrix}. \tag{B.9}$$

References

- [1] M. Abdelaal, M. Fränzle, and A. Hahn. Nonlinear model predictive control for tracking of underactuated vessels under input constraints. In *Proc. IEEE European Modelling Symposium*, Madrid, Spain, 6-8 Oct., 2015.
- [2] A. P. Aguiar and A. M. Pascoal. Dynamic positioning and way-point tracking of underactuated auvs in the presence of ocean currents. *International Journal of Control*, 80(7):1092–1108, 2007.
- [3] A. P. Aguiar and A. M. Pascoal. Dynamic positioning and way-point tracking of underactuated AUVs in the presence of ocean currents. In *Proc. 41st IEEE Conference on Decision and Control*, pages 2105–2110, Las Vegas, Nevada USA, Dec. 2002.
- [4] A. P. Aguiar, J. P. Hespanha, et al. Trajectory-tracking and path-following of underactuated autonomous vehicles with parametric modeling uncertainty. *IEEE Transactions on Automatic Control*, 52(8):1362–1379, 2007.
- [5] A. Alessandretti, A. P. Aguiar, and C. Jones. Trajectory-tracking and path-following controllers for constrained underactuated vehicles using model predictive control. In *Proc. IEEE European Control Conference*, pages 1371–1376, Zurich, Switzerland, 17-19 July, 2013.
- [6] M. Andreasson, D. V. Dimarogonas, H. Sandberg, and K. H. Johansson. Distributed control of networked dynamical systems: Static feedback, integral action and consensus. *IEEE Transactions on Automatic Control*, 59(7):1750–1764, 2014.
- [7] D. Angeli and E. D. Sontag. Forward completeness, unboundedness observability, and their lyapunov characterizations. *Systems & Control Letters*, 38(4):209–217, 1999.
- [8] F. Arrichiello. *Coordination control of multiple mobile robots*. PhD thesis, University of Cassino, 2006.
- [9] F. Arrichiello, S. Chiaverini, and T. I. Fossen. Formation control of underactuated surface vessels using the null-space-based behavioral control. In *IEEE/RSJ International Conference on Intelligent Robots and Systems*, pages 5942–5947, Beijing, China, Oct. 9-15, 2006.

- [10] K. J. Aström and R. M. Murray. *Feedback systems: An Introduction for Scientists and Engineers*. Princeton university press, 2010.
- [11] R. Bachmayer and N. E. Leonard. Vehicle networks for gradient descent in a sampled environment. In *41st IEEE Conference on Decision and Control*, pages 112–117, Las Vegas, Nevada, USA, 2002.
- [12] D. J. W. Belleter and K. Y. Pettersen. Path following with disturbance rejection for inhomogeneous formations with underactuated agents. In *IEEE European Control Conference (ECC)*, Linz, Austria, July, 2015.
- [13] D. J. W. Belleter and K. Y. Pettersen. Path following for formations of underactuated marine vessels under influence of constant ocean currents. In *53rd IEEE Conference on Decision and Control (CDC)*, pages 4521–4528, Los Angeles, California, USA, 2014.
- [14] D. J. W. Belleter and K. Y. Pettersen. Leader-follower synchronisation for a class of underactuated systems. In *Nonlinear Systems*, pages 157–179. Springer, 2017.
- [15] D. J. W. Belleter, C. Paliotta, M. Maggiore, and K. Pettersen. Path following for underactuated marine vessels. In *Proc. 10th IFAC Symposium on Nonlinear Control Systems*, Monterey, CA, USA 2016.
- [16] D. J. W. Belleter, M. Maghenem, C. Paliotta, and K. Y. Pettersen. Observer based path following for underactuated marine vessels in the presence of ocean currents: a global approach. *Submitted to IEEE Transactions on Control Systems and Technology*, 2017.
- [17] E. Biyık and M. Arcaç. Gradient climbing in formation via extremum seeking and passivity-based coordination rules. *Asian Journal of Control*, 10(2):201–211, 2008.
- [18] E. Børhaug and K. Y. Pettersen. Cross-track control for underactuated autonomous vehicles. In *44th IEEE Conference on Decision and Control- European Control Conference. (CDC-ECC)*, pages 602–608, Seville, Spain, Dec., 2005.
- [19] E. Børhaug, A. Pavlov, E. Panteley, and K. Y. Pettersen. Straight line path following for formations of underactuated marine surface vessels. *IEEE Transaction on Control Systems Technology*, 19(3), 2011.
- [20] E. Børhaug, A. Pavlov, and K. Y. Pettersen. Integral LOS control for path following of underactuated marine surface vessels in the presence of constant ocean currents. In *Proc. 47th IEEE Conference on Decision and Control*, pages 4984–4991, Cancun, Mexico, Dec. 9-11, 2008.
- [21] A. D. Bowen, D. R. Yoerger, C. Taylor, R. McCabe, J. Howland, D. Gomez-Ibanez, J. C. Kinsey, M. Heintz, G. McDonald, D. B. Peters, et al. The nereus hybrid underwater robotic vehicle for global ocean science operations to 11,000 m depth. In *Proc. of OCEANS*, pages 1–10, Quebec City, QC, Canada, 2008.

-
- [22] M. Breivik. *Topics in guided motion control of marine vehicles*. PhD thesis, Norwegian University of Science and Technology, Dept. Engineering Cybernetics, 2010.
- [23] M. Breivik and T. I. Fossen. Guidance laws for planar motion control. In *IEEE 47th Conference on Decision and Control*, pages 570–577, Cancun, Mexico, Dec. 2008.
- [24] M. Breivik and T. I. Fossen. Path following of straight lines and circles for marine surface vessels. In *6th IFAC Conference on Control Applications in Marine Systems (CAMS)*, Ancona, Italy, July 7-9, 2004.
- [25] M. Breivik, V. E. Hovstein, and T. I. Fossen. Straight-line target tracking for unmanned surface vehicles. *Modeling, Identification and Control*, 29(4): 131–149, 2008.
- [26] M. Breivik, V. E. Hovstein, and T. I. Fossen. Ship formation control: A guided leader-follower approach. In *Proc. IFAC World Congress*, pages 16008–16014, Seoul, South Korea, 2008.
- [27] F. Bullo. *Geometric control of mechanical systems*, volume 49. Springer Science & Business Media, 2005.
- [28] F. Bullo and R. M. Murray. Tracking for fully actuated mechanical systems: a geometric framework. *Automatica*, 35(1):17–34, 1999.
- [29] M. Burger. *Disturbance Rejection using Conditional Integrators: Applications to path manoeuvring under environmental disturbances for single vessels and vessel formations*. PhD thesis, Norwegian University of Science and Technology, Dept. Engineering Cybernetics, 2011.
- [30] M. Burger, A. Pavlov, and K. Pettersen. Conditional integrators for path following and formation control of marine vessels under constant disturbances. In *FAC Conference on Manoeuvring and Control of Marine Craft*, pages 179–184, Guarujá, Brazil, 2009.
- [31] W. Caharija. *Integral line-of-sight guidance and control of underactuated marine vehicles*. PhD thesis, Norwegian University of Science and Technology, Department of Engineering Cybernetics, 2014.
- [32] W. Caharija, K. Y. Pettersen, M. Bibuli, P. Calado, E. Zereik, J. Braga, J. T. Gravdahl, A. J. Sørensen, M. Milovanović, and G. Bruzzone. Integral line-of-sight guidance and control of underactuated marine vehicles: Theory, simulations, and experiments. *IEEE Transactions on Control Systems Technology*, 24(5):1623–1642, 2016.
- [33] W. Caharija, K. Y. Pettersen, J. T. Gravdahl, and E. Borhaug. Integral LOS guidance for horizontal path following of underactuated autonomous underwater vehicles in the presence of vertical ocean currents. In *Proc. 2012 American Control Conference*, pages 5427–5434, Montreal, Canada, June 2012.

- [34] Y. Cheng, M. W. Maimone, and L. Matthies. Visual odometry on the mars exploration rovers—a tool to ensure accurate driving and science imaging. *IEEE Robotics & Automation Magazine*, 13(2):54–62, 2006.
- [35] I. Colomina and P. Molina. Unmanned aerial systems for photogrammetry and remote sensing: A review. *ISPRS Journal of Photogrammetry and Remote Sensing*, 92:79–97, 2014.
- [36] W. Commons. Platform supply vessel., 1999. URL https://commons.wikimedia.org/wiki/File:Platform_Supply_Vessel.JPG. English: Enesco Ram: platform supply vessel.
- [37] I. D. Couzin, J. Krause, N. R. Franks, and S. A. Levin. Effective leadership and decision-making in animal groups on the move. *Nature*, 433(7025):513–516, 2005.
- [38] J. E. da Silva, B. Terra, R. Martins, and J. B. de Sousa. Modeling and simulation of the LAUV autonomous underwater vehicle. In *Proc. 13th IFAC Inter. Conf. on Methods and Models in Automation and Robotics*, Szczecin, Poland, August, 2007.
- [39] L. de Sistemas e Tecnologia Subaquatica (LSTS). Dune: Unified navigation environment,, 2015. URL <http://lsts.fe.up.pt/toolchain/dune>.
- [40] Z. Ding. Consensus disturbance rejection with disturbance observers. *IEEE Transactions on Industrial Electronics*, 62(9), 2015.
- [41] K. Do and J. Pan. Global tracking control of underactuated ships with nonzero off-diagonal terms in their system matrices. *Automatica*, 41(1):87–95, 2005.
- [42] K. Do, Z.-P. Jiang, and J. Pan. Universal controllers for stabilization and tracking of underactuated ships. *Systems & Control Letters*, 47(4):299–317, 2002.
- [43] K. D. Do. Global robust and adaptive output feedback dynamic positioning of surface ships. *Journal of Marine Science and Application*, 10(3):325, 2011.
- [44] K. D. Do and J. Pan. State-and output-feedback robust path-following controllers for underactuated ships using serret-frenet frame. *Ocean Engineering*, 31(5):587–613, 2004.
- [45] K. D. Do and J. Pan. Global robust adaptive path following of underactuated ships. *Automatica*, 42(10):1713–1722, 2006.
- [46] K. D. Do, Z.-P. Jiang, and J. Pan. Underactuated ship global tracking under relaxed conditions. *IEEE Transactions on Automatic Control*, 47(9):1529–1536, 2002.
- [47] M. I. El-Hawwary and M. Maggiore. Reduction theorems for stability of closed sets with application to backstepping control design. *Automatica*, 49(1):214–222, 2013.

-
- [48] P. Encarnacao and A. Pascoal. 3d path following for autonomous underwater vehicle. In *39th IEEE Conference on Decision and Control*, pages 2977–2982, Sydney, Australia, 2000.
- [49] P. Encarnação and A. Pascoal. Combined trajectory tracking and path following: an application to the coordinated control of autonomous marine craft. In *40th Conference on Decision and Control*, pages 964–969, Orlando, Florida, USA, 2001.
- [50] P. Encarnação, A. Pascoal, and M. Arcak. Path following for marine vehicles in the presence of unknown currents. In *6th IFAC Symposium on Robot Control*, pages 469–474, Vienna, Austria, 21-23 Sept., 2000.
- [51] P. M. M. Encarnação. *Nonlinear path following control systems for ocean vehicles*. PhD thesis, Universidade Técnica de Lisboa, 2002.
- [52] O. Faltinsen. *Sea loads on ships and offshore structures*, volume 1. Cambridge university press, 1993.
- [53] E. Fiorelli, N. E. Leonard, P. Bhatta, D. A. Paley, R. Bachmayer, and D. M. Fratantoni. Multi-AUV control and adaptive sampling in monterey bay. *IEEE Journal of Oceanic Engineering*, 31(4):935–948, 2006.
- [54] T. I. Fossen. *Handbook of marine craft hydrodynamics and motion control*. John Wiley & Sons, 2011.
- [55] T. I. Fossen and K. Y. Pettersen. On uniform semiglobal exponential stability (USGES) of proportional line-of-sight guidance laws. *Automatica*, 50(11), 2014.
- [56] T. I. Fossen, M. Breivik, and R. Skjetne. Line-of-sight path following of underactuated marine craft. In *Proc. 6th IFAC Inter. Conf. on Maneuvering and Control of Marine Crafts*, pages 244–249, Girona, Spain, 2003.
- [57] E. Fredriksen and K. Y. Pettersen. Global κ -exponential way-point manoeuvring of ships. In *Proc. 43rd IEEE Conference on Decision and Control*, pages 5360–5367, Atlantis, Bahamas, Dec. 14-17, 2004.
- [58] E. Fredriksen and K. Y. Pettersen. Global κ -exponential way-point manoeuvring of ships: Theory and experiments. *Automatica*, 42(4):677–687, 2006.
- [59] N. Ghods and M. Krstic. Multi-agent deployment around a source in one dimension by extremum seeking. In *American Control Conference (ACC)*, pages 4794–4799, 2010.
- [60] D. Goldberg, V. Cicirello, M. B. Dias, R. Simmons, S. Smith, T. Smith, and A. Stentz. A distributed layered architecture for mobile robot coordination: Application to space exploration. In *Proc. International NASA Workshop on Planning and Scheduling for Space*, Houston, Texas, USA, 2002.

- [61] J. Guckenheimer and P. J. Holmes. *Nonlinear oscillations, dynamical systems, and bifurcations of vector fields*, volume 42. Springer Science & Business Media, 2013.
- [62] B. J. Guerreiro, C. Silvestre, R. Cunha, and A. Pascoal. Trajectory tracking nonlinear model predictive control for autonomous surface craft. *IEEE Transactions on Control Systems Technology*, 22(6):2160–2175, 2014.
- [63] J. Han and Y. Chen. Multiple uav formations for cooperative source seeking and contour mapping of a radiative signal field. *Journal of Intelligent & Robotic Systems*, 74(1-2):323–332, 2014.
- [64] I.-A. Ihle, R. Skjetne, and T. I. Fossen. Nonlinear formation control of marine craft with experimental results. In *43rd IEEE Conference on Decision and Control*, pages 680–685, Atlanta, Georgia, USA, 2004.
- [65] I.-A. Ihle, J. Jouffroy, and T. I. Fossen. Formation control of marine surface craft using lagrange multipliers. In *44th IEEE Conference on Decision and Control*, pages 752–758, Seville, Spain, 2005.
- [66] I.-A. F. Ihle, J. Jouffroy, and T. I. Fossen. Formation control of marine surface craft: A Lagrangian approach. *IEEE Journal of Oceanic Engineering*, 31(4): 922–934, 2006.
- [67] I.-A. F. Ihle, M. Arcak, and T. I. Fossen. Passivity-based designs for synchronized path-following. *Automatica*, 43(9):1508–1518, 2007.
- [68] A. Isidori. *Nonlinear control systems*. Springer Science & Business Media, 1995.
- [69] A. Jadbabaie, J. Lin, and A. S. Morse. Coordination of groups of mobile autonomous agents using nearest neighbor rules. *IEEE Transactions on Automatic Control*, 48(6):988–1001, 2003.
- [70] M. Ji, A. Muhammad, and M. Egerstedt. Leader-based multi-agent coordination: Controllability and optimal control. In *Proc. 26th IEEE American Control Conference*, Minneapolis, Minnesota, USA, June 2006.
- [71] Z.-P. Jiang. Global tracking control of underactuated ships by Lyapunov’s direct method. *Automatica*, 38(2):301–309, 2002.
- [72] Z.-P. Jiang and H. Nijmeijer. A recursive technique for tracking control of nonholonomic systems in chained form. *IEEE Transactions on Automatic control*, 44(2):265–279, 1999.
- [73] K. Jo, J. Kim, D. Kim, C. Jang, and M. Sunwoo. Development of autonomous car—part i: distributed system architecture and development process. *IEEE Transactions on Industrial Electronics*, 61(12):7131–7140, 2014.

-
- [74] K. Jo, J. Kim, D. Kim, C. Jang, and M. Sunwoo. Development of autonomous car—part ii: A case study on the implementation of an autonomous driving system based on distributed architecture. *IEEE Transactions on Industrial Electronics*, 62(8):5119–5132, 2015.
- [75] T. A. Johansen and T. I. Fossen. Control allocation—a survey. *Automatica*, 49(5):1087–1103, 2013.
- [76] C. Johnson. Positive definite matrices. *The American Mathematical Monthly*, 77(3):259–264, 1970.
- [77] H. K. Khalil. *Nonlinear systems*. Prentice Hall, New Jersey, 2000.
- [78] S. Z. Khong, Y. Tan, C. Manzie, and D. Nešić. Multi-agent source seeking via discrete-time extremum seeking control. *Automatica*, 50(9):2312–2320, 2014.
- [79] D. Kingston, R. W. Beard, and R. S. Holt. Decentralized perimeter surveillance using a team of uavs. *IEEE Transactions on Robotics*, 24(6):1394–1404, 2008.
- [80] L. Lapierre and D. Soetanto. Nonlinear path-following control of an AUV. *Ocean Engineering*, 34(11):1734–1744, 2007.
- [81] L. Lapierre, D. Soetanto, and A. Pascoal. Nonlinear path following with applications to the control of autonomous underwater vehicles. In *42nd IEEE Conference on Decision and Control*, pages 1256–1261, Maui, Hawaii, USA, 2003.
- [82] J. R. Lawton, R. W. Beard, and B. J. Young. A decentralized approach to formation maneuvers. *IEEE Transactions on Robotics and Automation*, 19(6):933–941, 2003.
- [83] T. Lee. Robust adaptive attitude tracking on $so(3)$ with an application to a quadrotor uav. *IEEE Transactions on Control Systems Technology*, 21(5):1924–1930, 2013.
- [84] T. Lee. Geometric tracking control of the attitude dynamics of a rigid body on $SO(3)$. In *Proc. 2011 American Control Conference*, pages 1200–1205, San Francisco, CA, June 2011.
- [85] T. Lee, M. Leok, and N. H. McClamroch. Stable manifolds of saddle equilibria for pendulum dynamics on S^2 and $so(3)$. In *50th IEEE Conference on Decision and Control and European Control Conference (CDC-ECC)*, pages 3915–3921, Orlando, Florida, Dec. 2011.
- [86] T. Lee, M. Leoky, and N. H. McClamroch. Geometric tracking control of a quadrotor UAV on $SE(3)$. In *Proc. 49th IEEE Conference on Decision and Control*, Atlanta, USA, Dec. 2010.

- [87] E. Lefeber, K. Y. Pettersen, and H. Nijmeijer. Tracking control of an underactuated ship. *IEEE Transactions on Control Systems Technology*, 11(1): 52–61, 2003.
- [88] N. E. Leonard. Multi-agent system dynamics: Bifurcation and behavior of animal groups. *IFAC Proceedings Volumes*, 46(23):307–317, 2013.
- [89] N. E. Leonard. Multi-agent system dynamics: Bifurcation and behavior of animal groups. *Annual Reviews in Control*, 38(2):171–183, 2014.
- [90] N. E. Leonard and E. Fiorelli. Virtual leaders, artificial potentials and coordinated control of groups. In *Proc. 40th IEEE Conference on Decision and Control*, pages 2968–2973, Orlando, Florida, USA, Dec. 2001.
- [91] F. L. Lewis, H. Zhang, K. Hengster-Movric, and A. Das. *Cooperative Control of Multi-Agent Systems: Optimal and Adaptive Design Approaches*. Springer Science & Business Media, 2013.
- [92] Z. Li, Z. Duan, G. Chen, and L. Huang. Consensus of multiagent systems and synchronization of complex networks: a unified viewpoint. *IEEE Transactions on Circuits and Systems I: Regular Papers*, 57(1):213–224, 2010.
- [93] R. A. Lindemann and C. J. Voorhees. Mars exploration rover mobility assembly design, test and performance. In *Proc. IEEE International Conference on Systems, Man and Cybernetics*, pages 450–455, Waikoloa, HI, USA, 10-12 Oct, 2005.
- [94] K. D. Listmann and C. A. Woolsey. Output synchronization of systems in chained form. In *48th IEEE Conference on Decision and Control*, pages 3341–3346, Shanghai, Cina, 2009.
- [95] B. Liu, T. Chu, L. Wang, and G. Xie. Controllability of a leader-follower dynamic network with switching topology. *IEEE Transactions on Automatic Control*, 53(4):1009–1013, 2008.
- [96] D. A. B. Lombana and M. di Bernardo. Multiplex pi control for consensus in networks of heterogeneous linear agents. *Automatica*, 67:310–320, 2016.
- [97] A. Loría and E. Panteley. Cascaded nonlinear time-varying systems: Analysis and design. In *Advanced topics in control systems theory*, pages 23–64. Springer, 2005.
- [98] M. Ludvigsen, G. Johnsen, P. Lågstad, A. Sørensen, and Ø. Ødegård. Scientific operations combining ROV and AUV in the Trondheim Fjord. In *Proc. of OCEANS*, pages 1–7, Bergen, Norway, 2013.
- [99] M. Maghenem, D. J. W. Belleter, C. Paliotta, and K. Y. Pettersen. Observer based path following for underactuated marine vessels in the presence of ocean currents: a local approach. In *IFAC World Congress*, Toulouse, France, 2017.

-
- [100] P. Maurya, A. P. Aguiar, and A. Pascoal. Marine vehicle path following using inner-outer loop control. In *Proc. 8th IFAC Inter. Conf. on Manoeuvring and Control of Marine Craft*, pages 38–43, Guarujá, Brazil, 2009.
- [101] M. Mesbahi and M. Egerstedt. *Graph theoretic methods in multiagent networks*. Princeton University Press, 2010.
- [102] A. Micaelli and C. Samson. *Trajectory tracking for unicycle-type and two-steering-wheels mobile robots*. PhD thesis, INRIA, 1993.
- [103] S. Moe, W. Caharija, K. Y. Pettersen, and I. Schjølberg. Path following of underactuated marine surface vessels in the presence of unknown ocean currents. In *Proc. IEEE American Control Conference*, pages 3856–3861, 2014.
- [104] K. Narendra and A. Annaswamy. A new adaptive law for robust adaptation without persistent excitation. *IEEE Transactions on Automatic control*, 32(2):134–145, 1987.
- [105] P. Ögren, E. Fiorelli, and N. E. Leonard. Cooperative control of mobile sensor networks: Adaptive gradient climbing in a distributed environment. *IEEE Transactions on Automatic Control*, 49(8):1292–1302, 2004.
- [106] D. Pais and N. E. Leonard. Adaptive network dynamics and evolution of leadership in collective migration. *Physica D: Nonlinear Phenomena*, 267: 81–93, 2014.
- [107] C. Paliotta and K. Y. Pettersen. Leader-follower synchronization with disturbance rejection. In *Proc. IEEE Multi-Conference on Systems and Control*, Buenos Aires, Argentina, Sep. 2016.
- [108] C. Paliotta and K. Y. Pettersen. Source seeking with a variable leader multi-agent fixed topology network. In *Proc. European Control Conference*, Linz, Austria, 2015.
- [109] C. Paliotta and K. Y. Pettersen. Geometric path following with ocean current estimation for ASVs and AUVs. In *Proc. 2016 American Control Conference*, Boston, MA, USA, July 2016.
- [110] C. Paliotta, E. Lefeber, and K. Y. Pettersen. Trajectory tracking of under-actuated marine vehicles. In *Proc. 45th IEEE Conference on Decision and Control*, Las Vegas, Nevada, USA, Dec. 2016.
- [111] C. Paliotta, D. J. W. Belleter, and K. Y. Pettersen. Adaptive source seeking with leader-follower formation control. *IFAC-PapersOnLine, Presented at: 10th IFAC Conference on Maneuvering and Control of Marine Crafts*, 2015.
- [112] C. Paliotta, E. Lefeber, K. Y. Pettersen, J. Pinto, M. Costa, and J. Sousa. Trajectory tracking and path following for under-actuated marine vehicles. *Submitted to IEEE Transactions on Control Systems and Technology*, 2017.

- [113] E. Panteley and A. Loria. On global uniform asymptotic stability of nonlinear time-varying systems in cascade. *Systems & Control Letters*, 33(2):131–138, 1998.
- [114] E. Panteley and A. Loria. Growth rate conditions for uniform asymptotic stability of cascaded time-varying systems. *Automatica*, 37(3):453–460, 2001.
- [115] E. Panteley, E. Lefeber, A. Loria, and H. Nijmeijer. Exponential tracking control of a mobile car using a cascaded approach. In *Proc. of the IFAC workshop on motion control*, pages 221–226, Grenoble, France, Sept., 1998.
- [116] K. Pettersen and H. Nijmeijer. Tracking control of an underactuated surface vessel. In *Proc. 37th IEEE Conference on Decision and Control*, pages 4561–4566, Tampa, Florida, USA, Dec. 1998.
- [117] K. Y. Pettersen and H. Nijmeijer. Semi-global practical stabilization and disturbance adaptation for an underactuated ship. In *39th IEEE Conference on Decision and Control*, pages 2144–2149, Sydney, Australia, 2000.
- [118] K. Y. Pettersen and H. Nijmeijer. Underactuated ship tracking control: theory and experiments. *International Journal of Control*, 74(14):1435–1446, 2001.
- [119] A. Rahmani, M. Ji, M. Mesbahi, and M. Egerstedt. Controllability of multi-agent systems from a graph-theoretic perspective. *SIAM Journal on Control and Optimization*, 48(1):162–186, 2009.
- [120] W. Ren, R. W. Beard, and E. M. Atkins. Information consensus in multi-vehicle cooperative control. *IEEE Control systems magazine*, 2(27):71–82, 2007.
- [121] D. Ribas, N. Palomeras, P. Ridao, M. Carreras, and A. Mallios. Girona 500 auv: From survey to intervention. *IEEE ASME Transactions on Mechatronics*, 17(1):46, 2012.
- [122] E. J. Rodríguez-Seda, C. Tang, M. W. Spong, and D. M. Stipanović. Trajectory tracking with collision avoidance for nonholonomic vehicles with acceleration constraints and limited sensing. *The International Journal of Robotics Research*, 33(12):1569–1592, 2014.
- [123] W. J. Rugh. *Linear system theory*. Prentice Hall Upper Saddle River, NJ, 1996.
- [124] C. Samson. Path following and time-varying feedback stabilization of a wheeled mobile robot. In *Proc. International Conference on Advanced Robotics and Computer Vision*, Singapore, Sept., 1992.
- [125] G. S. Seyboth and F. Allgöwer. Synchronized model matching: a novel approach to cooperative control of nonlinear multi-agent systems*. In *19th IFAC World Congress*, pages 1985–1990, Cape Town, South Africa, 2014.

-
- [126] G. S. Seyboth and F. Allgower. Output synchronization of linear multi-agent systems under constant disturbances via distributed integral action. In *Proc. American Control Conference (ACC)*, pages 62–67, Chicago, IL, USA, 2015.
- [127] D. Shim, H. Chung, H. J. Kim, and S. Sastry. Autonomous exploration in unknown urban environments for unmanned aerial vehicles. In *Proc. AIAA Guidance, Navigation, Control Conf. Exhibit*, San Francisco, CA, 2005.
- [128] B. Siciliano, L. Sciavicco, L. Villani, and G. Oriolo. *Robotics: modelling, planning and control*. Springer Science & Business Media, 2010.
- [129] R. Skjetne, S. Moi, and T. I. Fossen. Nonlinear formation control of marine craft. In *41st IEEE Conference on Decision and Control*, pages 1699–1704, 2002.
- [130] C. R. Sonnenburg and C. A. Woolsey. Modeling, identification, and control of an unmanned surface vehicle. *Journal of Field Robotics*, 30(3):371–398, 2013.
- [131] A. J. Sørensen. Structural issues in the design and operation of marine control systems. *Annual Reviews in Control*, 29(1):125–149, 2005.
- [132] H. G. Tanner. On the controllability of nearest neighbor interconnections. In *43rd IEEE Conference on Decision and Control*, pages 2467–2472, Atlanta, Georgia, USA, 2004.
- [133] M. S. Triantafyllou and F. S. Hover. *Maneuvering and control of marine vehicles. Cambridge, Massachusetts, USA, 2003.*
- [134] M. S. Wiig, K. Y. Pettersen, and T. R. Krogstad. Uniform semiglobal exponential stability of integral line-of-sight guidance laws. In *10th IFAC Conference on Maneuvering and Control of Marine Craft (MCMC)*, pages 61–68, Copenhagen, Denmark, Aug. 2015.
- [135] C. A. Woolsey. Directional control of a slender, underactuated auv using potential shaping. In *45th IEEE Conference on Decision and Control*, pages 6826–6831, San Diego, CA, USA, 2006.
- [136] W. Wu, D. Chang, and F. Zhang. A bio-inspired robust 3d plume tracking strategy using mobile sensor networks. In *Proc. IEEE 52nd Conference on Decision and Control*, pages 4571–4578, Loas Angeles, California, Dec. 2013.
- [137] W. Wu, I. D. Couzin, and F. Zhang. Bio-inspired source seeking with no explicit gradient estimation. In *Proc. of 3rd IFAC Workshop on Distributed Estimation and Control in Networked Systems*, Santa Barbara, CA, USA, Sept. 2012.
- [138] E. Xidias, C. Paliotta, N. Aspragathos, and K. Y. Pettersen. Path planning for formation control of autonomous vehicles. In *Proc. 25th Conference on Robotics in Alpe-Adria-Danube Region (RAAD16)*, Belgrade, Serbia, 2016.

- [139] C. Zhang, D. Arnold, N. Ghods, A. Siranosian, and M. Krstic. Source seeking with non-holonomic unicycle without position measurement and with tuning of forward velocity. *Systems & control letters*, 56(3):245–252, 2007.
- [140] H. Zhang, F. L. Lewis, and A. Das. Optimal design for synchronization of cooperative systems: state feedback, observer and output feedback. *IEEE Trans. on Automatic Control*, 56(8):1948–1952, 2011.
- [141] S. Zhu, D. Wang, and C. B. Low. Cooperative control of multiple uavs for source seeking. *Journal of Intelligent & Robotic Systems*, 70(1-4):293–301, 2013.
- [142] S. Zhu, D. Wang, and C. B. Low. Cooperative control of multiple uavs for moving source seeking. *Journal of Intelligent & Robotic Systems*, 74(1-2): 333–346, 2014.